Investigating cognitive performance and major modulatory inhibitory interneurones in the humanised $App^{NL\text{-}F/NL\text{-}F}$ mouse model of Alzheimer's disease

Alexandra-Loredana Petrache

A dissertation submitted in partial fulfillment
of the requirements for the degree of
Doctor of Philosophy
of
University College London.

UCL School of Pharmacy
University College London

I, Alexandra-Loredana Petrache, confirm that the work presented in this thesis is my own. Where information has been derived from other sources, I confirm that this has been indicated in the work.

Abstract

Studies using human AD patients and mouse models of AD have shown abnormal synaptic hyperexcitation, which has been postulated to spread the pathology of AD leading to cognitive deficits. Since neuronal excitation is balanced by specialised inhibitory interneurones, we hypothesise that major inhibitory interneurones are disrupted in AD, could cause this imbalance and contribute to cognitive worsening. This study focused on three modulatory inhibitory interneurones that express cholecystokinin (CCK), somatostatin (SST) and a subtype that expresses calretinin (CR) and that are specialised to only contact other interneurones.

The focus was on the CA1 hippocampal region in the $App^{NL\text{-}F/NL\text{-}F}$ mouse model and age-matched wild-type mice. A top-down approach was taken to first investigate symptoms of AD such as memory impairment and anxiety with the T-arm maze and novel object recognition, and open arena, respectively. This was followed by investigation of anatomical interneurone and pyramidal cell density using immunohistochemistry and confocal microscopy, and the expression of α5-containing $GABA_A$ receptor subunit, which is important in memory formation. These parameters were correlated with typical hallmarks of AD such as amyloidβ (Aβ) accumulation and gliosis- proliferation of astrocytes and microglia. The results indicate modest memory impairment in the $App^{NL\text{-}F/NL\text{-}F}$ starting at 6-9 months and continuing to 18-22 months, accompanied by indicators of anxiety. Furthermore, in the $App^{NL\text{-}F/NL\text{-}F}$ model, Aβ selectively infiltrated CCK and SST cells, but not CR cells. This was associated with age-dependent CCK and SST cell

density decline, in contrast with the preserved CR cells. A closer look at receptor expression showed that all three interneuron subtypes in wild-type and $App^{NL\text{-}F/NL\text{-}F}$ animals, as well as pyramidal cells, expressed the $\alpha 5$ subunit.

The results highlight selective interneurone destruction in disease, accompanied by AD hallmarks and cognitive deficits. The widespread expression of the $\alpha 5$ subunit on multiple cell types emphasises its importance in disease.

Acknowledgements

I would first and foremost like to thank my supervisor, Dr. Afia B. Ali, for her academic guidance as well as for her unwavering support and mentorship. The MRC, for funding this research via the grant MR/N013867/1, as well as the UCL-Birkbeck Doctoral Training Programme for offering me a place on this prestigious course and for giving me the opportunity to make the most of my PhD at the School of Pharmacy.

I would also like to thank my family, faith and those who supported me at any moment in my journey, and also myself for being determined and resilient.

This thesis was created using Overleaf and the UCL Thesis template by (c) Ian Kirker, 2014.

Contents

List of Figures

List of Tables

Abbreviations

A1= activated astrocytes

A2= non-inflammatory astrocytes

Aβ= amyloid-β

ACSF= artificial cerebrospinal fluid

nACSF= normal artificial cerebrospinal fluid

AD= Alzheimer's Disease

APP= amyloid precursor protein

ATP= adenoside triphosphate

BACE1= beta-site amyloid precursor protein cleaving enzyme

CamKII-α= Ca2+/calmodulin-dependent protein kinase II- α

Cluster of Differentiation 68= CD68

CNS= central nervous system

Cornu ammonis 1-4= CA1-4

CR= calretinin

CTF= carbon terminal domain

EC= entorhinal cortex

fAD= familial Alzheimer's disease

GABA= gamma-aminobutyric acid

GAD67= glutamate decarboxylase

GAT1= GABA transporter 1

GFAP= glial fibrillary acidic protein

GTP= guanosine triphosphate

H_2O_2= hydrogen peroxide

LEC= lateral entorhinal cortex

LTP= long-term potentiation

M1/2= activated/neuroprotective microglia

MCI= mild cognitive impairment

NMDA= N-methyl-D-aspartate

PC= pyramidal cells

PD= Parkinson's disease

PSEN1/2= presenilin 1/2

Rs= receptors

SEM= standard error of the mean

sAPP= secreted amyloid precursor protein

SST= somatostatin

TBS-T= Tris Buffer Saline containing Triton-X

VGlut1= vesicular glutamate transporter 1

VIP= vasoactive intestinal peptide

Impact Statement

This study, through a top-to-bottom approach, tracked the physiological changes that accompanied cognitive impairment and indicators of anxiety in the $App^{NL\text{-}F/NL\text{-}F}$ preclinical mouse model of Alzheimer's disease and highlighted that three major inhibitory interneurone sub-classes which express calretinin, cholecystokinin and somatostatin, respectively, were differentially affected in disease, and also expressed α5-subunit-containing $GABA_A$ receptors important in learning and memory. Pathological changes reported include Aβ accummulation and an increase in neuroinflammatory markers as evidence by astrocytosis and microgliosis.

Firstly, the behavioural experiments in this study formed the basis for an on-going study in the research group, which utilises a novel mouse model, the $App^{NL\text{-}F/NL\text{-}F}$ crossed with a tau model that aims to further recapitulate AD pathology. This continuity indicates the impact of the study for the researchers in the same research group.

Secondly, the results reported are extremely important, as they help understand the pathology of AD and enrich the knowledge of the field with regards to therapeutic avenues. For example, research from this thesis was part of a publication (Petrache et al. 2020) which indicated that perhaps α5-subunit-containing $GABA_A$ receptors were not pertinent as a therapeutic target for AD, as it had been previously thought.

Thirdly, neuroinflammation, altered neuronal density, anxiety and impaired

cognition are characteristic not only of AD, but of other neurodegenerative diseases as well, meaning that work from this study has the potential to impact other fields of research beyond the field of AD.

Chapter 1

Introduction

1.1 Alzheimer's disease in the context of dementia

"Dementia" is a term used to describe a plethora of neurodegenerative diseases which result in progressive cognitive decline. It is estimated that it affects 1 in 14 people over the age of 65 in the UK (Prince et al.2014), costing the global economy $818 billion yearly (Prince et al. 2015). Alzheimer's Disease (AD) is the most common type of dementia, accounting for 60% of all cases (Blennow, Leon, and Zetterberg 2006).

AD is characterised by gradual memory loss and cognitive decline (Serrano-Pozo et al. 2011). Some of the first noticeable symptoms can be the loss of smell and an inability to form and recall memories, which later expands to loss of intellectual functions. In the late stages of the disease, patients are unable to perform simple daily tasks independently. The condition worsens progressively and ultimately leads to death.

1.2 Alzheimer's disease symptomatology

1.2.1 Memory loss and cognitive decline

A typical, well-known symptom of AD is losing the ability to form or recall memories. This is reflected in alterations of two main types of memory: working memory and reference memory. The former refers to a form of short-term memory and defines the ability to create memories and access them for a brief period as it is required on the spot. The latter is long-term memory, recalling events and facts that took place some time ago. Let us take the example of a doctoral student sitting their *viva*. Their working memory will help them recall questions asked of them in the *viva* and build a defence based on the current discussion, while reference memory will serve them to remember the methodology for a certain experiment they performed several years before and when exactly the experiment was performed.

Along with memory disturbances, patients suffer from speech difficulty. This is due to their semantic memory being affected. Semantic memory gives rise to abilities such as language and verbal fluency- for example, naming items of a category, such as ice-cream flavours, or pronouncing certain words, and loss of proficiency could occur years prior to an AD diagnostic as evidenced in meta-analysis studies (Chan, Salmon, and Pena 2001; Henry, Crawford, and Phillips 2004; Laws et al. 2007). Semantic memory might decrease with age and worsen as the disease progresses. However, a study comparing normal ageing subjects, preclinical AD patients and AD patients over the course of two years, found that dysfunction occurred at similar rates in the latter two and was significantly worse compared to the former (Clark et al. 2009).

This type of memory suffers in AD because of the disruption that occurs in brain regions such as the hippocampus. The hippocampus cements short-term memories into long-term and is one of the first areas of the brain to be affected in AD, together with the entorhinal and the association cortices. The functions of the hippocampus and entorhinal cortex and their fate in AD will be discussed more in detail in sections 1.6 and 1.8.

1.2.2 Anxiety and depression

Anxiety and depression are symptoms widely present in dementia patients. They may often be disregarded or overlooked in the face of more alarming symptoms such as cognitive dysfunction, but they should be placed at the forefront of therapy. The issues of anxiety and depression among AD patients are not uncommon. To highlight, 40%-50% of them encounter these issues, compared to 7% in the general population (Nelson 2021), and in some studies, the number of patients with such symptoms go as far as 75% (Kaiser et al. 2014). Interestingly, the incidence of anxiety symptoms varies even among the two different types of AD, which are early onset familial AD and late onset AD- both discussed in section

These symptoms, accompanied by lack of sleep, can have serious repercussion on the disease itself and could cause it to worsen. Seeing as there is no cure for AD and treatments are focusing on alleviating symptoms, targeting anxiety and depression would greatly improve the life quality of AD patients. First-line treatments for anxiety usually include the use of selective serotonin reuptake inhibitors (SSRIs), such as Prozac or Zoloft, but these treatments usually come with non-negligible side effects which can affect daily wellbeing and which include diarrhoea, constipation, loss of weight or even an increase in agitation (NHS 2021) .

Formerly, benzodiazepines were the course of action for anti-anxiety therapy.

However, there is a long history of addiction to benzodiazepines and the need for increases in dosage. Moreover, they also trigger side effects such as vomiting or diarrhoea or even memory impairment and confusion (Tamblyn et al. 2005), especially in the elderly- which is why now clinicias tend to avoid prescribing benzodiazepines in the older age groups of AD patients (AmGerSoc 2015).

1.3 Genetics of Alzheimer's disease

Although a precise diagnostic of AD can only be confirmed post-mortem, and the majority of AD cases are not inherited, there are certain factors that affect the risk of developing the disease, and they will be discussed below, as well as the genetics of different types of AD.

There are two forms of AD and both are characterised by intra- and extra-cellular aggregates of abnormal Aβ deposits and tau tangles, both of which destabilise neurons and the brain environment. There are no diagnosis markers for AD and the most definitive diagnostic is given post-mortem, upon identification of the abnormal types of protein deposits (Serrano-Pozo et al. 2011). The two forms of AD are classed based on genetics: familial AD has a heavy genetic component and is inherited, while sporadic AD is not inherited and cannot be clearly identified through genetics, although there are certain factors that increase the risk of developing the disease.

1.3.1 Familial AD

Familial AD (fAD) has been associated with mutations in three genes: the amyloid precursor protein (*APP*) gene and presenilin (*PSEN*)-1 and -2 genes, and has an autosomal dominant inheritance pattern (Campion et al. 1999). There are three mutations that have been identified in the *APP* gene, that lead to various levels of

disease severity, and several mutations in the *PSEN* genes, and a person can inherit multiple mutations. Depending on the genetic makeup, the severity of the disease varies between individuals. A striking difference between the sporadic and the familial forms of AD is the onset of the pathology. While sporadic AD appears late in life, the inherited form has an early onset, with symptoms appearing before or around 50 years of age. For example, the "Iberian" mutation in the *App* sequence was first identified in an individual who died of the disease at 33 years of age (Guerreiro et al. 2010). Relatives from his family tree that also had the disease died before 40 years of age.

Mutations in both the *APP* and the *PSEN* genes are implicated in defective cleavage of APP. Alterations in *APP* affect the protease complex that cleaves the gene product into smaller constructs. There are three protease enzymes: alpha, beta and gamma. Pathogenic mutations affect the latter two and result in APP being cleaved into longer products. Normal Aβ polypeptides are 35-38 amino acids in length, however, pathological forms are 40-42 amino acids long and the longer the product the more severe the pathology caused. Mutations in *PSEN*-1 and -2 also code for components of γ-secretase and affect APP cleavage (Li et al. 2016).

1.3.2 Sporadic AD

Sporadic or late-onset AD accounts for over 90% of AD cases and in Europe and the USA it affects 40% of people that are 85 or older (Hort et al. 2010). This form of AD is not associated with a particular genetic makeup, like familial AD. However, there are factors, some genetic, that increase the risk of developing the disease. One of these factors is being a carrier of the apolipoprotein (*APOE*) ε4 allele (Corder et al. 1993). APOE is involved in cholesterol metabolism, which is linked to APP cleavage. Mutations in the *APP* or *PSEN* genes are also associated

with a higher risk of developing late-onset AD (Qiu, Ronchi, and Fratiglioni 2007; Bekris et al. 2010), as does being a female, having a history of vascular disease, being a smoker, suffering trauma or lacking higher education (Launer et al. 1999). As most of AD cases occur in the elderly, the main risk factor is ultimately old age. The incidence of the disease increases progressively from 1% in the population aged 60-70 years, to over 6% in people aged 85 or over (Mayeux and Stern 2012).

The possible involvement of *APOE* in AD was first identified from linkage studies, which showed that the $\varepsilon 4$ allele followed the same segregation pathway as the disease. Furthermore, the same study analysed cerebrospinal fluid from patients and reported high-affinity binding between *APOE* and Aβ (Saunders et al. 1993). *APOE* was shown to be present in Aβ plaques in AD and other diseases that show amyloidosis (Namba et al. 1991).

The genetic and stochastic triggers of AD give rise to pathology that can be identified by characteristic markers. The pathological hallmarks of AD, namely Aβ accumulation, neurodegeneration (a loss of neurons and neuronal connections), abnormal activity identified in certain neuronal circuits, and increased toxicity of glial inflammatory cells, will be introduced in the next section.

1.4 Pathological hallmarks of Alzheimer's disease

Typical AD symptomatology reflects profound physiological changes. This study investigated established physiological hallmarks of AD, such as Aβ accumulation, neurodegeneration and neuroinflammation. There are other noticeable physiological changes, such as the intracellular accumulation of tau tangles, which has not been investigated presently due to its absence from the pathology exhibited by the animal model utilised in this study. However, it will be introduced, for a

better grounding of the disease and the implications of the research carried out.

1.4.1 Amyloid-β

A decrease in the number of neurones has long been considered a hallmark of AD, however, the focus has broadened and now an important hallmark is the neuronal dysfunction of signalling pathways, rather than just the number of neurones in itself. This dysfunction affects synapse formation and brain circuits (Palop, Chin, and Mucke 2006) and in AD its main triggers are abnormal protein aggregates Aβ and tau tangles. As discovered by Hardy and Higgins in 1992, Aβ is cleaved from APP and forms oligomers which are found mainly extracellularly (Hardy and Higgins 1992). Tau is a microtubule-associated protein found widely throughout the central nervous system. In AD, tau targets neurons by forming intracellular tangles (Weingarten et al. 1975; Binder, Frankfurter, and Rebhun 1985; Ittner and Gotz 2010). The central dogma of the field, the "amyloid cascade hypothesis" states that AD pathology is triggered by Aβ deposits that arise from processing of APP fragments via the pathological lysosomal pathway, as opposed to the secretase pathway. This results in plaque-forming residues that, through disruption of calcium homeostasis, trigger hyperphosphorylation of the microtubule associated protein tau, cell death and vascular damage. The toxic tau tangles, in turn, promote Aβ toxicity (Maccioni et al. 2018; Wu et al. 2016).

The peptide Aβ is 38-43 amino acids in length and it is produced via the amyloidogenic pathway by enzymatic β- and γ-secretase activity, from APP (Sinha and Lieberburg 1999). APP can also be cleaved via a non-amyloidogenic pathway, whereby α- and not β-secretase represents the first step in the cleavage process. The reason this latter pathway is non-amyloidogenic, meaning that it doesn't cause pathological amyloid aggregates, is that the cleavage site for α-secretase is found within the Aβ sequence, not outside, as for β-secretase

cleavage. This stops the production of pathological fragments. The fragment produced this way is called secreted APP (sAPP). After α- and β-secretase action, carboxyterminal fragments CTF83 and CTF99, respectively, are produced. They undergo γ-secretase activity, which produces P3 and Aβ, respectively, and the amino-terminal APP intracellular domain (AICD) (Chen et al. 2017). Figure 1.1 shows a simplified diagram of the two different APP-processing pathways. Due to its relevance to AD and to the current study, the pathological pathway will be further presented in more detail. There has been no clear role identified for the P3 APP-derived fragment produced via the non-amyloidogenic pathway. sAPPα, produced after α-secretase cleavage, has been found to be protective for neurones. *In vitro* studies show that sAPPα protects against excitotoxicity by stabilising the resting membrane potential by blocking Ca^{2+} currents and increasing K^{+} currents (Mattson et al. 1993), and that it also promotes synapse formation (Gakhar-Koppole et al. 2008). *In vivo* studies reported improvement in memory and learning in rodents upon intracerebroventricular injection of sAPPα (Meziane et al. 1998). The mechanisms of action are not entirely known, and some *in vivo* reports contradict *in vitro* findings, as they found that sAPPα increases long-term potentiation (LTP) and the activity of N-methyl-D-aspartate (NMDA) receptors (Taylor et al. 2008)- different from the reports highlighting a dampening of potassium currents and calcium currents.

In the brain, β-secretase activity is mainly mediated by beta-site APP cleaving enzyme 1 (BACE1) (Vassar 1999). The next enzyme in the amyloidogenic APP processing pathway, γ-secretase, is made of four protein domains: one of presenilins 1 or 2, nicastrin, presenilin enhancer 2 and anterior pharynx defective 1 (Wolfe 2008). sAPPβ, on the other hand, the APP product that results from APP cleavage by β-secretase, does not confer neuroprotection like sAPPα, and has been reported to be involved in synapse pruning and neuronal death by activating

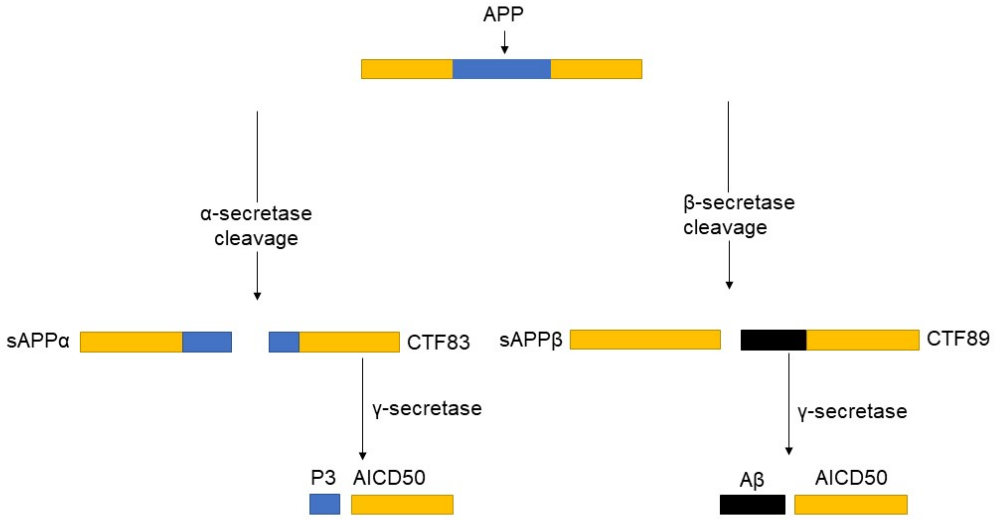

Figure 1.1: Schematic diagram of APP cleavage. APP= amyloid precursor protein, sAPP= secreted APP, CTF= carbon-terminal fragment, AICD= amyloid precursor protein intracellular domain.

caspase-6 which targets the axon (Nikolaev et al. 2009). BACE1 is mainly located in the trans-Golgi network and the endosomes (Huse et al. 2002). From here, it is transported to the plasma membrane via vesicle trafficking and recycled. Hence, the APP cleavage by BACE1 rarely happens at the plasma membrane, but mostly in the endocytic vesicles and trans-Golgi network. The APP fragment thus produced is eliminated out of the cell by exocitosis. However, even though its main forms are extracellular, intracellular Aβ has also been reported in both human AD patients and mouse models of the disease (Gómez-Ramos and Asunción Morán 2007; Petrache et al. 2019). Other forms of proteases with β-secretase activity include cathepsins (Klein, Felsenstein, and Brenneman 2008). After cleavage by β-secretase, CTF99 usually, or CTF89, are produced. There is no known role for them. They are cleaved by γ-secretase, which results in Aβ 1-40/42.

The full biological effects of APP and the fragments that arise from its enzymatic

processing are still unknown. However, the main hypothesis is that it causes disruption of excitatory, NMDA-mediated synaptic function, reduction of synapse number and loss of neuritic spines (Selkoe 2002).

It is clear that targeting Aβ processing would have therapeutical benefits, potentially by inhibiting BACE1 activity, but caution is required, so as not to disrupt healthy biological processes. It has been shown that mice homozygous for a BACE1 deletion ($BACE^{-}/^{-}$) show severe reduction in myelination of peripheral nerves (Willem et al.2006), higher seizure rates which increase even more when they are crossed with the AD model PDAPP (Kobayashi et al. 2008) , morphological changes in pyramidal neurones in the hippocampus and cognitive deficits (Savonenko et al. 2008). This could be due to the involvement of BACE1 in the processing of other biological entities apart from Aβ (Hunt and Turner 2009). Similarly, inhibiting γ-secretase or *PSEN-1* activity has been shown to lead to neurodegeneration or cognitive deficits in animal models of AD (Tabuchi et al. 2009).

What is the role of native APP? It isn't clear, although it seems that it could be involved in brain and body development, as mice lacking APP were reported to show reduced body and brain sizes, as well as neurological disruptions (Ring et al. 2007). In this thesis, an APP knock-in mouse line was utilised to model AD. The levels of Aβ were investigated and correlated with other markers, such as neurodegeneration or the presence of pro-inflammatory glial cells astrocytes and microglia.

1.4.2 Neurodegeneration

Like all neurodegenerative diseases, AD is characterised by progressive loss of neurons and neuronal connections (Przedborski, Vila, and Jackson-Lewis 2003).

Loss of synapses is present early in the disease stage, and it has been postulated that it starts in the entorhinal cortex (EC). A way of assessing neurodegeneration is by counting the anatomical density of cells. In the current study, the main excitatory units in the mammalian brain, pyramidal cells, were counted, as well as certain types of inhibitory interneurones. Notably, neurodegeneration has not yet been characterised in the $App^{NL-F/NL-F}$ mouse model used in the current study, therefore one of the focal points was to investigate this aspect and report on its extent. To do so, brain tissue was stained with antibodies to $Ca^{2}+$ /calmodulin-dependent protein kinase II-α (CaMKII-α), a marker for pyramidal cells and important in memory formation. Furthermore, the levels and organisation of the vesicular glutamate transporter 1 (VGluT1) and gamma-aminobutyric acid (GABA) transporter 1 (GAT1) were also investigated in the entorhinal cortex and CA1 region of the hippocampus, so as to assess the integrity of excitatory and inhibitory connections. Glutamate and GABA are important neurotransmitters in the cortex and hippocampus, being utilised in learning and memory formation, and long-term potentiation- the consolidation of synapses (McEntee and Crook 1993), therefore disruption of these pathways could indicate cognitive deficits (Greenamyre et al. 1987).

1.4.3 Proinflammatory glial cells

1.4.3.1 AD triggers pathological changes in glial cells

More and more studies show that AD pathology does not affect only neurons, but also components of the brain immune system, and that the disease triggers a chronic inflammatory response, which in turn plays an active part in perpetuating disease progression (Eikelenboom et al. 2002; Streit 2004; Maccioni et al. 2018).

Inflammation plays an active role in AD. It is triggered by pathology such as Aβ

deposits and it facilitates the further exacerbation of pathology. The toxic inflammatory pathways are evidenced by increased toxicity of the glial cells astrocytes and microglia. These are cells of the brain immune and support system and in a healthy individual they fulfill protective roles. The toxic inflammatory pathways are triggered under the form of activated microglia (Maccioni et al. 2018) and astrocytes (Liddelow and Barres 2017).

Alongside tangles and plaques, neuroinflammation also plays a key role in shaping hippocampal vulnerability. Previously overlooked in dementia research, neuroinflammatory factors have gained more focus recently. These include an increase in the density of glial cells such as astrocytes and microglia and a change in their secretory profile, from protective and anti-inflammatory to acute and pro-inflammatory. This triggers a cascade of changes at both the molecular level and at higher, macro levels, both of which alter the healthy brain homeostasis to promote pathology. Among the effects are impaired Aβ processing, a harmful increase in the level of cytokines such as tumour necrosis factor (TNF)-α (Baier et al. 2009) and glutamate excitotoxicity due to failure to reuptake excess neurotransmitter from the synaptic cleft (Semmler et al. 2012), to name a few, causing dysfunction of neuronal networks and memory impairment (Bartsch 2012).

Studies in both humans and rodents show that neuroinflammation is elevated in AD brain tissue compared to brain tissue from healthy age-matched subjects (reviewed in Lee et al. 2010). Analysis of gene regulatory networks in post-mortem samples from 1647 late-onset AD patients and healthy subjects revealed that the immune system is the molecular system most implicated in late-onset AD pathology (Zhang et al. 2013).

What causes the involvement of immunological mechanisms in AD pathology? It is

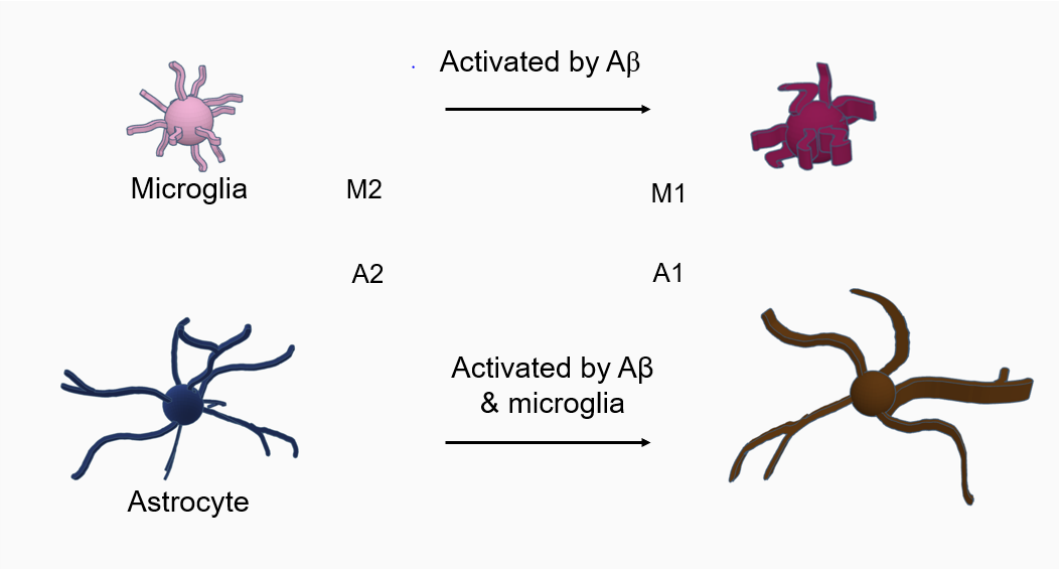

Figure 1.2: Glial cell activation. M2 and A2 are protective states for microglia and astrocytes, respectively, while M1 and A1 indicate reactive microglia and astrocytes.

hypothesised that toxic Aβ oligomers trigger inflammatory responses by employing microglia and astrocytes. Although inflammation is a healthy response to injury and it normally helps to clear cellular residues, in AD it becomes toxic, as glial cells fail to clear abnormal protein deposits, promote their aggregation and secrete proinflammatory molecules such as reactive oxygen species or cytokines (Tuppo and Arias 2005). Both astrocytes and microglia are glial cells which are involved in neurone network support, homeostasis maintenance and the brain immune system and their more specific roles are discussed below. Figure 1.2 shows a simplified representation of microglia and astrocytes switching from a protective state (M2 and A2, respectively) to a pro-inflammatory one (M1, A1) after "activation" by Aβ-driven pathology or indeed activation of astrocytes by microglia. These states are further discussed in the sections below.

1.4.3.2 Astrocytes in AD

As their name suggests, astrocytes are stellate-shaped cells with processes extending from the soma. The ends of the processes contact neurons and capillar vessels. Astrocytes are heavily involved in maintaining healthy neuronal networks and play a key part in the ”tripartite synapse”, whereby astrocytic processes wrap around the presynaptic and postsynaptic components and contribute to regulating neurotransmitter availability at the synaptic cleft (Araque et al. 1999).

When activated by cytokines from neuroinflammatory microglia, astrocytes switch from a neuro-protective state to a toxic state termed “A1” in which pro-inflammatory genes are upregulated and killing of neurons and oligodendrocytes takes place (Liddelow and Barres 2017). It has been suggested that, due to upregulation of key components of the pro-inflammatory complement system, A1 astrocytes are damaging to synapses. In contrast, astrocytes that are protective and promote neurotrophic factors are termed “A2”. Interestingly, in the Csf1r-/- mouse model that is microglia-deficient, A1 astrocytes could not be triggered, suggesting that reactive microglia are required to trigger that phenotype (Liddelow and Barres 2017), which helps pinpoint the specialist roles of glial cells. When they are found in the proximity of Aβ plaques, astrocytes secrete pro-inflammatory factors and they also collect Aβ. In pathology, they can lyse, expulsing the Aβ fragments and giving rise to more Aβ plaques (Nagele et al. 2003). Astrocytes are also vital components of the blood-brain barrier and when malfunctioning they can endanger its integrity.

What characterises astrocyte toxicity? Healthy astrocytes contribute to forming excitatory synapses through secretions of compounds such as glypicans (Gpc)-4 and -6 (Allen et al. 2012). The absence of Gpc-4 in mice has been shown to lead to impaired synapse formation and a reduction in the amplitude of hippocampal

excitatory synaptic currents (Allen et al. 2012), which could suggest that healthy astrocytes in the hippocampus are important in memory formation. Studies on synaptic preservation in retinal ganglionic cells (RGC) co-cultured with either A1 astrocytes or resting astrocytes show a significant 50% decrease in synapse number in the former compared to the latter, a number which was similar to the synapse formation in RGC cultured in the absence of astrocytes (Allen et al. 2012). In human AD patients, *in situ* hybridisation and immunohistochemistry studies in the central nervous system (CNS) using staining for glial acidic fibrillary protein (GFAP) show that almost 60% of all the astrocytes stained were expressing complement component 3, which is only expressed by toxic A1 astrocytes (Liddelow and Barres 2017). This suggests that the majority of astrocytes in AD are A1, toxic, and play a driving role in pathology progression.

1.4.3.3 Microglia in AD

Normal-functioning microglia fulfil the role of the brain resident phagocytes and clear out cellular debris to maintain neuronal health. They are the first glial cells to reach the brain and differentiate around the time that neurons are born, thus having the first chance to be involved in brain development (Li and Barres 2017).

Healthy microglia normally remove abnormal protein deposits such as Aβ aggregates. However, in a pathological state of neuroinflammation like the one in AD, those neuro-protective clearance mechanisms are impaired and microglia begin to secrete pro-inflammatory factors that exacerbate the pathology (Sarlus and Heneka 2017) - "activated" microglia.

Activated microglia become neurotoxic and dysfunctional, furthering the course of the disease in two ways: firstly, by being unable to clear Aβ deposits, which continue to accumulate and disrupt synapses, and secondly, by secreting toxic

inflammatory factors and failing to provide support to neurones.

Similarly to astrocyte classification, two states of microglia have been described: a pro-inflammatory state termed M1, whereby the cells produce pro-inflammatory factors such as cytokines and nitric oxide, and an anti-inflammatory M2 state during which microglia secrete anti-inflammatory compounds such as interleukin (IL)-4 or IL-13 (Gordon 2003). Until recently, it was thought that microglia could only be found in one or the other of the two opposing states. However, analysis of transcriptome data from models of neurodegenerative diseases shows that microglia can exhibit both states at the same time (Wes et al. 2015), which further contributes to disease complexity.

A certain involvement of the immune system is expected in disease. Even so, in AD, the microglial response is escalated from acute, which is a short-term activation of cytokine cascades that would normally lead to phagocytosis and clearance of Aβ, to chronic, whence the neuroprotective capacities of microglia are overwhelmed by the sustained neurotoxicity of heavy cytokine production which impairs microglial phagocytic functions (Bo et al. 1995). Such chronically-activated microglia undergo modification of their cytoplasm, which becomes denser and darker, and were found to contribute to synaptic damage in an APP/PS1 mouse model of AD (Bisht et al. 2016). Moreover, there is evidence that activated microglia can also affect the function of surrounding astrocytes, which, in turn, can lead to death of neurones (Liddelow and Barres 2017).

To sum up, there is strong evidence that microglia and astrocytes do more than just provide support for neurones and they can influence pathological progression of AD. The evidence presented above illustrates the mechanistic contribution to AD of these neuroinflammatory markers, from promoting the spread of Aβ to driving pathology such as synaptic disruption.

1.4.4 Abnormal hyperactivity

A dominant hypothesis in the field of AD is that Aβ deposits cause loss of neurons and synapses, which is what causes the cognitive impairment characteristic of the disease (Selkoe 2002). However, recent evidence suggests that this is not the whole extent of the disease. Human studies performed using patients with a genetic predisposition to AD show an abnormally heightened hippocampal activity (Bookheimer et al. 2000; Dennis et al. 2009; Bakker et al. 2012), suggesting a shift in the balance between synaptic excitation and inhibition. These findings were also replicated in mouse models of AD such as APP23X45 (Busche et al. 2012), $^{AppNL-F/NL-F}$ (Petrache et al. 2019). In the APP23X45 model, both hyperactivity and silencing of neurones was observed in cortical and hippocampal neurones (Busche and Konnerth 2016). Notably, a 16-fold increase in hyperactive neurones was reported compared to a 3-fold increase in silenced neurones, and both populations increased as the disease progressed. However, while the silenced neurones were evenly distributed throughout cortical regions, the hyperactive cells were notably found in proximity to the Aβ deposits (Busche et al. 2012). The observed hyperactivity was reported to have a synaptic nature, as an effect of reduced inhibition on the hyperactive neurones, resulting from reduced GABA input. This suggest that Aβ deposits affect the excitatory-inhibitory synaptic imbalance, and raises the plausible hypothesis that hyperactive neurones are a mark of AD themselves (Busche and Konnerth 2016), impair GABA inhibition and therefore points to a potential involvement of GABAergic inhibitory interneurones in pathological hyperactivity, as they control and fine-tune principal neurons and also form connections with each other.

Hyperactive neurons in AD include principal pyramidal cells, the major excitatory cells in cortical regions. Studies show that hyperactive pyramidal cells are found

around the sites of Aβ deposits, supporting the hypothesis that those aggregates might be contributing to the abnormally elevated activity of principal cells (Ovsepian et al. 2016). Interestingly, the hyperactivity of pyramidal interneurones in layer 5 of the cortex was reduced in a mouse model of amyotrophic lateral sclerosis (ALS) and frontotemporal dementia (FTD) by treatment with picrotoxin, which blocks $GABA_A$ receptors (Zhang et al. 2016). Moreover, inhibitory SST interneurones were also reported to be hyperactive in the ALS and FTD mouse model starting from 3 weeks of age and continuing throughout adulthood, which leads to the hypothesis that GABAergic SST cells may be disinhibited themselves or disinhibit pyramidal cells by inhibiting other populations of interneurones that control pyramidal cells (Zhang et al. 2016).

SST cell hyperactivity as well as reduced GABAergic inhibition on principal cells highlight the importance of inhibitory interneurones and the role they may play in the abnormal excitatory-inhibitory imbalance present in AD. Three major modulatory interneurones, SST-, CCK- and CR-expressing cells, form the focus of this study and are introduced in section 1.10.2. Moreover, studies show that treatment with glutamate receptor antagonists CNQX and APV, and diazepam, a $GABA_A$ receptor modulator reduces hyperexcitation in cortical neurones (Busche et al. 2008; Busche and Konnerth 2016). Hence, a better understanding of the major modulatory inhibitory networks would help understand the underlying mechanisms of hyperactivity in AD and perhaps would highlight novel therapeutic targets.

1.5 Mouse models of Alzheimer's disease

Many murine models of AD have been created with the aim of recapitulating pathology as seen in human patients. The focus has been on producing transgenic

models that exemplify Aβ or tau accumulation, or that carry a mutation in one of the presenilin genes or a risk variant of apolipoprotein (APOE) (reviewed in (Hall and Roberson 2012)). When it comes to investigating the amyloid hypothesis and modeling Aβ, animal models have largely been based on overexpression of APP, which is problematic as that causes overproduction not only of the Aβ fragments characteristic of AD, but also of other fragments that are not normally overproduced in human AD (Saito et al. 2014). Moreover, they do not use an endogenous promoter to express APP, therefore the transgene might not be expressed in the correct places.

1.5.1 First-generation models

The first wave of AD murine models was largely comprised of transgenic animals where the sequence of proteins linked to AD pathology were overexpressed. For example, models overexpressing APP or PSEN 1 or 2.

In terms of AD pathology, first generation animal models exhibit characteristics of the disease, such as Aβ accumulation. However, as mentioned, they also give rise to "by-product" additional pathology, which is not found in human patients. It is unknown how these additional phenotypes could affect the progress and intensity of the disease, hence the reasoning behind eliminating them and creating models that more faithfully recapitulate the human symptomatology and disease physiology.

Such single or double transgenic models were comprehensively reviewed by Sasaguri and colleagues (Sasaguri et al. 2017). Single transgenic models such as PDAPP or APP23 show arbitrary integration of the transgene and the overexpression of APP fragments (such as the AICD fragment) that are not overproduced in human AD. Sometimes, the animals die unexpectedly and unexplainably and, in the case of the TgCRND8 model, the cognitive impairment

characteristic of the disease predates the accumulation of Aβ.

When one talks about a reasonably good research model one should mention the feasibility of the genetic crosses. Indeed, for some of those strains, the background is too complex and there are multiple mutations that need to be managed. Such is the case of double transgenic mice that overexpress APP and PSEN, or even triple transgenic mice such as 3xTg-AD with mutations affecting the APP, PSEN and Tau genes. This makes breeding difficult from a logistical point of view, which can delay or impede research and which might introduce breeding errors (Sasaguri et al. 2017).

However, in spite of the limitations of these animal models, a wealthy body of research is based on them and they also represent the foundation on which new models can be based on and improved. These models allow for characterisation of Aβ and tau pathology and of analysis of cognitive functions.

1.5.2 Second generation models: the knock-in *App*$^{NL\text{-}F/NL\text{-}F}$

To bypass some of these problems, in this study we used a humanised knock-in mouse model that harbours two mutations of the *APP* gene identified in human patients: the Swedish (APP KM670/671NL) and Iberian (APP I716F) mutation, together with the mouse APP promoter (Saito et al. 2014). The model has the identifier *App*$^{NL\text{-}F/NL\text{-}F}$. In this model, APP is produced at wild-type levels. The Swedish mutation substitutes the amino acids lysine and methonine for asparagine and leucine, thus affecting the β-secretase site. This leads to the production of elevated levels of pathogenic Aβ40 and Aβ42 (Scheuner et al. 1996). The Iberian mutation results in the substitution of isoleucine to phenylalanine, which increases the ratio of Aβ42 to Aβ40 (Herl et al. 2009), the latter being the more pathogenic Aβ species.

Aside from the characteristic Aβ plaques, the *App*$^{NL\text{-}F/NL\text{-}F}$ model displays other pathological hallmarks of AD. It presents with neuroinflammation as shown by increased microgliosis and astrocytosis (Saito et al. 2014; Petrache et al. 2019), and loss of the number of pyramidal cells in the EC and hippocampus of aged animals, compared to healthy whild-type counterparts (Petrache et al. 2019), as well as disrupted synaptic function, which was apparent from a pronounced loss of immunoreactivity to synaptophysisn and post-synaptic density (PSD) 95.

It is important to note that this model does not, as a rule, exhibit neurofibrillary tau tangles, although stochastic phosphorylated tau has been observed after 24 months of age (Saido 2021, personal communication to Alzforum). Far from being discouraging, the lack of tau pathology in the model enables for a better disentangling and investigation of Aβ pathology. Importantly, it shows a pathologically elevated Aβ40/Aβ42 ratio, which is characteristic of the disease.

In terms of temporal and pathological progression of Aβ accumulation, *App*$^{NL\text{-}F/NL\text{-}F}$ closely recapitulates human pathology. Aβ accumulation was first reported by the authors at 6 months of age, and it increased progressively until 24 months (the last time-point tested in the original study).

Ultimately, the *App*$^{NL\text{-}F/NL\text{-}F}$ model was chosen by comparing its strengths and weaknesses against the other models and against the current need for preclinical models required for therapeutic research. Seminal studies have reported memory impairment in these mice from 8 months of age (Masuda et al. 2016) and 18 months of age (Saito et al. 2014), respectively. However, they used different behavioural testing and did not report memory impairment at other ages. Due to the lack of consistent significant memory impairment reporting in this mouse model, it is perhaps better to treat it as a preclinical model of AD when interpreting results. Carrying out further studies to investigate potential cognitive decline is

also important so as to establish a reference frame for therapeutic testing.

1.6 The hippocampus

The hippocampus is a brain structure found in the temporal lobe (Duvernoy, Cattin, and Risold 2013). For mammals, including humans, it is a paired structure, meaning there are two hippocampi, one in each brain hemisphere. It is an allocortical, archicortex structure and it is composed of Cornu Ammonis (CA) regions 1-4, which make up the 'hippocampus proper', and the dentate gyrus (DG) (Tatu and Vuillier, 2014) (Figure 1.3)- which are involved in synaptic circuits with one another. In this thesis, 'hippocampus' refers to the CA1-4 regions. The classification of the hippocampus sometimes includes the subiculum, presubiculum and EC, grouped under the 'hippocampal formation'. These regions have a similar layered construction and are connected, forming circuits with one another. Being part of the archicortex means that the hippocampus is one of the oldest brain structures as well as part of the most basic cortices.

Anatomically, the hippocampus has been compared to a sea horse, due to its S-like shape, and the horns (Cornu) of a ram. The cells of the hippocampus are organised neatly in layers, according to the different sections of the structure. The layers are, from top to bottom: stratum oriens (SO), stratum pyramidale (SP), stratum radiatum (SR) and stratum lacunosum moleculare (SLM) (labelled in Figure 1.4) . The CA3 region also has an intermediate layer, stratum lucidum (SL), between SP and SR. In anatomical slices, the hippocampus can be easily recognised by the densely packed pyramidal cells in SP, which have their axons in a lamellar layer called the alveus.

The hippocampus is part of the limbic system, a group of structures that govern spatial navigation and memory acquisition and recall (Bartsch 2012) and which include the EC. The hippocampus has a long evolutionary record and it is

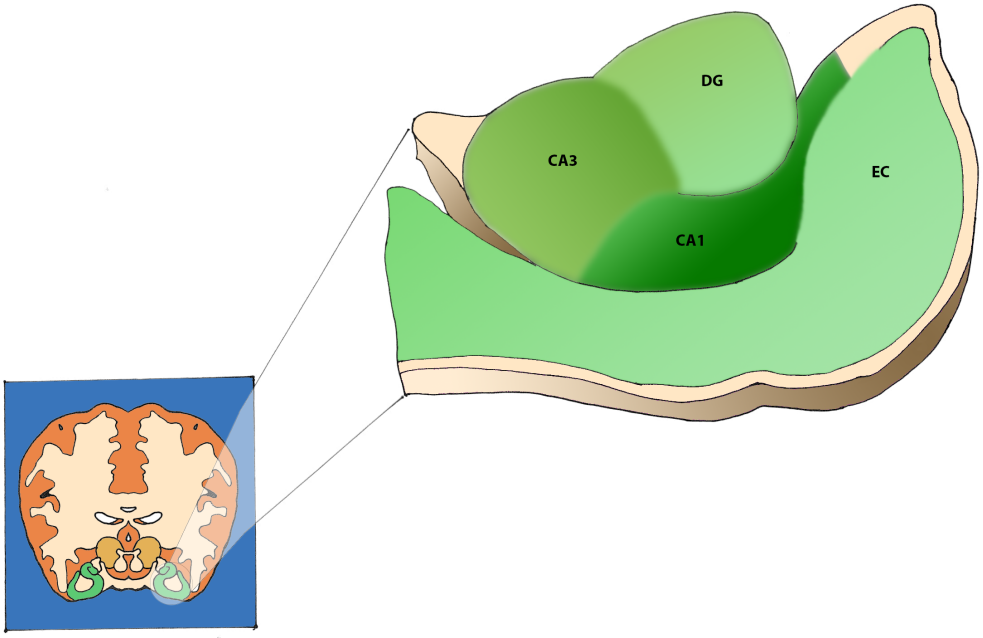

Figure 1.3: Location of the hippocampus formation in the brain. Hand-drawn, processed using Adobe Photoshop CC 2015.

characterised by traits that are preserved across vertebrate species and taxa, such as its connectivity with other brain structures, as well as characteristics that are more unique for different vertebrate groups, particularly the way different cell layers are organised (Bingman and Sharp 2006).

Since the discovery of 'place cells' by O'Keefe and Dostrovsky (O'Keefe and Dostrovsky 1971) and 'grid cells' (Moser, Rowland, and Moser 2015) in rodents, the importance of the hippocampus for spatial memory and navigation has been further cemented. Comparative evolutionary studies show that similar 'cognitive maps', representations of the world that allow the individual to utilise a spatial framework in which to position itself and of which to make use for navigation purposes, exist in other mammals and birds. Moreover, other vertebrates have similar structures to the hippocampus that allow them to navigate the surrounding world. As these structures help the subject remember their position in relation to

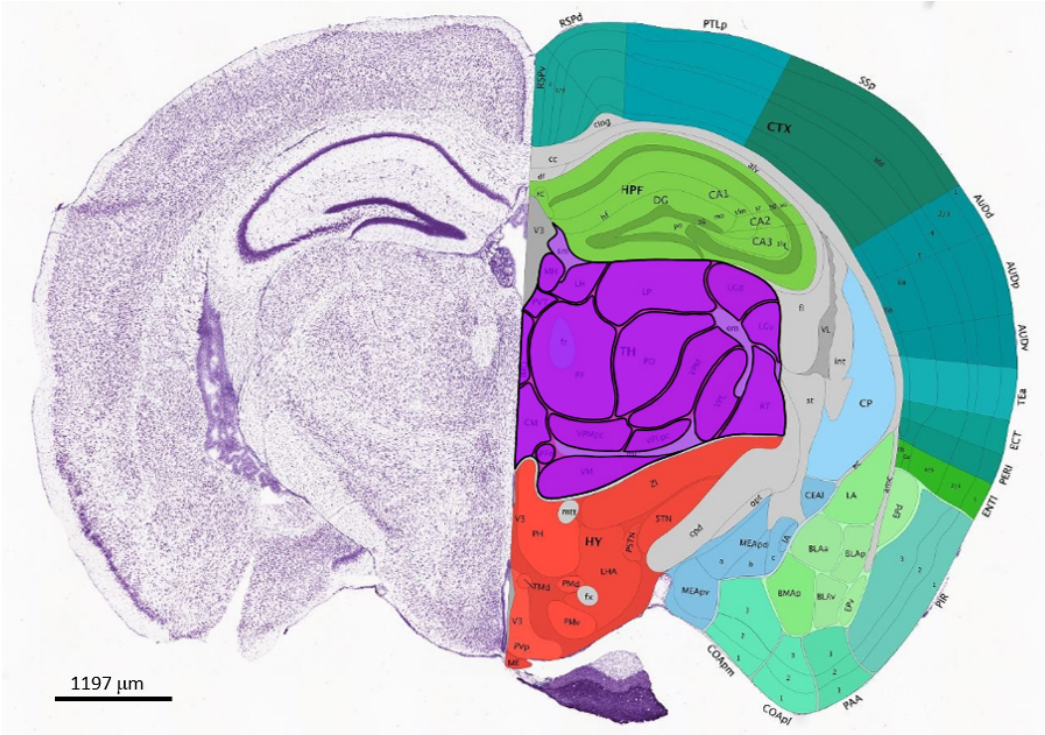

Figure 1.4: Location of the hippocampus in the brain, together with the main regions and layers. Coronal plane. Image credit: Allen Institute. © 2011 Allen Institute for Brain Science. Allen Adult Mouse Brain Atlas. Available from: atlas.brain-map.org. (Allen Institute for Brain Science 2011)

features on a map, the memories so formed are similar to episodic or declarative memories in humans (Clayton and Dickinson 1998). Indeed, the hippocampus is a key structure of great importance in the formation and retrieval of episodic memories.

Episodic memories are a type of 'declarative' memories, a collection of past events that an individual is able to recall at will, such as the duration of their PhD *viva* and the weather on that day. Another type of declarative memory is semantic memory, which refers to an individual's ability to learn and recall facts- for example, recalling that the Battle of Hastings took place in 1066.

The hippocampus receives input to and from various brain structures such as the EC, DG, the subiculum, and it also forms complex local circuits between the CA regions (Figure 1.5). One of those, the perforant pathway, connects the hippocampus with

the EC.

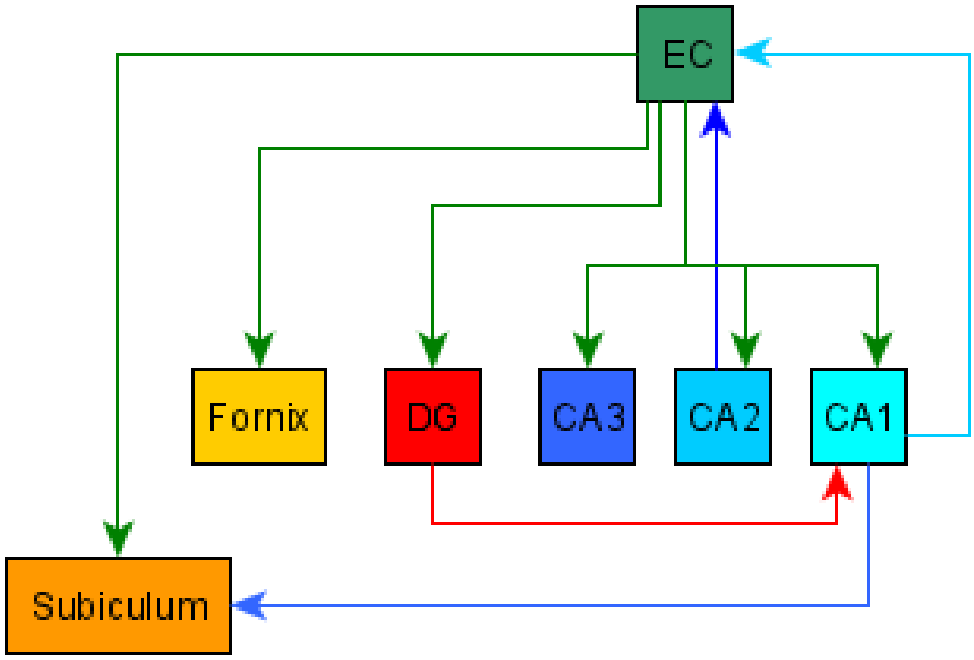

Figure 1.5: Main pathways connecting the hippocampus with other brain regions. EC= entorhinal cortex, DG= dentate gyrus, CA= cornu ammonis.

Long-term potentiation, which defines strengthening of synapses after a high-frequency stimulation and which is thought to be the basis of memory formation, was identified in the hippocampus in 1966 (Andersen, Andersen, and Lomo 1966), while studying the perforant pathway, which connects the hippocampus and the EC. Inputs from layers II and III of the EC arrive in the DG, CA1-3 and the subiculum. Outputs from the CA2 region return to layer II and those from CA1 and subiculum arrive in layers V/VI. The DG, CA1 and CA3 form the 'trisynaptic circuit': granule cells in the DG receive input from the EC via the perforant pathway, then mossy cell fibres from the DG arrive to pyramidal neurons in the CA3, which send Schaffer collaterals to pyramidal neurons in the CA1 (Lisman 1999), see Figure 1.5. The input is further transmitted to the subiculum and fornix. This circuit was first identified by Ramon y Cajal (Ramon-y-Cajal

1909).

1.7 The lateral entorhinal cortex

Much of the input that the hippocampus receives from other regions stems from the EC. Similar to the hippocampus, the EC is found in the medial temporal lobe and is involved in memory formation and spatial navigation, although it is not limited to these functions. Some classifications place the EC in the hippocampal formation.

The EC is extremely important as it is a relay point between the hippocampus and neocortical regions; the main source of excitation to the hippocampus, the perforant pathway, starts in layer II of the EC, while efferent projections from the hippocampus arrive in layer IV (Gomez-Isla et al. 1996). In Alzheimer's disease, both layer II and IV have been shown to be heavily infiltrated by Aβ plaques, and the perforant pathway heavily affected. Such a disruption in the region would rightly affect memory formation and be transmitted to the hippocampus through the connections it makes with the EC, which can, therefore, disrupt not only local circuits in the EC but also input and output to and from the hippocampus.

The EC is divided into lateral (LEC) and medial (MEC). Both communicate with the hippocampus, but their projections show preferential targeting of regions. For example, the MEC connects the proximal CA1, while the LEC connects distal CA1. Similarly, they innervate different parts of the dentate gyrus (DG). This is reflected by the different physiology between the two regions and different characteristics of cells in the respective CA1 region. For example, place cells, which are paramount for spatial orientation -in which both the EC and the hippocampus are involved- behave differently in proximal versus distal CA1 (Hargreaves et al. 2005).

1.8 The hippocampus and entorhinal cortex in Alzheimer's disease

Given its connectivity which links it to various brain structures, it is clear that disruptions in hippocampal function will have wide functional ramifications. In AD, the hippocampus is one of the first regions to be damaged by pathology, after the EC, which results in the progressive memory loss and cognitive decline that are characteristic of the disease. Incidentally, it could be the high degree of plasticity of the hippocampus and EC that makes these regions more vulnerable to damage stemming from AD and ageing (Neill 1995). Both regions are prone to atrophy with age, with atrophy levels ranging between 0.79%-2% (Jack et al. 1998) for the former and 0.3%-2.4% for the latter (Du et al. 2003).

As pathology develops, both the EC and the hippocampus show pronounced Aβ accumulation, as well as neurofibrillary tau tangles. A study carrying out stereological neuronal counting in brain tissue from the entirety of the EC of AD patients reported a 32% decrease in the overall number of neurones compared to cognitively normal subjects (Gomez-Isla et al. 1996). Notably, all affected patients showed mild clinically detectable dementia only, but presented with neurofibrillary tangles and senile plaques characteristic of AD. Layers II and IV of the EC were affected even more drastically, 60% and 40% reductions in neuron number, respectively. In tissue from patients with severe AD, the same two layers showed 90% and 70% reduction in the number of neurons, compared to samples from cognitively normal individuals.

1.9 Neurones of the CA1 and LEC

Complex local and distal circuits control the excitatory-inhibitory balance in the hippocampus. In AD, however, disruptions in those circuits overturn the balance and lead to an abnormal shift between excitation and inhibition.

Inhibition is crucial to maintaining healthy brain functions, as inhibitory interneurones are able to fine-tune the function of excitatory cells, synchronise neuronal populations and generally manage timing and expression of inhibitory outputs onto other cells.

1.9.1 Pyramidal cells

Pyramidal cells are the principal excitatory neurones in the human CNS. They were first identified by the Spanish neuroscientist Ramon y Cajal in 18933 (Cajal 1893). They have a pyramid-shaped soma, with multiple spiny dendrites, both basal and apical. They are large, usually with a diameter between 20-120μm and a length from the end of the basal dendrite to the top of the apical one of 200-1000 μm.

In the hippocampus, the soma of pyramidal cells is arranged in an ordered layer in the SP. Pyramidal cells in the CA1 and CA3 region are responsible for relaying information to and from the EC, DG and further to the subiculum and fornix. Their axons and dendrites branch broadly and they are bipolar cells, with an apical and a basal dendrite. The apical dendrite sometimes branches and gives rise to two apical dendrites that then branch even more extensively. The dendrites are covered in dendritic spines, the number of which has been used to estimate the number of excitatory synapses made on to the pyramidal cell- although some excitatory synapses can be formed between the spines. A typical pyramidal cell has thousands of dendritic spines.

Pyramidal cells receive inputs and outputs from other neurones and participate in retrograde signalling- for example, via the endocannabinoid system. They receive excitatory signals from one another and are fine-tuned by GABAergic interneurones. Inhibitory synapses on pyramidal cells are made on the dendritic shaft and the soma.

Synaptic signals made on pyramidal cells are integrated in a non-linear fashion- meaning that inputs arriving from proximal dendrites do not prevail over those from distal dendrites. Na^{+}, K^{+} and $Ca^{(2+)}$ voltage-gated channels are strewn across the dendrites, which plays a role in altering synaptic input (Stuart and Sakmann 1994).

The phenomenon of synaptic plasticity -changes in the strength of synapses based on the frequency of synaptic activation- is very apparent in pyramidal cells, which have been important in the study of long-term synaptic potentiation or depression, mechanisms that are thought to be important in memory formation (Kampa, Letzkus, and Stuart 2007).

1.9.2 Inhibitory interneurones

Interneurones make up to 20-25% of the total number of cortical neurones and are mostly inhibitory, utilising the neurotransmitter GABA (Whittington and Traub 2003; Wang et al. 2004). They perform modulatory functions, which allows them to alter cortical plasticity. Their population is highly heterogenous. There are various sub-types of interneurones in cortical regions, with at least 23 subtypes in CA1 alone and they are diverse in terms of morphology, physiology, function, or neuropeptide/s expressed (Freund and Buzsaki 1996), characteristics which are used to classify them. It is this heterogeneity that makes interneurones highly specialised and crucial in governing network operations to maintain the inhibitory-excitatory balance. They were first characterised by Ramon y Cajal,

based on the Golgi-staining method that used silver nitrate to mark a neurone, complete with soma and neurites (Cajal 1888). His student, Lorente de Nó, followed suit, working on the classification using the same method.

The wide interneurone diversity in terms of morphology, physiology and functionality could stem from their origins, which differ across different subpopulations of interneurones. In rodents, cortical interneurones originate mainly in the caudal and medial ganglionic eminences. In humans, on the other hand, interneurones of the cortex arise mostly in the cortical subventricular zone. Sonic hedgehog (Shh) signalling and the transcription factor *Nkx2.1* are involved in determining neuronal fate, and there are other factors that coordinate the migration from origin, such as *Dlx1*. This latter factor is normally only expressed during foetal development, but it is maintained postnatally in a subset of interneurones expressing the protein calretinin, which were investigated in this thesis and which are further discussed in section 1.9.2.1.

Interneurones do not exhibit many dendritic spines (they are aspiny in the cortex) and their axons project locally (Wonders and Anderson 2006), hence the name ”short axon neurons” that was given to them by Cajal. They make dendro-dendritic, axo-axonic, axo-dendritic and even axo-somatic connections. They form complex networks and are involved in local and distal circuits, for example the perforant pathway which spans the lateral entorhinal cortex and fields of the hippocampus such as the CA1 region or the subiculum. Interneurones make contact with principal pyramidal cells, both directly, and via disinhibition- by contacting and inhibiting other inhibitory interneurones. An example of the heterogeneity of interneurone function was highlighted by Wang and colleagues, which modeled a microcircuit modulated by different classes of interneurones (Wang et al. 2004). In their example, parvalbumin (PV)-expressing interneurones targeted the perisoma of excitatory pyramidal cells, calbindin (CB)-expressing

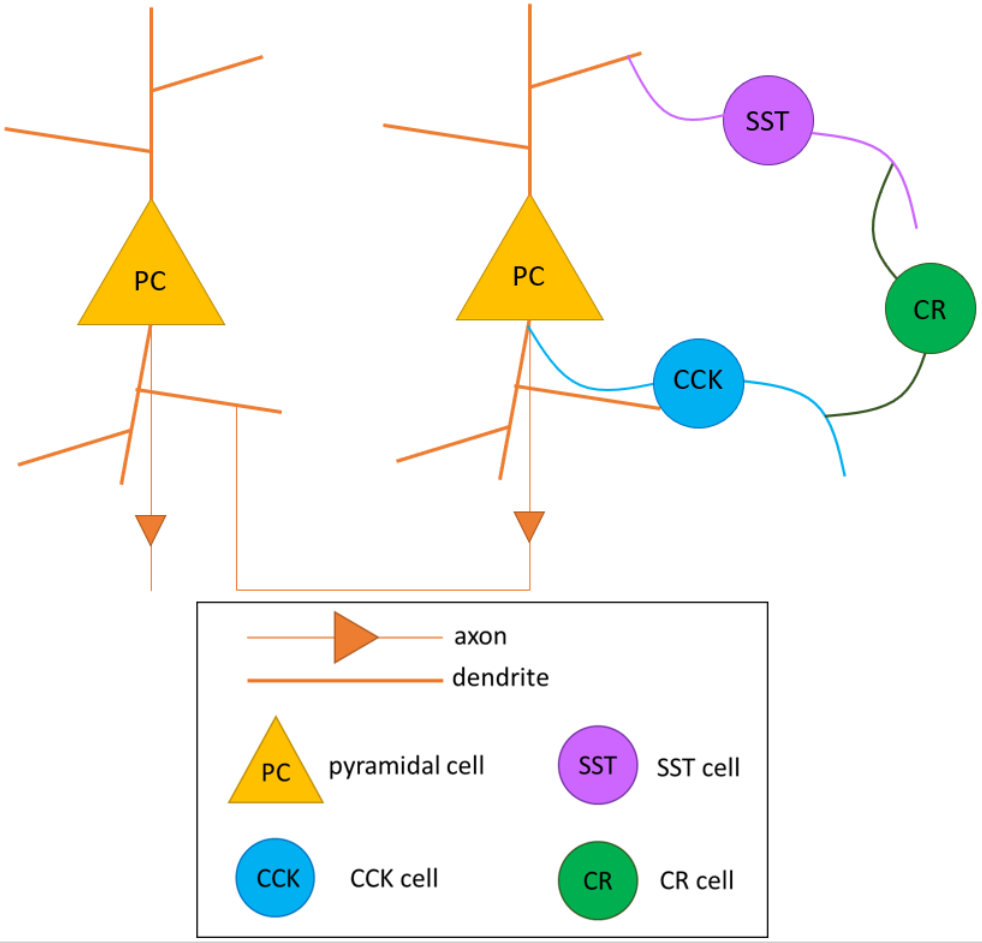

Figure 1.6: Example of a hippocampal microcircuit. CCK= cholecystokinin, CR= calretinin, SST= somatostatin, PC= pyramidal cell.

interneurones targeted their dendrites and CR cells made contact with the CB cells (Figure 1.6).

In fact, CR-expressing cells are interneurone-specific interneurones, as they only make contact with other inhibitory interneurones. They form the focus of the current study alongside another two subclasses of major modulatory inhibitory interneurones that express the neuropeptide somatostatin and the peptide hormone cholecystokinin, respectively. The onus of this study was on the interneurones of the CA1, with some aspects investigated in the LEC as well.

Apart from modulating established circuits, interneurones also aid in neuronal

proliferation during development, through manipulation of the neurotransmitter GABA, which they predominantly utilise. Studies of rat brains show that GABA facilitates neurite growth and that it also helps direct neuronal migration (Wolff, Joo, and Dames 1978). In the EC, cortical interneurones are distributed in layers numbered I to VI.

In short, interneurones are central modulators of neural circuits and involved in maintaining the balance between excitation and inhibition in the healthy brain. Due to this balance being affected in AD (see 1.4.4) and to them playing an important role in the health of cognitive functions, interneurones are increasingly becoming a focal point of AD research.

1.9.2.1 Calretinin-expressing interneurones

CR cells are a type of modulatory inhibitory interneurone that mainly expresses the calcium-binding protein calretinin. Although they were first characterised over two decades ago (Freund and Gulyas 1997), there still is a missing gap in the understanding of these cells.

As opposed to other classes of inhibitory interneurones such as cholecystokinin (CCK)- or somatostatin (SST)- expressing cells, or indeed even pyramidal cells, which show their numbers to be greatly reduced in disease, CR cells maintain their anatomical density in AD. Immunohistochemical studies of post-mortem tissue from AD patients that presented a heavy Aβ burden showed that CR cells are spared in AD, with their density intact throughout the brain and comparable to tissue from healthy subjects (Resibois and Rogers 1992; Hof et al. 1993; Fonseca and Soriano 1995).

CR cells are distributed throughout the entorhinal cortex, hippocampus (all strata), and neocortex and account for 10-30% of GABAergic interneurones (Cauli

et al. 2014). They are specialised in connecting with other interneurones, among which are SST and CCK cells (Cauli et al. 2014). They are usually bipolar cells, but can be multipolar, and can be visualised by staining for the calcium-binding protein calretinin (Freund and Buzsaki 1996).

An interesting characteristic of CR cells is the ability to form connections with other CR cells, a cell being in contact with several others at a time (Freund and Gulyas 1997). These contacts can be dendro-dendritic and axo-dendritic, while contacts with other cell types are dendro-dendritic only. They show a preference for contacting calbindin DK28 cells and vasointestinal peptide-expressing (VIP) cells. They avoid interneurones that express parvalbumin (PV) (Gulyas, Hajos, and Freund 1996). According to gross morphology and spatial distribution, two types of CR cells have been identified: spiny CR cells which are found in parts of the dentate gyrus and the CA3, and aspiny CR cells, which are evenly found in the hippocampus (Gulyas, Hajos, and Freund 1996). Interestingly, CR cells in the strata pyramidale (SP) and radiatum (SR) co-express VIP. These CR/VIP cells have been shown to make synapses on to oriens-lacunosum moleculare (OLM) SST cells, which in turn contact the distal dendrites of pyramidal cells (Freund and Gulyas 1997). This way, CR cells participate in disinhibition, by modulating excitation through the inhibition of SST cells.

Seeing that, as disinhibitory cells, CR interneurones are capable of modulating a variety of circuits and are seemingly unchanged in AD, a plausible hypothesis arises: are CR cells a key player in the excitatory-inhibitory imbalance in AD, and if so what exactly is their role?

1.9.2.2 Cholecystokinin-expressing interneurones

Cholecystokinin is a hormone peptide that regulates nutrient processing, with effects on the digestive tract and associated organs such as stomach, gallbladder and pancreas (Mutt, 1988), and it is synthesised both by endocrine cells in the small intestine and by neurones. CCK sulfated octapeptide (CCK-8S) is the form that is most widely expressed in the CNS and which has neurotransmitter properties (Acosta 2001).

Two CCK receptors have been identified to date, CCK_A and CCK_B. Both are present in the gastric system and the CNS, and show high concentration in the hippocampus - where CCK cells were investigated in this study. CCK is heavily involved in memory functions. In humans, administering the CCK peptide nasally led to an increase in ”familiarity-based recognition memory” compared to placebo (n=64 subjects, Schneider et al. 2008). In addition to CCK receptors and receptors for GABA, CCK cells express a wealth of other receptors, such as muscarinic acetylcholine receptors or the endocannabiniod receptor CB1 (Rio, McBain, and Pelkey 2012), which highlights the role these cells play in retrograde signalling and the regulation of neurotransmission.

In the hippocampus, CCK cells represent one of the two major types of basket cells, named so due to their dendritic branching, the other one being parvalbumin (PV)-expressing cells, with which they make contact (Karson et al. 2009). The somata and dendrites of CCK cells are located in SR, while their axon arborises in SP. They target different segments of pyramidal cells: soma, proximal dendrites and the axon initial segment (Halasy et al. 1996) and by doing this, they are in an excellent position to control perisomatic inhibition and the synchrony of pyramidal cells (Lee et al. 2010), which means they play a vital role coordinating the input and output of neuronal networks.

CCK interneurones are themselves targeted by PV, CR and SST cells, which shows the tight links between different interneurone subtype and circuits and the importance of CCK cells in normal brain functioning (Katona, Acsády, and Freund 1999).

CCK interneurones have slower membrane constants than the other class of basket cells, PV interneurones, and accommodating spike discharges, which makes this particular interneurone subtype more maleable and plastic to modulatory inputs arriving from the other interneurone subpopulations (Freund and Katona 2007). Studies have shown that CCK-8S bath-applied to hippocampal slices from rats led to an increase in the frequency of spontaneous postsynaptic currents in pyramidal cells in the CA1 hippocampal layer, as well as in cells of the dentate gyrus (Miller et al. 1997).

It is known that CCK interneurons are important in memory retrieval, therefore any alteration of their morphology, function or receptor composition is expected to have detrimental effects on cognitive function. CCK cells were optically silenced in mice, which resulted in significantly diminished performance in olfactory working memory in contrast with animals with unaltered background (Nguyen et al. 2020). Other studies showed that CCK knock-out rodents tested with the Morris water maze performed significantly more poorly than wild-type animals (Lo et al. 2008).

In AD, CCK cells have been largely unstudied. However, a study analysing the CSF from patients with AD or mild cognitive impairment (MCI) showed that higher amounts of CCK correlated with a decreased likelihood of developing AD or MCI (Plagman et al. 2019). When MCI was already present, higher volumes of CCK decreased the likelihood of progression to AD.

The CCK peptide also plays a role in anxiety behaviour, as seen from human studies; subjects injected with CCK tetrapeptide experienced significant anxiety

levels and panic attacks (Montigny 1989). Similar findings were identified in animals- rats were exposed to stressful situations and it was noted that the level of CCK peptide increased in the hippocampus, compared to the levels in animals which had not been subjected to stress (Harro et al. 1996). CCK cells also have been shown to postsynaptically contact α2-containing $GABA_A$ receptors (Koester et al. 2013). Moreover, agonists to CCK_B receptors have anxiogenic effects and antagonists to CCK_B receptors have anxiolytic effects, as seen from pharmacological studies (Hughes et al. 1990).

CCK interneurones play a consolidated role in brain circuitry, making contacts with pyramidal cells and with several sub-types of interneurones, as well as with each other, and are also important in memory processing and involved in anxiogenic behaviours, therefore they represented a focal point of this study. Understanding their survivability in the preclinical $App^{NL\text{-}F/NL\text{-}F}$ mouse model of AD would contribute to the understanding of AD pathology.

1.9.2.3 Somatostatin-expressing interneurones

SST OLM cells are GABAergic inhibitory interneurones (Ali and Thomson 1998) and have been the subject of many studies (reviewed in (Urban-Ciecko and Barth 2016)), being well characterised. The population is heterogenous, with SST neurons showing different morphology and electrophysiological properties: irregular spiking, fast-spiking or stuttering (Hu, Cavendish, and Agmon 2013). There are three types of SST cells: multipolar Martinotti cells, bitufted cells and basket cells (Jiang et al. 2015). In the developing mouse brain, hippocampal SST cells arise in the medial ganglionic eminence like all of the other interneurones, then migrate to the hippocampus (Butt et al. 2005).

This study focused on OLM SST cells, which get their name because their soma

is found in the stratum oriens in the CA1, while their axon spans the lacunosum-moleculare strata (Ali and Thomson 1998). Every instance that mentions CA1 SST cells henceforth refers to SST OLM cells.

SST cells in the CA1 form connections with the distal dendrites of PC- which is also the place where PC receive input from the EC (Maccaferri and McBain 1995). It has also been reported that OLM cells inhibit interneurones from the stratum radiatum (SR) in CA1 that form synapses with the dendrites of PC and that they reduce or promote LTP (Leao et al. 2012). All of this evidence suggests that OLM cells have an executive control over information flow in CA1 (Lovett-Barron et al. 2012), which means that any disturbance in their network during AD pathology has a spillover effect and can damage wider networks and information flow.

SST cells have been previously found to be hyperactive in animal models of AD (Busche et al. 2008; Zhang et al. 2016; Shi et al. 2019).In the $App^{NL\text{-}F/NL\text{-}F}$ mouse model of AD used in this study, SST cells have been found to show altered membrane properties from the early stage of 2 months of age, when compared to age-matched wild-type C56BL/6 animals (Shi et al. 2019). Specifically, whole-cell patch clamp recordings show that with increasing current injection steps (+200pA to -200pA), the firing of the interneurones increased, as well as the input resistance of the membrane and the time constant. This was significantly different between the two genotypes.

This pronounced SST cell hyperactivity in AD contributes to the heightened activity of pyramidal cells through disinhibition via cells such as PV interneurones (Zhang et al. 2016), with which SST cells make contact. Interestingly, somatostatin receptors and the peptide somatostatin are depleted in AD (Burgos-Ramos et al. 2008). This might be paradoxical, when one considers the hyperactivity of SST cells. Moreover, somatostatin has also been shown to be

amyloidogenic, one of the neuropeptides that binds to Aβ fragments in vitro, enabling their oligomerisation (Solarski et al. 2018), which cements their role in propagating AD pathology. Notably, SST cells are in close proximity to Aβ deposits in the hippocampus (Schettini 1991). This highlights SST cells as a potentially fundamental player in hippocampal AD pathology.

1.10 Gamma-aminobutyric acid

1.10.1 Overview and GABA receptors

GABA is the main inhibitory neurotransmitter in the cerebral cortex (Schwartz 1988) and GABAergic transmission plays an important role in all of the major brain functions. Dysfunction of this pathway leads to abnormal brain activity such as epileptic seizures (Treiman 2001).

GABA is produced in GABAergic neurons from glutamate via glutamate decarboxylase or glutamic acid decarboxylase (GAD). Glutamate comes from glutamatergic neurons, produced inside those from glutamine, which is in turn supplied by astrocytes. Figure 1.7 shows a simplified route of GABA production. This serves to illustrate the systems involved in producing GABA and the complexity of the networks involved. More on the involvement of astrocytes in GABA production can be found in section 1.4.3.2.

GABA is known as the main inhibitory neurotransmitter. However, it fulfills other roles as well. It has been shown that GABA is involved in the development of oligodendrocytes and Schwann cells, which myelinate axons in the CNS and PNS, respectively (Serrano-Regal et al. 2020). Through its role in developing these specialised cells, GABA contributes to the functioning and support of neurons. Moreover, in the forming of neuronal connection in the brain, GABA plays a

crucial role, as it helps regulate the balance between excitation and inhibition to modulate synaptic connections. To start with, during development, GABA is excitatory and leads to the depolarisation of synapses formed in newly-born neurons, due to the initial high concentration of Cl^- (Ben-Ari 2002).

This aspect of GABA contribution to the development of the immature brain is highly conserved among evolutionary taxa and GABAergic synapses appear before glutamatergic ones. Ben-Ari proposes a model through which excitatory GABA appears first, then GABAergic and glutamatergic synapses arise, after which giant depolarising potentials are generated to coordinate aspects of neuronal growth or circuit plasticity (Ben-Ari 2002). Only afterwards, the system reaches a point where GABA becomes inhibitory, through elimination of chloride ions from the intracellular space.

There are two main classes of GABA receptors: $GABA_A$ and $GABA_B$. $GABA_A$ receptors are ionotropic ligand-gated chloride channels, while $GABA_B$ are metabotropic. A special type of $GABA_A$-rho receptor exists, which is made up of ρ-subunits. $GABA_A$ receptors trigger fast inhibitory post-synaptic potentials (IPSPs), while $GABA_B$ are responsible for slower inhibition (Kuriyama, Hirouchi, and Nakayasu 1993).

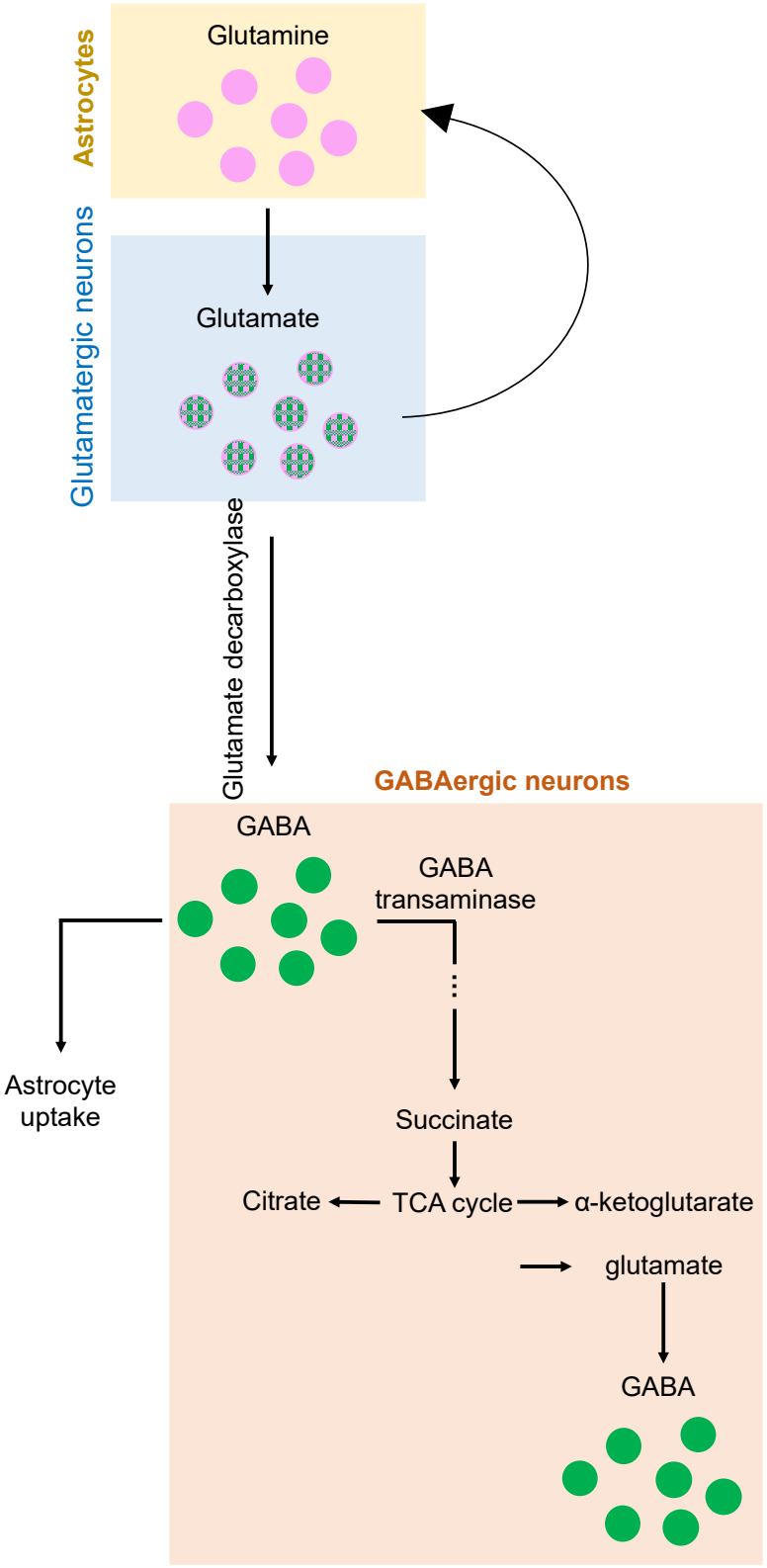

Figure 1.7: Schematic of GABA production. TCA= tricarboxylic acid cycle.

1.10.2 $GABA_A$ receptors

$GABA_A$ receptors have been extensively studied, as they contain the site of action for drugs with anticonvulsant, anxiolytic or sedative effects (Chambers et al. 2003). 19 different subunits have been discovered that make up the $GABA_A$ receptor in a heteropentameric fashion, not including alternative splicing (Wafford 2005), α(1–6), β(1–4), γ(1–3), δ, ε and θ. The subunits are part of a cys-loop super-family of ligand-gated ion channels, which include other receptors such as nicotinic acetylcholine receptors and glycine receptors (Schofield et al. 1987). These $GABA_A$ subunits are arranged in a 2α:2β:1γ stoichiometry, which gives rise to many potential combinations, the most common of which is $\alpha1\beta2\alpha1\beta2\gamma2$ (Pirker et al. 2000).

There are various ligands that bind to sites on the $GABA_A$ receptor (Solomon et al. 2019) and many are used pharmacologically. For example, the binding site of the allosteric modulator class benzodiazepines is between the α and γ subunits. GABA binds to the orthosteric site of the receptor, found between α and β subunits. The type of the α subunit is the one that dictates the pharmacological profile of the receptor. $\alpha1$ and $\alpha5$ subunits lead to more sedative effects of benzodiazepines, while $\alpha2$ or $\alpha3$ mediate more anxiolytic effects. Some $GABA_A$ receptors that contain $\alpha4$ or $\alpha6$ mediate alcohol activity. See Figure 1.8 for a schematic of the heteropentameric $GABA_A$ receptor.

It was reported that while $GABA_A$ receptor subunits such as $\alpha1$, β1-3 and $\gamma2$ show wide distribution throughout the brain, others like α2-6, $\gamma1$ and δ show a more specific distribution (Pirker et al. 2000).

The fact that the distribution of different subunits does not show large overlap suggests they fulfil specialised functions according to the different

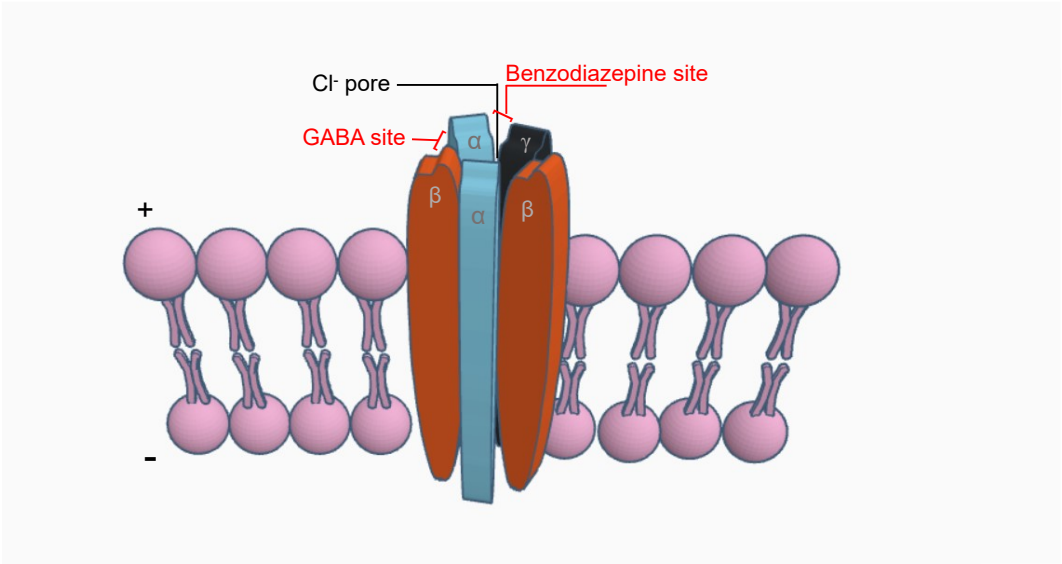

Figure 1.8: Representation of a $GABA_A$ receptor.

pharmacological profiles, which are determined by the α-subunit (Minier and Sigel 2004; Ali, Afia B. and A. M. Thomson 2008). The α5 subunit has been reported to be important in learning and memory formation (Collinson et al. 2002; Ghafari et al. 2016), and therefore alterations that affect its functions could have repercussions in AD. α5 knock-out mice show improved performance in spatial memory tests (Collinson et al. 2002) and studies show that α5-subunit-containing $GABA_A$ receptors are involved in associative memory and fear conditioning (Yee et al. 2004), which further highlights this subunit's importance in AD. Remarkably, $GABA_A$ receptors are preserved in AD in the hippocampus, unlike other types of receptors, such as glutamatergic receptors (Greenamyre et al. 1987; Jansen et al. 1990; Zilles et al. 1995), with only a slight reduction being reported in the stratum pyramidale of CA1 (Chu, Penney, and Young 1987). Interestingly, Prut and colleagues studied the effect of a reduction of the α-subunit in the alpha5(H105R) knock-in mouse and noted a shift in memory- namely, a reduction of spatial recognition and an increased preference for the use of object recognition memory (Prut et al. 2010). .

1.10.3 The α5 subunit and its role in AD

The α5-subunit is mainly found in the hippocampus (Fritschy and Mohler 1995), where it helps mediate tonic inhibition (Glykys, Mann, and Mody 2008). Studies found that it is anatomically and physiologically preserved in the hippocampus of AD patients (Howell et al. 2000), and that it mainly localises extrasynaptically on CA1 pyramidal cells (PC) (Brünig et al. 2001; Caraiscos et al. 2004). However, there is a lack of studies on α5 expression on interneurones, in particular on CR interneurones, which is why we further explored it in this study.

Coupling the apparent preservation in AD together with its importance in memory formation and involvement in inhibitory functions, the α subunit represents an important investigative point in this study.

The inhibitory function mediated by GABA can be modulated by different drug types, which affect either the metabolism of GABA, its synaptic release or reuptake (Meldrum 1982). When $GABA_A$ Rs contain α5-subunits combined with γ2, they show high affinity binding for benzodiazepines, compounds which enhance the GABA effect and that are used to treat anxiety and seizures (Pritchett and Seeburg 1990). However, benzodiazepines themselves have been strongly associated with an increased risk of developing dementia in the elderly (He et al. 2019) and they increase the risk of suicide, therefore a new form of therapy is required, perhaps one targeting the α5-subunit?

There are also compounds which bind to the benzodiazepinde site and enhance memory. Such a compound is L-655,708, an inverse agonist to α5 subunit-containing $GABA_A$ Rs, which recognises the benzodiazepine site with high selectivity (Caraiscos et al. 2004) and which has been shown to enhance performance in rats assessed with the Morris water maze memory test (Chambers

et al. 2003). This highlights $\alpha 5$ as a potential drug target in AD.

Seeing as the expression of the $\alpha 5$ subunit-containing $GABA_A$ receptors is mainly confined to the hippocampus and that a reduction in their functions seems to benefit learning and memory formation, it is in our interest to firstly report on their levels in the inhibitory interneurones investigated and then to discuss whether they could qualify as a potential drug target that could modulate the inhibitory interneurone network and harness it to help alleviate symptoms of AD such as memory loss.

1.11 Therapeutic Challenges

Current AD treatments focus on alleviating the symptoms and range from providing care and support to patients to implementing an exercise regime associated with a lower risk of dementia (Larson et al. 2006). Drug treatments include antidepressants and antipsychotics and, a popular treatment, acetylcholinesterase inhibitors such as donepezil or rivastigmine (Kumar, Singh, and Ekavali 2015). For patients with more severe cases of dementia, memantine is recommended (Wang et al. 2017). The common denominator of these treatments, however, is that although they help patients manage their symptoms, they do not treat the underlying causes of the disease and may trigger unwanted side effects such as vomiting, headaches or hallucinations (NICE 2011), exposing a missing gap in the field of pharmacological approaches to treat AD.

For example, acetylcholinesterase inhibitors such as donepezil or rivastigmine are used to compensate for the low levels of acetylcholine (ACh) in the brain by limiting its processing and its break-up into harmful products, not by treating the underlying cause that leads to the increased break-up.

BACE1 is the main mediator of β-secretase, which is the first enzyme of the APP

cleavage process (see section 7.5). Mutations in the APP sequence can lead to increased cleaving by BACE1 and increased Aβ productions and have been identified in familial AD. BACE1 inhibitors have, therefore, been trialed as AD treatment (Das and Yan 2019). However, treatments have not had the desired effect, perhaps due in part to the lack of understanding of the full functions of BACE1. Deleting BACE1 in the germline has led to reduced production of Aβ, reduced aggregation and a notable decrease in the risk of developing AD (Maloney et al. 2014).

Apart from being involved in APP cleavage, BACE1 has also been shown to be important in synapse maintenance. Therefore, using BACE1 inhibitors as medication for AD needs to become a balancing act of treating the disease and avoiding synaptic disruption.

Memantine, which is recommended for more severe cases of dementia (Wang et al. 2017), is an agonist for certain dopamine receptors and antagonist for N-methyl-D-aspartate (NMDA) receptors, which are part of glutamatergic transmission. Seeing as it is thought that glutamatergic transmission is impaired in AD and causes neuronal excitotoxicity, the use of memantine as a low-affinity blocker reduces the excess Ca^2+ transmission and lowers excitotoxicity. However, there are no clear results that the pharmacology is effective in treating the progression of the disease. One study found that the drug treated symptomatology rather than actual disease progression (Reisberg et al. 2006) and while that is helpful, there comes a time-point in disease progression when the drug will not be efficient, due to pathology that is too advanced. Indeed, after 28 weeks of receiving placebo instead of memantine, a cohort of patients was switched to the drug for 24 weeks and showed similar results in terms of improved symptomatology to the cohort that had received the medication from the beginning of the first study. This suggests that memantine only treats disease symptoms, otherwise the group that

had initially received placebo and that was further along with disease progression would not have shown a similar improvement trajectory to the cohort that had been medicated from the start (Leber 1997).

The proportion of the ageing population in the world is increasing, therefore so is the incidence of Alzheimer's disease. This problem is accentuated by the fact that treatments do not yet provide a cure for Alzheimer's disease: neither a halt nor a reversal of disease progression. Consequently, the call for developing more suitable and effective pharmaceutical treatments for AD is all the more urgent.

Chapter 2

Aims

The current study aimed to contribute to the understanding of the pathophysiological mechanisms of AD that underlie neuronal dysfunction correlated with neuroinflammation and Aβ aggregates. The following aspects were investigated:

- Memory impairment in the $App^{NL\text{-}F/NL\text{-}F}$ animal model of AD, as well as indicators of anxiety.
- The level of pathological hallmarks of AD sucha as Aβ accumulation as well as the proliferation of astrocytes and microglia as a sign of neuroinflammation.
- The anatomical density of pyramidal cells.
- The anatomical density of the interneurone-specific modulatory interneurone subclass that expresses calretinin and is specialised to connect other interneurones.
- The anatomical density of major inhibitory interneurones that express cholecystokinin and somatostatin and make contact with pyramidal cells as well as with other interneurones and which are important in learning and anxiety.

- The state of key neurotransmitter transporters GAT1 and VGlut1.
- The level of expression of α5-subunit-containing $GABA_A$ receptors, which are important in memory formation, on the cellular subtypes so as to evaluate the therapeutic potential of targeting those receptors.

Neuroinflammation, pathological hallmarks of AD and disruption of neuronal networks are all results and drivers of AD pathology progression and have not yet been fully explored, which is why they were investigated in the current study. The methods used in this study include behavioural tests of cognitive abilities, immunohistochemical staining and confocal microscopy in the first knock-in preclinical mouse model of AD, the $App^{NL-F/NL-F}$.

The findings in this thesis contribute to a better understanding of AD pathology and have the potential to inform therapeutic avenues. Firstly, there is immediate impact in the research group, which will build on the current study and extend it with other animal models of AD and additional methodology. Secondly, the results will contribute to the knowledge bank of the wider field of AD. Work from this thesis has already been published in peer-reviewed journals and cited by the wider field (Petrache et al. 2019; Shi et al. 2019; Petrache et al. 2020).

Chapter 3

Materials and Methods

3.1 Animal rearing and maintenance

The study was based on procedures carried out as per the British Home Office regulations of the Animal Scientific Procedure Act 1986, under the project licence PPL : 7007558 held by the principal investigator, Dr. Afia B. Ali.

$App^{NL-F/NL-F}$ mice obtained from RIKEN were crossed with wild-type C57BL/6J mice at the School of Pharmacy, ordered from Charles River, and the heterozygous animals that resulted were further used for breeding to yield homozygous wild-type and $App^{NL-F/NL-F}$ mice. Only the homozygous $App^{NL-F/NL-F}$ and wild-type from the same breeding were used in experiments. The animals were genotyped centrally at UCL, using tissue from the ear. The following primers were used for genotyping via polymerase chain reaction, as per the original publication Saito et al. 2014: 5-ATCTCGGAAGTGAAGATG-3, 5-TGTAGATGAGAACTTAAC-3, 5-ATCTCGGAAGTGAATCTA-3, and 5-CGTATAATGTATGCTATACGAAG-3.

The animals were housed in cages of up to 5 inhabitants and given ad-libitum access to food and water. The day: night cycle was 12 hours: 12 hours. 155 adult male animals were used in this study, the youngest age being one month and the oldest 22 months. No females were used in this study. $App^{NL-F/NL-F}$ and wild-type mice were grouped into the following age brackets: 1-3 months, 6-9

months, 12-16 months and 18-22 months. The grouping was decided based on previous observations in the laboratory which showed that no differences were observed within the respective age groups, as well as on comparable studies from the speciality literature.

All rodents that went through experimental procedures were thoroughly monitored for signs of discomfort. Their weight and general health were inspected and recorded twice daily before starting the experiments, during experiments, as well as up to a week afterwards to ensure there was no lasting harm to their health. Animals which underwent one type of cognitive test were generally not utilised in another test. If it was required they be utilised, a break of minimum one month was taken between tests to allow for the animals to recover their naïve state.

The animal welfare signs checked included: maintenance of weight levels, general grooming or mouse grimace scale (Wolfensohn and Lloyd 1998; Langford et al. 2010) .

3.2 Behavioural tests of cognitive deficits and anxiety

All experimental procedures were carried out blind to the genotype of the animal and the mice were sampled randomly from the existing colony of age-matched wild-type and $App^{NL-F/NL-F}$ mice.

In all behavioural studies, the behavioural arena and the the experimental objects were cleaned thoroughly between trials and between animal runs with 70% ethanol which was allowed to dry before placing the animal into the arena. The animals went though one particular experimental procedure only once during the lifespan, unless stated otherwise. All animals were handled by the experimenter for a minimum of 5 days prior to the experiment (3 if the animal was handled on a

regular basis), so as to minimise anxiety and to maximise optimal test performance. Preference was given to the use of a tunnel when handling the animals.

Table 10.1.1 displays the mouse allocation to each behavioural experiment type, by age and number. All of these mice were included in the statistical analysis. During the NOR test, at 12-16 months of age, a mouse was not included in analysis due to a fault in equipment (camera resetting).

Table 3.2.1: Mouse allocation for each experiment, by age and number. RAM= radial-arm maze, NOL= novel object location, NOR= novel object recognition. Further detail provided in text.

		Age (months)		
Experiment	Genotype	6-9	12-16	18-22
RAM	Wild-type	-	4	-
	$App^{NL\text{-}F/NL\text{-}F}$	-	4	-
T-maze	Wild-type	10	14	8
	$App^{NL\text{-}F/NL\text{-}F}$	10	14	8
NOL	Wild-type	9	12	13
	$App^{NL\text{-}F/NL\text{-}F}$	10	12	13
NOR	Wild-type	10	6	6
	$App^{NL\text{-}F/NL\text{-}F}$	11	12	13
Open Arena	Wild-type	11	11	13
	$App^{NL\text{-}F/NL\text{-}F}$	10	6	9

3.2.1 8-arm radial maze

Three of the eight arms of the maze were baited with a drop of condensed milk (Essential Waitrose & Partners Condensed Milk) as a reward, dissolved 1:1 in water and placed in a small plastic boat. To avoid olfactory bias, the non-baited arms had a drop of condensed milk under an inverted plastic boat so that the reward would be unreachable in those arms. For each animal, different arms were baited. A photograph of the 8-arm maze is shown in Figure 3.1. The maze and boats were cleaned with ethanol in between experimental runs so as to eliminate the odour of previous subjects.

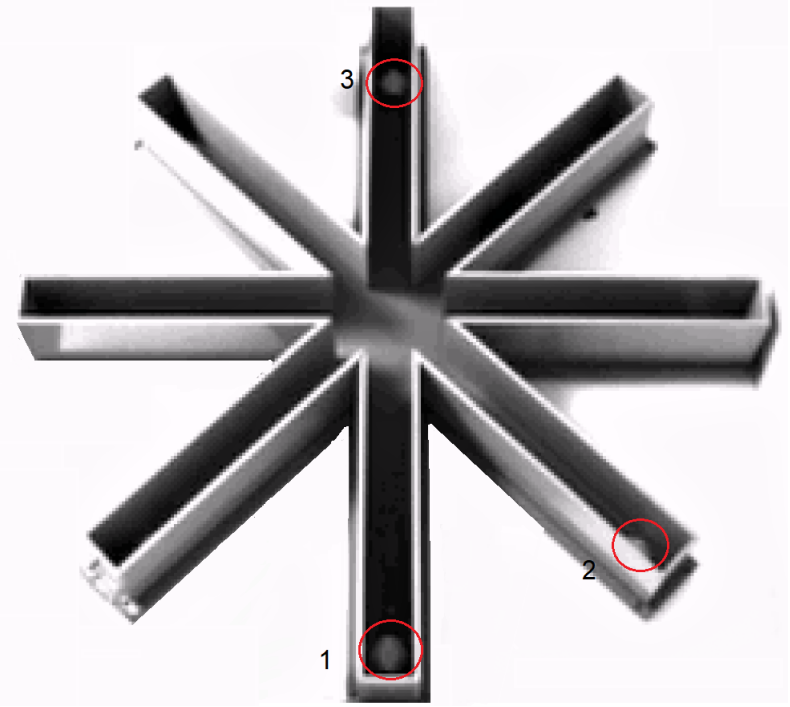

Figure 3.1: Representative photograph of the 8-arm radial maze. Numbers 1, 2 and 3 indicate arms baited with condensed milk. The red circles pinpoint the plastic boats.

The animals went through three experimental stages: acclimatisation with the experimenter and with the arena, training, and testing. For several days prior to any experimental procedures, the animals were intermittently deprived of food as per common practices to incentivise maze exploration and consumption of the food reward. During food deprivation, the weight of the animal was carefully monitored and maintained above 90% of the initial body weight over the course of the experiment. Normally, the food deprivation lasted between 1 and 14 hours each day. During food deprivation, the animals had ad-libitum access to water. Any weight drop below 90% of the initial body weight would result in the animal being immediately removed from the experimental procedure, but no animal reached this drop.

Wild-type mice and $App^{NL-F/NL-F}$ animals were tested in small cohorts of 2-4 animals per experimental group at one time, to ensure enough time was given to

complete the procedures without delays to the protocol or unnecessary prolongation of food deprivation.

The following protocol was used in the 8-arm maze experiments:

1. The week preceding the experiment:

    - Condensed milk was placed in the cage for the animal to become accustomed to it and develop a feeding interest.
    - Daily 1-2 minute encounters and handling by the experimenter.

2. Experimental procedure:

    - Six sessions of habituation to the maze were delivered over 3 days, one AM and one PM each day. The first two sessions were 10-minutes long, the remaining four sessions 5 minutes long. During the first three sessions, drops of condensed milk were scattered around the maze to encourage exploration. For the last three sessions, the drops were placed at the end of each of the 8 maze arms.
    - After the first two sessions it was noted that the mice were eating on average 2 out of 3 food rewards, therefore food restriction was introduced to encourage exploration and feeding off the condensed milk. Food restriction was done overnight for the first day, then 1 hour before the AM sessions and 4 hours before the PM sessions, after which the mice were given ad-libitum access to food again. Access to water was permanent. The experimental schedule was as follows:
    - Day 1-3 (AM): 2 x 5 minutes training with the baited arms, after food deprivation.
    - Day 4: resting day.

- Day 5 (AM): testing day: 2 x 5 minutes test trial.

The room contained the following visual cues outside of the maze:

- bottle of ethanol between arms 6 and 7;
- one orange A4 sheet on the wall behind the maze, to the left;
- one black A4 sheet on the wall behind the maze, to the right;
- laptop and camera on the right of the maze, on the bench;
- experimenter in front of the maze, approx. 1.5 m away, directly in front of arm 1, so as not to cause any bias.

The following outcomes were measured:

- Working memory error (WME), which measured the number of entries to a previously visited arm after food reward had already been collected.
- Reference memory error (RME), which measured the number of entries to non-baited arms.

3.2.2 Novel Object Location and Novel Object Recognition tests

During novel object location (NOL) and novel object recognition (NOR) tests, habituation of animals with experimenters took place for 1-2 minute daily for approximately one week before experiments if the animals had not been previously handled, and 3-5 days before experiments if previous handling had occurred regularly. Figure 3.2 shows an example of the experimental set-up. The arena was comprised of a 40x40x40 cm box made from light grey opaque plastic material. Objects utilised for the experiment comprised two green plastic tubes

approximately 10 cm in height with a diameter of 3 cm, and one yellow plastic sphere approximately 7 cm in height, with a diameter of 6 cm. The objects were selected based on established practice in the field so as to avoid preference bias.

Testing was done at 6-9 months, 12-16, and 18-22 months. The same animals were used for the latter two categories. However, ten animals died or had to be processed before they could be utilised in the 18-22-month study, during the nation-wide Covid-19 lockdown, therefore new animals were introduced to the study. The experiment was video recorded to allow for post-hoc analysis.

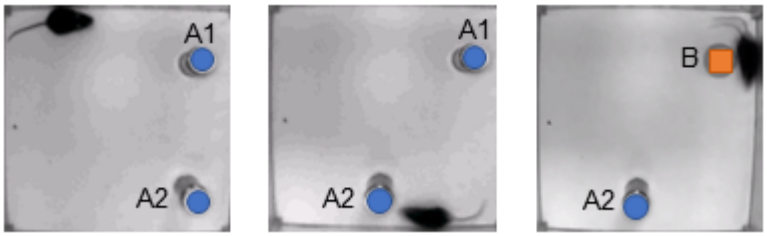

Figure 3.2: Experimental paradigm for novel object location and novel object recognition tasks detailing the habituation phase with the two identical objects (A1 and A2, leftmost panel), the object location task (A1 and A2, middle panel) and the novel object recognition task (A2 and B, rightmost panel).

In these experiments, the mice were run in groups of four. The following protocol was used in NOL/NOR tests:

1. Day 1: Arena Habituation

    - The mouse was habituated with the experimental room for 30 minutes, then placed for 10 minutes in the empty experimental arena.The arena was cleaned and then the next mouse was run. This step was done twice for all the animals.

2. Day 2: Arena Habituation

    - After a 30-minute habituation with the experimental room, the mouse was placed in the empty experimental arena for 10 minutes.

3. Day 3: Training and Testing

    - The animal was brought into the experimental room for a 30 minutes-rest.
    - Afterwards, it was allowed to explore the arena for 10 minutes with two identical objects in place: A1 and A2 (see Figure 3.2).
    - The animal was then returned to its cage in the experimental room and allowed to rest for 30 minutes. Afterwards, it was placed in the arena for a further 10 minutes with object A2 moved to a novel location within the arena, while object A1 stayed in place.
    - The animal was then returned to its cage in the experimental room for 30 minutes, then placed back in the arena, now with object A1 replaced by novel object B, while object A2 stayed in its place.

The experimental objects were placed at the same distance from the arena walls, in mirrored positions, to avoid any location bias. They were chosen based on literature standards as well as on recommendations from experienced staff within the Department of Pharmacology at the School of Pharmacy. The objects were immobile and did not have any movable parts nor any edible parts.

3.2.3 T-arm Maze: Spontaneous alternation

A T-arm maze was designed using Tinkercad and Inkscape and laser-cut from acrylic sheets (Figure 3.3). The design was based on the diagram and dimensions from (Denninger, Smith, and Kirby 2018), but was adapted to create a maze easy to disassemble and store (see Figure 3.3). The maze was brown and the inner walls were sanded to diminish reflection from the acrylic sheets. The maze had an end arm and two ”goal” arms that spread left and right. Each of the goal arms had a small white well made of plastic at the end filled with a drop of condensed milk

(Essential Waitrose and Partners Condensed Milk), diluted 1:1 in water. The aim of the experiment was for the animal to correctly identify a previously-visited arm and alternate its choice on a subsequent run. For example, if on the first run the animal visited the left arm, on its second run it would be expected to visit the right arm. Baiting the arms with milk is not necessary to carry out the experiment, but acts as another incentive for the mouse to follow its natural instincts and alternate its choices.

Prior to the experiment, the animals were habituated with the experimenter over several days, until they were relaxed and interacted readily. Overall, the mice were well-habituated and ran within seconds. Moreover, they were fed small drops of condensed milk in their home cage over several days to become accustomed with it and to avoid hyponeophagia.

The maze was cleaned with ethanol before the start of the experiment, as well as in between animal runs. Paper cues were placed on the room walls, at equal distances from the walls of the maze. A small drop of approx. 2 mL of condensed milk was placed in the food wells at the end of the two goal arms. Fresh wood chipping was placed on the floor of the maze. After each animal had had its runs, the wood chipping and food reward were replaced and the maze cleaned.

The animals were brought into the experimental room 5 to 10 minutes before testing. An individual animal was placed gently at the bottom of the vertical arm, into the ”start” zone (see Figure 3.3A). The experimenter then placed themselves 1m behind the maze and central to the end arm, to allow the animal to choose an arm without any bias. Once the animal entered an arm fully, with the four feet and the tail, a guillotine door was lowered and the mouse restricted in the zone for 30 seconds to allow time to consume the milk reward. After 30 seconds, the door was removed and the animal allowed to enter a plastic tube, from which it was

immediately replaced in the start zone for a new choice of arm. Once the choice was made, the mouse was restricted in the area for 30 seconds, then removed and replaced back in the home cage. If it visited the previously unvisited arm, the run was scored as an alternation. Otherwise it was scored as a non-alternation.

After the initial trial, two more trials followed where delays were introduced between the first and the second runs. The mouse was replaced in the home cage between the first and the second choice, for 30 seconds and one minute, respectively.

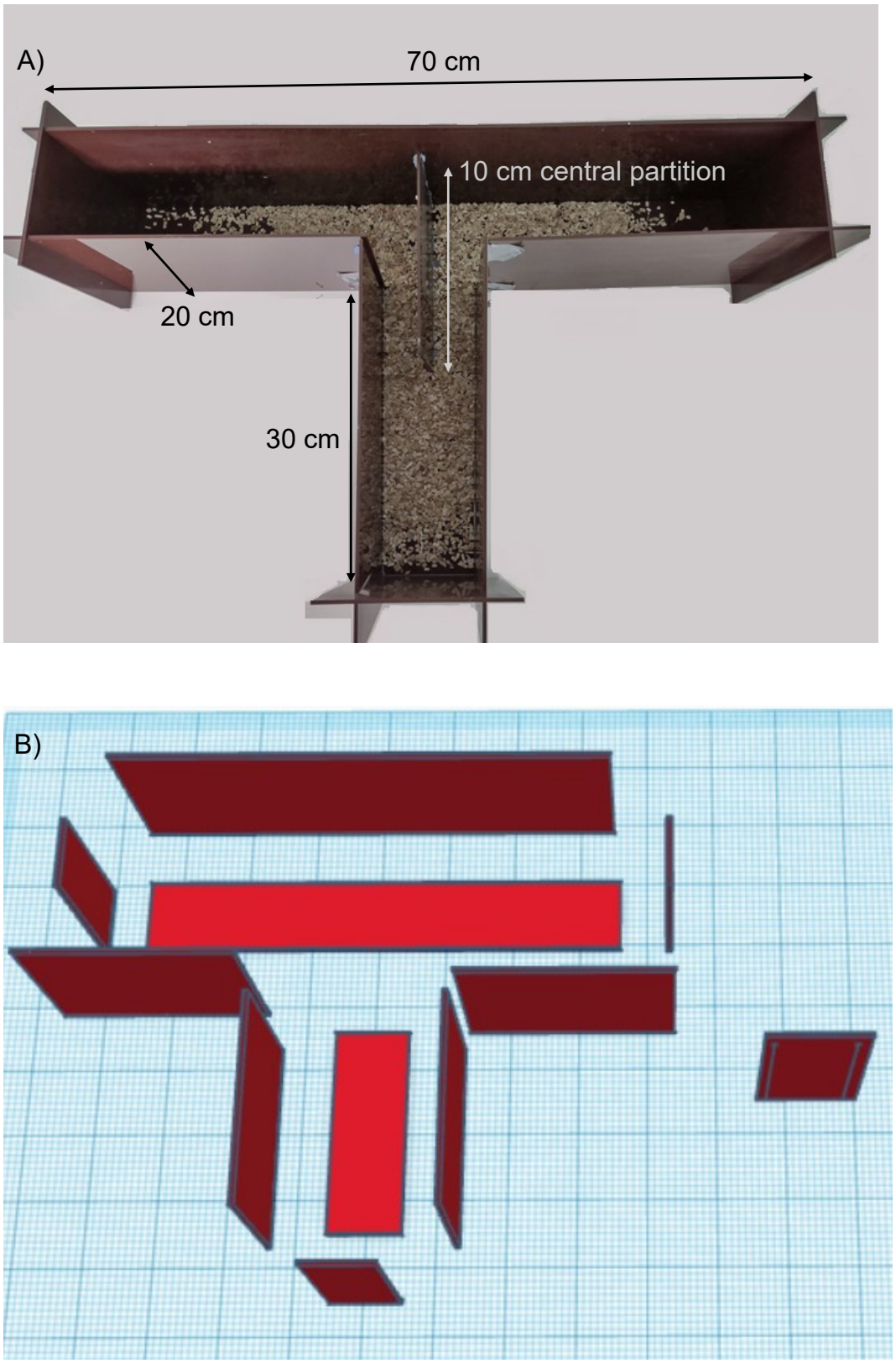

Figure 3.3: T-arm maze design and dimensions. A) Finalised maze, filled with wood chippings. B) Maze design, made using TinkerCad.

3.2.4 Open arena test for anxiety-related behaviour

An open arena was used to measure anxiety-related behaviours. This consisted of a 40x40x40 cm box made from light grey opaque plastic material, where animals were placed for 10 minutes and allowed to explore freely. The following parameters were measured: time spent in the centre of the arena (20x20x20 cm area in the centre), time spent in the periphery, distance run and average speed, as per norms widely accepted in the field REFREFREF. The main indicators of anxiety were based on the two zones the animals spent time in: more anxious animals were expected to spend more time in the periphery of the arena, away from the centre which made them feel exposed, see Figure 3.4. In terms of distance run and speed anxious animals have been found to run faster.

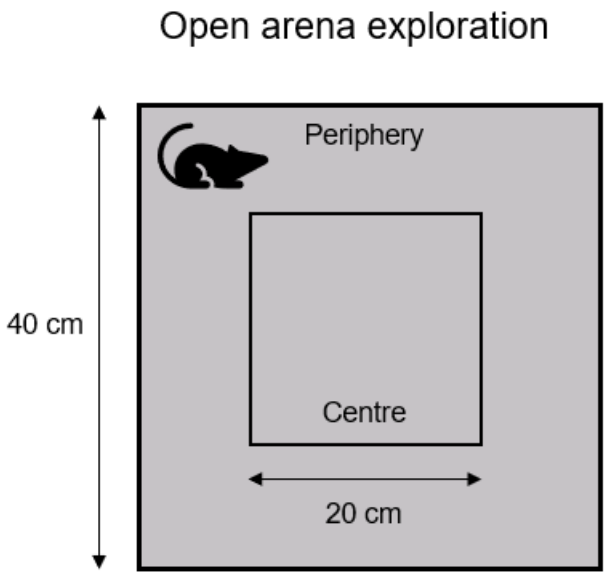

Figure 3.4: Open arena diagram showing the zone delimitation: centre and periphery, and arena dimensions.

3.3 Histological procedures

3.3.1 Tissue collection and preparation

Animals were anaesthetised with 60 mg/kg pentobarbitone, which was administered intraperitoneally prior to each transcardial perfusion. Pedal and tail pinch reflexes were monitored, as well as depth and pattern of respiration. The level of anaesthesia was determined to be adequate when there was no response to the pedal pinch reflex and when the breathing became shallow. Then, an incision was made through the abdomen of the animal, the skin pulled back to expose the thorax, the diaphragm cut and the rib cage removed to allow access to the heart for perfusion.

The animals were perfused transcardially with ice-cold artificial cerebrospinal fluid (ACSF) with sucrose, containing the following in mM: 248 sucrose, 3.3 KCl, 1.4 NaH_2PO_4, 2.5 $CaCl_2$, 1.2 $MgCl_2$, 25.5 $NaHCO_3$, and 15 glucose, which was bubbled with 95% O_2 and 5% CO_2. This step in the procedure helped to preserve the structural integrity of the brain tissue and it ensured exsanguination to eliminate peroxidase-containing red blood cells, which could interfere with histochemical experiments.

To perfuse an animal, a 23G butterfly needle (Greiner Bio-One) was inserted into the left ventricle of the heart and the peristalic pump (Waton-Marlow, 502s, Cornwall, UK) circulating blood at 5 mL/minute was turned on. The right atrium was cut, and the ice-cold sucrose solution was allowed to perfuse for approximately 10-15 seconds, until the fluid coming out of the animal showed no traces of blood. After perfusion, the animal was decapitated, an incision was made on the head along the anterior-posterior axis to reveal the skull and snips were made with fine scissors in the skull plates to allow for pulling of the plates away from the brain without

causing any damage to the soft tissue. The brain was collected and briefly placed in an ice-cold solution of ACSF containing the following (in mM):121 NaCl, 2.5 KCl, 1.3 NaH_2PO_4, 2 $CaCl_2$, 1 $MgCl_2$, 20 glucose, and 26 $NaHCO_3$, bubbled with with 95% O_2 and 5% CO_2. After the brief immersion, the tissue was distributed among experiments and experimenters accordingly, so as to be mindful of the ”Reduction” principle of the ”3Rs”.

For neuroanatomical studies, the tissue was fixed for 24 hours after collection in a solution of 0.1M phosphate buffer, 4% paraformaldehyde and 0.2% picric acid. Afterwards, the tissue was sectioned with a vibratome (Series 1000, Intracel, UK) in coronal slices with a thickness of 70 μm.

3.3.2 Immunofluorescence protocol

Brain slices obtained as per section 3.3.1 were placed into 24-well plates divided by age and genotype. To make the tissue readily permeable by the antibody solution, the slices were washed in 0.3% Triton X-100 detergent diluted in Tris Buffer Saline, (TBS-T 0.3%) in three 10-minute changes. The slices were incubated in 0.03% H_2O_2 at room temperature for 30 minutes as a blocking step to eliminate residual blood traces. After the H_2O_2 incubation, the three washing steps with TBS-T 0.3% were repeated, then slices were placed for one hour at room temperature in blocking serum (20%). This was followed by incubation in a TBS-T 0.5% solution containing primary antibody. For primary antibodies and blocking sera used in each experiment, please see Table 3.3.1.

After 72 hours in primary antibody at 4°C, the slices were washed in TBS-T 0.3% twice for 10 minutes and once in TBS-T 0.5% for 10 minutes, then incubated for 3 hours at room temperature in TBS-T 0.5% containing secondary fluorophore antibodies (see Table 3.3.2) and 0.05% blocking serum. The plates were wrapped

in aluminium foil to avoid light exposure and potential bleaching of the fluorophores. Next, the slices were washed in TBS-T 0.5% three times for 10 minutes. If staining of the nuclei was required, an 8-minute incubation with 4',6-diamidino-2-phenylindole (DAPI) was added in between the second and third wash. After washes, the slices were mounted on plain glass slides using a paintbrush and in dim light to minimise light exposure that could cause bleaching of the fluorophore. The excess fluid surrounding the slices was absorbed using filter paper, then the slides were placed in a dark drawer for a short period to dry. Antifade mouting medium Vectashield (Vector Laboratories) was applied on top of the slices and a cover slip gently lowered over it. Excess medium was removed using filter paper. After a brief drying time, the sides of the coverslip were sealed with transparent nailpolish to secure it in place.

Table 3.3.1: Primary antibodies and blocking sera for the immunofluorescence protocol. *NHS*: normal horse serum, *NDS*: normal donkey serum, *NGS*: normal goat serum

Antibody target	Company	Target species	Dilution	Blocking serum
VGlut1	Millipore	Goat	1:2500	NHS
GAT-1	Millipore	Goat	1:500	NHS
CaMKIIα	Cell Signaling Technology	Mouse	1:100	NHS
CR	Swant	Goat	1:1000	NDS
SST	Santa Cruz Biotechnology	Rabbit	1:200	NHS
CCK	Frontier Institute	Rabbit	1:750	NHS
GFAP	Agilent (Dako)	Rabbit	1:500	NGS
GFAP	Invitrogen	Rat	1:1000	NGS
CD68	BioRad	Goat	1:500	NGS
APP695	ThermoFisher	Mouse	1:1000	NHS
$GABA_A$ α5	Abcam	Mouse	1:100	NHS
GAD67	Millipore	Mouse	1:2000	NHS

3.3.3 Immunoperoxidase protocol

The first steps of the immunoperoxidase staining protocol were similar to those for immunofluorescence staining, up until the primary antibody incubation. For this

Table 3.3.2: Secondary antibodies for the immunofluorescence protocol.

Antibody	Company	Target species	Dilution
Alexa 488	Abcam	Goat	1:500
Alexa 568	Abcam	Rat	1:500
Alexa 647	Abcam	Mouse	1:500
DAPI	Sigma-Aldrich	Multiple	1:1000
Texas Red	Thermo-Scientific	Rabbit	1:750

step, the primary antibodies were diluted in TBS-T 0.3% and no sera added to the solution. The antibody concentration was much lower. This experimental procedure was carried out for astrocyte, microglia and Aβ staining (for concentrations and secondary antibodies see Table 3.3.3).

Table 3.3.3: Immunoperoxidase Antibodies

Primary antibody	Company	Target species	Dilution
AP695	Thermo-Fisher	Mouse	1:500
CD68	BioRad	Rat	1:8000
GFAP	Agilant(Dako)	Rat	1:2000
DAPI	Sigma-Aldrich	Multiple	1:2000
Secondary antibody	**Company**	**Target species**	**Dilution**
Biotinylated	Vector	Mouse, Rat	1:500

The primary antibody incubation lasted 48 hours, after which slices were washed in TBS-T 0.3% three times for 10 minutes and the slices incubated with secondary antibodies for 24 hours as per Table 3.3.3. Post incubation with secondary antibodies, the slices were placed in avidin–biotin–horseradish peroxidase complex (ABC, Vector Laboratories) for two hours, then washed three times with phosphate buffer saline (PBS), for a duration of five minutes per wash. Slices were then placed in 3–3-diaminobenzidine (DAB) with NiCl. Afterwards, a drop of 6 μL of H_2O_2 was added to each individual well and the staining allowed to develop until the reaction was stopped with TrisBuffer. Slices were washed twice in TrisBuffer and then placed on gelatin-coated slides.

After mounting, the slices were dried in a fume hood for a minimum of three hours

or overnight, then dehydrated with EtOH in several steps: 15 minutes in 50% EtOH, 15 minutes in 70% EtOH, 15 minutes in 90% EtOH, and two consecutive washes in 100% EtOH for 10 minutes. Post dehydration, slices were placed in Histoclear for 1-2 minutes. They were then briefly drained, DPX Mountant (Sigma-Aldrich) was placed on top and a coverslip gently lowered over the slide to avoid the formation of any bubbles. Slices were kept in designated boxes in a dry place away from sunlight.

3.3.4 Image analysis

Sections mounted on glass slides, stained with immunofluorescent dyes, were imaged using Zeiss 710 and Zeiss LSM 880 confocal microscope. Z-stacks spanning the whole thickness of the slice were taken, with particular care given to imaging as much as possible of the area of interest in order to obtain representative results. After imaging, the Z-stacks were compressed into one image using the Maximum Intensity Projection function in the Zen software.

Cell number was manually counted using a clicker. When colocalisation between different structures was investigated, the image with the channels corresponding to both structures of interest was imported into Fiji (Image J) and split into 8-bit channels corresponding to the structures of interest. Let's take the example of colocalisation between a subtype of interneurone and a receptor. There would be two 8-bit images corresponding to the channel for the interneurone and the channel for the receptor staining, respectively. The next step was adjusting the threshold using the automated function in Image J, so that any noise was removed. Afterwards, the outline of the interneurons was drawn manually as a region of interest (ROI), then, using the Coloc-2 module, a colocalisation report between the ROI and the same regions in the receptor image was obtained. From this, Pearson's correlation coefficient R was obtained as a measure of colocalisation.

When intensity levels of images processed with the immunofluorescence or immunoperoxidase protocols were measured (e.g. to obtain levels of expression in a whole section, rather than an ROI), the 'Measure' function from Fiji was used on the 8-bit images so as to obtain the mean of Integrated Density, which was then normalised by the slice volume. An overall average was obtained per animal and then a group average for cohort and age bracket, respectively.

3.4 Statistics and Data Presentation

Wherever possible, statistical analysis was done blinded. All of the statistical analysis was performed using GraphPad Prism version 8.01. A 95% confidence interval was utilised throughout the study. Figures display the data means with error bars representing the standard error of the mean. A power calculation was performed using information from preliminary experimental data or from data already available in the lab. The power calculations were performed using the online tool ClinCalc (Kane 2019), based on the following equation:

$N_1=\left\{z_1\text{-}\alpha/2*\sqrt{\overline{p}*\overline{q}*(1+\frac{1}{k})}+z_1\text{-}\beta*\sqrt{p_1*q_1+\frac{p_2*q_2}{k}}\right\}/\triangle^2$, where:

- q_1=1-p_1
- q_2=1-p_2
- $\overline{p}=\frac{p_1+kp_2}{1+K}$
- $\overline{q}=1-\overline{p}$
- p_1, p_2 = proportion (incidence) of groups 1 and 2
- $\triangle=|p_2-p_1|$ = absolute difference between two proportions
- n_1 = sample size for group 1

- n_2 = sample size for group 2
- α = probability of type I error (usually 0.05)
- β = probability of type II error (usually 0.2)
- z = critical Z value for a given α or β
- K = ratio of sample size for group 2 to group 1

The power (1-β) was set to 0.80. Before performing any statistical test, the normality of the raw data was verified using the test Shapiro-Wilk and a ROUT test to identify potential outliers. In almost all of the cases no outliers were identified. Where an outlier existed, it was removed from the data pool via the software. When comparing between three or more data sets from two genotypes, a one-way analysis of variance (ANOVA) was performed. When a second factor was taken into account, for example age, a two-way ANOVA was used. After any ANOVA, a post-hoc test for multiple comparisons was applied. Direct comparisons between only two data sets were performed using an unpaired two-tailed Student's t-test. All *P*-values below 0.05 were considered significant and asterisks added to the presentation of the data as follows: * $P<0.05$ ** $P<0.01$ *** $P<0.001$ **** $P<0.0001$.

Chapter 4

Results I: Behavioural testing

This chapter presents the findings from multiple behavioural paradigms conducted to assess hippocampal memory function and report on cognitive differences between $App^{NL\text{-}F/NL\text{-}F}$ and age-matched wild-type mice. These tests included the 8-arm radial maze, T-arm maze, novel object location and novel object recognition.

There has been very little published on cognitive deficits in the $App^{NL\text{-}F/NL\text{-}F}$ AD model. The initial study which characterised the model upon its creation reported a significantly reduced performance in the Y-maze test at 18 months of age (Saito et al. 2014), but there was no mention of cognitive deficits being identified at other ages. Another seminal paper identified cognitive deficits in the $App^{NL\text{-}F/NL\text{-}F}$ mice at 8-12 months in the learning and fear conditioning tests (Masuda et al. 2016), but no corroboration at 18 months with the previous study. Therefore, this current study was aimed at testing a range of age windows to robustly report on cognitive performance in these animals.

The age windows chosen for all behavioural paradigms were kept consistent and animals were tested at 6-9, 12-16 and 18-22 months, as these time-points were identified to be relevant testing points in experiments concerning this animal disease model (Saito et al. 2014; Masuda et al. 2016). The sample size was based on standard practice throughout the literature, where groups are normally made of a minimum of 6-8 animals per group. Initially, a pilot study of four animals from

each genotype was used to determine the power of the study, which resulted in a recommended sample of 18 animals per group. After inputting more data into the power calculator, the recommended sample size was of 12 animals, which is what was aimed for each cohort.

Firstly, the results from the 8-arm radial maze test are presented, then results from the T-arm maze and then novel object location (NOL) and novel object recognition (NOR) tests. The findings are discussed after chapter V, in a joint discussion for chapters IV and V.

By carrying out more than one memory test, it was ensured that the task was suitable for the animal. For example, the project started with an 8-arm radial maze, but after a pilot experiment the task was deemed as too difficult for the mice and the much simpler T-arm maze was used, which is also the standard in the field (Stewart, Cacucci, and Lever 2011).

4.1 8-arm radial maze

The 8-arm radial maze test relies on the mice making correct spatial choices and finding rewards in a number of the 8 arms which are baited with rewards (Stafstrom 2006), 3 arms in this case. After having had their food restricted for 12-14 hours, the mice were placed in the maze which had diluted drops of condensed milk as rewards. Mice had been previously habituated to the food rewards in their home cages for a minimum of one week. The mice went through a training phase of six sessions over three days (two sessions per day), where they habituated to the placement of the rewards in the maze. After a rest day, the mice were returned to the maze and tested twice. Healthy mice were expected to remember where the rewards were placed and to not visit other arms. If the mice visited any unbaited arms, that counted as a reference memory error (RME), as it meant that they did not remember the location of the reward. If they visited an arm they had already visited, that counted as a working memory error (WME), as they did not remember they had just visited that arm during the tests. These outcomes served to assess spatial hippocampus-dependent memory (Axmacher, Elger, and Fell 2009; Cassel and Vasconcelos 2015).

Due to the general interest of our lab, which had utilised the 8-arm maze test previously with rats, this was the first behavioural test performed.

$App^{NL\text{-}F/NL\text{-}F}$ and wild-type animals at 12-16 months of age were tested using the 8-arm radial maze and the amount of working and reference memory errors were measured (WME and RME). The graphs in Figure 4.1 show the results of the test sessions, while the graphs in Figure 4.2 show the progression of the mice through the six training sessions and two tests. There were no significant differences between the two genotypes, neither in the total number of errors made nor in the

behaviour exhibited over the 8 trials they were subjected to. The training sessions were analysed alongside the tests so as to observe the learning pattern of the mice.

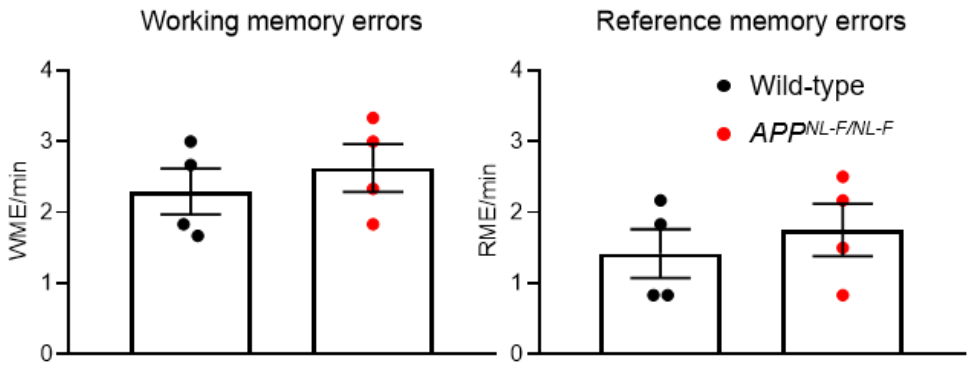

Figure 4.1: Working memory error (WME) and reference memory error (RME) averages in 12-16 months old $App^{NL\text{-}F/NL\text{-}F}$ mice and age-matched wild-type mice. n=4 animals per genotype. No changes were noted between the two genotypes.

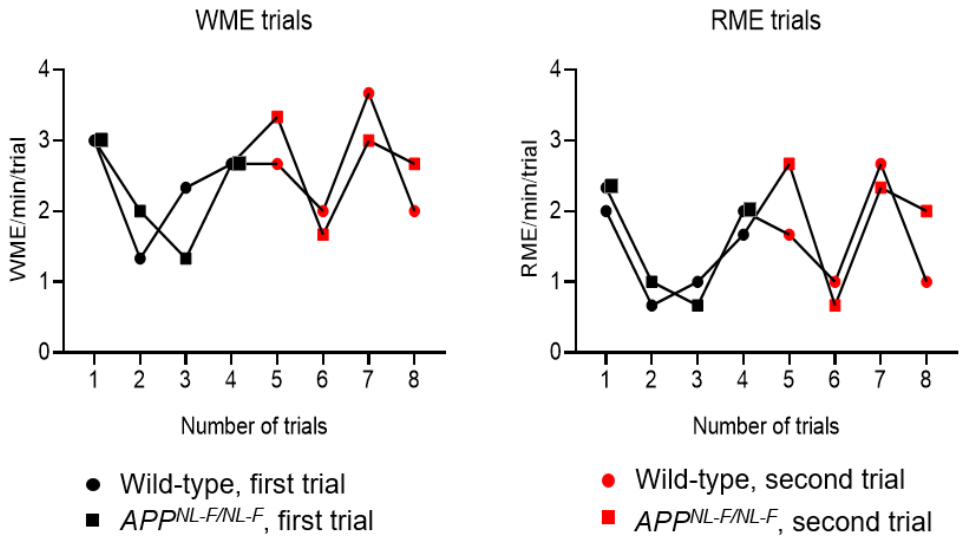

Figure 4.2: Working and reference memory error trials. 12-16 months old $App^{NL\text{-}F/NL\text{-}F}$ mice and age-matched wild-type mice. All individual trials are shown here: six training sessions and two test sessions. n=4 animals per genotype. Mice from both genotypes appeared to have difficulty learning the task, as their proficiency fluctuated over the 8 trials.

The experimental protocol was adjusted from methodology previously utilised with rats. Initially, the protocol consisted of two training sessions, a rest day then testing. For the mice, the training sessions were increased to six. The reason behind this was that some mouse strains have been shown to be slower learners than rats (Ellenbroek and Youn 2016), therefore a more robust training system could bypass such issues, if present. However, after the initial pilot study, it was observed that all of the tested mice showed inconsequential performance, rather than improving as they progressed through training and testing. After surveying the literature, it was also noted that the 8-arm maze was consistently used for rat testing rather than mice and in fact it had been designed for rat testing (Olton, Collison, and Werz 1977), therefore the task was deemed not appropriate to test the mice and the experiment was not continued, in favour of testing the mice with a T-arm maze instead, which represented a standard in the field (Stewart, Cacucci, and Lever 2011).

4.2 T-arm maze

The T-arm maze was used to test spontaneous alternation behaviour in $App^{NL\text{-}F/NL\text{-}F}$ and age-matched wild-type mice. The task was chosen as it represents a literature standard (Stewart, Cacucci, and Lever 2011) and it is based on the natural preference of mice and rats to alternate when presented with a choice of left-right options (Dember and Richman 1989). This represents a way of testing working memory controlled by the hippocampus (Olton, Becker, and Handelmann 1979). It has been noted that spontaneous alternation behaviour is the likely normal outcome in such a test, even when one considers that the animal could make an alternation by chance (Dember and Richman 1989). This test has been utilised for decades and one of the first mentions of rats showing an innate preference for alternation appears in 1914 (Hunter 1914). In addition, in a study reviewing methodology testing the Tg2576 AD mouse model with tasks such as T-arm maze, Y maze or Morris water maze, the T-arm maze was deemed to be the most appropriate to identify memory impairment (Stewart, Cacucci, and Lever 2011).

The maze measurements and protocol were adapted from (Deacon and Rawlins 2006). Each animal was tested in the maze three times, consecutively, then replaced to their home cage. Each of the three trials was made of two ”runs”, where the mouse was placed at the base of the ”T” and had to make a choice between the left and the right arm. On its second run, the mouse was replaced at the base and it had to make a choice again; a healthy animal with no cognitive impairment would be expected to visit the previously unvisited arm. In the first trial, the animal had no delay between the first and the second run. For the second trial, which took place approximately 2 minutes after the first, 30s delay was introduced between runs. Finally, after 2 more minutes in the home cage, a 60s delay was introduced between the two runs in the third trial. Figure 4.3 displays the percentage of animals that

performed an arm alternation - left-right or right-left - for the two genotypes.

In the no delay trial (Figure 4.3 A), the $App^{NL\text{-}F/NL\text{-}F}$ mice made only 40% correct alternations, compared to 60% in the case of wild-type mice. At 12-16 months, only 21.43% of the $App^{NL\text{-}F/NL\text{-}F}$ mice alternated, while the wild-type mice alternated in 42.86% of cases. At 18-22 months, where $App^{NL\text{-}F/NL\text{-}F}$ mice alternated in 25% of cases and the wild-type mice in 50% of cases.

When the 30-second delay was introduced, the $App^{NL\text{-}F/NL\text{-}F}$ mice alternated in 20% of cases at 609 months, compared to wild-type mice, which alternated 50% of the time. However, at 12-16 months, the AD model made alternations in 57.14% of cases, compared to 42.86% for the wild-type mice. At 18-22 months, the $App^{NL\text{-}F/NL\text{-}F}$ mice alternated 25% of the time compared to 75%, which was the case of the wild-type mice.

In the last trial, where a 60-second delay was introduced, the $App^{NL\text{-}F/NL\text{-}F}$ mice alternated in 30% of cases at 6-9 months, at 12-16 months in 57% of cases, and at 18-22 months in 25% of cases. In comparison, at the same ages wild-type mice alternated correctly 70% of the time, 58.33% and 75%, respectively.

A two-way ANOVA of the pooled data, with genotype and age as factors, identified genotype as making a significant contribution to the variation observed in the data, with $P < 0.01$ ($F_{(1,12)} = 14.36$, Figure 4.4). Overall, in the pooled data from all three trials at 6-9 months, the $App^{NL\text{-}F/NL\text{-}F}$ mice performed 50% ± 9.62 % fewer alternations than wild-type animals, a significant reduction in performance ($P < 0.05$, Holm-Sidak test for multiple comparisons).

At 12-16 months, in the pooled data, the $App^{NL\text{-}F/NL\text{-}F}$ mice alternated similarly to wild-type mice. However, at 18-22 months, the AD model cohort performed significantly worse than the age-matched wild-type mice, showing a 57.14 % ± 8.16

% reduction in the percentage of correct alternations ($P < 0.05$, Holm-Sidak test for multiple comparisons). This is comparable to results identified in the original paper which described the generation and features of the $App^{NL\text{-}F/NL\text{-}F}$ model (Saito et al. 2014), see figure 4.4.

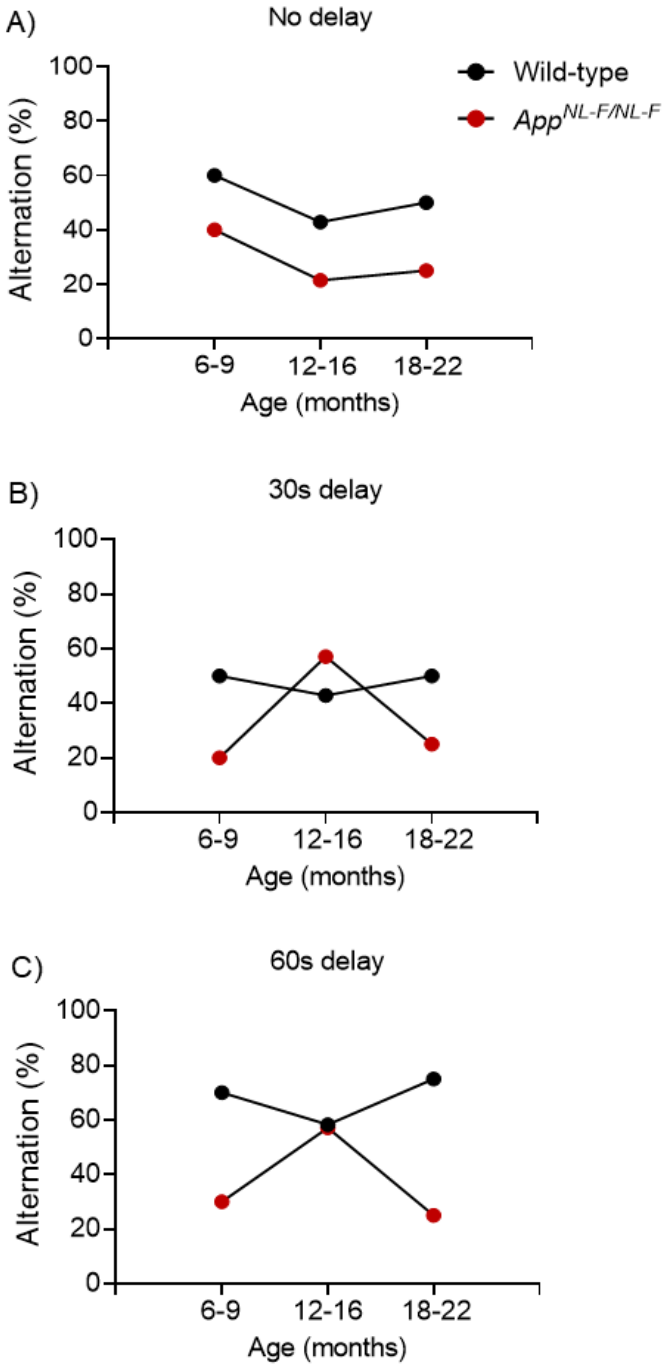

Figure 4.3: Percentage of mice that alternated in the T-arm maze test, in trials with no delay (A), 30 seconds delay (B) and 60 seconds delay (C), at 6-9 months, 12-16 months and 18-22 months. $App^{NL-F/NL-F}$ mice performed worse in the memory task than age-matched wild-type animals. n=10 each for both genotypes at 6-9 months, n=14 mice each for both genotypes at 12-16 months apart from the 60s delay trial where n=12 for the wild-type cohort, n=8 each for both genotypes at 18-22 months. As the figure displays the percentage of alternation in the whole age/genotype group, rather an average of individual values, error bars are not included.

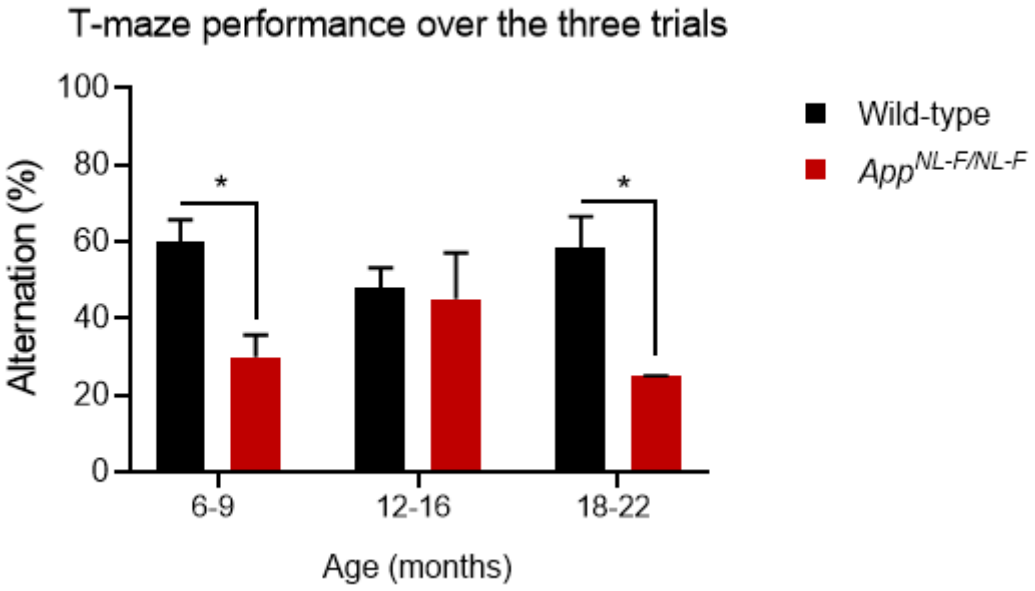

Figure 4.4: Overall performance in the T-arm maze. The $App^{NL-F/NL-F}$ mice show significantly impaired memory at 6-9 and 18-22 months. The graphs show the average of the alternations scores from the three trials: no delay, 30-second delay and 60-second delay, + SEM. Sample size for each of the three trials was between 8 and 14 mice. Two-way ANOVA with genotype and age as factors, and post-hoc Holm-Sidak test for multiple comparisons. * $P<0.05$.

4.3 Novel location and novel object recognition tests

Novel object location (NOL) and recognition (NOR) tests were performed successively in the same experimental setting. The subjects in the 6-9 month group were a separate cohort to the 12-16 month group and the 18-22 month group, which were part of the same longitudinal experiment.

NOL and NOR tests are a variation of the same task and are both based on the innate preference of mice to explore novel objects rather than familiar ones, and have been used to test hippocampal memory (Assini, Duzzioni, and Takahashi 2009; Barrett et al. 2011). In these tests, the mice are first allowed to familiarise themselves with two identical objects in an otherwise empty arena, after which one of the objects is moved to a novel location- a cognitively-normal mouse would be expected to spend more time investigating the object in the novel location, rather than the other object. After this test, the previously unmoved object is replaced with a novel one- again, the mouse would be expected to spend more time exploring this object than the familiar one (Denninger, Smith, and Kirby 2018). There is a 30 minute waiting time between each of the three phases: habituation with the identical objects, NOL and NOR.

Statistical analysis did not identify significant memory differences between between wild-type and $App^{NL\text{-}F/NL\text{-}F}$ animals at 6-9 months of age in neither the NOL nor the NOR test (Figure 4.5). Sample size in the NOL test was 9 wild-type mice and 10 $App^{NL\text{-}F/NL\text{-}F}$ mice, and 11 mice for each of the two genotypes in the NOR test.A two-way ANOVA with age and genotype as factors did not identify any of them as having a significant influence on the results.

At 12-16 months, the $App^{NL\text{-}F/NL\text{-}F}$ mice showed a significant reduction in memory in the $App^{NL\text{-}F/NL\text{-}F}$ animals compared to wild-type in the NOL test ($P < 0.05$, Holm-

Sidak test for multiple comparisons, Figure 4.5), concurrent with previous literature (Masuda et al. 2016). At the same age, the AD model cohort performed similarly to the wild-type mice in the NOR test, which was done immediately after NOL. Sample size in the NOL test was 12 mice for each of the two genotypes and for the NOR it was 12 wild-type mice and 11 $App^{NL\text{-}F/NL\text{-}F}$ mice.

When carrying out the longitudinal study at 18-22 months with animals from the 12-16 month cohort, there was large variance within groups. It has been reported that around this age, the $App^{NL\text{-}F/NL\text{-}F}$ animals exhibit attention deficits and pronounced impulsivity (Masuda et al. 2016), which can impact their ability to perform in this particular test and which can account for the large variance. Sample size for both the NOL and NOR test was 13 wild-type mice and 13 $App^{NL-F/NL-F}$ mice.

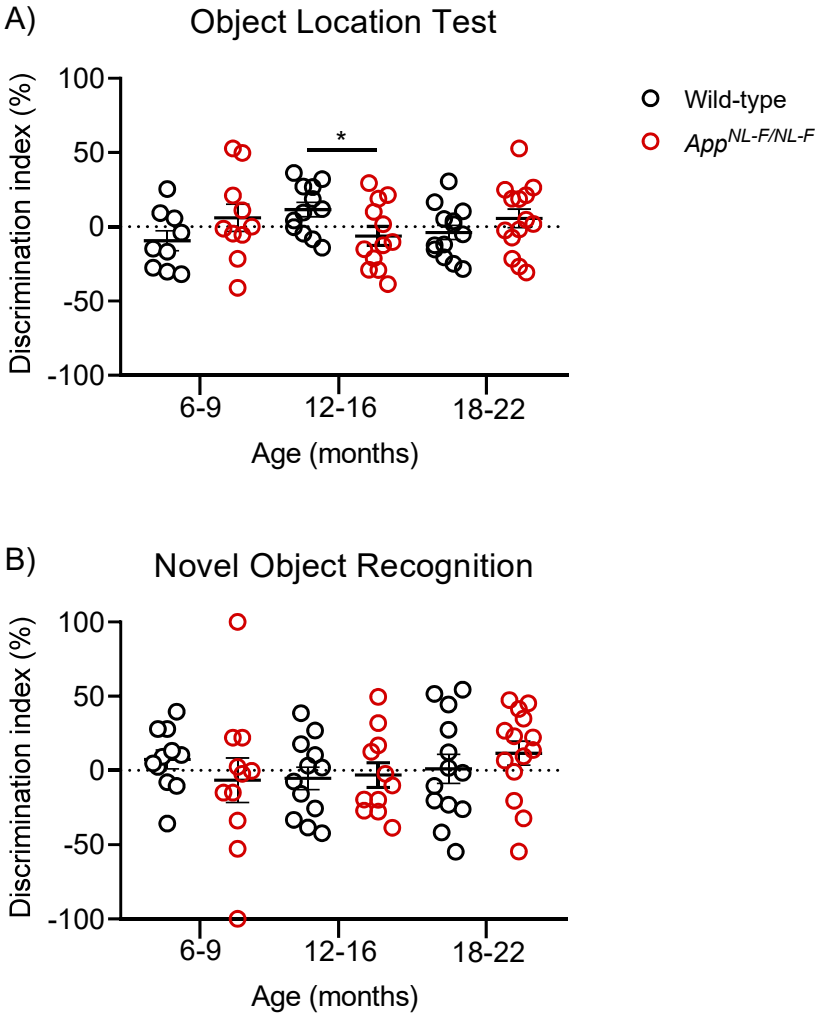

Figure 4.5: Novel object location test identified reduced cognitive performance at 12-16 months in the $App^{NL\text{-}F/NL\text{-}F}$ mice. Results are not significant. Two-way ANOVA with genotype and age as factors, and Holm-Sidak test for multiple comparisons. n=9-14 for each of the two genotypes at each age. The graphs display individual values around cohort averages ± SEM. * P 0.05.

Chapter 5

Results II: Indicators of anxiety

Following the identification of reduced cognitive performance in the AD mouse model, we investigated whether further behavioural changes were present in these animals.

Seeing as anxiety causes a large burden in dementia patients and also exacerbates the burden upon carers, the aim was to investigate anxiety-related behaviours in the $App^{NL\text{-}F/NL\text{-}F}$ animals. For this, an open arena test was used, where the following were measured: whether animals spent more time exploring the open centre of the arena or at the periphery, closer to the walls (thigmotaxis), the distance they travelled and their average speed, as previously described (Hefner and Holmes 2007). Different cohorts of wild-type and $App^{NL\text{-}F/NL\text{-}F}$ animals were tested at 6-9 months, 12-16 months and 18-22 months.

Anxiety-prone animals would be expected to spend more time in the periphery of the arena, as, naturally, that would shelter them from potential danger, compared to the more exposed central area. Likewise, the longer the distance run and the faster they run, the more anxiety-prone they are (Wable et al. 2015).

A two-way ANOVA with genotype and age as factors was performed for statistical analysis, with post-hoc Holm-Sidak test for multiple comparisons. In the case of centre exploration, significant sources of variation were the genotype ($F_{(1,41)}$ =

8.416, $P<0.01$), age ($F_{(2,41)} = 8.326$, $P<0.01$) and the interaction between the two factors ($F_{(2,41)} = 5.779$, $P<0.01$). For the time spent at the periphery, significant sources of variation were the genotype ($F_{(1,40)} = 7.953$, $P<0.01$), age ($F_{(2,40)} = 11.01$, $P<0.001$) and the interaction between the two factors ($F_{(2,40)} = 5.744$, $P<0.01$).

For distance run and speed, the two-way ANOVA did not identify any significant source of variation.

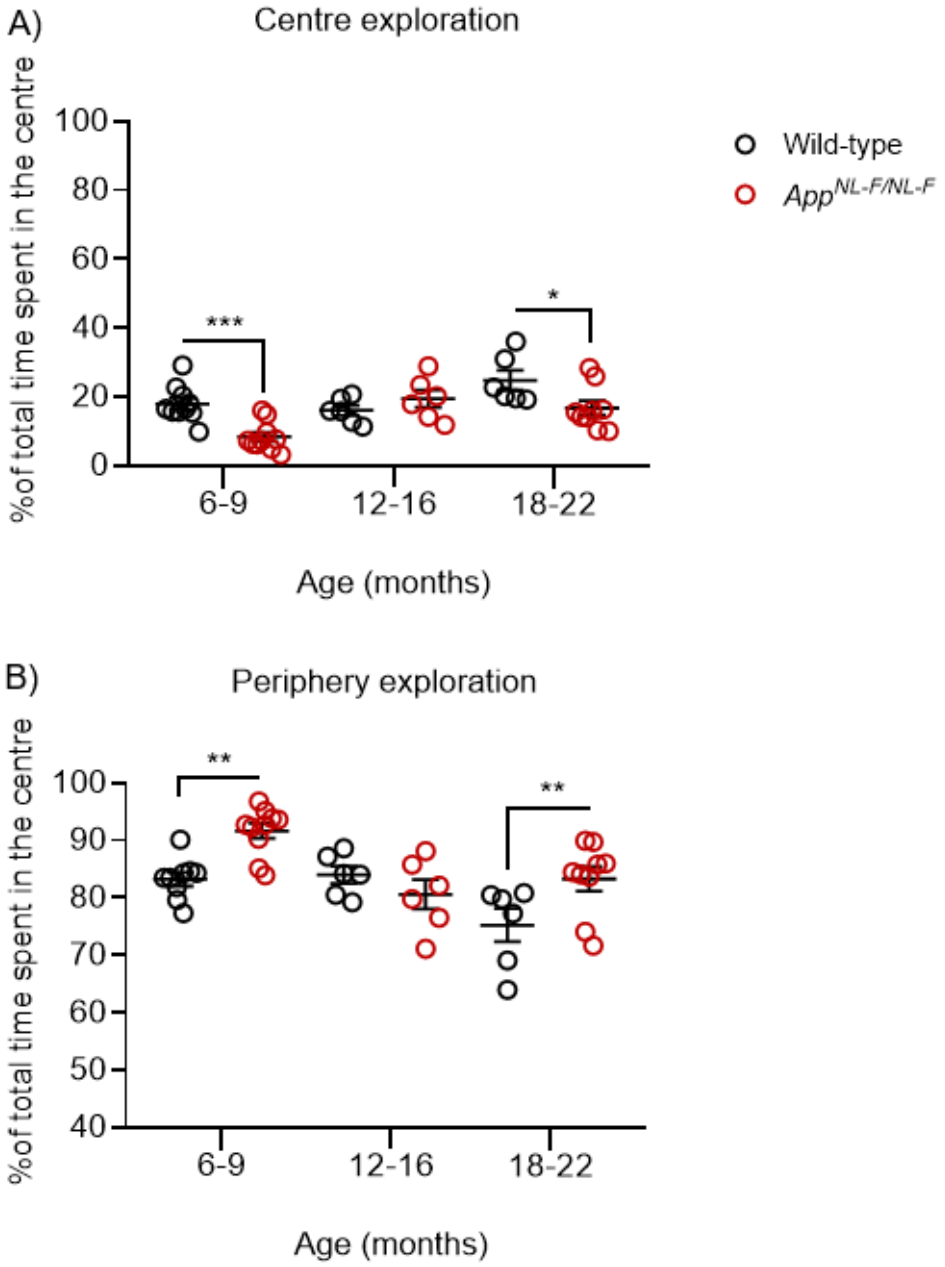

Figure 5.1: *App*$^{NL\text{-}F/NL\text{-}F}$ animals exhibited anxiety-related behaviour at 6-9 months and 18-22 months. Graphs show percentage of the total time spent exploring the centre of the arena (A) and periphery (B), respectively. The graphs display individual values around averages ± SEM. *n*=6-10 for each genotype and age. A two-way ANOVA with genotype and age was used for statistical analysis, followed by post-hoc Holm-Sidak test for multiple comparisons. * $P < 0.05$, ** $P < 0.01$. At 6-9 months one wild-type animal was removed following outlier analysis.

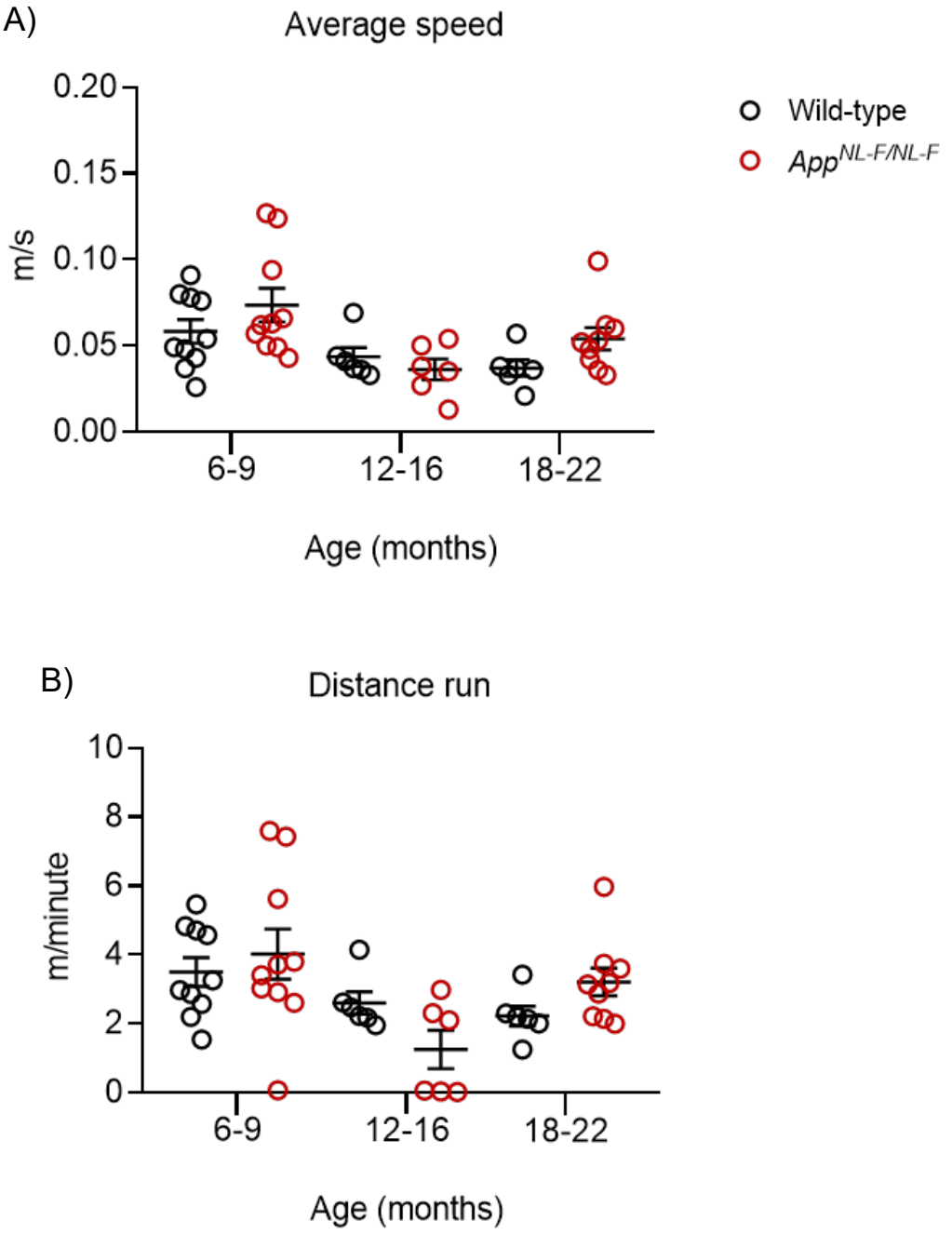

Figure 5.2: The average speed and distance run in a minute did not differ significantly between *App*$^{NL\text{-}F/NL\text{-}F}$ and wild-type mice. Graphs show the average speed (A, m/s) and distance run (B, m/minute), respectively. The graphs display individual values around averages ± SEM. *n*=6-10 for each genotype and age. A two-way ANOVA with genotype and age was used for statistical analysis, followed by post-hoc Holm-Sidak test for multiple comparisons.

App$^{NL\text{-}F/NL\text{-}F}$ animals exhibited anxiety-related behaviour at 6-9 months, as they

spent significantly less time, 53.58 % ± 8.39 % in the centre of the arena than the wild-type animals (P <0.001, Figure 5.1, post-hoc Holm-Sidak test for multiple comparisons). Conversely, they also spent significantly more time, 17.75 % ± 0.25 %, at the periphery (P <0.05, post-hoc Holm-Sidak test for multiple comparisons). No significant anxiety-related behaviour was identified in the $App^{NL\text{-}F/NL\text{-}F}$ animals at 12-16 months. They spent a similar amount of time in the centre and at the periphery and the average speed was similar. At 18-22 months of age, $App^{NL\text{-}F/NL\text{-}F}$ animals showed anxiety-related behaviour, as they spent 10.66 % ± 0.27 % significantly more time at the periphery of the arena than the wild-type animals (P <0.01, Holm-Sidak test for multiple comparisons), and they also spent 32.34 % ± 4.09 % significantly less time in the centre region than the wild-type cohort (P <0.01, Holm-Sidak test for multiple comparisons). The time spent in the periphery of the arena of the wild-type mice from the 6-9-month cohort was removed following its identification as an outlier via outlier analysis performed in GraphPad Prism.

At 6-9 months, the AD model animals performed similarly to wild-type mice in terms of distance travelled and average speed, with not significant differences between the two cohorts (P >0.05 for both measures, post-hoc Holm-Sidak test for multiple comparisons). There were no difference in perfomance at 12-16 months either (P >0.05, post-hoc Holm-Sidak test for multiple comparisons), however, there was great variance within the group.

In terms of distance and average speed observed at 18-22 months, the $App^{NL\text{-}F/NL\text{-}F}$ mice again performed similarly to age-matched wild-type mice (P >0.05 for both measures, post-hoc Holm-Sidak test for multiple comparisons). Even though neither distance nor average speed were significantly increased compared to wild-type animals, the trend was still strongly positive and it suggests that the $App^{NL\text{-}F/NL\text{-}F}$ animals were more anxiety-prone than their age-matched wild-type

counterparts.

The fact that animals from the youngest (6-9 months) and oldest (18-22 months) cohort showed memory deficits in the T-arm maze, corroborated with significantly higher anxiety indicators compared to wild-type is interesting, to say the least. It seems that at 12-16 months, memory deficits and indicators of anxiety are not easily identifiable, or they are attenuated.

5.1 Discussion- $App^{NL-F/NL-F}$ mice exhibit cognitive impairment and anxiety

By using several behavioural assays for cognitive deficits, this study corroborates evidence from previous studies that have investigated such differences in the $App^{NL-F/NL-F}$ animals (Saito et al. 2014; Masuda et al. 2016) and furthers our understanding of the model.

Interestingly, in the T-arm maze, the $App^{NL-F/NL-F}$ animals performed significantly worse overall both at 6-9 months and 18-22 months, but not at 12-16 months. In a neurodegenerative disease with progressive worsening such as AD, a consistent cognitive decline would be expected. However, the T-arm maze results from this study suggest perhaps not an improvement, but rather a temporary reduction in pathology acceleration, a brief plateau in memory impairment in the AD model at 12-16 months.

How these results compare to other similar studies?

Previously, the two seminal studies on this mouse model reported reduced cognitive performance at different ages: at 8-12 months (Masuda et al. 2016) and 18 months (Saito et al. 2014) in the IntelliCage and Y-maze, respectively. The IntelliCage study covered several parameters such as memory deficits or compulsive behaviour. It should be noted that the two different studies reported cognitive differences at different ages and used different behavioural tests. The present study aimed to bridge that gap by using three memory tests across three different age groups. The rationale behind using three different tests was to identify the most appropriate one for these animals by trialing tests commonly used in the literature (Deacon and Rawlins 2006; Stewart, Cacucci, and Lever 2011; Denninger, Smith, and Kirby

2018). Overall, in this study, cognitive impairment was identified starting at 6-9 months of age, through to old age at 18-22 months, which is consistent with the findings in the previous two studies.

To make matters even more noteworthy, the open arena test which was aimed at identifying anxiety-related behaviour, revealed that while $App^{NL\text{-}F/NL\text{-}F}$ animals showed increased anxiety behaviour at both 6-9 months and 18-22 months cohorts, that same behaviour was not present at 12-16 months. Arguably, the sample size for the 12-16 months was reduced compared to the other two age cohorts, however, the variability within the group was smaller and it can be seen that all the animals performed similarly. The sample size for this test should be increased in further research, but the current data are still indicating an important notion- that there might be a time-point during pathology where the progression of symptoms such as cognitive decline and anxiety slows down temporarily. Further research is required to confirm this assumption, and the time-point identified could be useful in at least two ways: if cognitive decline does slow reduced progression at this particular age in AD mouse models, behaviour analysis in response to drug administration should be carried out either at earlier or later stages, so as to increase chances of identifying improvements in cognitive performance. Secondly, if indeed cognitive worsening decelerates, this age represents a good point for administering therapy to halt further cognitive decline if and when such therapy becomes available.

Each of the three trials in the T-arm maze was considered a standalone measurement of the memory of the mice. However, if they were to be considered as repeated measures, performing a two-way ANOVA for repeated measures with a post-hoc Tukey test revealed that the AD model mice performed significantly worse than the wild-type animals across the board ($P < 0.01$, factors were age and genotype). This further reinforces the idea that there is a reduced performance in cognitive tasks

in the $App^{NL\text{-}F/NL\text{-}F}$ animals and although not straightforward to identify, it can be revealed experimentally.

5.1.1 Learning and performance in the maze

Could a larger deficit not have been detected due to poor performance in the control cohort? This is possible, and has been reviewed in (Stewart, Cacucci, and Lever 2011), which identified studies where control animals performed poorly in the T-arm maze (Zhuo et al. 2007; Deacon et al. 2008). They would normally be expected to perform correctly and to alternate in more than 50% of all trials. The wild-type animals in the current study have, overall in the three trials, alternated correctly 60% of the time at 6-9 months, 48% of the time at 12-16 months and 58% of the time at 18-22 months. Poor control performance could be linked to age, anxiety or apathy, that could be present in the wild-type mice as well $App^{NL\text{-}F/NL\text{-}F}$ animals. Therefore, data from wild-type animals where they only alternated correctly 50% of the time might be difficult to interpret correctly when compared to data from $App^{NL\text{-}F/NL\text{-}F}$ mice; with low alternation levels that are close to chance, the mice might not have formed a memory of the maze and the task might not have worked as planned. If wild-type animals consistently perform only 50% or lower correct alternations, changes to animal housing, handling or maze and testing conditions should be made.

The mice in this study were all motivated to run, as no apparent difference in task start latency was observed between genotypes and ages. One way to improve the likelihood of detecting a more significant memory impairment is to increase the sample size- this is being done in the research group, as another member of the lab is currently testing different mouse models and wild-type animals.

Moreover, the fact that the same level of cognitive impairment at the same age was

not detected through all tests utilised suggests the deficit between the AD model and wild-type mice is not extraordinary. However, the reduction in cognitive performance is significant enough to be detectable.

Looking at the graphics from the polled data in the T-arm maze where the $App^{NL\text{-}F/NL\text{-}F}$ mice failed to alternate, it might be suggested that these mice may have displayed a preference for the part of the maze they entered first and in fact, preference might have been measured instead of alternation. However, that was not the case, as none of the two genotypes showed any predisposition towards neither the ”left” nor the ”right” arm of the maze and first entries to arms were not biased towards one or the other.

To bypass this, in the future this experiment could be repeated by carrying out the first run without any rewards and then introducing a reward in the maze. This would influence the mouse to search for the reward and it might help activate the innate preference to alternate between the two arms of the T-maze.

All things considered, one also needs to be mindful of the shortcomings of AD mouse models. The $App^{NL\text{-}F/NL\text{-}F}$ is a second-generation mouse model, which has been shown to follow human progression of AD more faithfully. However, it is not perfect, and while investigation of cellular pathology in this model mirror pathology identified in human patients (see next chapters), it has been difficult to identify a clear cognitive deficit that worsens with age, as proven by this study and the two seminal studies discussed previously. More research is needed for a clear answer, but until that is done, the model is excellent for targeting and investigating physiological hallmarks of AD, as well as modest cognitive deficits.

The next step of the behavioural analysis was to investigate indicators of anxiety. Anxiety has been identified from tomographic scans of patients with cognitive impairment to be associated with increased Aβ deposition and to act as a predictor

of faster cognitive decline (Bensamoun et al. 2015; Johansson et al. 2020). Psychological symptoms such as anxiety are experienced by at least 6 out of 10 patients suffering from dementia (Lyketsos 2000), which can also lead to more pronounced stress in caregivers (Kaufer et al. 2000).

The main indicators of anxiety investigated in this study were preference for a sheltered area (arena periphery) and reluctance to spend time in an exposed area (centre of arena). Such anxiety indicators were significantly more pronounced at 6-9 and 18-22 months in the $App^{NL\text{-}F/NL\text{-}F}$ animals, both ages at which they showed reduced memory performance in the T-arm maze, but not at 12-16 months, age at which the AD mice performed similarly to wild-type animals in the T-arm maze, but at which they performed more poorly in the NOL test. As mentioned in chapter 4, this could indicate that, perhaps, after the initial onset of memory deficit, some mechanisms are at play which temporarily slow the progression of psychological symptoms such as anxiety. The anxiety indicators investigated in this study have not been measured in this mouse model. However, the model has been shown to exhibit compulsive behaviour from 8 to 13 months (Masuda et al. 2016). Moreover, apathy is also a known symptom of AD in human patients (Bensamoun et al. 2015) and perhaps at 12-16 months, apathy is a psychological symptom that is more heavily encountered than anxiety, which could mask the presence of anxiety in the $App^{NL\text{-}F/NL\text{-}F}$ animals, making detection unlikely, and also mask any memory deficits in the T-arm maze, unlike at the other ages- the animals could be more apathetic and indifferent to the choices they make. However, with all three age groups investigated, the mice ran well in the maze and no apparent difference in the start of different runs was detected.

Identifying anxiety as a symptom in the $App^{NL\text{-}F/NL\text{-}F}$ model improves its use as a preclinical model and could prove helpful in testing anxiolytic drugs.

5.2 Comparison of the $App^{NL/NL}$ and other mouse models of AD

First-generation AD mouse models, which were obtained through overexpression of APP, do present similarities with human AD pathology: neuronal loss, Aβ peptide accumulation, gliosis and memory deficits . However, it has been shown that these models also exhibit abnormal pathology such as overproduced APP fragments that are not Aβ, which could lead to yet unknown cellular or molecular interactions that are not relevant nor characteristic of human AD pathology (Sasaguri et al. 2017). On the other hand, the $App^{NL\text{-}F/NL\text{-}F}$ mouse does not characteristically express hyperphosphorylated tau tangles, a classical hallmark of AD, which only appears stochastichally in this mouse model after 24 months of age. It has been preferred over the $App^{NL/NL}$, which shows uncharacteristically slow progression of pathology, or the $App^{NL\text{-}G\text{-}F/NL\text{-}G\text{-}F}$, where A$\beta$ deposition takes place very early in the course of the disease, again not matching the pathological progression seen in human patients (Saito et al. 2014). The lack of tau expression in the $App^{NL\text{-}F/NL\text{-}F}$ model serves to disentangle tau and Aβ pathology. Furthermore, models expressing both pathological hallmarks have been difficult to breed and maintain. However, a novel knock-in APP and human tau model has been successfully bred, App^{NL-G-F}/MAPT, which harbours the Swedish (NL), Iberian (F) and Arctic (G) APP mutations of the original APP model crossed with MAPT knock-in mice, where the human tau gene has been inserted in the mouse genome (Saito et al. 2019). According to the original study, this model exhibits cognitive deficits at 12 months in the Y-maze, 6 months later than the original $App^{NL\text{-}G\text{-}F/NL\text{-}G\text{-}F}$ animals (Saito et al. 2014), but more in line to temporal progression of human AD. Current studies in the research group are using this mouse model to investigate memory deficits further as well as anxiety.

For now, the $App^{NL\text{-}G\text{-}F/NL\text{-}G\text{-}F}$ model represents a useful preclinical tool for studying and reporting on characteristic symptoms of AD.

Chapter 6

Results III: Pathological markers of AD

Following the identification of reduced cognitive performance in $App^{NL\text{-}F/NL\text{-}F}$ animals, a top-down approach was employed to investigate pathological changes at cellular levels. The study focused on the lateral entorhinal cortex (LEC) and CA1, as they are some of the first brain regions to be affected in AD (Neill 1995; Khan et al. 2013). The changes investigated concerned typical hallmarks of AD such as neuroinflammation, Aβ accumulation and pathological effects on neurotransmitter transporter systems and cell number. The changes were assessed in age-matched wild-type and $App^{NL\text{-}F/NL\text{-}F}$ animals at 1-3 months and 9-15 months.

To report on neuroinflammation, the levels of gliosis were assessed- the proliferation of microglia and astrocytes. For this, brain tissue from $App^{NL\text{-}F/NL\text{-}F}$ and age-matched wild-type mice was stained for glial fibrillary acidic protein (GFAP, marks astrocytes) and cluster of differentiation (CD) 68 (marks microglia), as is accepted in the field (Hol et al. 2003; Hopperton et al. 2017), and the levels of those two markers were measured.

Overall, there was a significant increase in Aβ, GFAP and CD68 levels at 9-15 months in the LEC and CA1.

6.1 Aβ, astrocytes and microglia significantly accumulate in disease

6.1.1 Immunofluorescence staining results

Aβ and neuroinflammatory markers microglia and astrocytes are highly interlinked in AD. Healthy microglia and astrocytes are protective and normally process Aβ to alleviate the pathological burden- however, in AD, they become dysfunctional, their processing mechanisms are affected and they promote Aβ accumulation as well as excitatory synaptic dysfunction (Nagele et al. 2003; Allen et al. 2012). Moreover, microglia and astrocytes also secrete pro-inflammatory factors and other toxic molecules in disease (Tuppo and Arias 2005), which contributes to further pathology increase.

Confocal microscopy analysis of tissue individually immunostained for Aβ, GFAP and CD68 showed a a significant increase of both Aβ and markers in the $App^{NL\text{-}F/NL\text{-}F}$ in both CA1 and LEC at 9-15 months, when compared to age-matched wild-type animals (Figure 6.1). The data was analysed with a two-way ANOVA with genotype and age as factors. For the Aβ data in the CA1, both age and genotype were identified to contribute significantly to the variation in data, as well as the interaction between the two: $F_{(1,12)} = 31.17$ ($P < 0.0001$), $F_{(1,12)} = 211.8$ ($P < 0.0001$), and $F_{(1,12)} = 31.14$ ($P < 0.0001$), respectively. In the LEC, both age and genotype as well as the interaction had a significant effect on the variation in the data, as well: $F_{(1,12)} = 41.26$ ($P < 0.0001$), $F_{(1,12)} = 168.0$ ($P = 0.0001$), and $F_{(1,12)} = 40.25$ ($P = 0.0001$), respectively.

For the CD68 data in the CA1, the factors introducing significant variation in the data were genotype ($F_{(1,11)} = 37.42$, $P < 0.0001$), age ($F_{(1,11)} = 28.52$, $P < 0.001$)

and their interaction ($F_{(1,11)}$ = 19.00, P <0.01). Similarly, all three components introduced variation in CD68 levels in the LEC: $F_{(1,14)}$ = 31.83 (P <0.0001), $F_{(1,14)}$ = 43.54 (P <0.0001) and $F_{(1,14)}$ = 30.47 (P <0.0001), respectively.

Variance in the GFAP CA1 data was introduced by the genotype factor ($F_{(1,18)}$ = 70.59, P <0.0001) and in the LEC data by genotype ($F_{(1,15)}$ = 40.86, P <0.0001), age ($F_{(1,15)}$ = 85.10, P <0.0001) and the interaction between the two ($F_{(1,15)}$ = 40.33, P <0.0001).

The results from the multiple comparison tests reported below come from the comparisons between the two genotypes: wild-type and $App^{NL\text{-}F/NL\text{-}F}$ mice, age-matched.

In the $App^{NL\text{-}F/NL\text{-}F}$ mice, Aβ was at similar levels to Aβ in wild-type animals in LEC at 1-3 months of age (P >0.05, post-hoc Holm-Sidak test for multiple comparisons, n=4 wild-type mice and 3 $App^{NL\text{-}F/NL\text{-}F}$ mice), but it increased by a hugely significant 124.34 % ± 20.66 % at 9-15 months in the $App^{NL\text{-}F/NL\text{-}F}$ model compared to wild-type animals of the same age (P<0.0001, post-hoc Holm-Sidak test for multiple comparisons, n=4 wild-type mice and 5 $App^{NL\text{-}F/NL\text{-}F}$ mice). In the CA1, Aβ levels in the $App^{NL\text{-}F/NL\text{-}F}$ cohort were no different to those in age-matched wild-type mice at 1-3 months (P >0.05, post-hoc Holm-Sidak test for multiple comparisons, n=4 wild-type mice and 3 $App^{NL\text{-}F/NL\text{-}F}$ mice). However, there was highly significant 191.69 % ± 33.99 %accumulation of Aβ in the AD model at 9-15 months compared to wild-type (P <0.0001, post-hoc Holm-Sidak test for multiple comparisons, n=5 wild-type mice and 4 $App^{NL\text{-}F/NL\text{-}F}$ mice).

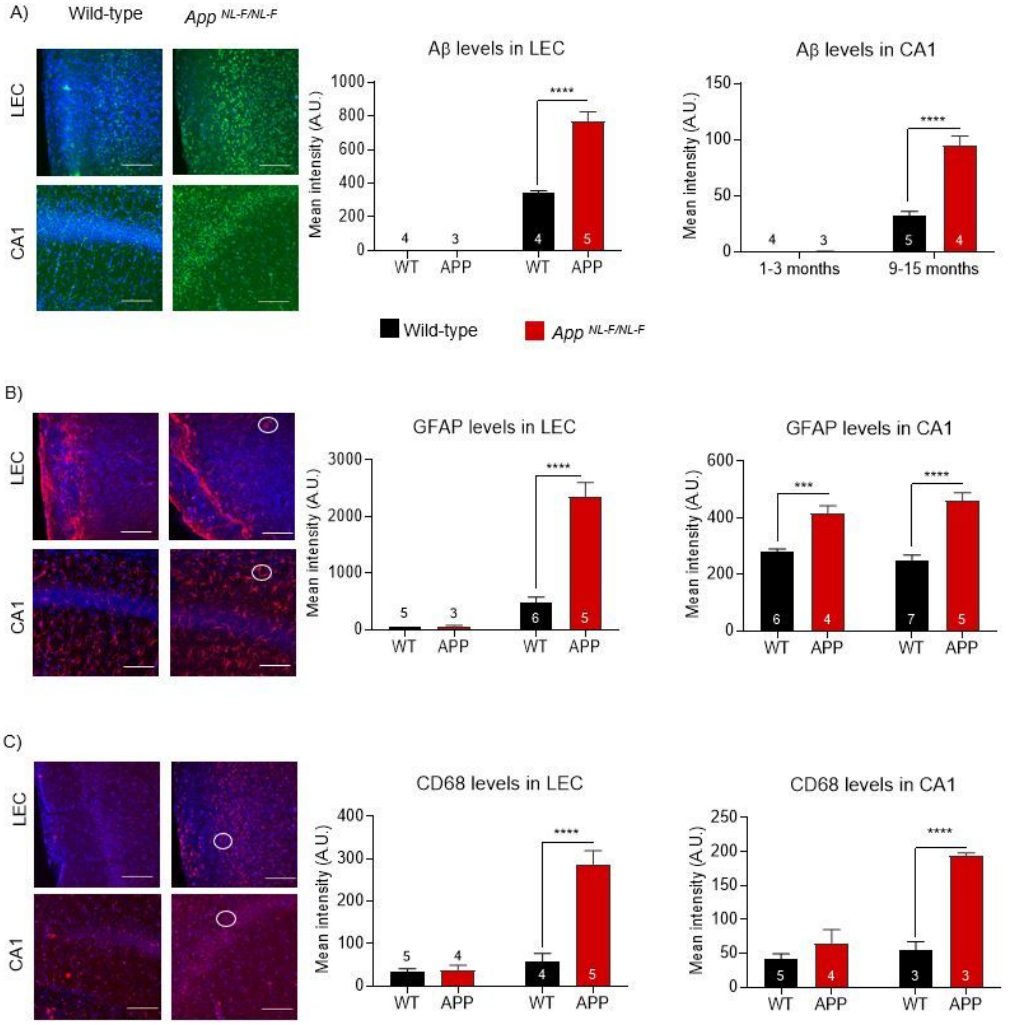

Figure 6.1: The levels of Aβ and neuroinflammatory markers GFAP and CD68 increased in the $App^{NL\text{-}F/NL\text{-}F}$ model at 9-15 months in both LEC and CA1. Panels show representative images for Aβ (A), GFAP (B, staining for astrocytes) and CD68 (C, staining for microglia) in wild-type and age-matched $App^{NL\text{-}F/NL\text{-}F}$ animals, at 20X magnification. Scale bars represent 10μm. White circles indicate pathology in the $App^{NL\text{-}F/NL\text{-}F}$. Marker levels are shown as cohort mean + SEM. Two-way ANOVA with genotype and age as factors, with post-hoc Holm-Sidak's test for multiple comparisons. Sample size displayed on each bar. *P <0.05, **P <0.01, ****P <0.0001. A.U. = arbitrary units.

The levels of GFAP in the LEC at 1-3 months were unchanged in the $App^{NL\text{-}F/NL\text{-}F}$ cohort (P>0.05, post-hoc Holm-Sidak's test for multiple comparisons, n=5 wild-type mice and 3 $App^{NL\text{-}F/NL\text{-}F}$ mice). However, at 9-15 months in LEC, there was a significant 390.72 % ± 22.29 % increase in GFAP levels in the $App^{NL\text{-}F/NL\text{-}F}$

group (P <0.0001, post-hoc Holm-Sidak's test for multiple comparisons, n=6 wild-type mice and 5 $App^{NL\text{-}F/NL\text{-}F}$ mice). At 1-3 months in CA1, there were significant increases in GFAP in the disease model: 49.80 % ± 5.97 % (P <0.001, post-hoc Holm-Sidak's test for multiple comparisons, n= 6 wild-type mice and 5 $App^{NL\text{-}F/NL\text{-}F}$ mice). In the CA1 at 9-15 months, the levels of GFAP also showed a large increase in the disease group by 83.66 % ± 11.94 % (P <0.0001, post-hoc Holm-Sidak's test for multiple comparisons, n=7 wild-type mice and 5 $App^{NL\text{-}F/NL\text{-}F}$ mice).

CD68 levels in the LEC did not show any difference between wild-type and the disease model at 1-3 months of age (P>0.05, post-hoc Holm-Sidak test for multiple comparisons, n=5 wild-type mice and 4 $App^{NL\text{-}F/NL\text{-}F}$ mice), while at 9-15 months there was a 405.37 % ± 98.20 % significant increase in the LEC in the same group (P <0.0001, post-hoc Holm-Sidak test for multiple comparisons, n=4 wild-type mice and 5 $App^{NL\text{-}F/NL\text{-}F}$ mice). At 1-3 months in the CA1 the levels were again unchanged between the two genotypes, (P >0.05, post-hoc Holm-Sidak test for multiple comparisons, n=5 wild-type mice and 4 $App^{NL\text{-}F/NL\text{-}F}$ mice). At 9-15 months there was a 251.76 % ± 11.18 % significant increase in CA1 in the $App^{NL\text{-}F/NL\text{-}F}$ experimental group (P <0.001, post-hoc Holm-Sidak test for multiple comparisons, n=3 wild-type mice and 3 $App^{NL\text{-}F/NL\text{-}F}$ mice).

6.1.2 Immunoperoxidase staining results

The findings from immunofluorescence staining presented in the previous section were corroborated with immunoperoxidase staining in the old-age cohort at 9-15 months, where levels of all three markers were found to increase significantly in both the LEC and CA1. Figure 6.2 shows how aggressive these markers become in disease, as they clump and aggregate at the site of AD injury. A two-way ANOVA with genotype and brain region as factors was performed for statistical analysis,

with post-hoc Holm-Sidak tests. For the Aβ data, the significant sources of variation were genotype ($F_{(1,24)}$ = 52.88, P <0.0001) as well as the interaction between genotype and region ($F_{(1,24)}$ = 11.32, P <0.01). The post-hoc results reported below represent comparisons of the two genotypes: wild-type and $App^{NL\text{-}F/NL\text{-}F}$ mice.

In the LEC, Aβ levels were significantly more abundant in the $App^{NL\text{-}F/NL\text{-}F}$ group, by 120.18 % ± 6.76 % (P <0.0001, post-hoc Holm-Sidak test for multiple comparisons, n=3 wild-type mice and 8 $App^{NL\text{-}F/NL\text{-}F}$ mice). In the CA1 region of $App^{NL\text{-}F/NL\text{-}F}$, levels of Aβ from immunoperoxidase staining showed an increase in the disease model by 37.47 % ± 1.19 % (P <0.01, post-hoc Holm-Sidak test for multiple comparisons test, n=6 wild-type mice and 11 $App^{NL\text{-}F/NL\text{-}F}$ mice)

Significant variation in the CD68 data was introduced by genotype ($F_{(1,16)}$ = 71.97, P <0.0001) and in the GFAP data by genotype as well ($F_{(1,16)}$ = 71.97, P <0.0001). Both CD68 and GFAP markers significantly increased in the AD model, by 82.11 % ± 9.09 % and 69.77 % ± 6.87 %, respectively (P <0.01 for both comparisons, post-hoc Holm-Sidak test for multiple comparisons, n=4 wild-type mice and 5 $App^{NL\text{-}F/NL\text{-}F}$ mice for each of the two markers). In the CA1, GFAP increased by 20.09 % ± 0.78 % (P <0.05, post-hoc Holm-Sidak test for multiple comparisons, n=5 wild-type mice and 6 $App^{NL\text{-}F/NL\text{-}F}$ mice), while CD68 showed a 202.82 % increase ± 1.19 % (P <0.001, post-hoc Holm-Sidak test for multiple comparisons, n=5 wild-type mice and 6 $App^{NL\text{-}F/NL\text{-}F}$ mice).

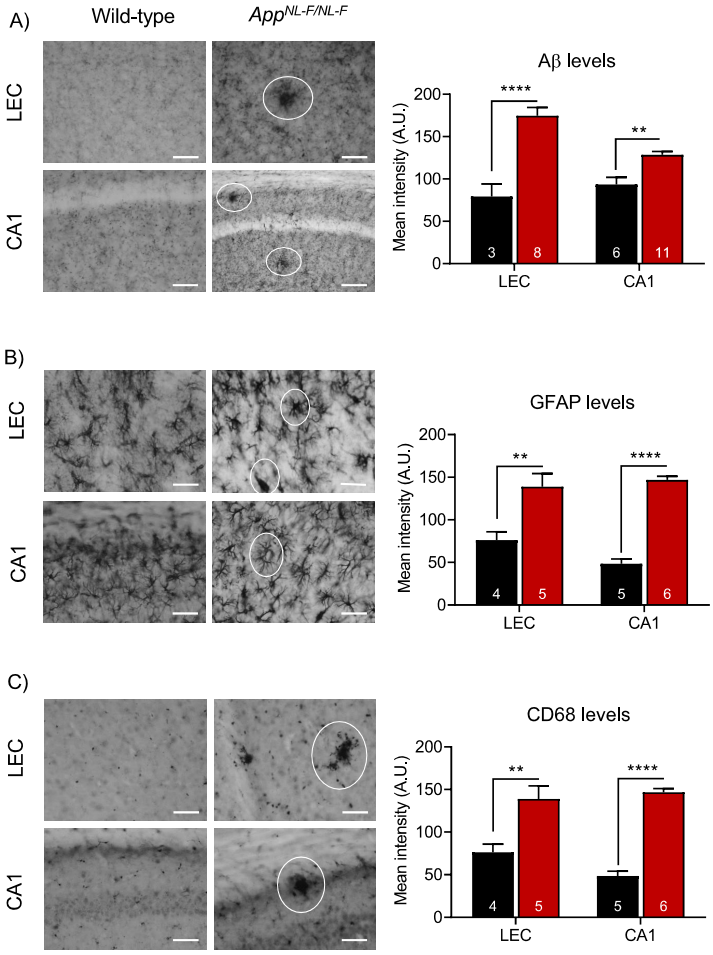

Figure 6.2: The levels of Aβ and neuroinflammatory markers increased in the $App^{NL\text{-}F/NL\text{-}F}$ model at 9-15 months in both LEC and CA1. Panels show representative images for Aβ (A), GFAP (B) and CD68 (C) in wild-type animals and age-matched $App^{NL\text{-}F/NL\text{-}F}$ animals, taken at 40X magnification. White circles indicate pathology in the $App^{NL\text{-}F/NL\text{-}F}$. Scale bars represent 50μm. Marker levels are shown as cohort mean + SEM. Two-way ANOVA with genotype and brain region as factors, with post-hoc Holm-Sidak's test for multiple comparisons. Sample size displayed on each bar. *P <0.05, **P <0.01, ****P <0.0001. A.U. = arbitrary units.

6.2 Discussion

6.3 Aβ, GFAP and CD68 levels increase in the AD model

Significant increases in Aβ, GFAP and CD68 were observed in both LEC and CA1 in the $App^{NL-FNL-F}$ mice at 9-15 months, compared to wild-type age-matched mice. The increase in these three markers matches known pathology in human AD patients: Aβ accumulation, astrocytosis and microgliosis (Hardy and Higgins 1992; Hol et al. 2003; Khan et al. 2013; Hopperton et al. 2017).

Both microglia and astrocytes become "activated" in AD and secrete proinflammatory factors such as toxic cytokines (e.g. tumour necrosis factor), which leads to damage of neurones and neuronal connections (Tuppo and Arias 2005; Liddelow and Barres 2017). Moreover, both types of glial cells become dysfunctional with age, which impairs clearing mechanisms of toxic cellular compartments or aggregates such as Aβ oligomers and results in failure to clear them out of the intercellular space, leading to further pathological build-up. However, the contribution of these neuroinflammatory markers to AD pathology does not stop here. Indeed, astrocytes have been shown to internalise Aβ peptide, fail to degrade it, thus amassing large amounts of Aβ, then lyse and expel the fragments in the intercellular space in toxic fragments which perpetuate neurodegeneration (Nagele et al. 2003). Furthermore, activated astrocytes affect synapse formation directly, by failing to provide key compounds glypicans, which promote synapse formation (Allen et al. 2012).

The link between astrocytes and microglia and their role in AD goes even deeper and it proves that dysfunctional glial cells are not just pathological by-products.

Indeed, the two types of glial cells secrete APOE and TREM-2, both two major risk factors for AD. APOE helps metabolise fats, is associated with a higher risk of AD and cardiovascular disease and secreted in the liver and brain- in the brain astrocytes are the major secretor of APOE (Zhao et al. 2017). Not all APOE isoforms are associated with a higher risk of AD, but rather the isoform $\varepsilon 4$ (Kim, Basak, and Holtzman 2009). The full degree of the $\varepsilon 4$ involvement in AD is yet unknown, however, the association between APOE and astrocytes highlights the importance of assessing the astrocyte contribution to AD genetic risk, through its association with APOE, as the latter is responsible for instigating an Aβ clearance response (Koistinaho et al. 2004). This risk translates to impaired processing of Aβ or hyperphosphorylation of tau (Kim, Basak, and Holtzman 2009). It should be noted that the $\varepsilon 2$ allele of apoE has been reported to be protective in AD, reducing the risk of developing the disease (Corder et al. 1993).

TREM2 dysfunction does not directly affect the accumulation of Aβ, but rather the behaviour of microglia, which becomes inefficient at internalising and processing the peptide, thus contributing to its accumulation (Gratuze, Leyns, and Holtzman 2018). The highest level of *TREM2* expression in the brain can be found in the hippocampus (Forabosco et al. 2013) and certain variants of *trem2* can have a similar effect on the genetic risk of AD, as one copy of the $\varepsilon 4$ allele (Gratuze, Leyns, and Holtzman 2018).

The findings in this study show that increased levels of microgliosis and astrocytosis are present in the $App^{NL\text{-}F/NL\text{-}F}$ model, which could, at least in part, explain the high levels of Aβ that characterise AD pathology. Perhaps targeting microglia and astrocytes in AD can represent the next focus for therapy.

Chapter 7

Results IV: Neurones show differential survival in AD

It is important to understand the changes that different cell types undergo in AD so as to decode the mechanisms of the disease and the full involvement of the different cells that make up vast and complex networks. Understanding their individual role in AD would help to better disentangle their contribution to pathology. Moreover, it would help us understand how they affect other cells with which they are in contact. One of the key aims of this study was to assess how pyramidal cells and major modulatory interneurones were affected in disease. The study reports on pyramidal cells- the main excitatory units in the mammalian cortex and on major inhibitory interneurones- calretinin (CR)-expressing, somatostatin (SST)- expressing and cholecystokinin (CCK)-expressing cells. These three interneurone sub-types were chosen based on the knowledge that they are modulatory inhibitory interneurones, which make contact with a wide array of other cell populations. For example, SST and CCK cells fine-tune the activity of pyramidal cells, as they make contacts on pyramidal cells (Maccaferri and McBain 1995; Halasy et al. 1996). CR cells are specialised to only make connections onto other inhibitory interneurones, including SST and CCK cells and other CR cells as well, playing a very important role in disinhibition (Freund and Gulyas 1997)- the inhibition of inhibitory cells. Moreover, CCK, SST and Ca^{2+}/calmodulin-dependent protein kinase II (CaMKII)-α (which stains pyramidal cells) are important in memory formation and CCK has been reported to

be involved in anxiogenic behaviour (Montigny 1989; Schneider et al. 2008). Seeing as a gradual loss of the ability to form and recall memory as well as the presence and increase risk of anxiety are key AD symptoms, the cells studied in this chapter are of great importance to the fundamental mechanisms of the disease.

The hippocampus is one of the regions to show atrophy in AD, as evidenced by imaging studies in AD patients compared to healthy subjects. On a microscopic level, this is manifested by dystrophic neurites, loss of synapses, somatic shrinkage and loss of cell numbers (Gomez-Isla et al. 1996). In this chapter, the densities of pyramidal cells and the inhibitory interneurones that express CR, CCK and SST were investigated so as to assess the level of cell density loss in the $App^{NL\text{-}F/NL\text{-}F}$ mouse model.

To assess the anatomical density of pyramidal cells, tissue from $App^{NL\text{-}F/NL\text{-}F}$ and wild-type animals was immunostained for CaMKII-α.

To investigate the anatomical density of interneurones, $App^{NL\text{-}F/NL\text{-}F}$ and age-matched wild-type tissue was immunostained with either antibody to CR, CCK or SST in conjunction with antibody to the enzyme GAD67. Inhibitory cells utilise GAD67 to produce the neurotransmitter GABA from glutamate, therefore this was done to ensure that only cells that maintained neurotransmitter production were selected for analysis. All cells that stained for CR, CCK and SST expressed GAD67 and they were all included in analysis.

7.1 Pyramidal cell density is affected in AD

A characteristic process of AD is the age-dependent loss of pyramidal cells, especially in the hippocampus (Mann 1996). Pyramidal cells are the main excitatory units in the mammalian cortex and are a fundamental part of major

pathways connecting the CA1 hippocampal region with the lateral and medial entorhinal cortex, such as the perforant pathway (Amaral and Witter 1989). Therefore, in this study, the density of pyramidal cells in CA1 and LEC was investigated in the $App^{NL\text{-}F/NL\text{-}F}$ model, especially since it has not been reported before in this mouse model. Cell density was assessed through stereological counts of pyramidal cells in brain tissue. Overall, there was an age-dependent loss of pyramidal cell number in both LEC and CA1 in the $App^{NL\text{-}F/NL\text{-}F}$ mouse model.

The $App^{NL\text{-}F/NL\text{-}F}$ model exhibited significant decrease in the density of pyramidal cells, obtained from anatomical cell counts of confocal microscopy Z-stacks, in both the LEC and CA1 regions in $App^{NL\text{-}F/NL\text{-}F}$ animals compared to age-matched wild-type animals. In the LEC, data from $App^{NL\text{-}F/NL\text{-}F}$ animals showed a significant reduction in pyramidal cell density at all three age groups investigated, measured with a two-way ANOVA with genotype and age as factors, n=3-5 animals per cohort (Figure 7.1). The source of variation in the CA1 data was given by the genotype ($F_{(1,13)} = 5.171$, $P < 0.05$), while in the LEC it was given by the genotype ($F_{(1,14)} = 48.16$, $P < 0.0001$) and age ($F_{(2,14)} = 8.705$, $P < 0.01$).

There were significant reductions in the number of pyramidal cells in the $App^{NL\text{-}F/NL\text{-}F}$ mice: 25.48 % ± 1.07 % at 1-3 months ($P<0.01$), 32.11 % ± 2.92 % ($P < 0.01$) at 4-6 months and 45.70 % ± 9.85 % ($P < 0.01$), at 9-15 months, all results from Holm-Sidak test for multiple comparisons. A reduction in density was also observed in the CA1 in the $App^{NL\text{-}F/NL\text{-}F}$ animals at 9-15 months compared to wild-type: 65.32 % ± 9.95 % ($P < 0.05$, Sidak's test for multiple comparisons). There were no differences between the AD model and wild-type mice neither at 1-3 months nor at 4-6 months when compared to age-matched wild-type mice.

This significant decrease in the number of pyramidal cells follows the typical pathological progression of AD from LEC to CA1. This indicates that pyramidal

cell loss takes place in the $App^{NL\text{-}F/NL\text{-}F}$ model, which has not been previously reported in the literature. The finding reinforces the validity of the $App^{NL\text{-}F/NL\text{-}F}$ as an AD model.

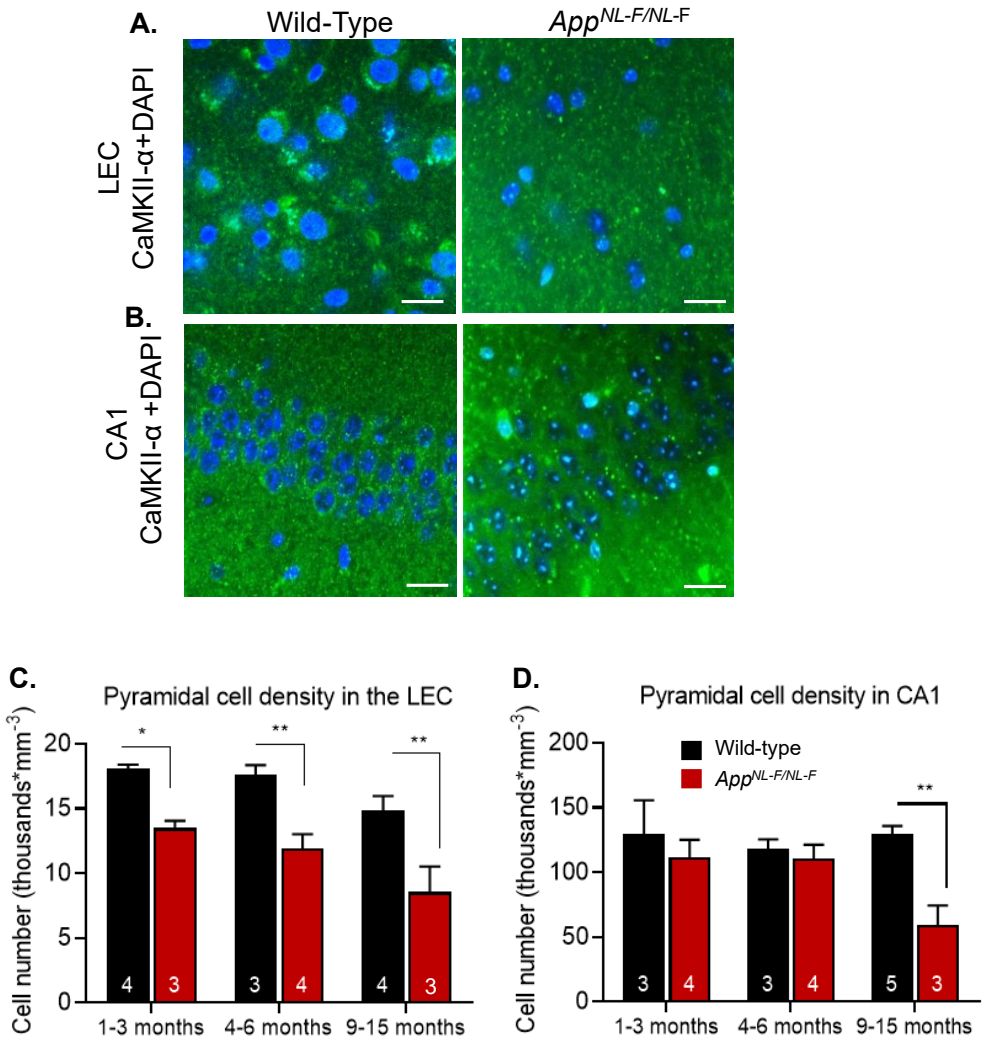

Figure 7.1: Density of pyramidal cells in LEC and CA1 declined in the AD model. Pyramidal cells labelled with antibody to calcium/calmodulin-dependent protein kinase II (CaMKII)- α and secondary antibody Alexa Green 488, costained with the nucleic acid stain DAPI (blue). Panels show representative images from confocal Z-stacks at x63 magnification in the LEC (A) and CA1 (B) of 13-months old wild-type and $App^{NL\text{-}F/NL\text{-}F}$F animals. Scale bars represent 20um. There is gradual decline in DAPI colocalised with CaMKII-α, suggesting neurodegeneration of principal cells. C-D) Cell density is shown as cohort mean + SEM. Two-way ANOVA factoring for age and genotype, with Holm-Sidak test for multiple comparisons. $*P < 0.05$, $**P < 0.01$. Sample size displayed on each bar.

7.1.1 CR interneurones are resilient to alteration in AD

CR cells are specialised to only make connections onto other inhibitory interneurones (themselves included), and this has the ability to trigger a cascade of events: through their inhibition of inhibitory cells they affect excitatory cells that are contacted by these middle players.

A fundamental focus was to assess the anatomical density of the CR cells as this would inform whether they are spared or targeted in disease. Moreover, it would also allow for a comparison with human AD pathology and an assessment of whether the $App^{NL\text{-}F/NL\text{-}F}$ model presents similar pathology. For example, it is known that CR cells are anatomically preserved in human AD patients (Resibois and Rogers 1992; Hof et al. 1993; Fonseca and Soriano 1995), therefore in this study it was investigated whether their density was also maintained in the $App^{NL\text{-}F/NL\text{-}F}$ model, especially in the later stages of the disease in CA1. CR cells are distributed throughout the entorhinal cortex, hippocampus (all strata), and neocortex and account for 10-30% of GABAergic interneurones (Cauli et al. 2014). They are specialised in connecting with other interneurones, among which are SST cells (Cauli et al. 2014). Usually, CR cells are bipolar, but they can also be multipolar. In brain tissue they are visualised by staining for the calcium-binding protein calretinin. Interestingly, CR cells can form connections with other CR cells, even to several cells at a time (Freund and Gulyas 1997).

A two-way ANOVA with genotype and age as factors was performed for statistical analysis and no significant variation within the data was identified.

There were no significant differences in CR cell density between $App^{NL\text{-}F/NL\text{-}F}$ animals and age-matched healthy controls at neither 1-3 months nor at 9-15 months in the CA1 (Figure 7.2D, $P > 0.05$, Sidak test for multiple comparisons,

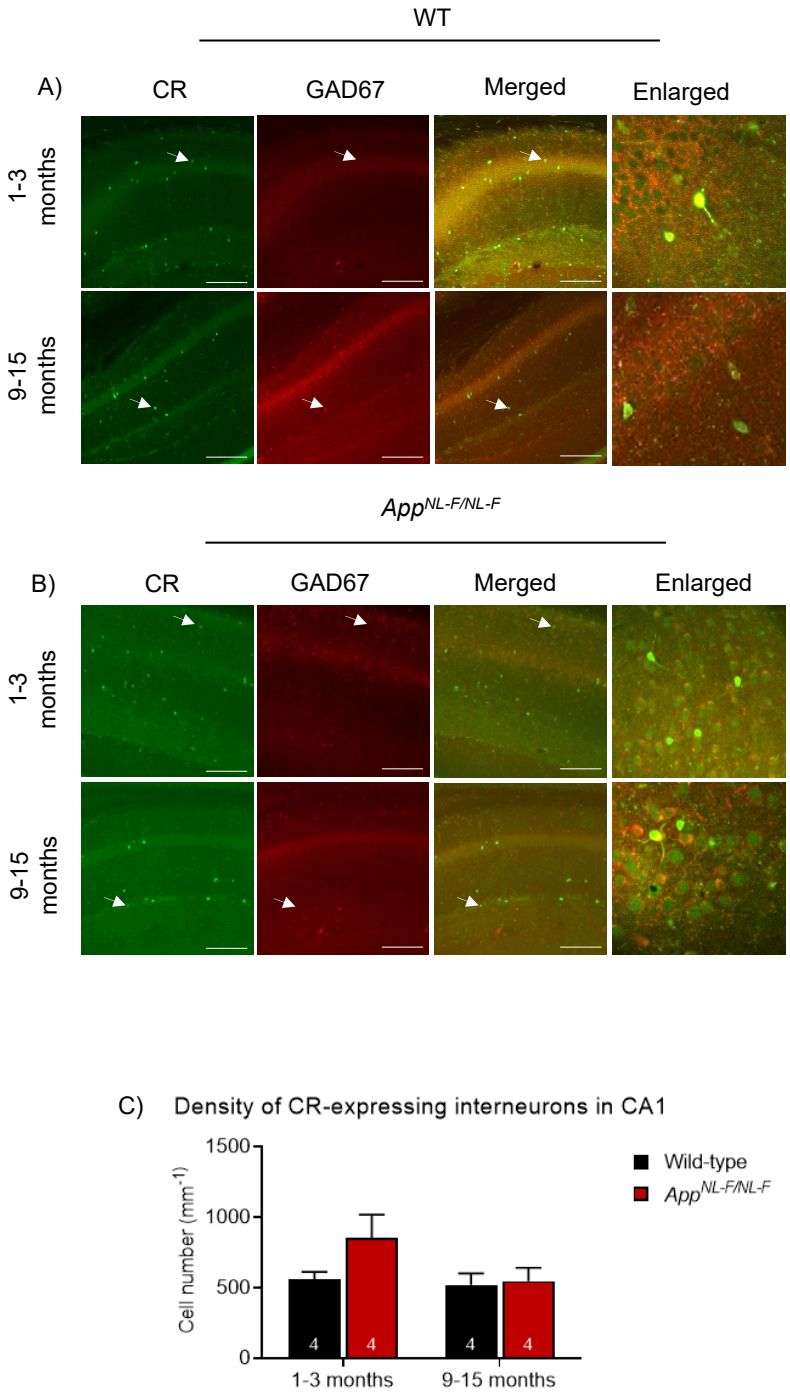

Figure 7.2: The density of CR interneurones was preserved in the $App^{NL\text{-}F/NL\text{-}F}$ model in CA1. A-B) Collapsed confocal microscopy Z-stacks at 20X magnification show CR cells (green, secondary antibody Alexa 488), the enzyme GAD67 (red, secondary antibody Texas Red), merged channels and enlarged. White arrows indicate representative cells. Scale bars represent 100 μm. C) Cell density at 1-3 and 9-15 months in the $App^{NL\text{-}F/NL\text{-}F}$ model and age-matched wild-type animals. A two-way ANOVA factoring for age and genotype did not identify either of them as introducing significant variance to the data. The bars represent the cohort means + SEM. Sample size is displayed on each bar.

n=4 animals per cohort).

7.1.2 Density of CCK interneurones declines in AD

CCK interneurones fine-tune pyramidal cells and are also contacted by CR cells, therefore they are very important components of local CA1 circuits and of interest in this study. In the hippocampus CCK represent one of the two major types of basket cells, named so due to their dendritic branching, the other one being parvalbumin (PV)- expressing cells (Karson et al. 2009). The somata and dendrites of CCK cells are located in SR, while their axon arborises in SP. They target different segments of pyramidal cells: soma, proximal dendrites and the axon initial segment (Halasy et al. 1996). Furthermore, CCK cells also make contact with and are targeted by PV cells (Karson et al. 2009). SST and CR cells also target CCK interneurones, which shows the tight links between different interneurone subtype and circuits (Katona, Acsády, and Freund 1999).

A two-way ANOVA with genotype and age was used for statistical analysis with a post-hoc Holm-Sidak test for multiple comparisons. The ANOVA did not identify neither age nor genotype as contributing significantly to the variation in the data. However, post-hoc tests identified the number of CCK interneurones decreased significantly in the old age in the AD model compared to age-matched wild-type animals (Figure 7.3): 43.92% ± 13.82% (P <0.05, Holm-Sidak test for multiple comparisons n=9 wild-type mice and 7 $App^{NL\text{-}F/NL\text{-}F}$ *mice*). At 1-3 months, there were no significant changes between the AD mouse model and the wild-type cohort (P >0.05, Holm-Sidak test for multiple comparisons, n=6 wild-type mice and 5 $App^{NL\text{-}F/NL\text{-}F}$ mice).

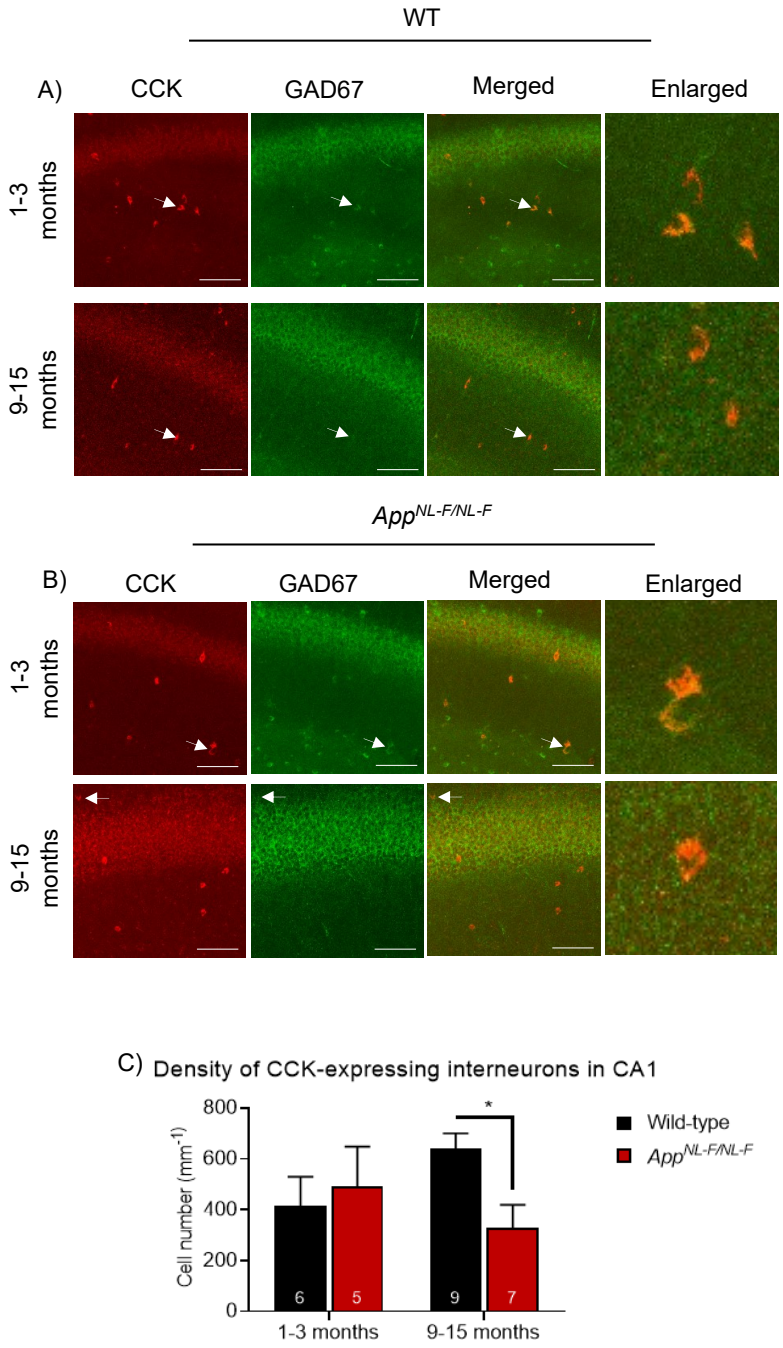

Figure 7.3: The density of CCK interneurones declined in late life in the $App^{NL\text{-}F/NL\text{-}F}$ model in CA1. Collapsed confocal microscopy Z-stacks at 20X magnification show CCK cells (red, secondary antibody Texas Red), the enzyme GAD67 (green, secondary antibody FIT-C), merged channels and enlarged. White arrows indicate representative cells. Scale bars represent 100 μm. C) Cell density at 1-3 and 9-15 months in the $App^{NL\text{-}F/NL\text{-}F}$ model and age-matched wild-type animals.There is a significant drop in the number of CCK interneurones in late life. Two-way ANOVA factoring for age and genotype with post-hoc Holm-Sidak tests. The bars represent the cohort means + SEM. * P <0.05. Sample size is displayed on each bar.

7.1.3 SST interneurones show reduced density in AD

SST interneurones are of much interest in AD, as they are required for modulation of pyramidal cell activity and important in fear conditioning (Kluge et al. 2008). Research shows that their function is disrupted in disease (Ali, Afia B. and A. M. Thomson 2008; Zhang et al. 2016; Shi et al. 2019) and that the neuropeptide SST has been shown to decrease in AD (Davies, Katzman, and Terry 1980). This study focused on OLM SST cells, which get their name because their soma is found in the stratum oriens in the CA1, while their axon spans the lacunosum- moleculare stratum (Ali and Thomson 1998). SST cells in the CA1 form connections with the distal dendrites of PC- which is also the place where PC receive input from the EC (Maccaferri and McBain 1995). It has also been reported that OLM cells inhibit interneurones from SR in CA1 that form synapses with the dendrites of PC and that they reduce or promote LTP (Leao et al. 2012). All of this evidence suggests that OLM cells have an executive control over information flow in CA1 (Lovett-Barron et al. 2012).

A two-way ANOVA with genotype and age as factors was used for statistical analysis, the significant source of variation to the data being the interaction between the two factors ($F_{(1,18)} = 6.217$, $P < 0.01$).

SST cell density was found to decrease in the late stages of AD in the $App^{NL\text{-}F/NL\text{-}F}$ animals compared to age-matched wild-type controls. (Figure 7.4). In the 1-3 months cohort, there were no significant differences between wild-type and $App^{NL\text{-}F/NL\text{-}F}$ animals ($P > 0.05$, n=7 mice per cohort). However, at 9-15 months, there was a 39.22% ± 7.90% significant reduction in the density of SST cells in the $App^{NL\text{-}F/NL\text{-}F}$ group compared to age-matched WT animals ($P < 0.05$, Holm-Sidak test for multiple comparisons, n=4 mice per cohort).

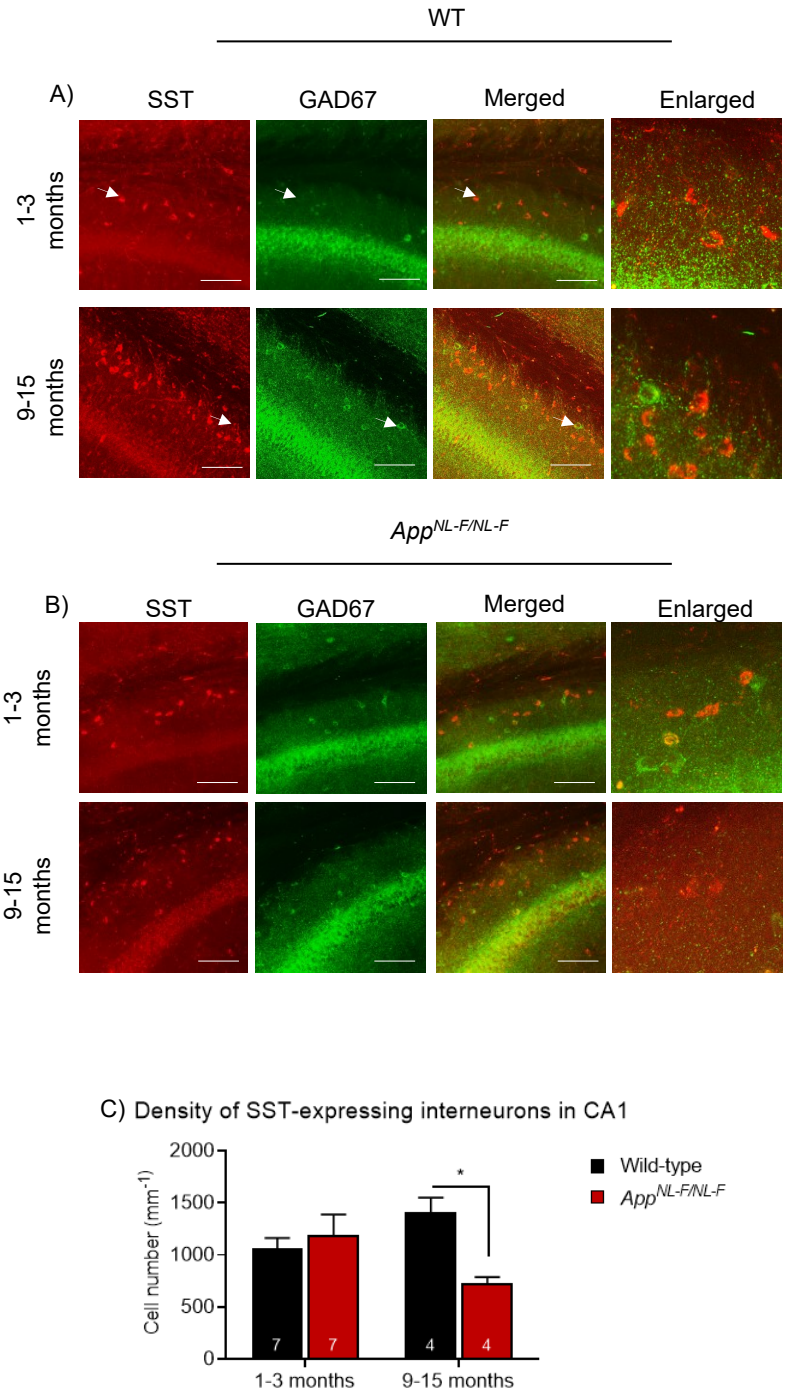

Figure 7.4: The density of SST interneurones declined in late life in the $App^{NL\text{-}F/NL\text{-}F}$ model in CA1. Collapsed confocal microscopy Z-stacks at 20X magnification show SST cells (red, secondary antibody Texas Red), the enzyme GAD67 (green, secondary antibody FIT-C), merged channels and enlarged. White arrows indicate representative cells. Scale bars represent 100 μm. C) Cell density at 1-3 and 9-15 months in the $App^{NL\text{-}F/NL\text{-}F}$ model and age-matched wild-type animals. There is a significant drop in the number of SST interneurones in late life. Two-way ANOVA factoring for age and genotype with post-hoc Holm-Sidak tests. The bars represent the cohort means + SEM. $^*P < 0.05$. Sample size is displayed on each bar.

7.2 Vulnerable CCK and SST cells correlate with Aβ infiltration

After identifying that CCK and SST cell density was significantly reduced in the AD model compared to age-matched wild-type animals, but that CR cell density was maintained, the next step was to investigate whether this differential vulnerability in disease was due to Aβ targeting. Therefore, separate co-staining experiments of Aβ and CCK, SST or CR cells were performed and analysed the data obtained from confocal imaging of the samples. CCK and SST cells showed significant colocalisation with Aβ, while there was limited to no traces of colocalisation between the peptide and CR. It is this differential permeability of Aβ into the cells that could be the contributing factor to cellular and functional disruption.

Aβ deposits are a hallmark of AD which disrupts neuronal function and integrity, causing a dysfunction of signaling pathways and affecting synapse formation and brain circuits (Palop, Chin, and Mucke 2006). Pathological Aβ is cleaved from APP and forms oligomers (Hardy and Higgins 1992). Therefore, in this study, the levels of Aβ were investigated, so as to assess whether they could represent a factor that influences the significant drop in the density of CCK and SST interneurones. Tissue was co-stained with Aβ and staining for CR, CCK and SST, respectively, and the colocalisation between the two stains was investigated. High levels of colocalisation with Aβ would represent an indication of Aβ proximity to those cells and, perhaps, infiltration, which could cause cellular function disruption and would help identify interneurone sub-types that are vulnerable in disease. A one-way ANOVA with interneurone type as factor was used for statistical analysis ($F_{2,7}$=0.4464, P <0.01.) with post-hoc Holm-Sidak tests for multiple comparisons.

Immunostaining for Aβ, CR, CCK and SST cells showed marked infiltration of soluble Aβ into CCK and SST cells, but only traces of Aβ in CR cells (Figure 7.5). Analysis of Z-stacks from confocal images taken at 63X magnification showed a significant 3114.73 % ± 231.79 % more accumulation in CCK cells compared to CR cells (P <0.05, Holm-Sidak test for multiple comparisons) and a striking 4403.16% ± 966.69% (P <0.01, Holm-Sidak test for multiple comparisons) significant increase in soluble Aβ levels in SST interneurones compared to CR cells (Figure 7.5 D), n=cells from 3-4 mice per cohort.

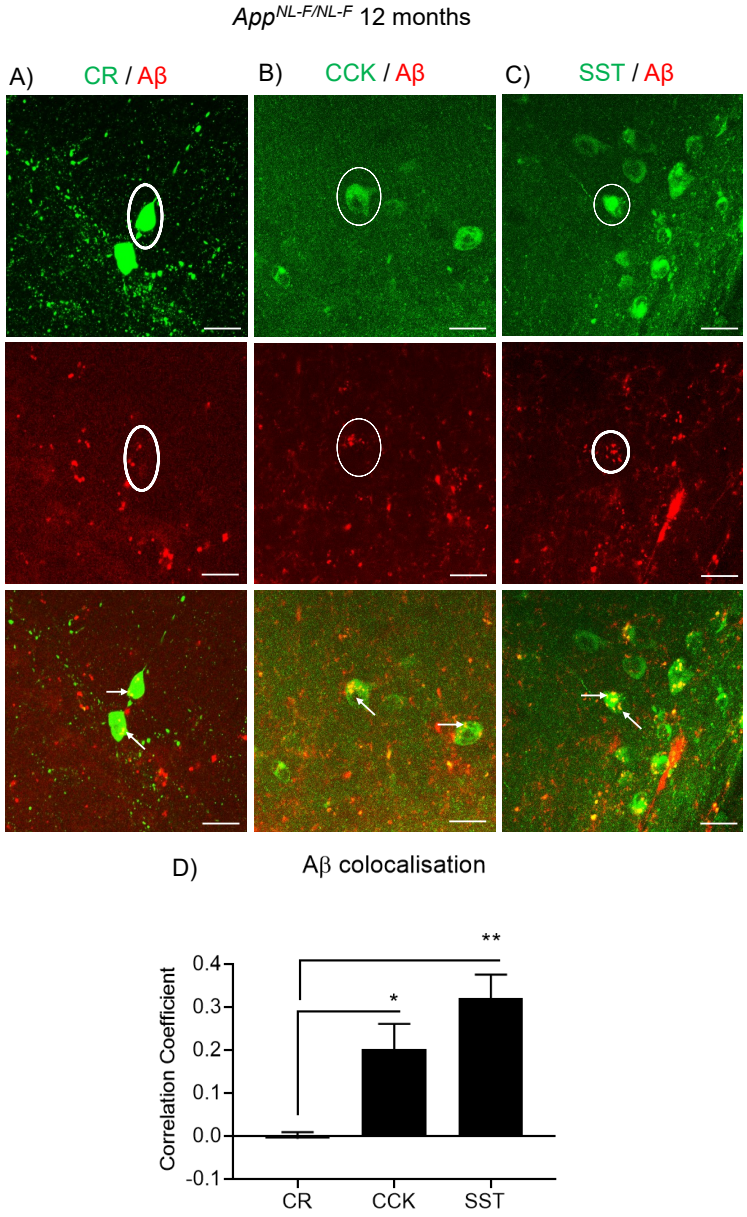

Figure 7.5: Aβ preferentially infiltrated SST and CCK cells. (A-C)Images taken at 63 Xmagnification. Aβ deposits (red) and interneurones (green) are indicated with white outline circles. Colocalization with Aβ deposits (yellow) is identified with white arrows. D) The level of colocalisation is shown as cohort mean + SEM. One-way ANOVA with Sidak's test for multiple comparisons. Data from cells obtained from 3-4 animals per group. *P <0.05, **P <0.01. Scale bars represent 20 μm.

7.3 Discussion

7.3.1 Time-dependent reduction of pyramidal cell density

In this study, a reduction of pyramidal cell density was reported along the LEC-CA1 axis in late stages of AD for the first time in the $App^{NL\text{-}F/NL\text{-}F}$ model (Petrache et al. 2019). This is an important finding and it had not been previously reported in the $App^{NL\text{-}F/NL\text{-}F}$ model. It represents a pathological change which mimics human AD. Not only does this finding increase the robustness of the $App^{NL\text{-}F/NL\text{-}F}$ model as a model of AD, but it also helps identify which neuronal cell types are affected in disease, which further helps identify which cell networks might be vulnerable. The loss or restoration of cell density can also be an important parameter to assess when investigating whether therapies are protective in AD.

There was a decline in CamKII-α staining levels in both the LEC and CA1 concurrent with nucleic DAPI staining, which indicates loss of pyramidal cells. $App^{NL\text{-}F/NL\text{-}F}$ animals expressed significantly less CamKII-α in the LEC compared to healthy mice, at all three ages investigated. In the later stages of AD, when pathology worsened, neurodegeneration reached the CA1 region in the AD model. This followed temporal pathophysiological progression in AD, which was reported to affect the LEC first and then the CA1 as the disease progresses (Brun and Gustafson 1976; Braak and Braak 1991; Solodkin, Veldhuizen, and Hoesen 1996).

In this study, cell nuclei also seemed affected in AD, as they appeared swollen in disease, suggesting cellular injury. Swollen cell nuclei, or “cytotoxic oedema” (Liang et al. 2007) represent a sign of impeding necrotic cell death in response to trauma (Berghe et al. 2014). This was also corroborated with a disorganised pattern of VGlut1 expression, which could suggested that glutamate transport is

affected. Seeing as glutamate is the main excitatory neurotransmitter in the cortex and hippocampus, dysfunction in this pathway could have negative repercussions on memory (Greenamyre et al. 1987).

There is a tight link between pyramidal cells and interneurones in the circuitry studied. For example, CCK and SST cells make contact on the proximal and distal dendrites of pyramidal cells, specifically, therefore any alteration, either in cell number or function, of any cell subtype, has repercussions on this very important pathway which is involved in learning and memory formation. More specifically, SST OLM cells form connection with the distal dendrites of pyramidal cells (Ali and Thomson 1998). This is also the place where pyramidal cells receive input from the entorhinal cortex (Maccaferri and McBain 1995). Moreover, studies have reported that CA1 SST cells also inhibit interneurones from the stratum radiatum in CA1 which form synapses with the dendrites of pyramidal cells, and that this can lead to alterations of LTP (Leao et al. 2012).

CCK cells make contact with the proximal dendrites, soma and axon initial segment of pyramidal cells (Halasy et al. 1996) and they express a variety of receptors such as $GABA_A$ or endocannabinoid receptor 1, and are involved in regulating neurotransmission, learning, anxiety and stress (Rio, McBain, and Pelkey 2012). These interneurones have been largely unstudied in AD. Nevertheless, studies have shown that in patients with AD or mild cognitive impairment, higher amounts of the CCK peptide in the CSF correlated with a decreased likelihood of developing either of the conditions (Plagman et al. 2019).

All of this evidence shows the tight interlink between pyramidal cells and interneurones and the LEC and CA1 region. More specific information about CR-, CCK- and SST-expressing interneurones in AD is discussed in the sections below.

7.3.2 CR interneurones survive in AD

CR cells were identified as being resilient in AD and spared from Aβ infiltration, potentially due to calretinin being a calcium-binding protein that confers protection from excitotoxicity in disease. Notably, the density of another type of interneurons that expresses a calcium-binding protein, parvalbumin, decreases in old animals in the LEC (Petrache et al. 2019). Moreover, previously it has been reported that the intrinsic function of individual CR cells (membrane properties such as time constant, input resistance or action potential discharge) were unchanged in the $App^{NL-F/NL-F}$ animals even in the old age bracket (Shi et al. 2019). However, there was a shift in spontaneous inhibition at the level of CR cells, which results in hyperinhibition, perhaps as a way to compensate for the observed hyperactivity of cells such as pyramidal neurones (Shi et al. 2019).

Not all studies on mouse models of AD have identified CR cells as preserved in AD. In a PS1/APP transgenic model, it was found that CR cells are preferentially targeted by Aβ and that their density decreases by up to 45% of that of age-matched healthy wild-type animals across the hippocampus and at the young age of 4 months (Baglietto-Vargas et al. 2010). However, this is a first generation mouse model that does not replicate findings from studies of post-mortem human AD tissue. The study does mention that Cajal-Retzius cells, a subclass of CR-positive cells, are on the other hand unaffected.

There was a preservation of CR cell density in the LEC-CA1 axis in the $App^{NL-F/NL-F}$ animals compared to age-matched WT mice, even in the later stages of the disease, at 9-15 months. The CR cells included in the analysis showed colocalisation with GAD67, which shows they are functional and producing GABA from glutamate. These findings are consistent with human studies reporting a resilience of CR cells (Hof et al. 1993; Fonseca and Soriano

1995). However, even without knowing precisely which sub-groups of CR cells are likely to survive in disease, this study still demonstrated that that population of neurones was resilient and preserved from alteration of cell number, unlike other interneurones. Could CR cells exert enhanced disinhibition of other inhibitory interneurones and therefore contribute to the abnormal excitatory-inhibitory imbalance and hyperactivity of pyramidal neurones observed in AD?

Electrophysiological recordings performed by Dr. Afia Ali (Shi et al. 2019) show unchanged individual cell behaviour in the $App^{NL-F/NL-F}$ animals at 12 months compared to age-matched wild-type counterparts. However, there was a reported increase in the amplitude and frequency of inhibitory postsynaptic potentials (IPSPs) in CR cells in the disease model at 12 months. This could indicate an enhanced inhibitory effect at the level of CR networks rather than cells. Interestingly, studies showed that in a transgenic *APP* mouse model of AD, pathological seizure activity in the cortex and hippocampus was accompanied by enhanced inhibitory activity (Palop et al. 2007).

Could a putative elevated inhibitory network of CR cells be a result of a compensatory effect? That remains to be established by analysing the density of putative CR-CR contacts made in the AD mouse model compared to contacts in the wild-type healthy animals. In addition, it is known that there are two types of CR cells: those that express solely CR and those that co-express vaso-intestinal peptide (VIP) (Gulyas, Hajos, and Freund 1996). Investigating whether there is a differential survival or GABA production between the two types in AD would help further understand the involvement of the calcium-binding protein and the factors that contribute to the resilience of CR immunoreactive cells. Elucidating the mechanisms of CR resilience in AD is of vital importance to understanding their full involvement in the local circuits. Experiments with double-staining with flurophores for CR and VIP cells were trialled, however, they resulted in leak

between the two channels when imaging, and it was concluded that there was an interaction between the CR and VIP primary antibodies that did not allow mixing of the two in the same preparation. Staggered incubation with anti-CR primary antibody and then with anti-VIP after a subsequent wash was trialled and it did not offer viable results either, therefore the experiment was discontinued.

7.3.3 CCK and SST cell density is significantly reduced in AD

A significant decline of CCK and SST cell density was found in the late stages of the disease (9-15 months) in the $App^{NL-F/NL-F}$ mice compared to age-matched WT animals, suggesting loss of CCK and SST interneurones as the disease progresses on to late stages. This corroborates previous reports of loss of SST immunoreactivity. What is the reason for this pronounced decline in disease and what are the possible mechanisms of SST loss? One reason could be the effect of pathological Aβ infiltrates into the cells. It has been shown that Aβ deposits negatively affect neighbouring synapses in transgenic mouse models of AD (Bittner et al. 2010), therefore Aβ infiltrates could be the reason for SST cell dysfunction and death in AD. It was observed that Aβ heavily infiltrates SST interneurones, significantly more compared to the Aβ infiltrates present in CR cells, so this is a plausible hypothesis. It would be interesting to see if neuroinflammatory markers are also present in higher numbers around CCK and SST cells compared to neighbouring regions so as to assess other factors that might contribute to the decline of neurones. The location of hippocampal SST cells to the OLM region of CA1, close to where Aβ deposits were observed in this study, could mean that SST interneurones are among the first cells to be affected in AD due to the proximal physicality between the two. This proximity of the SST peptide and Aβ in the hippocampus has been reported before (Schettini 1991). Interestingly, both SST peptide and APP undergo similar cleavage processes to

form SST and Aβ, which could facilitate interactions between the two even before their release from cells (LaFerla, Green, and Oddo 2007), which has led to the SST neuropeptide being termed "amyloidogenic".

Notably, it has been reported that the SST peptide shows "natural" decreases with ageing and it normally helps reduce levels of Aβ fragments (Saito et al. 2005), so perhaps what makes SST interneurones vulnerable in AD is the already low levels of SST peptide which cannot protect the cell, triggering a cycle of Aβ-inflicted damage. These findings are important: a linear correlation between SST reduction and Aβ levels has been reported in a PS1xAPP mouse model of AD, which suggests that a rescue of SST hippocampal immunoreactivity could be used as a method to detect the therapeutic efficacy of AD treatments (Ramos et al. 2006).

CCK interneurones have been found to be among the interneurones which express APP in the $App^{NL-G-F/NL-G-F}$ mouse model of AD (Rice et al. 2020). The study also reported SST cells to be APP-positive, but not CR cells. It is noteworthy that CCK cells were found to be among the cells with the highest immunopositivity for APP, which could indicate that they are vulnerable to AD pathology. Perhaps, as with the SST interneurones, this vulnerability to AD pathology leads to their significant decrease in the $App^{NL-F/NL-F}$ mouse model.

The literature concerning the anatomical density of CCK cells in AD is not very extensive. A very recent meta-analysis that aimed to identify studies of CCK cells in AD models of human patients in the CA1 region identified five publications only based on their criteria, two of which focused on rats and three on mice (Reid et al. 2021). Not all of the studies assessed the integrity of CCK cells at multiple time points, however, all pointed to the fact that CCK cells were the most affected in the late stages of the disease, around the time-point identified in this study, 9-15 months of age (Ramos et al. 2006; Villette et al. 2012; Aguado-Llera et al. 2018;

Shi et al. 2019).

The CR, CCK and SST interneurones investigated in this study all expressed GAD67, although work in the research group has previously shown that the level of expression is reduced in CCK and SST interneurones in the $App^{NL-G-F/NL-G-F}$ mouse model compared to wild-type mice (Shi et al. 2019). Interestingly, GAD67 deficiency has been found to reduce Aβ burden in a mouse model. Perhaps initially it is protective, as that is also when a slowing down of memory reduction was found in this study, around 9-15 months of age, a similar age to that at which the GAD67 deficit was reported. This apparent protection that results from GAD67 deficiency could be due to a reduction in GABA neurotransmitter at the synaptic cleft, which normally is too abundant in disease as it fails to be cleared out. Production of GABA is also intensified by astrocytes, which secrete excess glutamine, the basis of glutamate- from which GABA is made. Moreover, astrocytes also produce GABA directly and spill it in the synaptic cleft. Indeed, in the study, excess GABA from astrocytes (but not from neurones) and abnormal tonic GABA currents were significantly reduced by the GAD67 deficiency, which also reduced microglia reactivity (Wang et al. 2017). This contributes not only to a better health of neurones but also to improved Aβ clearance by microglia with a ”normalised” activity.

Chapter 8

Results IV: VGlut1 and GAT1 are maintained in the AD mice

Patterns of neurotransmitter transporter alteration were investigated by staining for glutamate transporter VGlut1 and GABA transporter GAT1 to asses the integrity of the transporter system. GAT1 is the most abundant GABA transporter in the brain of mammals (Conti, Minelli, and Melone 2004). It is located presynaptically on neurones and thought to be the main presynaptic GABA transporter (Govindpani et al. 2017). The health of the neurotransmitter system is linked to the integrity of the glial system, as GAT1 is found on astrocytes as well (Minelli et al. 1995), which further cements the importance of assessing these two systems in disease, to uncover the fundamental mechanisms of disease pathology.

VGlut1 has been reported to be important in memory formation, through its role as the most widely-expressed glutamate transporter in the hippocampus and cortex and its involvement in long-term potentiation, ass studies show that a higher level of the VGLUT1 protein was associated with better learning and memory abilities (Cheng et al. 2011). In AD and other neurodegenerative diseases, reduced levels of VGLUT1 have shown significant correlation with memory deficits (Kashani et al. 2008).

Being the main transporters of glutamate (Wojcik et al. 2004) and GABA (Conti,

Minelli, and Melone 2004; Govindpani et al. 2017), respectively, and contributing learning and memory formation, VGlut1 and GAT1 play important roles in AD pathology. Neurotransmitter availability and uptake are affected in AD, as there is deficient re/uptake and transport of neurotransmitter at the synaptic cleft (Govindpani et al. 2017), which could suggest defective functions of VGlut1 and GAT1. In the current study, the main interest was to report on the status of those two transporters in the $App^{NL-F/NL-F}$ animals during AD pathology, at 13 months. Overall, there was a noticeable disorganisation of GAT1 and VGlut1 staining in the AD model compared to age-matched wild-type animals.

The levels of both VGlut1 and GAT1 were maintained between wild-type and $App^{NL\text{-}F/NL\text{-}F}$ animals at 13 months of age in both LEC ($P > 0.05$, two-tailed unpaired student's t-test, n=3-7 mice) and CA1 ($P > 0.05$, two-tailed unpaired student's t-test, n=4-7 animals).

A comparison across the two regions and the two genotypes with a two-way ANOVA did not identify any of the two factors as being a source of variation in the levels of neurotransmitter.

The altered levels in the AD model of both neurotransmitter transporters across the two brain regions were not significant. However, the distribution patterns of pf VGlut1 (Figure 8.1, green) and GAT1 (red) in the $App^{NL\text{-}F/NL\text{-}F}$ animals appeared to be less ordered than in wild-type age-matched groups in both LEC and CA1, suggesting an alteration of the both excitatory and inhibitory pathways in disease. For example, GAT1 staining in the AD mouse model appeared sparser and concentrated into larger but fewer punctae.

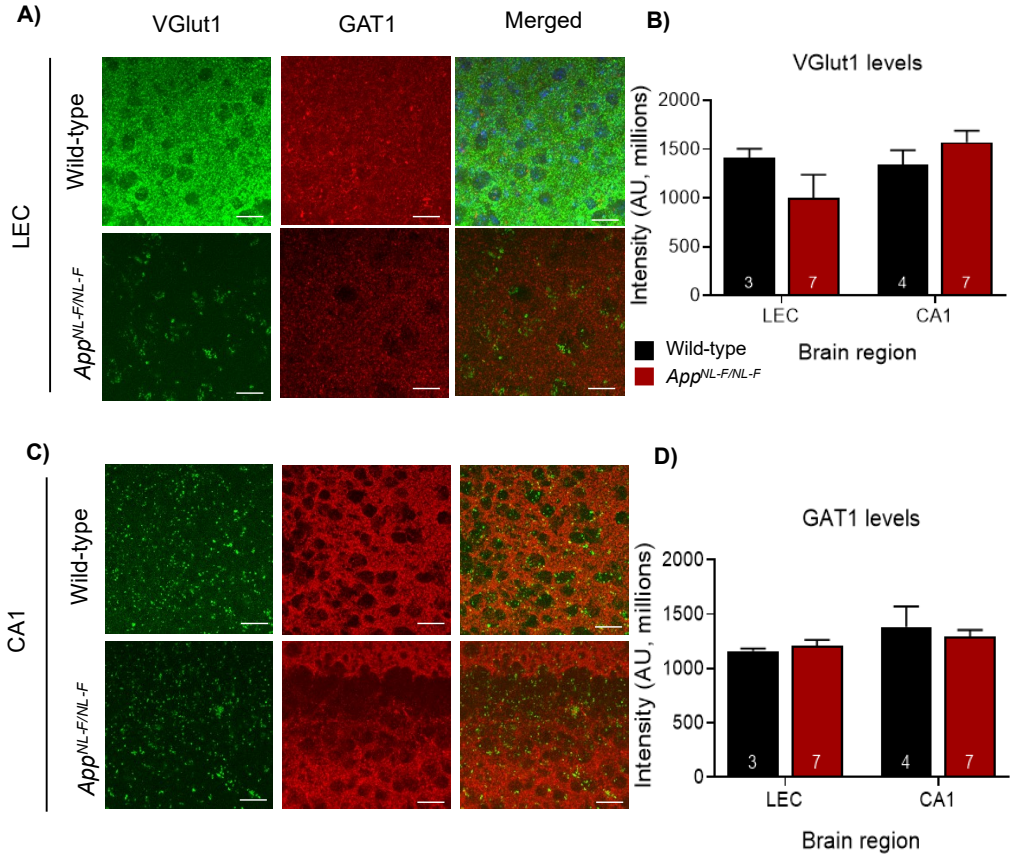

Figure 8.1: Distribution patterns of VGlut1 and GAT1 changed between wild-type and $App^{NL\text{-}F/NL\text{-}F}$ animals. Confocal microscope images of VGlut1 (green, Alexa 488) and GAT1 (red, Texas Red) in LEC (A) and CA1 (C) . Panels show collapsed Z-stacks at X63 for the two merged channels in 13-month old wild-type and $App^{NL\text{-}F/NL\text{-}F}$ animals. The pattern of distribution of both VGlut1 and GAT1 appears disorganised in the AD mouse model. Scale bars are 20 μm. B and D) Confocal microscopy analysis of Vglut1 and GAT1 from Z-stacks at 20x magnification in LEC and CA1. The graphs display cohort means + SEM. A two-tailed unpaired student's t-test was used for statistical analysis between the wild-type and $App^{NL\text{-}F/NL\text{-}F}$ animals at each region. n=3-7 animal. Sample size is displayed on each bar.

8.1 Discussion

It has been previously shown that VGlut1 levels were reduced in in Tg2576 mice, primary cell culture from Tg2576 mice and AD patients (Rodriguez-Perdigon et al. 2016). Other studies have also reported that a reduction in VGLUT1 levels strongly correlated with cognitive deficits (Kashani et al. 2008; Cheng et al. 2011).

In this study, no significant differences were observed between the $App^{NL\text{-}F/NL\text{-}F}$ mice and age-matched wild-type mice, in neither VGlut1 nor GAT1. However, a different pattern of staining was noticed in disease, one which appears more sparse, disorganised, with punctae that are clumped together. This could pin-point to the beginning of pathology among the neurotransmitter transporters, which perhaps affects this particular animal model at later stages.

A preservation of of GAT1 in AD patients has been previously reported (Nägga, Bogdanovic, and Marcusson 1999). In the cited study, post-mortem brain tissue was analysed from 18 AD patients and 23 control subjects that were age-matched. Radiolabelling was used to determine the levels of GAT1 in three brain regions, frontal cortex, temporal cortex and caudal nucleus, and no difference in binding capacity or affinity was reported (Nägga, Bogdanovic, and Marcusson 1999). This represents an interest finding which could indicate a preservation of GABAergic neurones in disease. On the other hand, the apparent disorganisation of GAT1 and indeed of VGlut1 in the present study in the LEC and CA1 could be due to networks of neurones being locally affected in disease.

Chapter 9

Results V: Interneurones and pyramidal cells of the CA1 region express cognitively-important α5-containing GABA$_A$ receptors

---

In the brain of AD patients, GABA$_A$ receptors are preserved in density compared to other types of receptors, such as NMDA, or even GABA$_B$ (Greenamyre et al. 1987; Jansen et al. 1990; Zilles et al. 1995). Of particular focus in these receptors is the α5 subunit, which has been found to be important in memory formation and expressed solely in the hippocampus (Fritschy and Mohler 1995; Howell et al. 2000; Collinson et al. 2002; Yee et al. 2004; Glykys, Mann, and Mody 2008).

In this study, the expression of the α5 subunit-containing GABA$_A$ receptors was investigated on pyramidal cells (stained for CaMKII-α) and interneurones that express CR, CCK and SST, respectively. This particular subtype of GABA$_A$ receptor was chosen because it is preserved in AD as well as important in memory formation (Collinson et al. 2002). If they are expressed and preserved on a particular cell type, perhaps they could be used as a modulatory therapeutic target through which to manipulate that specific cell sub-type and, consequently, the network it is part of.

The CA1 region in tissue from wild-type and *App*$^{NL\text{-}F/NL\text{-}F}$ animals was imaged with a confocal microscope (area imaged for each cell type can be seen in Figure 9). No

age-based differences were noted during the analysis, therefore the data across all age groups were pooled.

Z-stacks spanning the thickness of the tissue were taken at x63 magnification and analysed in three different ways: the intensity of $\alpha 5$ signal in the whole Z-stack was measured, then the levels of expression on the cell soma, and then the level of expression on their dendrites. Pearson's correlation coefficient R with Fisher's transformation was used for statistical analysis.

A two-way ANOVA with cell type and genotype was performed for statistical analysis and none of the factors introduced any significant variation to the data.

Pyramidal cells expressed the $\alpha 5$ subunit and preserved its expression in disease (Figure 9), as was expected, based on previous studies (Howell et al. 2000; Brünig et al. 2001), with no significant differences between wild-type and $App^{NL\text{-}F/NL\text{-}F}$ animals ($P > 0.05$). All three interneurone types also showed preservation of the subunit on their soma (Figure 9, n=5-7 animals per cohort). The AD model showed similar levels of $\alpha 5$ expression to wild-type mice in all three interneurone types investigated: CR, CCK and SST cells.

Seeing as the $\alpha 5$ subunit has been found postynaptically on dendrites where CR cells target SST cells (Magnin et al. 2018), as well as postynaptically on dendrites of pyramidal cells (Ali, Afia B. and A. M. Thomson 2008), we investigated its presence on the dendrites of CR and SST interneurons, as well as pyramidal cells. It is known that the dendrites of CCK cells are also targeted by interneurones (Ali, Afia B. and A. M. Thomson 2008), however we could not investigate $\alpha 5$ expression on CCK dendrites due to a lack of a CCK-targeting antibody that shows high specificity and staining of CCK dendrites in mouse. The dendrites of up to 5 cells were examined and a two-way ANOVA with cell type and genotype as factors revealed no significant difference in $\alpha 5$ expression between the different groups of

neurons nor between genotypes.

These results highlight the preservation of the $\alpha 5$ subunit in the $App^{NL\text{-}F/NL\text{-}F}$ mouse model and at multiple sites on several cell sub-types.

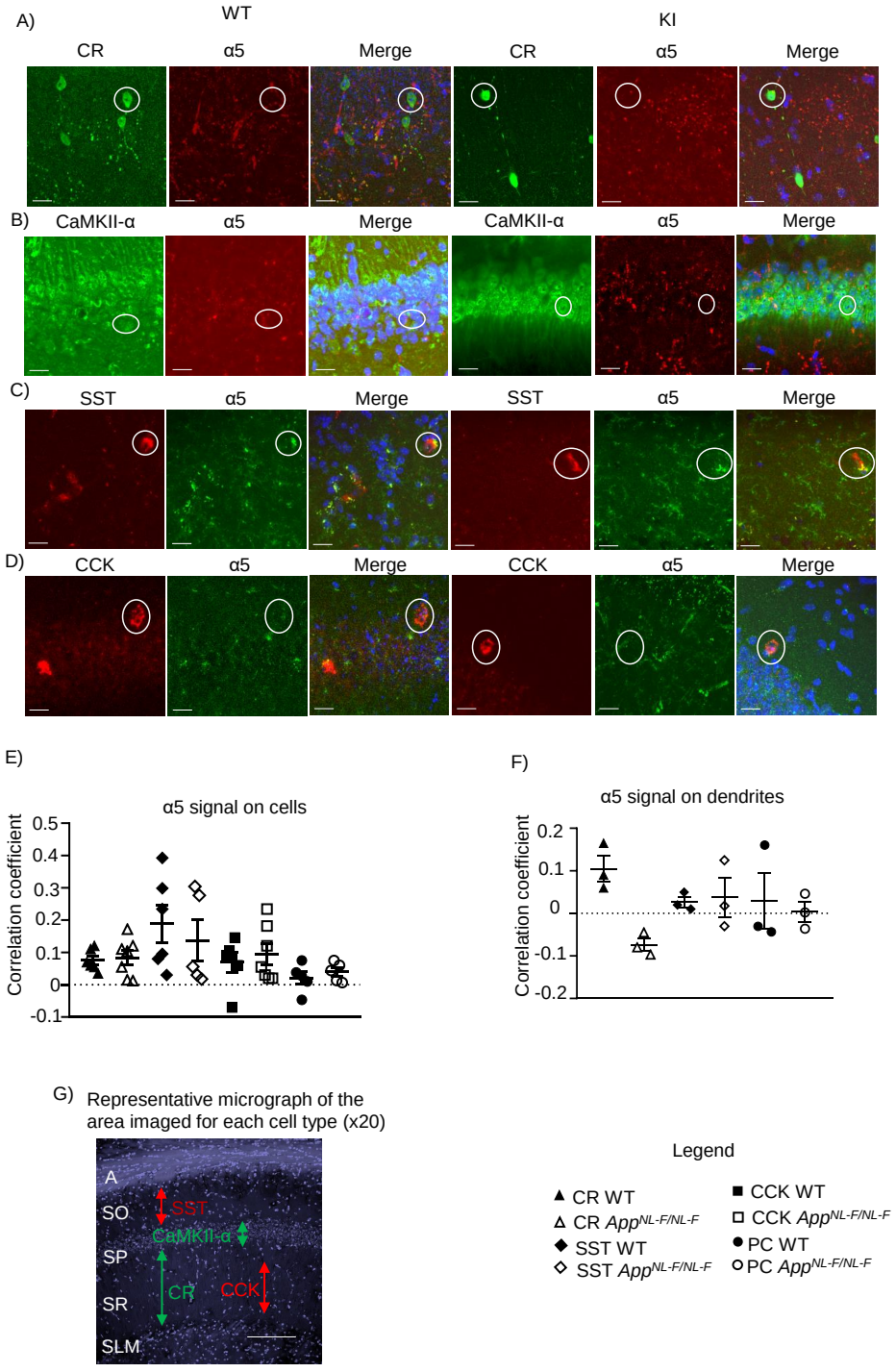

Figure 9.1: Expression of α5-subunit-containing $GABA_A$ receptors in CA1 pyramidal cells and CR, CCK and SST interneurones. Caption continued on the following page.

(A–D) Z-stacks at 63× magnification showing α5-subunit-containing $GABA_A$ receptor expression on pyramidal neurons (CaMKII- α), CR interneurons, SST interneurons, and CCK interneuronesin wild-type and $APP^{NLF/NLF}$ animals. Panels show individual channels and merged image with the nuclear stain DAPI (blue). White circles outline representative soma, while arrows indicate dendritic co-localization of α5. E) α5 expression on soma (PC= pyramidal cells). Each data point represents an average value of five cells from individual animals at 12–18 months (n = 5–7 animals per cohort). F) Analysis of α5 subunit-containing $GABA_AR$ expression on CR- SST- and pyramidal cell (PC) dendrites (n = 3 mice per genotype, visible proximal dendrites analyzed in five cells per animal). G) Representative micrograph of α5 (red) and DAPI (blue) at 20× magnification in $APP^{NL\text{-}F/NLF}$ CA1 to exemplify the region of data acquisition, arrows indicate the location of cell sub-type in the strata: alveus (A), stratum oriens (SO), stratum pyramidale (SP), stratum radiatum (SR), stratum lacunosum moleculare (SLM). Individual data points around averages ± SEM, of Pearson correlation coefficient with Fisher's transformation. Data analyzed with a two-way ANOVA with cell type and genotype as factors. Own figure, data first published in (Petrache et al. 2020).

9.1 Discussion: α5 $GABA_A$ Rs do not make a good therapeutic target

Previously, it has been shown that the α5-subunit-containing $GABA_A$ receptors are preserved in human AD patients (Howell et al. 2000), although which neuronal types they are expressed on beyond pyramidal cells is unclear. Since the current study shows that CR interneurones are preserved, it was investigated whether these cells localised those receptors, alongside the major inhibitory interneurones that express CCK and SST, and pyramidal cells.

For the first time, a more comprehensive study was conducted on interneurones that expressed the α5 subunit and maintained its expression in the $App^{NL\text{-}F/NL\text{-}F}$ model even in the late stages of the disease. This suggests that the activity of those cells is facilitated by the use of the α5 subunit-containing $GABA_A$ receptor. CR cells could be using these receptors postsynaptically to facilitate network communication between CR-CR cells.

As previously reported (Caraiscos et al. 2004), the expression and preservation of α5 in the late stages of the disease in the AD model was observed on pyramidal cells, and on CCK and SST interneurones. The widespread expression of the α5-subunit-containing $GABA_A$ shows they are essential for various cell networks and not specific to one subpopulation, as it had been previously hypothesised. This has wide implications, particularly for therapeutic studies. Negative allosteric modulators of α5-subunit-containing $GABA_A$ receptors have been unsuccessful in clinical trials aimed at improving memory in adults (Atack et al. 2009; Atack 2010), in spite of apparent success in animal studies which resulted in improved cognitive abilities in rodent models of neurodegenerative diseases (Atack et al. 2006; Ballard et al. 2009; Braudeau et al. 2011). This could suggest either that the proposed therapy is not specific enough for the target, or that the target is not appropriate. Collaborative work at the School of Pharmacy including our research group showed that the formulation of a highly specific negative allosteric modulator was possible. However, when this drug was bath applied to brain tissue from $App^{NL\text{-}F/NL\text{-}F}$ animals, whole-cell electrophysiology recordings did not detect a restoration of cell function to normality, on the contrary (Petrache et al. 2020). Specifically, the hyperactivity of pyramidal cells, CCK and SST interneurones was accentuated, and the hyperinhibition detected at the level of CR cell network was exacerbated as well. This is indication that α5-subunit-containing $GABA_A$ receptors do not make appropriate therapeutic targets to restore memory deficits observed in neurodegenerative diseases and that this could be due to their wide expression on multiple cell types, which reduces the specificity of any treatment and instead leads to a ”blanket” effect which negatively affects cell function that is already abnormal.

Chapter 10

Discussion, Limitations and Future Experiments

10.1 Overview

This thesis aimed to further the understanding of the mechanisms of AD pathology. The study took a top-down approach and investigated characteristic AD symptoms such as memory impairment and anxiety indicators were in the preclinical $App^{NL\text{-}F/NL\text{-}F}$ familial AD (fAD) mouse model, together with the anatomical alteration of pyramidal cells and major inhibitory interneurones expressing CR, CCK and SST, respectively, correlated with neuroinflammation and Aβ aggregates. The following are key findings from the study:

- The $App^{NL\text{-}F/NL\text{-}F}$ fAD model showed modest memory impairment at 6-9 and 18-22 months, compared to age-matched wild-type mice, in the T-arm maze. At 12-16 months, memory impairment was detected in the NOL test, but not in any of the other behavioural tests.

- At 6-9 months and 18-22 months the $App^{NL\text{-}F/NL\text{-}F}$ mice also exhibited indicators of anxiety.

- At 9-15 months in the AD model, memory impairment and indicators of anxiety were accompanied by increased accumulation of Aβ, microgliosis and astrocytosis.

- The expression of neurotransmitter transporters GAT1 and VGlut1 was maintained in disease even in at 9-15 months of age, although the expression pattern appears disorganised in $App^{NL\text{-}F/NL\text{-}F}$ mice.

- The density of pyramidal cells dropped significantly in the AD mice at 9-15 months in key regions important for memory formation: CA1 and LEC, when compared to age-matched wild-type mice.

- CR cells, specific to only contact interneurones, maintained their cell density in CA1 in the $App^{NL\text{-}F/NL\text{-}F}$ mice even at 9-15 months.

- CCK cells, which are important in both memory formation and anxiety, showed a significant reduction in density at 9-15 months in the $App^{NL\text{-}F/NL\text{-}F}$ mice compared to age-matched wild-type animals.

- SST cells, which fine-tune pyramidal cell activity and have been reported to associate with the APP peptide in vitro, also exhibited a significant reduction in anatomical density in the AD mouse model at 9-15 months.

- α5-subunit-containing $GABA_A$ receptors were expressed on the soma of pyramidal cells, CR-, CCK- and SST cells, and on the proximal dendrites of pyramidal cells, CR- and SST- cells, as detected from signal measured in confocal microscopy stacks. The levels of expression were unchanged between the wild-type and KI mice.

This research serves to enrich our knowledge of the factors that play a role in the abnormal inhibitory-excitatory synaptic imbalance that is characteristic of AD- and of other neurodegenerative diseases. This was achieved by conducting behavioural tests(T-arm maze, NOL and NOR) of $App^{NL\text{-}F/NL\text{-}F}$ and healthy age-matched wild-type animals, as well as testing anxiety in the open arena, at three time-points: 6-9 months, 12-16 and 18-22 months. The levels of Aβ as well as

Table 10.1.1: A tabulated overview of the results from this study, indicating identified changes. N/A= experiment was not carried out at that respective age. IN= interneurones. [1]= results from one memory test, NOL, which were not replicated in the subsequent NOR test.

Behavioural testing observations			
	6-9 months	12-16 months	18-22 months
Memory impairment	Yes	Yes[1]	Yes
Anxiety	Yes	No	Yes
Anatomical observations			
Changes in AD markers	1-3 months	9-15 months	
Aβ	No	LEC and CA1	
CD68	No	LEC and CA1	
GFAP	CA1	LEC and CA1	
Changes in cell density	1-3 months	4-6 months	9-15 months
Pyramidal cells	LEC	LEC	LEC and CA1
CR IN	CA1-No	N/A	CA1-No
CCK IN	CA1-No	N/A	CA1-Yes
SST IN	CA1-No	N/A	CA1-Yes
Changes in expression levels	1-3 months	9-15 months	
VGlut1	N/A	No	
GAT1	N/A	No	
α5	N/A	No	

gliosis were measured via immunohistochemistry and confocal microscopy, as were the levels of neurotransmitter transporters VGlut1 and GAT1, the anatomical density of pyramidal cells and interneurones, and the expression of the α5-subunit containing $GABA_A$ receptors on these cells.

10.2 $App^{NL\text{-}F/NL\text{-}F}$ animals exhibit reduced cognitive performance and anxiety

One of the aims of this study was to investigate memory impairment in the $App^{NL\text{-}F/NL\text{-}F}$ mouse model, so as to inform the field on its feasibility as an AD model, focusing on the hallmark symptom of memory impairment.

The $App^{NL\text{-}F/NL\text{-}F}$ mice indeed showed significant memory impairment when tested

with the T-arm maze at 6-9 months and 18-22 months against age-matched wild-type counterparts. Memory was also noticeable in the novel object location test at 12-16 months of age in the $App^{NL\text{-}F/NL\text{-}F}$ tested with the NOL test. This was not replicated with the NOR test or T-arm maze.

This bridges the knowledge from the two seminal papers that have studied this mouse model, as they have identified memory impairment from 8 months of age (Masuda et al. 2016) and 18 months of age (Saito et al. 2014) and have not reported on other ages in this particular model. The T-arm maze appeared to be better at detecting memory deficits between the $App^{NL\text{-}F/NL\text{-}F}$ mice and has been indicated in the field as perhaps the most appropriate tool for memory tests (Stewart, Cacucci, and Lever 2011). After identifying that the $App^{NL\text{-}F/NL\text{-}F}$ mice exhibited memory impairment in the T-arm maze at 6-9 months and 18-22 months, it was interesting to discover that the AD model also exhibited indicators of anxiety at the same age groups. This was made apparent by the preference of the $App^{NL\text{-}F/NL\text{-}F}$ mice for the sheltered periphery of the open arena and their reluctance to spend time exploring the centre.

How do the memory and anxiety symptoms translate with respects to AD pathology and the integrity of neuronal circuits in AD?

10.3 Pyramidal cells are not protected in AD

The number of pyramidal cells decreased significantly in the $App^{NL\text{-}F/NL\text{-}F}$ at 9-15 months of age in both the CA1 and LEC, when compared to age-matched wild-type animals. It is interesting that CaMKII, which was used as a pyramidal cell marker, is one of the proteins involved in tau phosphorylation (O'Day, Eshak, and Myre 2015), which leads to AD pathology. The $App^{NL\text{-}F/NL\text{-}F}$ mouse model does not show expression of tau tangles, otherwise it would have been interesting to study

the results of reduced CaMKII on hyperphosphorylated pathogenic tau.

Pyramidal cells are contacted on their soma, proximal dendrites and the axon initial segment by CCK cells and on the distal dendrites by SST cells (Halasy et al. 1996). CCK cells also make contact with the other type of basket cells in the hippocampus, PV cells (Karson et al. 2009), therefore any alteration to this group of interneurones also has repercussions on inhibitory interneurones and results in reduced inhibition in the hippocampus. CR cells, in turn, make contact with both CCK and SST cells, as well as with other CR cells. These results highlight the complexity of neuronal networks.

10.4 CR cell density is maintained in the $App^{NL\text{-}F/NL\text{-}F}$ model

Out of all three interneurone subtypes investigated, CR cells were found to be the most spared in disease, maintaining their anatomical density in the $App^{NL\text{-}F/NL\text{-}F}$ model both in the early stages at 1-3 months and at 9-15months of age. CR cells were also found to express little to no Aβ infiltrates (Shi et al. 2019). CR cells also show preserved membrane properties, as membrane time constant, input resistance and action potential discharge were unchanged in the $App^{NL\text{-}F/NL\text{-}F}$ mice, even at 9-15 months of age (Shi et al. 2019).

Is there a particular characteristic of CR cells that confers them protection in AD over CCK and SST cells?

Several reports suggest that expression of calcium-binding proteins such as calretinin or calbindin could protect neurones in neurodegenerative diseases (D'Orlando et al. 2001). This is based on the calmodulin hypothesis, which is focused on the fact that proteins involved in the production of Aβ appeared to

express calmodulin-binding domains, which suggests that perhaps calmodulin holds the key to regulating this process (O'Day and Myre 2004). APP and BACE1, the main APP cleaving enzyme, both bind to calmodulin, for example. The calmodulin hypothesis is based in turn on the calcium hypothesis, which states that the APP cleaving pathways influence and remodel calcium signalling pathways- namely, soluble oligomeric Aβ increases the amount of Ca^{2+} found in the endoplasmic reticulum (Berridge 2009). Other modifications that result from the alteration of Ca^{2+} pathways can lead to long-term depression, which induces memory loss (Berridge 2009). Alterations in calcium signalling appear before worsening of neurones and other signalling path-ways in the disease, and calcium could be involved in maintaining cell homeostasis, potentially resulting in calcium-binding proteins protecting the neurones that express them (Khachaturian 1994). Therefore, CR could be protective of CR-expressing interneurones by shielding them from calcium-triggered toxicity. Interestingly, our own research shows that interneurones immunoreactive for parvalbumin (PV), another calcium-binding protein, decline in the*App$^{NLF/NLF}$* model in the LEC in old age (Petrache et al. 2019), which indicates the complexity of the mechanisms involved in the preservation of CR cells. Moreover, CaMKII- Calmodulin-dependent protein kinase II-, a calcium-binding protein, did not seem to confer protection to pyramidal cells, as this study has identified them to decrease significantly in the *App$^{NL\text{-}F/NL\text{-}F}$* model at 9-15 months of age.

Notably, the amount of GAD67 expressed in CCK and SST interneurons varies as well, but not the amount expressed in CR cells, suggesting a reduction in normal inhibitory function of CCK and SST cells (Shi et al. 2019). An overall decrease in GAD67 in AD has been reported in other studies as well, in both animal models and human patients, in the hippocampus, cortex and cerebellum (Krantic et al. 2012; Leung et al. 2012; Burbaeva et al. 2014).

10.5 CCK cell density is significantly reduced in the $App^{NL\text{-}F/NL\text{-}F}$ model

CCK cells, which are vital in learning and mediate anxiety and stress responses (Montigny 1989; Harro et al. 1996; Schneider et al. 2008), show significant reduction in density in the hippocampus of $App^{NL\text{-}F/NL\text{-}F}$ mice, identified in this study from 9 months of age, when both memory impairment and anxiety symptoms appeared in the AD model. This, together with the apparent predisposition of CCK cells to soluble Aβ infiltration and the fact that they have been previously shown to express the highest levels of endogenous Aβ among GABAergic interneurones (Rice et al. 2020), indicate that this interneurone subpopulation is heavily involved in AD pathology. This could also pinpoint CCK cells as key drivers of pathology, not just merely afflicted, as they could be releasing soluble Aβ into the environment upon the death of the cell. Moreover, an age-dependent reduction in GAD67 was observed in hippocampal CCK cells in the $App^{NL\text{-}F/NL\text{-}F}$ mice, in particular after 9 months of age (Shi et al. 2019), suggesting a defficiency in their inhibitory function.

CCK cells have been found to be infiltrated by soluble Aβ in this study, and exhibit aberrant hyperexcitability in the AD model, starting from early on in the disease process, around 2 months of age (Shi et al. 2019). This, corroborated with the vulnerability to Aβ and the heavy loss of cell number, results in an alteration of CCK density and function, which leads to hyperexcitability of pyramidal cells- as CCK interneurones are tasked with contacting the soma, proximal dendrites and the axon initial segment of pyramidal cells. CCK cells also make contact with PV cells, therefore any alteration to this group of interneurones results also has repercussions on inhibitory interneurones and results in hipoinhibition in the hippocampus.

CCK interneurones are important both in memory formation and in anxiogenic processes. Indeed, the CCK peptide has been found to be anxiogenic in murine studies, but also in human studies where injections with CCK tetrapeptide induced intense anxiety and panic attacks (Montigny 1989). Pharmacological studies show that agonists to CCK_B receptors have anxiogenic effects and antagonists, anxiolytic (Hughes et al. 1990). Specifically, in an experiment were rats were exposed to stressful situations, the levels of CCK peptide were increased in the hippocampus of those animals compared to the control group (Harro et al. 1996). It would be interesting to investigate any differences in CCK among $App^{NL\text{-}F/NL\text{-}F}$ animals exposed to stresses, unstressed $App^{NL\text{-}F/NL\text{-}F}$ animals and stressed and unstressed wild-type animals, respectively.

The involvement of CCK interneurones in memory formation and generation of anxiety, as well as their place as modulatory interneurones which connect other interneurones as well as pyramidal cells, highlight that any affliction of this cellular subtype contributes to AD pathology. However, through their association with memory and anxiety, CCK cells could represent a therapeutic target for the alleviation of those key symptoms.

10.6 SST cell density is significantly reduced in the $App^{NL\text{-}F/NL\text{-}F}$ model

SST cell density followed a similar age-dependent declining trajectory in the CA1 as CCK cells. By 9-15 months of age, the SST cell density in $App^{NL\text{-}F/NL\text{-}F}$ mice declined significantly in comparison to wild-type animals. What is the reason for this pronounced decline in disease and what are the possible mechanisms of SST loss? One reason could be the effect of pathological Aβ infiltrates into the cells. It has been shown that Aβ deposits negatively affect neighbouring synapses in

transgenic mouse models of AD (Bittner et al. 2010), therefore Aβ infiltrates could be the reason for the significant decline of SST cell density. We observed a heavy infiltration of Aβ into SST interneurones, so this is a plausible hypothesis. SST cells are located in the OLM region, in proximity to Aβ deposits and the SST peptide has been shown to undergo similar cleavage processes as Aβ, which could contribute to this proclivity of SST cells to be targeted by Aβ (LaFerla, Green, and Oddo 2007). The fact that both CCK and SST cells are infiltrated by Aβ also pinpoints them as drivers of pathology, not just merely afflicted, as they could be releasing soluble Aβ into the environment upon their death or damage.

The functions of SST, as well as CCK cells also show alterations (Shi et al. 2019). Recordings performed by Dr. Afia Ali have shown that CCK and SST interneurones, which show significantly age-dependent decreases in density in the AD model, are abnormally hyperactive in the$App^{NL\text{-}F/NL\text{-}F}$ model from the age of 2 months (Shi et al. 2019). This precedes Aβ pathology, neuroinflammation and alteration of cell number.

10.7 Interneurones are preferentially targeted by Aβ

Out of all three interneuron sub-types investigated, CR cells were found to be the most spared in disease, maintaining their anatomical density in the $App^{NL\text{-}F/NL\text{-}F}$ model both in the early stages at 1-3 months and at 9-15 months of age. In contrast, both CCK and SST cells showed a significantly pronounced decline at 9-15 months 10.

The preferential Aβ targeting of interneurons was accompanied by alterations in their function, as electrophysiological recordings performed in the research group by Dr. Afia Ali have shown (Shi et al. 2019). CCK and SST interneurons, which showed significantly decreased numbers in disease, were hyperactive in the AD

mouse model, from the age of 2 months, preceding Aβ pathology, neuroinflammation and alteration of cell numbers. CR cells on the other hand, showed preserved membrane properties, as membrane time constant, input resistance and action potential discharge are unchanged in the AD model at neither young nor old age.

It has been shown that Aβ impacts inhibitory neurones negatively, as it causes reductions in their number (Verret et al. 2012) and also leads to aberrant neural network activity; this, in turn, leads to memory impairment in both human AD patients and mouse models of AD. The strong colocalisation of CCK and SST interneurones with Aβ highlights them as vulnerable in AD and targetetd by pathology.

10.8 α5-subunit-containing $GABA_A$ receptors are widely expressed

All of the cellular subtypes investigated were found to express the α5 subunit of $GABA_A$ receptors. It is known that this subunit is important in learning and memory formation, which is further testimony that the cellular subtypes investigated are involved in memory formation. However, the wide expression of these receptors in the hippocampus, on the three interneurone subpopulations and on pyramidal cells as well, also decreseases their suitability as a therapeutic target and could represent one of the reasons why α5 modulators have failed human trials- their actions target multiple cell populations and have the overall effect of increasing abnormal cell function in the hippocampus and deepening pathological cell activity (Petrache et al. 2020). This results in even more hyperactive pyramidal cells and a failure to correct the existing abnormal activity.

In terms of the expression of α5-subunit-containing GABA$_A$ receptors, it has previously been shown that they are preserved on pyramidal cells, mainly extrasynaptically, as well as postsynaptically on dendrite targetting interneurones. However, we help pinpoint that they are expressed on all three sub-classes of interneurones investigated. For the first time, we report that CCK, CR and SST cells express the α5 subunit and maintain its expression in the *App*$^{NL\text{-}F/NL\text{-}F}$ model even in the late stages of the disease. This suggests that their activity is facilitated by the use of the α5 subunit-containing GABA$_A$ receptor. We are hypothesising that these receptors are used postsynaptically to facilitate network communication between cells.

The α5-subunit-containing GABA$_A$ receptors might be expressed on even more cell types than assessed in this study. What the current study highlights is that these receptors are widely expressed in the hippocampus. This is important, as immense effort has been putting into targeting them pharmacologically with negative allosteric modulators in an attempt to improve cognitive function or to halt the progress of cognitive deficits. In spite of all the success in animal studies, these compounds have not worked in clinical trials. In a recent study we discuss that the α5-subunit-containing GABA$_A$ receptors might not be a good therapeutic target, and one of the reasons could be the wide expression of these subunits by such a vast network of cells, which results in an exacerbation of aberrant function when modulation is attempted. Instead of normalising brain function, modulation of α5-subunit-containing GABA$_A$ receptors negatively affect already impacted cellular function and deepens effect of AD pathology.

10.9 The *App$^{NL\text{-}F/NL\text{-}F}$* exhibits high levels of astrogliosis and microgliosis at 9-15 months

At the same ages at which the cognitive symptoms are noticeable and interneurone density is reduced, and even before, glial cells microglia and astrocytes develop a pathologic pro-inflammatory state, which intertwines with AD pathology as it influences Aβ deposition, neurotransmitter uptake at the synaptic cleft or synapse formation (Nagele et al. 2003; Tuppo and Arias 2005).

GFAP has been found in the serum of AD patients in significantly high amounts that correlate with memory impairment (Oeckl et al. 2019). The involvement of microglia and astrocytes in disease spans not only their immediate effects, but they are also involved in the genetic risk for AD. Astrocytes are the main APOE secretor in the brain (Ries and Sastre 2016) and microglia express the TREM2 receptor (Guerreiro et al. 2013), both of which are coded by for genes responsible for the highest genetic risk to AD. These genes also affect the mechanisms of Aβ clearance- for example, deficient TREM2 does not directly affect the production of Aβ, but rather the way microglia react to it, impairing the processing of the peptide. TREM2 is a cell-surface receptor which in the brain is mostly expressed in microglia and which in normal conditions coordinates a protective anti-inflammatory phenotype in microglia. One risk variant identified in TREM2, called R47H,which substitutes the 47th amino acid from arginine to histidine, leads to heightened risk of developing AD, even similar to the risk posed by APOEε4 variant (Rayaprolu et al. 2013). This variant has also been observed in other neurodegenerative diseases where neuroinflammation causes a pathological burden, such as Parkinson's disease (Rayaprolu et al. 2013). Genome-wide association studies and linkage studies highlight that TREM2 is highly involved in

regulating microglia and that deficits in its function lead to impaired microglial function and exacerbation of pathology (Guerreiro et al. 2013; Rayaprolu et al. 2013; Sims et al. 2017).

10.10 Limitations of the mouse model: The $App^{NL\text{-}F/NL\text{-}F}$ models familial AD

The $App^{NL\text{-}F/NL\text{-}F}$ mouse model utilised in this study models late onset fAD, being based on two fAD mutations first identified in families of Swedish and Iberian descent, respectively, that revolve around faulty cleavage of APP (Saito et al. 2014). However, most cases of AD are sporadic, and while there are genetic factors such as being a carrier for APOE $\varepsilon 4$ or TREM2 mutations, the consensus is that the majority of AD cases are caused by a combination of genetic and environmental factors.

Another limitation is that the $App^{NL\text{-}F/NL\text{-}F}$ model does not account for tau pathology, which is a hallmark of AD. A way to circumvent this would be to introduce tau pathology in the model for future studies. There are several methods of doing this: viral injection, induction of pathology by inoculates from experimental brain trauma (Zanier et al. 2018), or cross-breeding with a genetic mouse model that carries tau pathology.

Nevertheless, the $App^{NL\text{-}F/NL\text{-}F}$ model presents typical soluble and plaque Aβ pathology that is characteristic of AD and of the Aβ hypothesis around which AD pathology is centred. As shown in the current studies, it exhibits memory impairment, although not large, anxiety, increases in neuroinflammatory markers and characteristic cell density reduction. Moreover, a novel mouse model has been created, which combines the $App^{NL\text{-}F/NL\text{-}F}$ APP model with a MAPT model where

the murine tau gene has been replaced with the human one.

The $App^{NL\text{-}F/NL\text{-}F}$ model is a robust model of AD and a reliable model for studies that aim to disentangle Aβ pathology from tau. This is particularly useful as Aβ pathology is upstream of tau pathology, so the onset of Aβ deposits represents a desirable time point for therapeutic intervention.

10.11 Future Experiments

10.11.1 Sample size increase

The sample size in the experiments presented has been informed by power calculations or literature standards. However, the challenging situations over the past year meant that in one case the sample size was slightly below what was desired. The anxiety analysis of the 12-16-month wild-type animals was based on 6 animals only, compared to normal standards which range from 8-12 usually. Therefore, that experiment would benefit from an increase in sample size.

10.11.2 Molecular methods for study validation

The immunohistochemical studies performed in the current study were robust, replicated and published in peer-reviewed articles. Performing both immunofluorescence and immunoperoxidase experiments when possible contributed to the validity of the study. However, for a better and more exact understanding of the processes involved, it might be beneficial to complement them with molecular biology techniques. For example, quantification of cellular mRNA by RT-PCR would better inform on the levels of receptor expression in wild-type versus $App^{NLF/NLF}$ and would reveal subtle changes in gene expression. Similarly, Western Blotting methods could help identify cytokines, such as tumour

necrosis factor, that are released by pro-inflammatory glial cells, so as to help identify a panel of such toxic compounds to target in the current mouse model.

10.11.3 CR-VIP co-staining

It was not possible to co-stain tissue for CR and VIP and obtain satisfactory staining results. It would be informative if one could differentiate between interneurones that express only CR and those that co-express CR and VIP. Therefore, in the future, this avenue should be considered if more appropriate antibodies are identified.

10.11.4 Therapeutic Avenues

Ultimately, the aim of the research project is to contribute to the identification of a therapy. The next viable steps in this direction would be to test whether pharmacological compounds administered to the $App^{NL\text{-}F/NL\text{-}F}$ normalise any of the pathology observed. One avenue is to target astrocytes and microglia, as successful manipulation of their network would have beneficial repercussions on neuronal transmission and Aβ-triggered pathology, as well as an effect on the genetic risk of developing AD.

For example, a way to drive the project forward would be to inject the AD model mice with anti-inflammatory drugs and then assess the effects on AD markers, neurone density and memory impairment. A crucial aspect of such a therapy would be to ensure that the drugs pass the blood-brain barrier. This could be done via viral vectors (Vagner et al. 2016), nanoparticles (Saraiva et al. 2016), or, in the case of small molecules, attaching a transporter that would take the drugs through the blood brain barrier (Rajora et al. 2017).

Another aspect to consider is the treatment of anxiety, which could be pursued in this mouse model and the anxiety indicators measured as in chapter 5. This could be

accomplished by targeting CCK_B receptors with antagonists (Hughes et al. 1990) in $App^{NL\text{-}F/NL\text{-}F}$ to see whether anxiety is alleviated. It would be also interesting to see how this intervention would affect CCK function, by recording the cells' activity with whole-cell electrophysiology.

10.12 Conclusions and implications

The $App^{NL\text{-}F/NL\text{-}F}$ mouse model of AD exhibited reduced cognitive performance starting from 6-9 months through to 18-22 months and anxiety at the same ages. Very interestingly, at 12-16 months of age there seemed to be a slowing down in pathology affecting cognitive differences, as well as a slowing down of anxiety indicators. However, cells important in learning and anxiety, such as major excitatory units, pyramidal cells, and inhibitory interneurones CCK and SST were affected around the 12-month mark, as their densities decreased significantly in the $App^{NL\text{-}F/NL\text{-}F}$ mouse model. Similarly, there were pronounced increases in astrocyte and microglia signal at the 9-15 month age bracket, as well as Aβ deposition.

These signs point to an involvement of inhibitory interneurones in disease. Linked with the fact that in this study CCK and SST cells were found to be heavily infiltrated with Aβ around 9-15 months of age in the CA1 and to previous mentions that GABAergic interneurones express APP and could be drivers of Aβ pathology, it could be that once the density of interneurones is affected at a certain age, together with their function, this leads to cognitive impairment and to anxiety.

The α5-subunit-containing $GABA_A$ receptors were expressed on CR, CCK and SST interneurones, together with pyramidal cells. This finding is very informational, as it indicates that modulating these receptors will not have the clear-cut desired effect of reducing abnormal function in the hippocampus and restoring normality,

but rather that it would affect several neuronal populations, which could contribute to an increase in pathology.

To conclude, the $App^{NL\text{-}F/NL\text{-}F}$ is a useful preclinical model of AD, which can be utilised to study pathological markers of AD and cellular alteration in disease, as well as to test therapeutic avenues. This study contributed to deepening the understanding on cognitive deficits, anxiety, pyramidal cells and interneurones, as well as the expression of the α5-subunit-containing $GABA_A$ receptors on pyramidal cells and CR-, CCK- and SST- interneurones. Further work is necessary in order to unravel more layers of AD pathology in this and second-generation mouse model, at a molecular level, to be able in obtain even more informative results that can help in finding a therapy for AD.

The experimental flow in this thesis was designed with the aim of informing future therapeutic avenues. Memory impairment and anxiety indicators are symptoms that can be monitored for improvement when administering therapy. Anatomical cell densities, neuroinflammation and Aβ accumulation can also be measured to determine therapy success.

Bibliography

Acosta, G. 2001. “A possible interaction between CCKergic and GABAergic systems in the rat brain”. *Comparative Biochemistry and Physiology Part C: Toxicology & Pharmacology* 128, no. 1 (): 11–17. doi:10.1016/s1532-0456(00)00175-7. https://doi.org/10.1016/s1532-0456(00)00175-7.

Aguado-Llera, David, et al. 2018. “The Protective Effects of IGF-I against -Amyloid-related Downregulation of Hippocampal Somatostatinergic System Involve Activation of Akt and Protein Kinase A”. *Neuroscience* 374 (): 104–118. doi:10.1016/j.neuroscience.2018.01.041. https://doi.org/10.1016/j.neuroscience.2018.01.041.

Ali, Afia B. and A. M. Thomson. 2008. “Synaptic alpha5 Subunit-Containing GABAA Receptors Mediate IPSPs Elicited by Dendrite-Preferring Cells in Rat Neocortex”. *Cerebral Cortex* 18, no. 6 (): 1260–1271. doi:10.1093/cercor/bhm160. https://doi.org/10.1093/cercor/bhm160.

Ali, Afia B, and A. M. Thomson. 1998. “Facilitating pyramid to horizontal oriens-alveus interneurone inputs: dual intracellular recordings in slices of rat hippocampus”. *The Journal of Physiology* 507, no. 1 (): 185–199. doi:10.1111/j.1469-7793.1998.185bu.x. https://doi.org/10.1111/j.1469-7793.1998.185bu.x.

Allen Institute for Brain Science. 2011. “Personal communication to Alzforum.” *Allen Institute for Brain Science. Allen Adult Mouse Brain Atlas.* 1:1–10. http://atlas.brain-map.org/.

Allen, Nicola J., et al. 2012. “Astrocyte glypicans 4 and 6 promote formation of excitatory synapses via GluA1 AMPA receptors”. *Nature* 486, no. 7403 (): 410–414. doi:10.1038/nature11059. https://doi.org/10.1038/nature11059.

Amaral, D. G., and M. P. Witter. 1989. “The three-dimensional organization of the hippocampal formation: A review of anatomical data”. *Neuroscience* 31, no. 3 (): 571–591. doi:10.1016/0306-4522(89)90424-7. https://doi.org/10.1016/0306-4522(89)90424-7.

AmGerSoc. 2015. “American Geriatrics Society 2015 Updated Beers Criteria for Potentially Inappropriate Medication Use in Older Adults”. *Journal of the American Geriatrics Society* 63, no. 11 (): 2227–2246. doi:10.1111/jgs.13702. https://doi.org/10.1111/jgs.13702.

Andersen, P., S. A. Andersen, and T. Lomo. 1966. “Patterns of Spontaneous Rhythmic Activity within Various Thalamic Nuclei”. *Nature* 211, no. 5051 (): 888–889. doi:10.1038/211888b0. https://doi.org/10.1038/211888b0.

Araque, Alfonso, et al. 1999. “Tripartite synapses: glia, the unacknowledged partner”. *Trends in Neurosciences* 22, no. 5 (): 208–215. doi:10.1016/s0166-2236(98)01349-6. https://doi.org/10.1016/s0166-2236(98)01349-6.

Assini, Fabrıcio Luiz, Marcelo Duzzioni, and Reinaldo Naoto Takahashi. 2009. “Object location memory in mice: Pharmacological validation and further evidence of hippocampal CA1 participation”. *Behavioural Brain Research*

204, no. 1 (): 206–211. doi:10.1016/j.bbr.2009.06.005. https://doi.org/10.1016/j.bbr.2009.06.005.

Atack, John R. 2010. "Preclinical and clinical pharmacology of the GABAA receptor 5 subtype-selective inverse agonist 5IA". *Pharmacology & Therapeutics* 125, no. 1 (): 11–26. doi:10.1016/j.pharmthera.2009.09.001. https://doi.org/10.1016/j.pharmthera.2009.09.001.

Atack, John R., et al. 2009. "In Vitro and in Vivo Properties of 3-tert-Butyl-7-(5-methylisoxazol-3-yl)-2-(1-methyl-1H-1, 2, 4-triazol-5-ylmethoxy)-pyrazolo[1, 5-d]-[1, 2, 4]triazine (MRK-016), a GABAA Receptor 5 Subtype-Selective Inverse Agonist". *Journal of Pharmacology and Experimental Therapeutics* 331, no. 2 (): 470–484. doi:10.1124/jpet.109.157636. https://doi.org/10.1124/jpet.109.157636.

Atack, John R., et al. 2006. "L-655, 708 enhances cognition in rats but is not proconvulsant at a dose selective for 5-containing GABAA receptors". *Neuropharmacology* 51, no. 6 (): 1023–1029. doi:10.1016/j.neuropharm.2006.04.018. https://doi.org/10.1016/j.neuropharm.2006.04.018.

Axmacher, N., C. E. Elger, and J. Fell. 2009. "Working Memory-Related Hippocampal Deactivation Interferes with Long-Term Memory Formation". *Journal of Neuroscience* 29, no. 4 (): 1052–1060. doi:10.1523/jneurosci.5277-08.2009. https://doi.org/10.1523/jneurosci.5277-08.2009.

Baglietto-Vargas, David, et al. 2010. "Calretinin Interneurons are Early Targets of Extracellular Amyloid- Pathology in PS1/APP Alzheimer Mice Hippocampus". *Journal of Alzheimer's Disease* 21, no. 1 (): 119–132. ISSN:

18758908, 13872877. doi:10.3233/JAD-2010-100066. https://doi.org/10.3233/JAD-2010-100066.

Baier, Paul Christian, et al. 2009. "Impaired hippocampus-dependent and -independent learning in IL-6 deficient mice". *Behavioural Brain Research* 200, no. 1 (): 192–196. doi:10.1016/j.bbr.2009.01.013. https://doi.org/10.1016/j.bbr.2009.01.013.

Bakker, Arnold, et al. 2012. "Reduction of Hippocampal Hyperactivity Improves Cognition in Amnestic Mild Cognitive Impairment". *Neuron* 74, no. 3 (): 467–474. doi:10.1016/j.neuron.2012.03.023. https://doi.org/10.1016/j.neuron.2012.03.023.

Ballard, Theresa M., et al. 2009. "RO4938581, a novel cognitive enhancer acting at GABAA 5 subunit-containing receptors". *Psychopharmacology* 202, **numbers** 1-3 (): 207–223. doi:10.1007/s00213-008-1357-7. https://doi.org/10.1007/s00213-008-1357-7.

Barrett, Ruth M, et al. 2011. "Hippocampal Focal Knockout of CBP Affects Specific Histone Modifications, Long-Term Potentiation, and Long-Term Memory". *Neuropsychopharmacology* 36, no. 8 (): 1545–1556. doi:10.1038/npp.2011.61. https://doi.org/10.1038/npp.2011.61.

Bartsch, Thorsten, ed. 2012. *The Clinical Neurobiology of the Hippocampus*. Oxford University Press. doi:10.1093/acprof:oso/9780199592388.001.0001. https://doi.org/10.1093/acprof:oso/9780199592388.001.0001.

Bekris, Lynn M., et al. 2010. "Review Article: Genetics of Alzheimer Disease". *Journal of Geriatric Psychiatry and Neurology* 23, no. 4 (): 213–227. doi:10.1177/0891988710383571. https://doi.org/10.1177/0891988710383571.

Ben-Ari, Yehezkel. 2002. "Excitatory actions of gaba during development: the nature of the nurture". *Nature Reviews Neuroscience* 3, no. 9 (): 728–739. doi:10.1038/nrn920. https://doi.org/10.1038/nrn920.

Bensamoun, David, et al. 2015. "Associations between Neuropsychiatric Symptoms and Cerebral Amyloid Deposition in Cognitively Impaired Elderly People". *Journal of Alzheimer's Disease* 49, no. 2 (): 387–398. ISSN: 13872877, 18758908. doi:10.3233/JAD-150181.

Berghe, Tom Vanden, et al. 2014. "Regulated necrosis: the expanding network of non-apoptotic cell death pathways". *Nature Reviews Molecular Cell Biology* 15, no. 2 (): 135–147. doi:10.1038/nrm3737. https://doi.org/10.1038/nrm3737.

Berridge, Michael J. 2009. "Calcium hypothesis of Alzheimer's disease". *Pflügers Archiv - European Journal of Physiology* 459, no. 3 (): 441–449. doi:10.1007/s00424-009-0736-1. https://doi.org/10.1007/s00424-009-0736-1.

Binder, L I, A Frankfurter, and L I Rebhun. 1985. "The distribution of tau in the mammalian central nervous system." *The Journal of Cell Biology* 101, no. 4 (): 1371–1378. doi:10.1083/jcb.101.4.1371. https://doi.org/10.1083/jcb.101.4.1371.

Bingman, Verner P., and Patricia E. Sharp. 2006. "Neuronal Implementation of Hippocampal-Mediated Spatial Behavior: A Comparative Evolutionary Perspective". *Behavioral and Cognitive Neuroscience Reviews* 5, no. 2 (): 80–91. doi:10.1177/1534582306289578. https://doi.org/10.1177/1534582306289578.

Bisht, Kanchan, et al. 2016. "Dark microglia: A new phenotype predominantly associated with pathological states". *Glia* 64, no. 5 (): 826–839.

doi:10.1002/glia.22966. https://doi.org/10.1002/glia.22966.

Bittner, Tobias, et al. 2010. "Multiple Events Lead to Dendritic Spine Loss in Triple Transgenic Alzheimer's Disease Mice". Ed. by Sven G. Meuth. *PLoS ONE* 5, no. 11 (): e15477. doi:10.1371/journal.pone.0015477. https://doi.org/10.1371/journal.pone.0015477.

Blennow, Kaj, Mony J. de Leon, and Henrik Zetterberg. 2006. "Alzheimer's disease". *The Lancet* 368, no. 9533 (): 387–403. doi:10.1016/s0140-6736(06)69113-7. https://doi.org/10.1016/s0140-6736(06)69113-7.

Bo, Roberto Del, et al. 1995. "Reciprocal control of inflammatory cytokines, IL-1 and IL-6, and -amyloid production in cultures". *Neuroscience Letters* 188, no. 1 (): 70–74. doi:10.1016/0304-3940(95)11384-9. https://doi.org/10.1016/0304-3940(95)11384-9.

Bookheimer, Susan Y., et al. 2000. "Patterns of Brain Activation in People at Risk for Alzheimer's Disease". *New England Journal of Medicine* 343, no. 7 (): 450–456. doi:10.1056/nejm200008173430701. https://doi.org/10.1056/nejm200008173430701.

Braak, H., and E. Braak. 1991. "Neuropathological stageing of Alzheimer-related changes". *Acta Neuropathologica* 82, no. 4 (): 239–259. doi:10.1007/bf00308809. https://doi.org/10.1007/bf00308809.

Braudeau, J, et al. 2011. "Specific targeting of the GABA-A receptor 5 subtype by a selective inverse agonist restores cognitive deficits in Down syndrome mice". *Journal of Psychopharmacology* 25, no. 8 (): 1030–1042. doi:10.1177/0269881111405366. https://doi.org/10.1177/0269881111405366.

Brun, A., and L. Gustafson. 1976. “Distribution of cerebral degeneration in Alzheimer’s disease”. *Archiv für Psychiatrie und Nervenkrankheiten* 223 (1): 15–33. doi:10.1007/bf00367450. https://doi.org/10.1007/bf00367450.

Brünig, Ina, et al. 2001. “Intact sorting, targeting, and clustering of -aminobutyric acid A receptor subtypes in hippocampal neurons in vitro”. *Journal of Comparative Neurology* 443, no. 1 (): 43–55. doi:10.1002/cne.10102. https://doi.org/10.1002/cne.10102.

Burbaeva, G. Sh., et al. 2014. “Glutamate and GABA-Metabolizing Enzymes in Post-mortem Cerebellum in Alzheimer’s Disease: Phosphate-Activated Glutaminase and Glutamic Acid Decarboxylase”. *The Cerebellum* 13, no. 5 (): 607–615. doi:10.1007/s12311-014-0573-4. https://doi.org/10.1007/s12311-014-0573-4.

Burgos-Ramos, E., et al. 2008. “Somatostatin and Alzheimer’s disease”. *Molecular and Cellular Endocrinology* 286, **numbers** 1-2 (): 104–111. doi:10.1016/j.mce.2008.01.014. https://doi.org/10.1016/j.mce.2008.01.014.

Busche, M. A., et al. 2008. “Clusters of Hyperactive Neurons Near Amyloid Plaques in a Mouse Model of Alzheimer’s Disease”. *Science* 321, no. 5896 (): 1686–1689. doi:10.1126/science.1162844. https://doi.org/10.1126/science.1162844.

Busche, M. A., et al. 2012. “Critical role of soluble amyloid- for early hippocampal hyperactivity in a mouse model of Alzheimer’s disease”. *Proceedings of the National Academy of Sciences* 109, no. 22 (): 8740–8745. doi:10.1073/pnas.1206171109. https://doi.org/10.1073/pnas.1206171109.

Busche, Marc Aurel, and Arthur Konnerth. 2016. “Impairments of neural circuit function in Alzheimer’s disease”. *Philosophical Transactions of the Royal Society B: Biological Sciences* 371, no. 1700 (): 20150429. doi:10.1098/rstb.2015.0429. https://doi.org/10.1098/rstb.2015.0429.

Butt, Simon J.B., et al. 2005. “The Temporal and Spatial Origins of Cortical Interneurons Predict Their Physiological Subtype”. *Neuron* 48, no. 4 (): 591–604. doi:10.1016/j.neuron.2005.09.034. https://doi.org/10.1016/j.neuron.2005.09.034.

Cajal, D. Santiago Ramon Y. 1893. “NUEVA CONCEPTA DE LA HISTOLOGIA DE LOS CENTROS NERVOSOS”. *Annals of Surgery* 18 (): 122. doi:10.1097/00000658-189307000-00018. https://doi.org/10.1097/00000658-189307000-00018.

Cajal, Santiago R. y. 1888. “Estructura de los centros nerviosos de las aves”. *evista trimestral de Histologıa normal y patológica*.

Campion, Dominique, et al. 1999. “Early-Onset Autosomal Dominant Alzheimer Disease: Prevalence, Genetic Heterogeneity, and Mutation Spectrum”. *The American Journal of Human Genetics* 65, no. 3 (): 664–670. doi:10.1086/302553. https://doi.org/10.1086/302553.

Caraiscos, V. B., et al. 2004. “Tonic inhibition in mouse hippocampal CA1 pyramidal neurons is mediated by 5 subunit-containing -aminobutyric acid type A receptors”. *Proceedings of the National Academy of Sciences* 101, no. 10 (): 3662–3667. doi:10.1073/pnas.0307231101. https://doi.org/10.1073/pnas.0307231101.

Cassel, Jean-Christophe, and Anne Pereira de Vasconcelos. 2015. “Importance of the ventral midline thalamus in driving hippocampal functions”. In *The Connected Hippocampus*, 145–161. Elsevier.

doi:10.1016/bs.pbr.2015.03.005. https://doi.org/10.1016/bs.pbr.2015.03.005.

Cauli, Bruno, et al. 2014. "Revisiting enigmatic cortical calretinin-expressing interneurons". *Frontiers in Neuroanatomy* 8 (). doi:10.3389/fnana.2014.00052. https://doi.org/10.3389/fnana.2014.00052.

Chambers, Mark S., et al. 2003. "Identification of a Novel, Selective GABAA5 Receptor Inverse Agonist Which Enhances Cognition". *Journal of Medicinal Chemistry* 46, no. 11 (): 2227–2240. doi:10.1021/jm020582q. https://doi.org/10.1021/jm020582q.

Chan, Agnes S., David P. Salmon, and Jody De La Pena. 2001. "Abnormal Semantic Network for "Animals" But not "Tools" in Patients with Alzheimer's Disease". *Cortex* 37 (2): 197–217. doi:10.1016/s0010-9452(08)70568-9. https://doi.org/10.1016/s0010-9452(08)70568-9.

Chen, Guo-fang, et al. 2017. "Amyloid beta: structure, biology and structure-based therapeutic development". *Acta Pharmacologica Sinica* 38, no. 9 (): 1205–1235. doi:10.1038/aps.2017.28. https://doi.org/10.1038/aps.2017.28.

Cheng, Xiao-Rui, et al. 2011. "Expression of VGLUTs contributes to degeneration and acquisition of learning and memory". *Neurobiology of Learning and Memory* 95, no. 3 (): 361–375. doi:10.1016/j.nlm.2011.01.010. https://doi.org/10.1016/j.nlm.2011.01.010.

Chu, Dorothy C.M., John B. Penney, and Anne B. Young. 1987. "Quantitative autoradiography of hippocampal GABAB and GABAA receptor changes in Alzheimer's disease". *Neuroscience Letters* 82, no. 3 (): 246–252. doi:10.1016/0304-3940(87)90264-3. https://doi.org/10.1016/0304-3940(87)90264-3.

Clark, Linda J., et al. 2009. "Longitudinal Verbal Fluency in Normal Aging, Preclinical, and Prevalent Alzheimer's Disease". *American Journal of Alzheimer's Disease & Other Dementiasr* 24, no. 6 (): 461–468. doi:10.1177/1533317509345154. https://doi.org/10.1177/1533317509345154.

Clayton, Nicola S., and Anthony Dickinson. 1998. "Episodic-like memory during cache recovery by scrub jays". *Nature* 395, no. 6699 (): 272–274. doi:10.1038/26216. https://doi.org/10.1038/26216.

Collinson, Neil, et al. 2002. "Enhanced Learning and Memory and Altered GABAergic Synaptic Transmission in Mice Lacking the α5 Subunit of the $GABA_A$Receptor". *The Journal of Neuroscience* 22, no. 13 (): 5572–5580. doi:10.1523/jneurosci.22-13-05572.2002. https://doi.org/10.1523/jneurosci.22-13-05572.2002.

Conti, Fiorenzo, Andrea Minelli, and Marcello Melone. 2004. "GABA transporters in the mammalian cerebral cortex: localization, development and pathological implications". *Brain Research Reviews* 45, no. 3 (): 196–212. doi:10.1016/j.brainresrev.2004.03.003. https://doi.org/10.1016/j.brainresrev.2004.03.003.

Corder, E., et al. 1993. "Gene dose of apolipoprotein E type 4 allele and the risk of Alzheimer's disease in late onset families". *Science* 261, no. 5123 (): 921–923. doi:10.1126/science.8346443. https://doi.org/10.1126/science.8346443.

D'Orlando, Cristina, et al. 2001. "Calretinin and calbindin D-28k delay the onset of cell death after excitotoxic stimulation in transfected P19 cells". *Brain Research* 909, **numbers** 1-2 (): 145–158. doi:10.1016/s0006-8993(01)02671-3. https://doi.org/10.1016/s0006-8993(01)02671-3.

Das, Brati, and Riqiang Yan. 2019. "A Close Look at BACE1 Inhibitors for Alzheimer's Disease Treatment". *CNS Drugs* 33, no. 3 (): 251–263. doi:10.1007/s40263-019-00613-7. https://doi.org/10.1007/s40263-019-00613-7.

Davies, Peter, Robert Katzman, and Robert D. Terry. 1980. "Reduced somatostatin-like immunoreactivity in cerebral cortex from cases of Alzheimer disease and Alzheimer senile dementa". *Nature* 288, no. 5788 (): 279–280. doi:10.1038/288279a0. https://doi.org/10.1038/288279a0.

Deacon, R.M.J., and J.N.P. Rawlins. 2006. "T-maze alternation in the rodent". *Nature Protocols* 1, no. 1 (): 7–12. doi:10.1038/nprot.2006.2. https://doi.org/10.1038/nprot.2006.2.

Deacon, R.M.J., et al. 2008. "Age-dependent and -independent behavioral deficits in Tg2576 mice". *Behavioural Brain Research* 189, no. 1 (): 126–138. doi:10.1016/j.bbr.2007.12.024. https://doi.org/10.1016/j.bbr.2007.12.024.

Dember, W.N., and C.L. Richman. 1989. *Spontaneous Alternation Behavior*. Springer, New York.

Denninger, Jiyeon K., Bryon M. Smith, and Elizabeth D. Kirby. 2018. "Novel Object Recognition and Object Location Behavioral Testing in Mice on a Budget". *Journal of Visualized Experiments*, no. 141 (). doi:10.3791/58593. https://doi.org/10.3791/58593.

Dennis, Nancy A., et al. 2009. "Temporal lobe functional activity and connectivity in young adult APOE ε4 carriers". *Alzheimer's & Dementia* 6, no. 4 (): 303–311. doi:10.1016/j.jalz.2009.07.003. https://doi.org/10.1016/j.jalz.2009.07.003.

Du, A. T., et al. 2003. “Atrophy rates of entorhinal cortex in AD and normal aging”. *Neurology* 60, no. 3 (): 481–486. doi:10.1212/01.wnl.0000044400.11317.ec. https://doi.org/10.1212/01.wnl.0000044400.11317.ec.

Duvernoy, Henri M., Francoise Cattin, and Pierre-Yves Risold. 2013. *The Human Hippocampus*. Springer Berlin Heidelberg. doi:10.1007/978-3-642-33603-4. https://doi.org/10.1007/978-3-642-33603-4.

Eikelenboom, P., et al. 2002. “Neuroinflammation in Alzheimer’s disease and prion disease”. *Glia* 40, no. 2 (): 232–239. doi:10.1002/glia.10146. https://doi.org/10.1002/glia.10146.

Ellenbroek, Bart, and Jiun Youn. 2016. “Rodent models in neuroscience research: is it a rat race?” *Disease Models & Mechanisms* 9, no. 10 (): 1079–1087. doi:10.1242/dmm.026120. https://doi.org/10.1242/dmm.026120.

Fonseca, Montserrat, and Eduardo Soriano. 1995. “Calretinin-immunoreactive neurons in the normal human temporal cortex and in Alzheimer’s disease”. *Brain Research* 691, **numbers** 1-2 (): 83–91. doi:10.1016/0006-8993(95)00622-w. https://doi.org/10.1016/0006-8993(95)00622-w.

Forabosco, Paola, et al. 2013. “Insights into TREM2 biology by network analysis of human brain gene expression data”. *Neurobiology of Aging* 34, no. 12 (): 2699–2714. doi:10.1016/j.neurobiolaging.2013.05.001. https://doi.org/10.1016/j.neurobiolaging.2013.05.001.

Freund, T.F., and G. Buzsaki. 1996. “Interneurons of the hippocampus”. *Hippocampus* 6, no. 4 (): 347–470. doi:10.1002/(sici)1098-1063(1996)6:4<347::aid-hipo1>3.0.co;2-i.

https://doi.org/10.1002/(sici)1098-1063(1996)6:4%3C347::aid-hipo1%3E3.0.co;2-i.

Freund, T.F., and A.I. Gulyas. 1997. "Inhibitory control of GABAergic interneurons in the hippocampus". *Canadian Journal of Physiology and Pharmacology* 75, no. 5 (): 479–487. doi:10.1139/y97-033. https://doi.org/10.1139/y97-033.

Freund, Tamás F., and István Katona. 2007. "Perisomatic Inhibition". *Neuron* 56, no. 1 (): 33–42. doi:10.1016/j.neuron.2007.09.012. https://doi.org/10.1016/j.neuron.2007.09.012.

Fritschy, Jean-Marc, and Hanns Mohler. 1995. "GABAA-receptor heterogeneity in the adult rat brain: Differential regional and cellular distribution of seven major subunits". *The Journal of Comparative Neurology* 359, no. 1 (): 154–194. doi:10.1002/cne.903590111. https://doi.org/10.1002/cne.903590111.

Gakhar-Koppole, Nidhi, et al. 2008. "Activity requires soluble amyloid precursor protein to promote neurite outgrowth in neural stem cell-derived neurons via activation of the MAPK pathway". *European Journal of Neuroscience* 28, no. 5 (): 871–882. doi:10.1111/j.1460-9568.2008.06398.x. https://doi.org/10.1111/j.1460-9568.2008.06398.x.

Ghafari, Maryam, et al. 2016. "Formation of GABAA receptor complexes containing 1 and 5 subunits is paralleling a multiple T-maze learning task in mice". *Brain Structure and Function* 222, no. 1 (): 549–561. doi:10.1007/s00429-016-1233-x. https://doi.org/10.1007/s00429-016-1233-x.

Glykys, J., E. O. Mann, and I. Mody. 2008. "Which GABAA Receptor Subunits Are Necessary for Tonic Inhibition in the Hippocampus?" *Journal of Neuroscience*

28, no. 6 (): 1421–1426. doi:10.1523/jneurosci.4751-07.2008. https://doi.org/10.1523/jneurosci.4751-07.2008.

Gomez-Isla, Teresa, et al. 1996. "Profound Loss of Layer II Entorhinal Cortex Neurons Occurs in Very Mild Alzheimer's Disease". *The Journal of Neuroscience* 16, no. 14 (): 4491–4500. doi:10.1523/jneurosci.16-14-04491.1996. https://doi.org/10.1523/jneurosci.16-14-04491.1996.

Gómez-Ramos, Pilar, and M. Asunción Morán. 2007. "Ultrastructural Localization of Intraneuronal A-Peptide in Alzheimer Disease Brains". *Journal of Alzheimer's Disease* 11, no. 1 (): 53–59. ISSN: 1875-8908. doi:10.3233/JAD-2007-11109. http://doi.org/10.3233/JAD-2007-11109.

Gordon, Siamon. 2003. "Alternative activation of macrophages". *Nature Reviews Immunology* 3, no. 1 (): 23–35. doi:10.1038/nri978. https://doi.org/10.1038/nri978.

Govindpani, Karan, et al. 2017. "Towards a Better Understanding of GABAergic Remodeling in Alzheimer's Disease". *International Journal of Molecular Sciences* 18, no. 8 (): 1813. doi:10.3390/ijms18081813. https://doi.org/10.3390/ijms18081813.

Gratuze, Maud, Cheryl E. G. Leyns, and David M. Holtzman. 2018. "New insights into the role of TREM2 in Alzheimer's disease". *Molecular Neurodegeneration* 13, no. 1 (). doi:10.1186/s13024-018-0298-9. https://doi.org/10.1186/s13024-018-0298-9.

Greenamyre, J. Timothy, et al. 1987. "Dementia of the Alzheimer's Type: Changes in Hippocampal L-[3H]Glutamate Binding". *Journal of Neurochemistry* 48, no. 2 (): 543–551. doi:10.1111/j.1471-4159.1987.tb04127.x. https://doi.org/10.1111/j.1471-4159.1987.tb04127.x.

Guerreiro, Rita Joao, et al. 2010. “Genetic screening of Alzheimer’s disease genes in Iberian and African samples yields novel mutations in presenilins and APP”. *Neurobiology of Aging* 31, no. 5 (): 725–731. doi:10.1016/j.neurobiolaging.2008.06.012. https://doi.org/10.1016/j.neurobiolaging.2008.06.012.

Guerreiro, Rita, et al. 2013. “TREM2 Variants in Alzheimer’s Disease”. *New England Journal of Medicine* 368, no. 2 (): 117–127. doi:10.1056/nejmoa1211851. https://doi.org/10.1056/nejmoa1211851.

Gulyas, Attila I., Norbert Hajos, and Tamas F. Freund. 1996. “Interneurons Containing Calretinin Are Specialized to Control Other Interneurons in the Rat Hippocampus”. *The Journal of Neuroscience* 16, no. 10 (): 3397–3411. doi:10.1523/jneurosci.16-10-03397.1996. https://doi.org/10.1523/jneurosci.16-10-03397.1996.

Halasy, Katalin, et al. 1996. “Synaptic target selectivity and input of GABAergic basket and bistratified interneurons in the CA1 area of the rat hippocampus”. *Hippocampus* 6 (3): 306–329. doi:10.1002/(sici)1098-1063(1996)6:3<306::aid-hipo8>3.0.co;2-k. https://doi.org/10.1002/(sici)1098-1063(1996)6:3%3C306::aid-hipo8%3E3.0.co;2-k.

Hall, Alicia M., and Erik D. Roberson. 2012. “Mouse models of Alzheimer’s disease”. *Brain Research Bulletin* 88, no. 1 (): 3–12. doi:10.1016/j.brainresbull.2011.11.017. https://doi.org/10.1016/j.brainresbull.2011.11.017.

Hardy, J., and G. Higgins. 1992. “Alzheimer’s disease: the amyloid cascade hypothesis”. *Science* 256, no. 5054 (): 184–185.

doi:10.1126/science.1566067. https://doi.org/10.1126/science.1566067.

Hargreaves, Eric L, et al. 2005. "Major dissociation between medial and lateral entorhinal input to dorsal hippocampus". *science* 308 (5729): 1792–1794.

Harro, Jaanus, et al. 1996. "Cholecystokinin peptides and receptors in the rat brain during stress". *Naunyn-Schmiedeberg's Archives of Pharmacology* 354, no. 1 (). doi:10.1007/bf00168707. https://doi.org/10.1007/bf00168707.

He, Qian, et al. 2019. "Risk of Dementia in Long-Term Benzodiazepine Users: Evidence from a Meta-Analysis of Observational Studies". *Journal of Clinical Neurology* 15 (1): 9. doi:10.3988/jcn.2019.15.1.9. https://doi.org/10.3988/jcn.2019.15.1.9.

Hefner, K., and A. Holmes. 2007. "Ontogeny of fear-, anxiety- and depression-related behavior across adolescence in C57BL/6J mice". *Behavioural Brain Research* 176, no. 2 (): 210–215. doi:10.1016/j.bbr.2006.10.001. https://doi.org/10.1016/j.bbr.2006.10.001.

Henry, Julie D, John R Crawford, and Louise H Phillips. 2004. "Verbal fluency performance in dementia of the Alzheimer's type: a meta-analysis". *Neuropsychologia* 42, no. 9 (): 1212–1222. doi:10.1016/j.neuropsychologia.2004.02.001. https://doi.org/10.1016/j.neuropsychologia.2004.02.001.

Herl, Lauren, et al. 2009. "Mutations in amyloid precursor protein affect its interactions with presenilin/-secretase". *Molecular and Cellular Neuroscience* 41, no. 2 (): 166–174. doi:10.1016/j.mcn.2009.02.008. https://doi.org/10.1016/j.mcn.2009.02.008.

Hof, Patrick R., et al. 1993. "Calretinin-immunoreactive neocortical interneurons are unaffected in Alzheimer's disease". *Neuroscience Letters* 152, **numbers** 1-2 (): 145–149. doi:10.1016/0304-3940(93)90504-e. https://doi.org/10.1016/0304-3940(93)90504-e.

Hol, E M, et al. 2003. "Neuronal expression of GFAP in patients with Alzheimer pathology and identification of novel GFAP splice forms". *Molecular Psychiatry* 8, no. 9 (): 786–796. doi:10.1038/sj.mp.4001379. https://doi.org/10.1038/sj.mp.4001379.

Hopperton, K E, et al. 2017. "Markers of microglia in post-mortem brain samples from patients with Alzheimer's disease: a systematic review". *Molecular Psychiatry* 23, no. 2 (): 177–198. doi:10.1038/mp.2017.246. https://doi.org/10.1038/mp.2017.246.

Hort, J., et al. 2010. "EFNS guidelines for the diagnosis and management of Alzheimer's disease". *European Journal of Neurology* 17, no. 10 (): 1236–1248. doi:10.1111/j.1468-1331.2010.03040.x. https://doi.org/10.1111/j.1468-1331.2010.03040.x.

Howell, O., et al. 2000. "Density and pharmacology of 5 subunit-containing $GABA_A$ receptors are preserved in hippocampus of Alzheimer's disease patients". *Neuroscience* 98, no. 4 (): 669–675. doi:10.1016/s0306-4522(00)00163-9. https://doi.org/10.1016/s0306-4522(00)00163-9.

Hu, Hang, John Z. Cavendish, and Ariel Agmon. 2013. "Not all that glitters is gold: off-target recombination in the somatostatin–IRES-Cre mouse line labels a subset of fast-spiking interneurons". *Frontiers in Neural Circuits* 7. doi:10.3389/fncir.2013.00195. https://doi.org/10.3389/fncir.2013.00195.

Hughes, J., et al. 1990. “Development of a class of selective cholecystokinin type B receptor antagonists having potent anxiolytic activity.” *Proceedings of the National Academy of Sciences* 87, no. 17 (): 6728–6732. doi:10.1073/pnas.87.17.6728. https://doi.org/10.1073/pnas.87.17.6728.

Hunt, Clare E., and Anthony J. Turner. 2009. “Cell biology, regulation and inhibition of -secretase (BACE-1)”. *FEBS Journal* 276, no. 7 (): 1845–1859. doi:10.1111/j.1742-4658.2009.06929.x. https://doi.org/10.1111/j.1742-4658.2009.06929.x.

Hunter, Walter S. 1914. “The Auditory Sensitivity of the White Rat”. *Journal of Animal Behaviour* 4:429–41. doi:10.1016/0023-9690(77)90054-6. https://doi.org/10.1016/0023-9690(77)90054-6.

Huse, Jason T., et al. 2002. “-Secretase Processing in the Trans-Golgi Network Preferentially Generates Truncated Amyloid Species That Accumulate in Alzheimer’s Disease Brain”. *Journal of Biological Chemistry* 277, no. 18 (): 16278–16284. doi:10.1074/jbc.m111141200. https://doi.org/10.1074/jbc.m111141200.

Ittner, Lars M., and Jurgen Gotz. 2010. “Amyloid- and tau — a toxic pas de deux in Alzheimer’s disease”. *Nature Reviews Neuroscience* 12, no. 2 (): 67–72. doi:10.1038/nrn2967. https://doi.org/10.1038/nrn2967.

Jack, C. R., et al. 1998. “Rate of medial temporal lobe atrophy in typical aging and Alzheimer’s disease”. *Neurology* 51, no. 4 (): 993–999. doi:10.1212/wnl.51.4.993. https://doi.org/10.1212/wnl.51.4.993.

Jansen, K.L.R., et al. 1990. “Alzheimer’s disease: Changes in hippocampal N-methyl-d-aspartate, quisqualate, neurotensin, adenosine, benzodiazepine, serotonin and opioid receptors—an autoradiographic study”. *Neuroscience*

39, no. 3 (): 613–627. doi:10.1016/0306-4522(90)90246-z. https://doi.org/10.1016/0306-4522(90)90246-z.

Jiang, X., et al. 2015. “Principles of connectivity among morphologically defined cell types in adult neocortex”. *Science* 350, no. 6264 (): aac9462–aac9462. doi:10.1126/science.aac9462. https://doi.org/10.1126/science.aac9462.

Johansson, Maurits, et al. 2020. “Apathy and anxiety are early markers of Alzheimer’s disease”. *Neurobiology of Aging* 85 (): 74–82. doi:10.1016/j.neurobiolaging.2019.10.008. https://doi.org/10.1016/j.neurobiolaging.2019.10.008.

Kaiser, Natalie C., et al. 2014. “Differences in Anxiety Among Patients With Early- Versus Late-Onset Alzheimer’s Disease”. *The Journal of Neuropsychiatry and Clinical Neurosciences* 26, no. 1 (): 73–80. doi:10.1176/appi.neuropsych.12100240. https://doi.org/10.1176/appi.neuropsych.12100240.

Kampa, Bjorn M., Johannes J. Letzkus, and Greg J. Stuart. 2007. “Dendritic mechanisms controlling spike-timing-dependent synaptic plasticity”. *Trends in Neurosciences* 30, no. 9 (): 456–463. doi:10.1016/j.tins.2007.06.010. https://doi.org/10.1016/j.tins.2007.06.010.

Kane, S.P. 2019. “Sample Size Calculator” (). https://clincalc.com/stats/samplesize.aspx.%20Updated%20July%2024,%202019.%20Accessed%20May%2023,%202021.

Karson, M. A., et al. 2009. “Synaptic Cross Talk between Perisomatic-Targeting Interneuron Classes Expressing Cholecystokinin and Parvalbumin in Hippocampus”. *Journal of Neuroscience* 29, no. 13 (): 4140–4154.

doi:10.1523/jneurosci.5264-08.2009. https://doi.org/10.1523/jneurosci.5264-08.2009.

Kashani, Alireza, et al. 2008. "Loss of VGLUT1 and VGLUT2 in the prefrontal cortex is correlated with cognitive decline in Alzheimer disease". *Neurobiology of Aging* 29, no. 11 (): 1619–1630. doi:10.1016/j.neurobiolaging.2007.04.010. https://doi.org/10.1016/j.neurobiolaging.2007.04.010.

Katona, I, L Acsády, and T.F Freund. 1999. "Postsynaptic targets of somatostatin-immunoreactive interneurons in the rat hippocampus". *Neuroscience* 88, no. 1 (): 37–55. doi:10.1016/s0306-4522(98)00302-9. https://doi.org/10.1016/s0306-4522(98)00302-9.

Kaufer, Daniel I., et al. 2000. "Validation of the NPI-Q, a Brief Clinical Form of the Neuropsychiatric Inventory". *The Journal of Neuropsychiatry and Clinical Neurosciences* 12, no. 2 (): 233–239. doi:10.1176/jnp.12.2.233. https://doi.org/10.1176/jnp.12.2.233.

Khachaturian, Z. S. 1994. "Calcium Hypothesis of Alzheimer's Disease and Brain Aging". *Annals of the New York Academy of Sciences* 747, no. 1 (): 1–11. doi:10.1111/j.1749-6632.1994.tb44398.x. https://doi.org/10.1111/j.1749-6632.1994.tb44398.x.

Khan, Usman A, et al. 2013. "Molecular drivers and cortical spread of lateral entorhinal cortex dysfunction in preclinical Alzheimer's disease". *Nature Neuroscience* 17, no. 2 (): 304–311. doi:10.1038/nn.3606. https://doi.org/10.1038/nn.3606.

Kim, Jungsu, Jacob M. Basak, and David M. Holtzman. 2009. "The Role of Apolipoprotein E in Alzheimer's Disease". *Neuron* 63, no. 3 (): 287–303. doi:10.1016/j.neuron.2009.06.026. https://doi.org/10.1016/j.neuron.2009.06.026.

Klein, Donna M., Kevin M. Felsenstein, and Douglas E. Brenneman. 2008. "Cathepsins B and L Differentially Regulate Amyloid Precursor Protein Processing". *Journal of Pharmacology and Experimental Therapeutics* 328, no. 3 (): 813–821. doi:10.1124/jpet.108.147082. https://doi.org/10.1124/jpet.108.147082.

Kluge, C., et al. 2008. "Role of the somatostatin system in contextual fear memory and hippocampal synaptic plasticity". *Learning & Memory* 15, no. 4 (): 252–260. doi:10.1101/lm.793008. https://doi.org/10.1101/lm.793008.

Kobayashi, Dione, et al. 2008. "BACE1 gene deletion: Impact on behavioral function in a model of Alzheimer's disease". *Neurobiology of Aging* 29, no. 6 (): 861–873. doi:10.1016/j.neurobiolaging.2007.01.002. https://doi.org/10.1016/j.neurobiolaging.2007.01.002.

Koester, Christina, et al. 2013. "Dissecting the role of diazepam-sensitive -aminobutyric acid type A receptors in defensive behavioral reactivity to mild threat". *Pharmacology Biochemistry and Behavior* 103, no. 3 (): 541–549. doi:10.1016/j.pbb.2012.10.004. https://doi.org/10.1016/j.pbb.2012.10.004.

Koistinaho, Milla, et al. 2004. "Apolipoprotein E promotes astrocyte colocalization and degradation of deposited amyloid- peptides". *Nature Medicine* 10, no. 7 (): 719–726. doi:10.1038/nm1058. https://doi.org/10.1038/nm1058.

Krantic, Slavica, et al. 2012. "Hippocampal GABAergic Neurons are Susceptible to Amyloid- Toxicity in vitro and are Decreased in Number in the Alzheimer's Disease TgCRND8 Mouse Model". *Journal of Alzheimer's Disease* 29, no.

2 (): 293–308. ISSN: 18758908, 13872877. doi:10.3233/JAD-2011-110830. https://doi.org/10.3233/JAD-2011-110830.

Kumar, Anil, Arti Singh, and Ekavali. 2015. "A review on Alzheimer's disease pathophysiology and its management: an update". *Pharmacological Reports* 67, no. 2 (): 195–203. doi:10.1016/j.pharep.2014.09.004. https://doi.org/10.1016/j.pharep.2014.09.004.

Kuriyama, Kinya, Masaaki Hirouchi, and Hiroshi Nakayasu. 1993. "Structure and function of cerebral GABAA and GABAB receptors". *Neuroscience Research* 17, no. 2 (): 91–99. doi:10.1016/0168-0102(93)90087-7. https://doi.org/10.1016/0168-0102(93)90087-7.

LaFerla, Frank M., Kim N. Green, and Salvatore Oddo. 2007. "Intracellular amyloid- in Alzheimer's disease". *Nature Reviews Neuroscience* 8, no. 7 (): 499–509. doi:10.1038/nrn2168. https://doi.org/10.1038/nrn2168.

Langford, Dale J., et al. 2010. "Coding of facial expressions of pain in the laboratory mouse". *Nature Methods* 7, no. 6 (): 447–449. doi:10.1038/nmeth.1455. https://doi.org/10.1038/nmeth.1455.

Larson, Eric B., et al. 2006. "Exercise Is Associated with Reduced Risk for Incident Dementia among Persons 65 Years of Age and Older". *Annals of Internal Medicine* 144, no. 2 (): 73. doi:10.7326/0003-4819-144-2-200601170-00004. https://doi.org/10.7326/0003-4819-144-2-200601170-00004.

Launer, L. J., et al. 1999. "Rates and risk factors for dementia and Alzheimer's disease: Results from EURODEM pooled analyses". *Neurology* 52, no. 1 (): 78–78. doi:10.1212/wnl.52.1.78. https://doi.org/10.1212/wnl.52.1.78.

Laws, Keith R., et al. 2007. “A meta-analytic review of category naming in Alzheimer’s disease”. *Neuropsychologia* 45 (12): 2674–2682. doi:10.1016/j.neuropsychologia.2007.04.003. https://doi.org/10.1016/j.neuropsychologia.2007.04.003.

Leao, Richardson N, et al. 2012. “OLM interneurons differentially modulate CA3 and entorhinal inputs to hippocampal CA1 neurons”. *Nature Neuroscience* 15, no. 11 (): 1524–1530. doi:10.1038/nn.3235. https://doi.org/10.1038/nn.3235.

Leber, P. 1997. “Slowing the progression of Alzheimer disease: methodologic issues”. *Alzheimer’s disease and associated disorders* 11:s10–21. https://pubmed.ncbi.nlm.nih.gov/9348423/.

Lee, Young-Jung, et al. 2010. “Inflammation and Alzheimer’s disease”. *Archives of Pharmacal Research* 33, no. 10 (): 1539–1556. doi:10.1007/s12272-010-1006-7. https://doi.org/10.1007/s12272-010-1006-7.

Leung, Laura, et al. 2012. “Apolipoprotein E4 Causes Age- and Sex-Dependent Impairments of Hilar GABAergic Interneurons and Learning and Memory Deficits in Mice”. Ed. by Steven Estus. *PLoS ONE* 7, no. 12 (): e53569. doi:10.1371/journal.pone.0053569. https://doi.org/10.1371/journal.pone.0053569.

Li, Qingyun, and Ben A. Barres. 2017. “Microglia and macrophages in brain homeostasis and disease”. *Nature Reviews Immunology* 18, no. 4 (): 225–242. doi:10.1038/nri.2017.125. https://doi.org/10.1038/nri.2017.125.

Li, Yanfang, et al. 2016. “Implications of GABAergic Neurotransmission in Alzheimer’s Disease”. *Frontiers in Aging Neuroscience* 8 ().

doi:10.3389/fnagi.2016.00031. https://doi.org/10.3389/fnagi.2016.00031.

Liang, Danny, et al. 2007. "Cytotoxic edema: mechanisms of pathological cell swelling". *Neurosurgical Focus* 22, no. 5 (): 1–9. doi:10.3171/foc.2007.22.5.3. https://doi.org/10.3171/foc.2007.22.5.3.

Liddelow, Shane A., and Ben A. Barres. 2017. "Reactive Astrocytes: Production, Function, and Therapeutic Potential". *Immunity* 46, no. 6 (): 957–967. doi:10.1016/j.immuni.2017.06.006. https://doi.org/10.1016/j.immuni.2017.06.006.

Lisman, John E. 1999. "Relating Hippocampal Circuitry to Function". *Neuron* 22, no. 2 (): 233–242. doi:10.1016/s0896-6273(00)81085-5. https://doi.org/10.1016/s0896-6273(00)81085-5.

Lo, Chun-Min, et al. 2008. "Characterization of mice lacking the gene for cholecystokinin". *American Journal of Physiology-Regulatory, Integrative and Comparative Physiology* 294, no. 3 (): R803–R810. doi:10.1152/ajpregu.00682.2007. https://doi.org/10.1152/ajpregu.00682.2007.

Lovett-Barron, Matthew, et al. 2012. "Regulation of neuronal input transformations by tunable dendritic inhibition". *Nature Neuroscience* 15, no. 3 (): 423–430. doi:10.1038/nn.3024. https://doi.org/10.1038/nn.3024.

Lyketsos, C. G. 2000. "Mental and Behavioral Disturbances in Dementia: Findings From the Cache County Study on Memory in Aging". *American Journal of Psychiatry* 157, no. 5 (): 708–714. doi:10.1176/appi.ajp.157.5.708. https://doi.org/10.1176/appi.ajp.157.5.708.

Maccaferri, Gianmaria, and Chris J. McBain. 1995. “Passive propagation of LTD to stratum oriens-alveus inhibitory neurons modulates the temporoammonic input to the hippocampal CA1 region”. *Neuron* 15, no. 1 (): 137–145. doi:10.1016/0896-6273(95)90071-3. https://doi.org/10.1016/0896-6273(95)90071-3.

Maccioni, Ricardo B., et al. 2018. “Alzheimer´s Disease in the Perspective of Neuroimmunology”. *The Open Neurology Journal* 12, no. 1 (): 50–56. doi:10.2174/1874205x01812010050. https://doi.org/10.2174/1874205x01812010050.

Magnin, Elise, et al. 2018. “Input-Specific Synaptic Location and Function of the 5 GABAA Receptor Subunit in the Mouse CA1 Hippocampal Neurons”. *The Journal of Neuroscience* 39, no. 5 (): 788–801. doi:10.1523/jneurosci.0567-18.2018. https://doi.org/10.1523/jneurosci.0567-18.2018.

Maloney, Janice A., et al. 2014. “Molecular Mechanisms of Alzheimer Disease Protection by the A673T Allele of Amyloid Precursor Protein”. *Journal of Biological Chemistry* 289, no. 45 (): 30990–31000. doi:10.1074/jbc.m114.589069. https://doi.org/10.1074/jbc.m114.589069.

Mann, David M. A. 1996. “Pyramidal Nerve Cell Loss in Alzheimer’s Disease”. *Neurodegeneration* 5, no. 4 (): 423–427. doi:10.1006/neur.1996.0057. https://doi.org/10.1006/neur.1996.0057.

Masuda, Akira, et al. 2016. “Neurobiology of learning and memory”. 135 (): 73–82. doi:10.1016/j.nlm.2016.07.001. https://pubmed.ncbi.nlm.nih.gov/27377630/.

Mattson, Mark P., et al. 1993. “Evidence for excitoprotective and intraneuronal calcium-regulating roles for secreted forms of the -amyloid precursor protein”. *Neuron* 10, no. 2 (): 243–254.

doi:10.1016/0896-6273(93)90315-i. https://doi.org/10.1016/0896-6273(93)90315-i.

Mayeux, R., and Y. Stern. 2012. "Epidemiology of Alzheimer Disease". *Cold Spring Harbor Perspectives in Medicine* 2, no. 8 (): a006239–a006239. doi:10.1101/cshperspect.a006239. https://doi.org/10.1101/cshperspect.a006239.

McEntee, William J., and Thomas H. Crook. 1993. "Glutamate: its role in learning, memory, and the aging brain". *Psychopharmacology* 111, no. 4 (): 391–401. doi:10.1007/bf02253527. https://doi.org/10.1007/bf02253527.

Meldrum, Brian. 1982. "Pharmacology of GABA". *Clinical Neuropharmacology* 5 (3): 293–316. doi:10.1097/00002826-198205030-00004. https://doi.org/10.1097/00002826-198205030-00004.

Meziane, H., et al. 1998. "Memory-enhancing effects of secreted forms of the -amyloid precursor protein in normal and amnestic mice". *Proceedings of the National Academy of Sciences* 95, no. 21 (): 12683–12688. doi:10.1073/pnas.95.21.12683. https://doi.org/10.1073/pnas.95.21.12683.

Miller, Karen K., et al. 1997. "Cholecystokinin Increases GABA Release by Inhibiting a Resting KConductance in Hippocampal Interneurons". *The Journal of Neuroscience* 17, no. 13 (): 4994–5003. doi:10.1523/jneurosci.17-13-04994.1997. https://doi.org/10.1523/jneurosci.17-13-04994.1997.

Minelli, A, et al. 1995. "GAT-1, a high-affinity GABA plasma membrane transporter, is localized to neurons and astroglia in the cerebral cortex". *The Journal of Neuroscience* 15, no. 11 (): 7734–7746.

doi:10 . 1523 / jneurosci . 15 - 11 - 07734 . 1995. https://doi.org/10.1523/jneurosci.15-11-07734.1995.

Minier, F., and E. Sigel. 2004. "Positioning of the -subunit isoforms confers a functional signature to -aminobutyric acid type A receptors". *Proceedings of the National Academy of Sciences* 101, no. 20 (): 7769–7774. doi:10 . 1073 / pnas . 0400220101. https://doi.org/10.1073/pnas.0400220101.

Montigny, Claude de. 1989. "Cholecystokinin Tetrapeptide Induces Panic-like Attacks in Healthy Volunteers". *Archives of General Psychiatry* 46, no. 6 (): 511. doi:10 . 1001 / archpsyc . 1989 . 01810060031006. https : //doi.org/10.1001/archpsyc.1989.01810060031006.

Moser, May-Britt, David C. Rowland, and Edvard I. Moser. 2015. "Place Cells, Grid Cells, and Memory". *Cold Spring Harbor Perspectives in Biology* 7, no. 2 (): a021808. doi:10.1101/cshperspect.a021808. https://doi.org/10.1101/cshperspect.a021808.

Nagele, Robert G., et al. 2003. "Astrocytes accumulate A42 and give rise to astrocytic amyloid plaques in Alzheimer disease brains". *Brain Research* 971, no. 2 (): 197–209. doi:10 . 1016 / s0006 - 8993(03) 02361 - 8. https://doi.org/10.1016/s0006-8993(03)02361-8.

Nägga, K., N. Bogdanovic, and J. Marcusson. 1999. "GABA transporters (GAT-1) in Alzheimer's disease". *Journal of Neural Transmission* 106, **numbers** 11-12 (): 1141–1149. doi:10.1007/s007020050230. https://doi.org/10.1007/s007020050230.

Namba, Yoshio, et al. 1991. "Apolipoprotein E immunoreactivity in cerebral amyloid deposits and neurofibrillary tangles in Alzheimer's disease and kuru plaque amyloid in Creutzfeldt-Jakob disease". *Brain Research* 541, no. 1 ():

163–166. doi:10.1016/0006-8993(91)91092-f. https://doi.org/10.1016/0006-8993(91)91092-f.

Neill, D. 1995. "Alzheimer's Disease: Maladaptive Synaptoplasticity Hypothesis". *Neurodegeneration* 4, no. 2 (): 217–232. doi:10.1006/neur.1995.0027. https://doi.org/10.1006/neur.1995.0027.

Nelson, Andrea. 2021. "Beyond Memory Loss: How to Handle the Other Symptoms of Alzheimer's". https://www.hopkinsmedicine.org/health/conditions-and-diseases/alzheimers-disease/beyond-memory-loss-how-to-handle-the-other-symptoms-of-alzheimers.%20Accessed%20May%2025,%202021.

Nguyen, Robin, et al. 2020. "Cholecystokinin-Expressing Interneurons of the Medial Prefrontal Cortex Mediate Working Memory Retrieval". *The Journal of Neuroscience* 40, no. 11 (): 2314–2331. doi:10.1523/jneurosci.1919-19.2020. https://doi.org/10.1523/jneurosci.1919-19.2020.

NHS. 2021. "Side effects - Selective serotonin reuptake inhibitors (SSRIs)" (). https://www.nhs.uk/mental-health/talking-therapies-medicine-treatments/medicines-and-psychiatry/ssri-antidepressants/side-effects/7.

NICE. 2011. "Donepezil, galantamine, rivastigmine and memantine for the treatment of Alzheimer's disease" (). https://www.nice.org.uk/guidance/ta217/resources/donepezil-galantamine-rivastigmine-and-memantine-for-the-treatment-of-alzheimers-disease-pdf-82600254699973.%20Accessed%20May%2025,%202021.

Nikolaev, Anatoly, et al. 2009. "APP binds DR6 to trigger axon pruning and neuron death via distinct caspases". *Nature* 457, no. 7232 (): 981–989. doi:10.1038/nature07767. https://doi.org/10.1038/nature07767.

O'Day, Danton H., and Michael A. Myre. 2004. "Calmodulin-binding domains in Alzheimer's disease proteins: extending the calcium hypothesis". *Biochemical and Biophysical Research Communications* 320, no. 4 (): 1051–1054. doi:10.1016/j.bbrc.2004.06.070. https://doi.org/10.1016/j.bbrc.2004.06.070.

O'Keefe, J., and J. Dostrovsky. 1971. "The hippocampus as a spatial map. Preliminary evidence from unit activity in the freely-moving rat". *Brain Research* 34, no. 1 (): 171–175. doi:10.1016/0006-8993(71)90358-1. https://doi.org/10.1016/0006-8993(71)90358-1.

O'Day, Danton H., Kristeen Eshak, and Michael A. Myre. 2015. "Calmodulin Binding Proteins and Alzheimer's Disease". *Journal of Alzheimer's Disease* 46, no. 3 (): 553–569. doi:10.3233/JAD-142772. https://doi.org/10.3233/JAD-142772.

Oeckl, Patrick, et al. 2019. "Glial Fibrillary Acidic Protein in Serum is Increased in Alzheimer's Disease and Correlates with Cognitive Impairment". *Journal of Alzheimer's Disease* 67, no. 2 (): 481–488. ISSN: 13872877, 18758908. doi:10.3233/JAD-180325. https://doi.org/10.3233/JAD-180325.

Olton, David S., James T. Becker, and Gail E. Handelmann. 1979. "Hippocampus, space, and memory". *Behavioral and Brain Sciences* 2, no. 3 (): 313–322. doi:10.1017/s0140525x00062713. https://doi.org/10.1017/s0140525x00062713.

Olton, David S., Christine Collison, and Mary Ann Werz. 1977. “Spatial memory and radial arm maze performance of rats”. *Learning and Motivation* 8, no. 3 (): 289–314. doi:10.1016/0023-9690(77)90054-6. https://doi.org/10.1016/0023-9690(77)90054-6.

Ovsepian, Saak Victor, et al. 2016. “Ambient Glutamate Promotes Paroxysmal Hyperactivity in Cortical Pyramidal Neurons at Amyloid Plaques via Presynaptic mGluR1 Receptors”. *Cerebral Cortex* (). doi:10.1093/cercor/bhw267. https://doi.org/10.1093/cercor/bhw267.

Palop, Jorge J., Jeannie Chin, and Lennart Mucke. 2006. “A network dysfunction perspective on neurodegenerative diseases”. *Nature* 443, no. 7113 (): 768–773. doi:10.1038/nature05289. https://doi.org/10.1038/nature05289.

Palop, Jorge J., et al. 2007. “Aberrant Excitatory Neuronal Activity and Compensatory Remodeling of Inhibitory Hippocampal Circuits in Mouse Models of Alzheimer’s Disease”. *Neuron* 55, no. 5 (): 697–711. doi:10.1016/j.neuron.2007.07.025. https://doi.org/10.1016/j.neuron.2007.07.025.

Petrache, Alexandra L., et al. 2020. “Selective Modulation of 5 GABAA Receptors Exacerbates Aberrant Inhibition at Key Hippocampal Neuronal Circuits in APP Mouse Model of Alzheimer’s Disease”. *Frontiers in Cellular Neuroscience* 14 (). doi:10.3389/fncel.2020.568194. https://doi.org/10.3389/fncel.2020.568194.

Petrache, Alexandra L, et al. 2019. “Aberrant Excitatory–Inhibitory Synaptic Mechanisms in Entorhinal Cortex Microcircuits During the Pathogenesis of Alzheimer’s Disease”. *Cerebral Cortex* 29, no. 4 (): 1834–1850.

doi:10.1093/cercor/bhz016. https://doi.org/10.1093/cercor/bhz016.

Pirker, S, et al. 2000. "GABAA receptors: immunocytochemical distribution of 13 subunits in the adult rat brain". *Neuroscience* 101, no. 4 (): 815–850. doi:10.1016/s0306-4522(00)00442-5. https://doi.org/10.1016/s0306-4522(00)00442-5.

Plagman, Alexandra, et al. 2019. "Cholecystokinin and Alzheimer's disease: a biomarker of metabolic function, neural integrity, and cognitive performance". *Neurobiology of Aging* 76 (): 201–207. doi:10.1016/j.neurobiolaging.2019.01.002. https://doi.org/10.1016/j.neurobiolaging.2019.01.002.

Prince, M., et al. 2015. "World Alzheimer Report 2015 The Global Impact of Dementia An analysis of prevalence, incidence, cost and trends". *Alzheimer's Disease International*.

Pritchett, Dolan B., and Peter H. Seeburg. 1990. "?-Aminobutyric AcidAReceptor ?5-Subunit Creates Novel Type II Benzodiazepine Receptor Pharmacology". *Journal of Neurochemistry* 54, no. 5 (): 1802–1804. doi:10.1111/j.1471-4159.1990.tb01237.x. https://doi.org/10.1111/j.1471-4159.1990.tb01237.x.

Prut, L., et al. 2010. "A reduction in hippocampal GABAAreceptor 5 subunits disrupts the memory for location of objects in mice". *Genes, Brain and Behavior* (). doi:10.1111/j.1601-183x.2010.00575.x. https://doi.org/10.1111/j.1601-183x.2010.00575.x.

Przedborski, Serge, Miquel Vila, and Vernice Jackson-Lewis. 2003. "Series Introduction: Neurodegeneration: What is it and where are we?" *Journal of Clinical Investigation* 111, no. 1 (): 3–10. doi:10.1172/jci200317522. https://doi.org/10.1172/jci200317522.

Qiu, Chengxuan, Diana De Ronchi, and Laura Fratiglioni. 2007. "The epidemiology of the dementias: an update". *Current Opinion in Psychiatry* 20, no. 4 (): 380–385. doi:10.1097/yco.0b013e32816ebc7b. https://doi.org/10.1097/yco.0b013e32816ebc7b.

Rajora, M. A., et al. 2017. "Tailored theranostic apolipoprotein E3 porphyrin-lipid nanoparticles target glioblastoma". *Chemical Science* 8 (8): 5371–5384. doi:10.1039/c7sc00732a. https://doi.org/10.1039/c7sc00732a.

Ramon-y-Cajal, Santiago. 1909. *Histologie du système nerveux de l'homme & des vertébrés*. Maloine, doi:10.5962/bhl.title.48637. https://doi.org/10.5962/bhl.title.48637.

Ramos, Blanca, et al. 2006. "Early neuropathology of somatostatin/NPY GABAergic cells in the hippocampus of a PS1×APP transgenic model of Alzheimer's disease". *Neurobiology of Aging* 27, no. 11 (): 1658–1672. doi:10.1016/j.neurobiolaging.2005.09.022. https://doi.org/10.1016/j.neurobiolaging.2005.09.022.

Rayaprolu, Sruti, et al. 2013. "TREM2 in neurodegeneration: evidence for association of the p.R47H variant with frontotemporal dementia and Parkinson's disease". *Molecular Neurodegeneration* 8, no. 1 (). doi:10.1186/1750-1326-8-19. https://doi.org/10.1186/1750-1326-8-19.

Reid, Hannah M.O., et al. 2021. "Understanding Changes in Hippocampal Interneurons Subtypes in the Pathogenesis of Alzheimer's Disease: A Systematic Review". *Brain Connectivity* 11, no. 3 (): 159–179. doi:10.1089/brain.2020.0879. https://doi.org/10.1089/brain.2020.0879.

Reisberg, Barry, et al. 2006. “A 24-Week Open-Label Extension Study of Memantine in Moderate to Severe Alzheimer Disease”. *Archives of Neurology* 63, no. 1 (): 49. doi:10.1001/archneur.63.1.49. https://doi.org/10.1001/archneur.63.1.49.

Resibois, A., and J.H. Rogers. 1992. “Calretinin in rat brain: An immunohistochemical study”. *Neuroscience* 46, no. 1 (): 101–134. doi:10.1016/0306-4522(92)90012-q. https://doi.org/10.1016/0306-4522(92)90012-q.

Rice, Heather C., et al. 2020. “Contribution of GABAergic interneurons to amyloid- plaque pathology in an APP knock-in mouse model”. *Molecular Neurodegeneration* 15, no. 1 (). doi:10.1186/s13024-019-0356-y. https://doi.org/10.1186/s13024-019-0356-y.

Ries, Miriam, and Magdalena Sastre. 2016. “Mechanisms of A Clearance and Degradation by Glial Cells”. *Frontiers in Aging Neuroscience* 8 (). doi:10.3389/fnagi.2016.00160. https://doi.org/10.3389/fnagi.2016.00160.

Ring, S., et al. 2007. “The Secreted -Amyloid Precursor Protein Ectodomain APPs Is Sufficient to Rescue the Anatomical, Behavioral, and Electrophysiological Abnormalities of APP-Deficient Mice”. *Journal of Neuroscience* 27, no. 29 (): 7817–7826. doi:10.1523/jneurosci.1026-07.2007. https://doi.org/10.1523/jneurosci.1026-07.2007.

Rio, Christian A. Cea-del, Chris J. McBain, and Kenneth A. Pelkey. 2012. “An update on cholinergic regulation of cholecystokinin-expressing basket cells”. *The Journal of Physiology* 590, no. 4 (): 695–702. doi:10.1113/jphysiol.2011.225342. https://doi.org/10.1113/jphysiol.2011.225342.

Rodriguez-Perdigon, Manuel, et al. 2016. “Down-regulation of glutamatergic terminals (VGLUT1) driven by A in Alzheimer’s disease”. *Hippocampus* 26, no. 10 (): 1303–1312. doi:10.1002/hipo.22607. https://doi.org/10.1002/hipo.22607.

Saido, Takaomi. 2021. “Personal communication to Alzforum.” *Alzforum* (). https://www.alzforum.org/research-models/app-nl-f-knock.

Saito, Takashi, et al. 2019. “Humanization of the entire murine Mapt gene provides a murine model of pathological human tau propagation”. *Journal of Biological Chemistry* 294, no. 34 (): 12754–12765. doi:10.1074/jbc.ra119.009487. https://doi.org/10.1074/jbc.ra119.009487.

Saito, Takashi, et al. 2014. “Single App knock-in mouse models of Alzheimer’s disease”. *Nature Neuroscience* 17, no. 5 (): 661–663. doi:10.1038/nn.3697. https://doi.org/10.1038/nn.3697.

Saito, Takashi, et al. 2005. “Somatostatin regulates brain amyloid peptide A42 through modulation of proteolytic degradation”. *Nature Medicine* 11, no. 4 (): 434–439. doi:10.1038/nm1206. https://doi.org/10.1038/nm1206.

Saraiva, Cláudia, et al. 2016. “Nanoparticle-mediated brain drug delivery: Overcoming blood–brain barrier to treat neurodegenerative diseases”. *Journal of Controlled Release* 235 (): 34–47. doi:10.1016/j.jconrel.2016.05.044. https://doi.org/10.1016/j.jconrel.2016.05.044.

Sarlus, Heela, and Michael T. Heneka. 2017. “Microglia in Alzheimer’s disease”. *Journal of Clinical Investigation* 127, no. 9 (): 3240–3249. doi:10.1172/jci90606. https://doi.org/10.1172/jci90606.

Sasaguri, Hiroki, et al. 2017. “APP mouse models for Alzheimer’s disease preclinical studies”. *The EMBO Journal* 36, no. 17 (): 2473–2487. doi:10.15252/embj.201797397. https://doi.org/10.15252/embj.201797397.

Saunders, A. M., et al. 1993. “Association of apolipoprotein E allele 4 with late-onset familial and sporadic Alzheimer’s disease”. *Neurology* 43, no. 8 (): 1467–1467. doi:10.1212/wnl.43.8.1467. https://doi.org/10.1212/wnl.43.8.1467.

Savonenko, A. V., et al. 2008. “Alteration of BACE1-dependent NRG1/ErbB4 signaling and schizophrenia-like phenotypes in BACE1-null mice”. *Proceedings of the National Academy of Sciences* 105, no. 14 (): 5585–5590. doi:10.1073/pnas.0710373105. https://doi.org/10.1073/pnas.0710373105.

Schettini, G. 1991. “Brain somatostatin: Receptor-coupled transducing mechanisms and role in cognitive functions”. *Pharmacological Research* 23, no. 3 (): 203–215. doi:10.1016/s1043-6618(05)80080-5. https://doi.org/10.1016/s1043-6618(05)80080-5.

Scheuner, D., et al. 1996. “Secreted amyloid –protein similar to that in the senile plaques of Alzheimer’s disease is increased in vivo by the presenilin 1 and 2 and APP mutations linked to familial Alzheimer’s disease”. *Nature Medicine* 2, no. 8 (): 864–870. doi:10.1038/nm0896-864. https://doi.org/10.1038/nm0896-864.

Schneider, Ronald, et al. 2008. “Effect of intranasally administered cholecystokinin on encoding of controlled and automatic memory processes”. *Psychopharmacology* 202, no. 4 (): 559–567. doi:10.1007/s00213-008-1332-3. https://doi.org/10.1007/s00213-008-1332-3.

Schofield, Peter R., et al. 1987. “Sequence and functional expression of the GABAA receptor shows a ligand-gated receptor super-family”. *Nature* 328, no. 6127 (): 221–227. doi:10.1038/328221a0. https://doi.org/10.1038/328221a0.

Schwartz, Rochelle D. 1988. “The GABAa receptor-gated ion channel: Biochemical and pharmacological studies of structure and function”. *Biochemical Pharmacology* 37, no. 18 (): 3369–3375. doi:10.1016/0006-2952(88)90684-3. https://doi.org/10.1016/0006-2952(88)90684-3.

Selkoe, D. J. 2002. “Alzheimer’s Disease Is a Synaptic Failure”. *Science* 298, no. 5594 (): 789–791. doi:10.1126/science.1074069. https://doi.org/10.1126/science.1074069.

Semmler, Alexander, et al. 2012. “Persistent cognitive impairment, hippocampal atrophy and EEG changes in sepsis survivors”. *Journal of Neurology, Neurosurgery & Psychiatry* 84, no. 1 (): 62–69. doi:10.1136/jnnp-2012-302883. https://doi.org/10.1136/jnnp-2012-302883.

Serrano-Pozo, A., et al. 2011. “Neuropathological Alterations in Alzheimer Disease”. *Cold Spring Harbor Perspectives in Medicine* 1, no. 1 (): a006189–a006189. doi:10.1101/cshperspect.a006189. https://doi.org/10.1101/cshperspect.a006189.

Serrano-Regal, Mari Paz, et al. 2020. “Expression and Function of GABA Receptors in Myelinating Cells”. *Frontiers in Cellular Neuroscience* 14 (). doi:10.3389/fncel.2020.00256. https://doi.org/10.3389/fncel.2020.00256.

Shi, Anqi, et al. 2019. “Preserved Calretinin Interneurons in an App Model of Alzheimer’s Disease Disrupt Hippocampal Inhibition via Upregulated P2Y1

Purinoreceptors". *Cerebral Cortex* 30, no. 3 (): 1272–1290. doi:10.1093/cercor/bhz165. https://doi.org/10.1093/cercor/bhz165.

Sims, Rebecca, et al. 2017. "Rare coding variants in PLCG2, ABI3, and TREM2 implicate microglial-mediated innate immunity in Alzheimer's disease". *Nature Genetics* 49, no. 9 (): 1373–1384. doi:10.1038/ng.3916. https://doi.org/10.1038/ng.3916.

Sinha, S., and I. Lieberburg. 1999. "Cellular mechanisms of beta -amyloid production and secretion". *Proceedings of the National Academy of Sciences* 96, no. 20 (): 11049–11053. doi:10.1073/pnas.96.20.11049. https://doi.org/10.1073/pnas.96.20.11049.

Solarski, Michael, et al. 2018. "Somatostatin in Alzheimer's disease: A new Role for an Old Player". *Prion* 12, no. 1 (): 1–8. doi:10.1080/19336896.2017.1405207. https://doi.org/10.1080/19336896.2017.1405207.

Solodkin, Ana, Stacy D. Veldhuizen, and Gary W. Van Hoesen. 1996. "Contingent Vulnerability of Entorhinal Parvalbumin-Containing Neurons in Alzheimer's Disease". *The Journal of Neuroscience* 16, no. 10 (): 3311–3321. doi:10.1523/jneurosci.16-10-03311.1996. https://doi.org/10.1523/jneurosci.16-10-03311.1996.

Solomon, Viswas Raja, et al. 2019. "GABA allosteric modulators: An overview of recent developments in non-benzodiazepine modulators". *European Journal of Medicinal Chemistry* 171 (): 434–461. doi:10.1016/j.ejmech.2019.03.043. https://doi.org/10.1016/j.ejmech.2019.03.043.

Stafstrom, Carl E. 2006. "Behavioral and Cognitive Testing Procedures in Animal Models of Epilepsy". In *Models of Seizures and Epilepsy*, 613–628. Elsevier.

doi:10.1016/b978-012088554-1/50051-7. https://doi.org/10.1016/b978-012088554-1/50051-7.

Stewart, Sarah, Francesca Cacucci, and Colin Lever. 2011. "Which Memory Task for My Mouse? A Systematic Review of Spatial Memory Performance in the Tg2576 Alzheimer's Mouse Model". *Journal of Alzheimer's Disease* 26, no. 1 (): 105–126. ISSN: 18758908, 13872877. doi:10.3233/JAD-2011-101827. https://doi.org/10.3233/JAD-2011-101827.

Streit, Wolfgang J. 2004. "Microglia and Alzheimer's disease pathogenesis". *Journal of Neuroscience Research* 77 (1): 1–8. doi:10.1002/jnr.20093. https://doi.org/10.1002/jnr.20093.

Stuart, Greg J., and Bert Sakmann. 1994. "Active propagation of somatic action potentials into neocortical pyramidal cell dendrites". *Nature* 367, no. 6458 (): 69–72. doi:10.1038/367069a0. https://doi.org/10.1038/367069a0.

Tabuchi, K., et al. 2009. "Conditional Forebrain Inactivation of Nicastrin Causes Progressive Memory Impairment and Age-Related Neurodegeneration". *Journal of Neuroscience* 29, no. 22 (): 7290–7301. doi:10.1523/jneurosci.1320-09.2009. https://doi.org/10.1523/jneurosci.1320-09.2009.

Tamblyn, Robyn, et al. 2005. "A 5-Year Prospective Assessment of the Risk Associated with Individual Benzodiazepines and Doses in New Elderly Users". *Journal of the American Geriatrics Society* 53, no. 2 (): 233–241. doi:10.1111/j.1532-5415.2005.53108.x. https://doi.org/10.1111/j.1532-5415.2005.53108.x.

Taylor, Chanel J., et al. 2008. "Endogenous secreted amyloid precursor protein-regulates hippocampal NMDA receptor function, long-term potentiation and spatial memory". *Neurobiology of Disease* 31, no. 2 (): 250–260. doi:10.

1016/j.nbd.2008.04.011. https://doi.org/10.1016/j.nbd.2008.04.011.

Treiman, David M. 2001. "GABAergic Mechanisms in Epilepsy". *Epilepsia* 42 (): 8–12. doi:10.1046/j.1528-1157.2001.042suppl.3008.x. https://doi.org/10.1046/j.1528-1157.2001.042suppl.3008.x.

Tuppo, Ehab E., and Hugo R. Arias. 2005. "The role of inflammation in Alzheimer's disease". *The International Journal of Biochemistry & Cell Biology* 37, no. 2 (): 289–305. doi:10.1016/j.biocel.2004.07.009. https://doi.org/10.1016/j.biocel.2004.07.009.

Urban-Ciecko, Joanna, and Alison L. Barth. 2016. "Somatostatin-expressing neurons in cortical networks". *Nature Reviews Neuroscience* 17, no. 7 (): 401–409. doi:10.1038/nrn.2016.53. https://doi.org/10.1038/nrn.2016.53.

Vagner, Tatyana, et al. 2016. "Systemic application of AAV vectors targeting GFAP-expressing astrocytes in Z -Q175-KI Huntington's disease mice". *Molecular and Cellular Neuroscience* 77 (): 76–86. doi:10.1016/j.mcn.2016.10.007. https://doi.org/10.1016/j.mcn.2016.10.007.

Vassar, R. 1999. "Beta-Secretase Cleavage of Alzheimer's Amyloid Precursor Protein by the Transmembrane Aspartic Protease BACE". *Science* 286, no. 5440 (): 735–741. doi:10.1126/science.286.5440.735. https://doi.org/10.1126/science.286.5440.735.

Verret, Laure, et al. 2012. "Inhibitory Interneuron Deficit Links Altered Network Activity and Cognitive Dysfunction in Alzheimer Model". *Cell* 149, no. 3 (): 708–721. doi:10.1016/j.cell.2012.02.046. https://doi.org/10.1016/j.cell.2012.02.046.

Villette, Vincent, et al. 2012. “A new neuronal target for beta-amyloid peptide in the rat hippocampus”. *Neurobiology of Aging* 33, no. 6 (): 1126.e1–1126.e14. doi:10.1016/j.neurobiolaging.2011.11.024. https://doi.org/10.1016/j.neurobiolaging.2011.11.024.

Wable, Gauri S., et al. 2015. “Anxiety is correlated with running in adolescent female mice undergoing activity-based anorexia.” *Behavioral Neuroscience* 129 (2): 170–182. doi:10.1037/bne0000040. https://doi.org/10.1037/bne0000040.

Wafford, Keith A. 2005. “GABAA receptor subtypes: any clues to the mechanism of benzodiazepine dependence?” *Current Opinion in Pharmacology* 5, no. 1 (): 47–52. doi:10.1016/j.coph.2004.08.006. https://doi.org/10.1016/j.coph.2004.08.006.

Wang, Jun, et al. 2017. “A systemic view of Alzheimer disease — insights from amyloid- metabolism beyond the brain”. *Nature Reviews Neurology* 13, no. 10 (): 612–623. doi:10.1038/nrneurol.2017.111. https://doi.org/10.1038/nrneurol.2017.111.

Wang, X.-J., et al. 2004. “Division of labor among distinct subtypes of inhibitory neurons in a cortical microcircuit of working memory”. *Proceedings of the National Academy of Sciences* 101, no. 5 (): 1368–1373. doi:10.1073/pnas.0305337101. https://doi.org/10.1073/pnas.0305337101.

Weingarten, M. D., et al. 1975. “A protein factor essential for microtubule assembly.” *Proceedings of the National Academy of Sciences* 72, no. 5 (): 1858–1862. doi:10.1073/pnas.72.5.1858. https://doi.org/10.1073/pnas.72.5.1858.

Wes, Paul D., et al. 2015. “Next generation transcriptomics and genomics elucidate biological complexity of microglia in health and disease”. *Glia* 64, no. 2 ():

197–213. doi:10.1002/glia.22866. https://doi.org/10.1002/glia.22866.

Whittington, Miles A, and Roger D Traub. 2003. "Interneuron Diversity series: Inhibitory interneurons and network oscillations in vitro". *Trends in Neurosciences* 26, no. 12 (): 676–682. doi:10.1016/j.tins.2003.09.016. https://doi.org/10.1016/j.tins.2003.09.016.

Wojcik, S. M., et al. 2004. "An essential role for vesicular glutamate transporter 1 (VGLUT1) in postnatal development and control of quantal size". *Proceedings of the National Academy of Sciences* 101, no. 18 (): 7158–7163. doi:10.1073/pnas.0401764101. https://doi.org/10.1073/pnas.0401764101.

Wolfe, Michael S. 2008. "Inhibition and modulation of -secretase for Alzheimer's disease". *Neurotherapeutics* 5, no. 3 (): 391–398. doi:10.1016/j.nurt.2008.05.010. https://doi.org/10.1016/j.nurt.2008.05.010.

Wolfensohn, Sarah, and Maggie Lloyd. 1998. *Handbook of Laboratory Animal Management and Welfare, 4th Edition*. Wiley-Blackwell.

Wolff, Joachim R., Ferenc Joo, and Wendelin Dames. 1978. "Plasticity in dendrites shown by continuous GABA administration in superior cervical ganglion of adult rat". *Nature* 274, no. 5666 (): 72–74. doi:10.1038/274072a0. https://doi.org/10.1038/274072a0.

Wonders, Carl P., and Stewart A. Anderson. 2006. "The origin and specification of cortical interneurons". *Nature Reviews Neuroscience* 7, no. 9 (): 687–696. doi:10.1038/nrn1954. https://doi.org/10.1038/nrn1954.

Wu, Jessica W, et al. 2016. "Neuronal activity enhances tau propagation and tau pathology in vivo". *Nature Neuroscience* 19, no. 8 (): 1085–1092. doi:10.1038/nn.4328. https://doi.org/10.1038/nn.4328.

Yee, Benjamin K., et al. 2004. "GABAA receptors containing the alpha5 subunit mediate the trace effect in aversive and appetitive conditioning and extinction of conditioned fear". *European Journal of Neuroscience* 20, no. 7 (): 1928–1936. doi:10.1111/j.1460-9568.2004.03642.x. https://doi.org/10.1111/j.1460-9568.2004.03642.x.

Zanier, Elisa R, et al. 2018. "Induction of a transmissible tau pathology by traumatic brain injury". *Brain* (). doi:10.1093/brain/awy193. https://doi.org/10.1093/brain/awy193.

Zhang, Bin, et al. 2013. "Integrated Systems Approach Identifies Genetic Nodes and Networks in Late-Onset Alzheimer's Disease". *Cell* 153, no. 3 (): 707–720. doi:10.1016/j.cell.2013.03.030. https://doi.org/10.1016/j.cell.2013.03.030.

Zhang, Wen, et al. 2016. "Hyperactive somatostatin interneurons contribute to excitotoxicity in neurodegenerative disorders". *Nature Neuroscience* 19, no. 4 (): 557–559. doi:10.1038/nn.4257. https://doi.org/10.1038/nn.4257.

Zhao, Jing, et al. 2017. "APOE 4/4 diminishes neurotrophic function of human iPSC-derived astrocytes". *Human Molecular Genetics* 26, no. 14 (): 2690–2700. doi:10.1093/hmg/ddx155. https://doi.org/10.1093/hmg/ddx155.

Zhuo, Jia-Min, et al. 2007. "Early discrimination reversal learning impairment and preserved spatial learning in a longitudinal study of Tg2576 APPsw mice". *Neurobiology of Aging* 28, no. 8 (): 1248–1257.

doi:10.1016/j.neurobiolaging.2006.05.034. https://doi.org/10.1016/j.neurobiolaging.2006.05.034.

Zilles, K, et al. 1995. “Plasticity and neurotransmitter receptor changes in Alzheimer’s disease and experimental cortical infarcts”. *Drug Res* 45:361–6.

Appendix A

Publications

OXFORD

Cerebral Cortex, 2019; 1–17

doi: 10.1093/cercor/bhz016
Original Article

ORIGINAL ARTICLE

Aberrant Excitatory–Inhibitory Synaptic Mechanisms in Entorhinal Cortex Microcircuits During the Pathogenesis of Alzheimer's Disease

Alexandra L. Petrache[1], Aarib Rajulawalla[1], Anqi Shi[1], Andrea Wetzel[1], Takashi Saito[2], Takaomi C. Saido[2], Kirsten Harvey[1] and Afia B. Ali [1]

[1]UCL School of Pharmacy, University College London, London WC1N 1AX, UK and [2]RIKEN Center for Brain Science, Wako-shi, Saitama, Japan

Address correspondence to Dr Afia B. Ali, UCL School of Pharmacy, 29-39 Brunswick Square, London, WC1N 1AX, UK. Email: afia.b.ali@ucl.ac.uk orcid.org/0000-0001-5203-5609

Alexandra L. Petrache, Aarib Rajulawalla, Anqi Shi had equal contribution

Abstract

Synaptic dysfunction is widely proposed as an initial insult leading to the neurodegeneration observed in Alzheimer's disease (AD). We hypothesize that the initial insult originates in the lateral entorhinal cortex (LEC) due to deficits in key interneuronal functions and synaptic signaling mechanisms, in particular, Wnt (Wingless/integrated). To investigate this hypothesis, we utilized the first knock-in mouse model of AD ($App^{NL\text{-}F/NL\text{-}F}$), expressing a mutant form of human amyloid-β (Aβ) precursor protein. This model shows an age-dependent accumulation of Aβ, neuroinflammation, and neurodegeneration. Prior to the typical AD pathology, we showed a decrease in canonical Wnt signaling activity first affecting the LEC in combination with synaptic hyperexcitation and severely disrupted excitatory–inhibitory inputs onto principal cells. This synaptic imbalance was consistent with a reduction in the number of parvalbumin-containing (PV) interneurons, and a reduction in the somatic inhibitory axon terminals in the LEC compared with other cortical regions. However, targeting $GABA_A$ receptors on PV cells using allosteric modulators, diazepam, zolpidem, or a nonbenzodiazepine, L-838,417 (modulator of α2/3 subunit-containing $GABA_A$ receptors), restored the excitatory–inhibitory imbalance observed at principal cells in the LEC. These data support our hypothesis, providing a rationale for targeting the synaptic imbalance in the LEC for early stage therapeutic intervention to prevent neurodegeneration in AD.

Key words: Alzheimer's disease, $GABA_A$ receptor, interneurons, synapse, Wnt signaling

Introduction

The axis between the entorhinal cortex and the hippocampus, important for the formation and consolidation of memories, is thought to be the first brain region to be significantly affected in patients with Alzheimer's disease (AD), characterized by synaptic loss leading to neurodegeneration and progressive cognitive deficits (Palop et al. 2006). Postmortem AD brains present with amyloid-β (Aβ) plaques, neurofibrillary tangles, dystrophic neurites, and signs of neuroinflammation, including astrocytosis and gliosis (Holtzman et al. 2011). Further to these contributors to the disease, deregulation of canonical Wingless/integrated (Wnt) signaling, important for synaptic maintenance, has long been proposed as a key contributor to neurodegeneration including AD pathogenesis (Inestrosa and Toledo

2008; Inestrosa and Arenas 2010; Toledo and Inestrosa 2010; Berwick and Harvey 2014).

One of the first changes observed during the early stages of AD pathogenesis is "hyperexcitability" in neuronal circuits. This is evidenced by imaging studies from preclinical and symptomatic AD patients during memory tasks (Buckner et al. 2005; O'Brien et al. 2010; Bero et al. 2012). It has been shown that the observed hyperexcitability is initiated in the lateral entorhinal cortex (LEC) before it spreads to other cortical regions (Khan et al. 2014). This abnormal hyperactivity is thought to be detrimental by causing Aβ release, spreading and accumulating during AD progression (Kamenetz et al. 2003; Busche et al. 2008; Cirrito et al. 2008; Yamamoto et al. 2015). This idea is further supported by studies reporting that a low dose of the antiepileptic drug levetiracetam can reduce hippocampal hyperactivity in humans and improve amnestic mild cognitive impairment (Bakker et al. 2012).

Although the precise neuronal circuits that are responsible for the hyperexcitability in AD patients observed from imaging studies remain largely unknown, it is generally accepted that glutamatergic principal pyramidal cells play a fundamental role in this neuronal hyperexcitation. The overall excitability of pyramidal cells is tuned by γ-aminobutyric acid (GABA)ergic inhibitory interneurons comprising ~20% of all neurones present in the cerebral cortex. As GABAergic cells are highly diverse in their properties and synapse on specific postsynaptic subcellular domains, (Maccaferri and Lacaille 2003; Markram et al. 2004; Ascoli et al. 2008; Klausberger and Somogyi 2008; Pelkey et al. 2017) even subtle disruption in interneuron behavior could unequivocally impact glutamatergic release, resulting in aberrant cortical excitation (Marin 2012; Verret et al. 2012; Palop and Mucke 2016; Khan et al. 2018).

Interestingly, fine regulatory mechanisms of Wnt signaling are crucial for synaptic maintenance that includes presynaptic neurotransmitter release, glutamate receptor trafficking and postsynaptic receptor clustering by postsynaptic density protein 95 (PSD-95) (Inestrosa and Arenas 2010; Cerpa et al. 2010, 2011; Park and Shen 2012). This signaling system has recently been shown to be important for the fine regulation of the entorhinal cortex–hippocampal circuitry (Oliva and Inestrosa 2015), and proposed to be critical for learning and memory-related synaptic plasticity (Jensen et al. 2012; Oliva et al. 2013a,b). However, it is unclear when neuronal hyperexcitability and Wnt signaling dysregulation occurs during the pathogenesis of AD.

The reported hyperexcitability in the brains of AD patients could be perceived as paradoxical, since several reports have shown that the inhibitory GABA receptor ($GABA_A$) family is actually preserved in human brains of AD patients (Howell et al. 2000; Rissman et al. 2007), although the $GABA_A$ receptors subtype that survives remains largely unclear. This receptor family is known to play a vital role in cognitive functions, including learning and memory through the actions of GABA-containing inhibitory interneurons. The prominent subclass of fast-spiking parvalbumin (PV)-containing (FS-PV) interneurons, namely, the basket cells targeting somatic and proximal dendrites of postsynaptic cells and chandelier cells targeting axon initial segments (Kawaguchi and Kubota 1993; Klausberger et al. 2005; Ascoli et al. 2008), accounts for ~40% of cortical GABAergic neurons (Rudy et al. 2011). FS-PV cells mediate inhibition via specific α1 and either α2 or α3 subunit-containing inhibitory $GABA_A$ receptors found on postsynaptic principal cells (Ali and Thomson 2008). This $GABA_A$ receptors, combination results in these cells showing activation in the γ frequency range in AD mice thereby reducing the spread of Aβ 1–40 and Aβ 1–42 isoforms before the onset of plaque formation or cognitive decline (Iaccarino et al. 2016). This suggests that the correct physiological function of FS-PV interneurons is important in preventing the spread of neurodegeneration in early stages of AD. The underlying mechanisms of this paradox and its significance for the expression of AD symptoms is not however, fully understood.

In our present study, we addressed this knowledge gap and deepened our understanding of synaptic dysfunction during AD progression using the first β-amyloid precursor protein (*App*) knock-in mouse model ($App^{NL\text{-}F/NL\text{-}F}$). This novel model is unique in resembling human AD progression more accurately than *App* overexpression models, showing age-related Aβ pathology, memory impairment and neuroinflammation (Saito et al. 2014; Masuda et al. 2016; Sasaguri et al. 2017). We hypothesize that Wnt signaling dysregulation is correlated with disrupted activity of the major inhibitory PV interneuron microcircuitry, which results in hyperexcitability initiated in the LEC and that these pathomechanisms precede the formation of Aβ plaques and neuroinflammation in App knock-in mice. Therefore, we investigated the excitatory–inhibitory synaptic inputs in principal cells and Wnt signaling dysregulation in cortical regions including the LEC of the AD mouse model relative to wild-type controls. We further investigated whether pharmacological modulation of PV cell activity could rescue the aberrant synaptic hyperactivity in AD.

Methods

Animals

Experimental Animals

All of the procedures in the study were carried out in accordance with the British Home Office regulations under the Animal Scientific Procedure Act 1986, under the project license PPL: 7007558 held by the principal investigator, Dr Afia Ali. All procedures were approved by both internal and external UCL ethics committees, and in accordance with the ARRIVE guidelines for reporting experiments involving animals (McGrath et al. 2010). A total of 85 animals (disease model and wild-type) were used in this study. The animals had ad-libitum access to food and water and were reared in cages of maximum 5 inhabitants, with a day: night cycle of 12 h:12 h.

The knock-in $APP^{NL\text{-}F/NL\text{-}F}$ AD mouse model was used for experiments (Saito et al. 2014). This particular mouse model was chosen because it follows the progression of human AD more faithfully. Since amyloid β-peptide (Aβ) plaque deposition is a key AD pathological hallmark, the model exhibits pathogenic Aβ accumulation whilst also maintaining biological amyloid precursor protein (APP) levels without overexpression artefacts. The $APP^{NL\text{-}F}$ model consists of the introduction of 2 familial AD (FAD) mutations: KM670/671NL and I716F. The former, identified as the Swedish mutation, increases β-site cleavage of APP to produce elevated amounts of both $Aβ_{40}$ and $Aβ_{42}$, whereas the latter, known as the Beyreuther/Iberian mutation, promotes γ-site cleavage at C-terminal position 42, thereby increasing the $Aβ_{42}/Aβ_{40}$ ratio in favor of the more hydrophobic $Aβ_{42}$ (Saito et al., 2014). Both features are key to the integrity of the disease phenotype. The transgenic line was crossed with C57BL/6 mice and the resulting heterozygous pairs were used for breeding, but excluded from experiments.

The knock in line was crossed with C57BL/6 mice and the resulting heterozygous pairs were used for breeding, but excluded from experiments. Only male $APP^{NL\text{-}F/NL\text{-}F}$ and age-

matched wild-type (C57BL/6) mice from the same breeding were used as control. $APP^{NL\text{-}F/NL\text{-}F}$ and control mice were investigated at 3 different ages: grouped into 3 age groups: 1–2, 4–6, and 10–18 months.

Animals were genotyped via standard polymerase chain reaction using the following 4 primers: 5′-ATCTCGGAAGTGAAG ATG-3′, 5′-TGTAGATGAGAACTTAAC-3′, 5′-ATCTCGGAAGTGAA TCTA-3′, and 5′-CGTATAATGTATGCTATACGAAG-3′ as previously described (Saito et al. 2014).

Tissue Collection and Preparation

Mice were anesthetized by an intraperitoneal injection of 60 mg/kg phenobarbitone and perfused transcardially with artificial cerebrospinal fluid (ACSF) containing sucrose. The level of anesthesia was monitored using pedal, tail pinch reflexes, rate, depth, and pattern of respiration through observation and color of mucous membranes and skin. The ACSF comprised of (in mM) 248 sucrose, 3.3 KCl, 1.4 NaH_2PO_4, 2.5 $CaCl_2$, 1.2 $MgCl_2$, 25.5 $NaHCO_3$, and 15 glucose, which was bubbled with 95% O_2 and 5% CO_2. The animals were then decapitated and the brain removed and parasagittal slices of cortex and hippocampus—300 μm thick—were cut in ice-cold standard ACSF using an automated vibratome (Leica, Germany). This standard ACSF contained (in mM): 121 NaCl, 2.5 KCl, 1.3 NaH_2PO_4, 2 $CaCl_2$, 1 $MgCl_2$, 20 glucose, and 26 $NaHCO_3$, equilibrated with 95% O_2 and 5% CO_2. Slices were incubated in ACSF for 1 h at room temperature (20–23 °C) prior to recording. Brain slices were placed in a submerged chamber and superperfused with ACSF at a rate of 1–2 mL min^{-1} for electrophysiological recordings. For neuroanatomical studies, brains were immediately fixed after perfusion in 4% paraformaldehyde plus 0.2% picric acid in 0.1 M phosphate buffer (PB) for 24 h prior to sectioning.

Electrophysiology

Whole-cell somatic recordings were performed in LEC (or CA1 and layer 2/3 of the neocortex) pyramidal cells and interneurons. Patch electrodes with resistances of 8–11 MΩ were made from filamented borosilicate glass capillaries (Harvard Apparatus, UK) and filled with a solution containing (in mM): 134 K gluconate, 10 HEPES, 10 phosphocreatine, 2 Na_2ATP, 0.2 Na_2GTP, and 0.2% w/v biocytin. Neurons were selected for recording based on the shape of their soma using video microscopy under near infrared differential interference contrast illumination, and further characterized by their electrophysiological properties obtained from injecting a series of 500 ms depolarizing and hyperpolarizing current pulses. Action potential parameters were measured from responses to depolarizing current steps (+50 to 150 pA, 500 ms), which induced a single or a trains of action potentials. The input resistance and membrane time constant were determined from voltage changes in response to hyperpolarizing current steps (−100 pA, 500 ms).

Spontaneous postsynaptic potentials were recorded from passive membrane responses and mixed spontaneous excitatory postsynaptic potentials (sEPSPs) and spontaneous inhibitory postsynaptic potentials (sIPSPs) were collected in 60 s frame samples, repeated at 0.33 Hz. Recordings were carried out under the current clamp mode of operation (NPI SEC 05LX amplifier; NPI electronics, Germany), low pass filtered at 2 KHz and digitized at 5 KHz using a CED 1401 interface (Cambridge Electronic Design, UK). Input resistance was monitored throughout experiments by means of a hyperpolarizing current step (−0.001 nA, 10 ms). Signal (Cambridge Electronic Design, UK) was used to acquire recordings and generate current steps. The average amplitudes of spontaneous events and their frequency was measured manually from single sweep data sets of 60 s recordings, including a total sweep range of 30–50 frames (i.e., 30–50 min of recording). For in vitro pharmacological studies, the $GABA_A$ receptor allosteric modulators—diazepam, zolpidem, or L-838,417 (0.5–1 μM, Tocris Bioscience, UK), the $GABA_A$ receptor antagonist GABAzine (SR95531 hydrobromide), and tetrodotoxin (TTX) were bath-applied. Average data points after drug application were obtained after steady-state responses were attained with the drugs, which was ~15–20 min after onset of the bath-application.

Neuroanatomical Procedures and Analysis

Parasagittal sections containing the entorhinal cortex, cerebral cortex, and hippocampus were sectioned at 100 μm-thickness using a vibratome (Vibroslice, Camden Instrument, Loughborough, UK), and placed in a 24-well plate containing 10% PB. Each experiment consisted of slices from wild-type and $APP^{NL\text{-}F/NL\text{-}F}$ age-matched mice and kept in separate 24-well plates. The sections per brain were randomly allocated to the antibody and procedure, but all sections underwent identical protocols for either immunofluorescence or immunoperoxidase procedures. Prior to these specific procedures, all sections were washed in 0.1% Triton X-100 in Tris-buffered saline (TBS-T), followed by incubation in 1% hydrogen peroxide aqueous solution for 30 min. After further rinses in TBS-T, sections were incubated in phosphate buffer saline (PBS) containing 10% normal goat serum (Sigma-Aldrich, USA) for 1 h at room temperature. This followed incubation in the specific primary antibodies to target the desired proteins shown in Table 1.

Immunofluorescence procedures, confocal image acquisition and analysis. For example, the anti-PV and anti-GAD67 primary antibodies were both added to the same wells to allow for colocalization assessments to be performed, whilst the anti-APP695, anti-CD68 and anti-GFAP primary antibodies were added to independent wells.

After incubation for 48 h in primary antibody on a platform shaker at a temperature at 4 °C, and a further 3 washes in TBS-T, the sections were incubated in the appropriate secondary antibodies for 3 h (fluorophores for immunofluorescence are shown in Table 1). The sections were then washed (3 × 10 min 0.3% TBS-T per well) and slices allocated for either CD68 or GFAP- selective immunofluorescence staining were then incubated further with DAPI (1:1000 dilution) for 15 min. After further washes, the slices were then mounted on glass slides using the antifade mounting medium, Vectarshield (Vector Lab. UK) ready for confocal microscopy.

The acquisition of fluorescence images was obtained using a LSM 710 confocal microscope which processed images using the Zen Black 2009 ZEISS software. An overview image (Tile-Scan) was taken of each whole brain slice using the ×10 lens, and then 3D images (Z-stack) were taken at 6 different positions within each brain section: the dorsal entorhinal cortex 1), ventral entorhinal cortex 2), layers 2/3 of the somatosensory neocortex 3), CA1 4), CA2 5) and CA3 regions 6), using the ×20 lens. The first and last 10 μm were discarded from each section to prevent repeated capture of the same cell.

The mean intensity and standard deviation (SD) of the light emitted by the fluorophores within a maximum projection of the Z-stacks was calculated using the confocal image processing software ZEN. To distinguish PV-expressing cells from any background fluorescence, a threshold was determined; any

Table 1 Antibodies used in immunohistochemistry experiments.

Immunofluorescence primary antibodies			
Antibody target	Company	Targeted species	Dilution
Parvalbumin	SWANT	Rabbit	1:1000
GAD67	Millipore	Mouse	1:2000
CD68	BioRad	Goat	1:500
GFAP	Agilent (Dako)	Rabbit	1:500
VGlut1	Millipore	Goat	1:2500
GAT-1	Millipore	Goat	1:500
CamKII-α	Cell Signaling Technology	Mouse	1:100
Immunofluorescence secondary antibodies			
Antibody	Company	Targeted species	Dilution
Texas Red	Thermo-Scientific	Rabbit	1:500
FITC	Sigma-Aldrich	Mouse	1:875
Alexa 488	abcam	Rabbit	1:1000
Alexa 568	Molecular Probes	Goat	1:500
DAPI	Sigma-Aldrich	Multiple	1:1000
Immunoperoxidase primary antibodies			
Antibody target	Company	Targeted species	Dilution
Parvalbumin	SWANT	Rabbit	1:5000
APP695	Thermo-Fisher	Mouse	1:10 000
CD68	BioRad	Goat	1:8000
GFAP	Agilant (Dako)	Rabbit	1:2000
Immunoperoxidase secondary antibodies			
Antibody	Company	Targeted species	Dilution
Biotinylated	Vector	Rabbit, Mouse, Rat	1:500

emission that exceeded a value of the mean intensity plus twice the standard deviation (e.g., PV or GAD67-positive interneuron = mean intensity + [2 × SD mean intensity]). Colocalization was confirmed when fluorophores marking both PV and GAD67 were at an intensity that exceeded the threshold. Somata that exceeded the threshold were counted in the individual levels of the Z-stack; any positive cells that appeared on consecutive levels of the Z-stack were considered to be the same cell and were not recounted. The total positive cell number of each Z-stack was then divided by the volume of the Z-stack (4.99×10^{-2} mm^3) to determine the density of PV + GAD67-coexpressing interneurons in each of the areas of interest.

Cell counts for each individual segment, were performed manually by circling each cell with the intent of avoiding counting the same cell twice. The total volume of each segment was calculated to allow for the conversion of cell counts to signify neuronal cell density (number of cells/mm^3).

Immunoperoxidase procedure and analysis. After washes in TBS-T, the sections were then incubated in secondary biotinylated antibodies (see Table 1 for individual antibody detail). Postincubation with secondary fluorescent antibody and after washes in TBS-T, there was a further incubation in avidin–biotin–horseradish peroxidase complex (ABC; Vector Laboratories, UK) solution, for 2 h at room temperature. The sections were then washed further in TBS-T, and processed with 3–3-diaminobenzidine (DAB), and subsequently dehydrated and mounted (Khan et al. 2018).

The darkness density of slices was measured using the Fiji imaging package. DAB-stained pictures were taken under 10× light microscope and kept consistent background. Pictures were processed by color deconvolution and "H DAB," and "Mean Gray Value" was used to measure the darkness density. Mean gray values were normalized into optical density numbers by the formula: OD = log (max intensity/mean intensity), where max intensity = 255 for 8-bit images.

Recovery of biocytin labeled-cells postelectrophysiological recordings and morphometric analysis. After electrophysiological recordings of pyramidal cells in the entorhinal cortex, slices were fixed in 4% paraformaldehyde plus 0.2% picric acid in 0.1 M PB for 24 h and then re-sectioned at 70 μm. Slices were incubated in ABC overnight at 4 °C, followed by the above DAB protocol. Anatomically recovered cells were reconstructed manually from consecutive slices at 100× objective under a Leica DMR microscope with an attached drawing tube. Images from the consecutive slices were digitally superimposed so as to be analyzed using Sholl analysis in ImageJ (version 1.49, RBS, Maryland, USA). Only neurons that were fully stained and had intact dendritic arbors were included in the study. The Sholl analysis was carried out with a radius step size of 10 μm and the area under the curve was regarded as a determinant of dendritic complexity, meaning that any deviations of this feature represented morphological alterations (Ristanovic et al. 2006).

Canonical Wnt Signaling Analysis via Immunoblotting

Brains were collected from *App*$^{NL\text{-}F/NL\text{-}F}$ knock-in mice and age-matched wild-type controls, micro dissected into cortex,

entorhinal cortex and cerebellum and directly transferred to ice. All following steps were performed on ice. Brain lysates were generated in lysis buffer composed of 5 mM $MgCl_2$, 150 mM NaCl, 50 mM Tris, pH 7.5, 1% (v/v) Igepal, supplemented with 1× complete protease inhibitor cocktail (Roche) and 1:100 phosphatase inhibitor cocktail (Pierce) using a dounce homogenizer (Merck). Lysates were cleared through a 10 min centrifugation step at 14 000 *g* and protein concentration was determined with the bicinchoninic acid (BCA) assay (Pierce). Equal protein amounts were analyzed by SDS Polyacrylamide gel electrophoresis (SDS-PAGE) and immunoblotting. Thereafter, 4× LDS sample loading buffer and 10× sample reducing agent (Invitrogen) were added to the samples followed by incubation for 10 min at 98 °C. The denatured samples were loaded onto a 4–12% (w/v) BisTris precast gel (Invitrogen). Proteins were blotted on polyvinylidine fluoride (PVDF) membranes (Millipore), blocked with 5% (w/v) nonfat dry milk in Tris-buffered saline plus 0.1% (v/v) Tween 20 (TBS-T) for 30 min and labeled using the following primary antibodies: active β-catenin (clone 8E7, Millipore), full-length β-Amyloid (clone 6E10, BioLegend) and β-actin (Sigma) in blocking buffer overnight at 4 °C. Membranes were washed 3 times in TBS-T the following morning, prior to incubation in HRP-conjugated secondary antibodies (Santa Cruz) in blocking buffer for 2 h at room temperature on a rocking shaker. Washing was repeated and the signal detected using SuperSignal West Pico Chemiluminescent Substrate or SuperSignal West Femto Chemiluminescent Substrate (Pierce) and a Syngene GeneGnome Imaging system. For the quantification, ImageJ software was employed. Please refer to supplementary files for further Western blots.

Statistics

A one-way analysis of variance (ANOVA) was used to determine whether there were any significant differences between the different experimental cohorts. If there was a difference, the Student *t*-test (2-tailed, unpaired) was used to compare $App^{NL\text{-}F/NL\text{-}F}$ animals to wild-type counterparts separately at the age group of interest. *P*-values below 0.05 were deemed significant. All figures displaying error bars represent the standard deviation from the mean, unless stated otherwise. The bar graphs display cohort means.

The "*n*" are given as the total number of observations (cells) and the number of animals used, unless otherwise stated.

Results

The $App^{NL\text{-}F/NL\text{-}F}$ Mouse Model Shows Time-Dependent Accumulation of Aβ and Neuroinflammation Associated With a Steady Decline of Principal Cell Density

In the $App^{NL\text{-}F/NL\text{-}F}$ mouse model, we observed age-dependent phenotypic changes of AD, including neuroinflammation indicated by astrocytosis, microgliosis and the progressive Aβ accumulation and deposition leading to plaque formation, which advocates progressive neurodegeneration, accurately recapitulating progression in AD patients. These data are also consistent with the study by Saito et al. (2014).

There was a higher level of $A\beta_{42}/A\beta_{40}$ associated in the $App^{NL\text{-}F/NL\text{-}F}$ mouse model at 10–18 months as opposed to their age-matched wild-type control mice (Fig. 1*A*,*B*,*G*). This accumulation of Aβ protein plaques is known to be initiated in the LEC and layer 2/3 of the neocortex border ((Braak and Braak 1991; Holtzman et al. 2011), which is consistent with our study showing an increase of Aβ protein plaques in the LEC of $App^{NL\text{-}F/NL\text{-}F}$ mice by, 12.64 ± 2.21%, 44.95 ± 4.29% and 286.61 ± 74.13% of control mice at 1–2, 4–6, and 10–18 months, respectively, $P < 0.01$, $n = 6$ animals).

Immunoreactivity to the neuroinflammatory markers cluster of differentiation 68 protein (CD68) and glial fibrillary acidic protein (GFAP) were also shown to be differentially expressed in the wild-type mice age-matched to $App^{NL\text{-}F/NL\text{-}F}$ mice. An age-dependent, gradual increase in CD68-positive glial cells in the LEC of $App^{NL\text{-}F/NL\text{-}F}$ mice was also observed (increase by, 4.32 ± 0.98% and by, 48.08 ± 16.11%, and 71.29 ± 12.72% of control mice at 1–2, 4–6, and 10–18 months, respectively), however these differences were only significant at 10–18 months ($P < 0.01$, $n = 6$ animals, Fig. 1*C*,*D*,*H*).

A slight decrease of GFAP-positive reactive astrocytes in the LEC was observed in the $App^{NL\text{-}F/NL\text{-}F}$ mouse model at 1–2 and 4–6 months compared with wild-type control mice (decreased by, 5.80 ± 1.21%, 6.38 ± 1.29% of control wild-type mice at 1–2 and 4–6 months, respectively); however, a significant accumulation of active astrocytes was seen in $APP^{NL\text{-}F/NL\text{-}F}$ mice at 10–18 months (31.50 ± 8.74% of control mice, $P < 0.07$, $n = 6$ animals) (Fig. 1*E*,*F*,*I*).

Figure 1 illustrates analysis from results obtained from immunoperoxidase procedures, however, these observations were consistent with complementary immunofluorescence labeling.

Furthermore, to investigate whether principal pyramidal cells showed neurodegeneration in the $App^{NL\text{-}F/NL\text{-}F}$ mouse model, we performed immunohistochemistry using antibody against CaMKII-α which is expressed in principal cells (Wang et al. 2013), and costained the tissue with DAPI (nuclei staining). An age-dependent decline in pyramidal cell density in CA1 and LEC was observed, suggesting a physiological progression of neurodegeneration in the $App^{NL\text{-}F/NL\text{-}F}$ mouse model of AD (Fig. 1*J*,*K*). Analysis of confocal imaging *Z*-stacks revealed that in the LEC, there was a significant decline in pyramidal cells in the $App^{NL\text{-}F/NL\text{-}F}$ animals compared with age-matched wild-type mice at all 3 age windows investigated. At 1–2 months, a reduction of 28.72 ± 2.63%, at 4–6 months, a reduction of 32.11 ± 5.84%, and at 10–18 months, a reduction of 45.07 ± 14.71% was observed (these data were all significantly different from the control, $P < 0.05$, $n = 5$ animals per cohort). In the CA1 and neocortex, there was also a significant reduction in the expression of CaMKII-α expressed in pyramidal cells costained with DAPI in the $App^{NL\text{-}F/NL\text{-}F}$ mouse brains compared with the healthy age-matched controls in the age window of 10–18 months, showing a reduction of 60.51 ± 3.98% ($P < 0.001$, $n = 4$ animals per group) in CA1 and 40.94 ± 6.23% ($P < 0.05$, $n = 4$ animals per group), in the neocortex. The reduction in the number of cells and fragmented staining also associated with a shrinkage of cells, were characteristic signs of cellular neurodegeneration in the cortical regions studied in the $App^{NL\text{-}F/NL\text{-}F}$ model.

Time-Dependent Wnt Signaling Changes in the $App^{NL\text{-}F/NL\text{-}F}$ Mouse Model of AD

Decreased canonical Wnt signaling has previously been suggested to play a role in AD pathogenesis in patients and has also been observed in other AD animal models (Inestrosa and Varela-Nallar 2014; Jin et al. 2017; Dengler-Crish et al. 2018; Huang et al. 2018; Tapia-Rojas and Inestrosa 2018a, b). Our aim was to investigate these findings in the $App^{NL\text{-}F/NL\text{-}F}$ mouse model. In addition, we asked the question of when and in what brain areas, changes in canonical Wnt signaling can first be

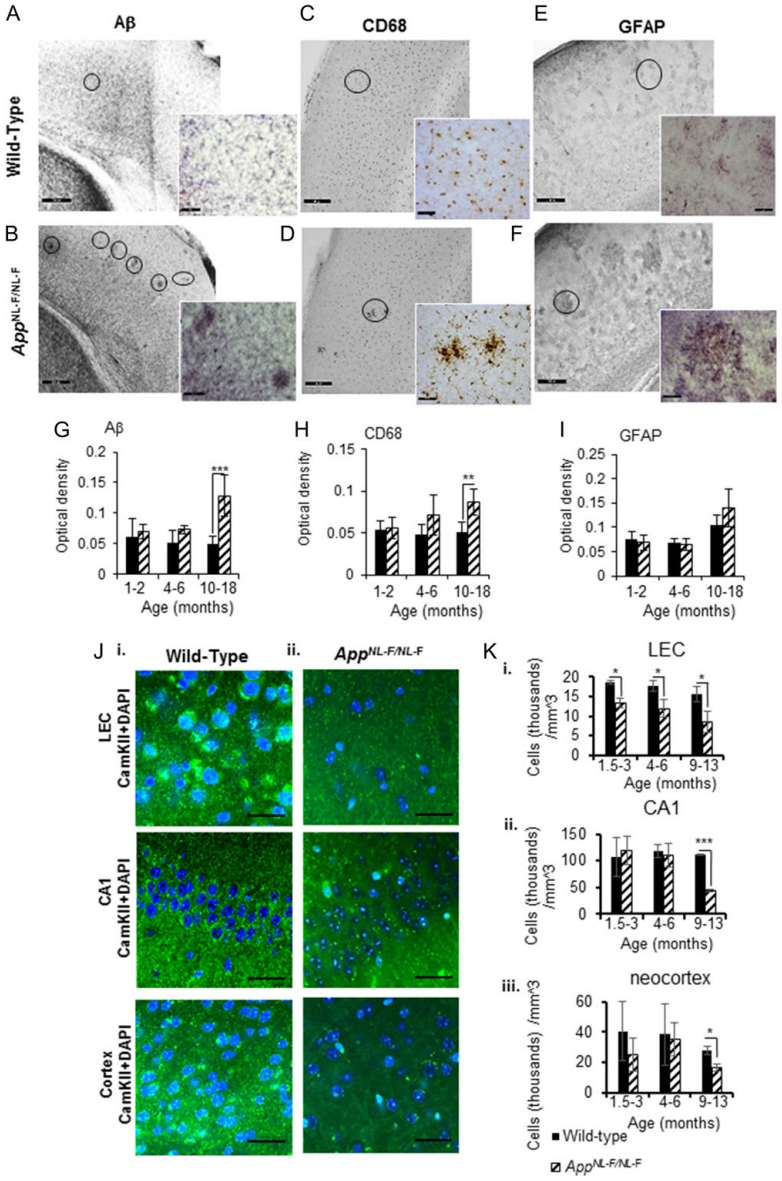

Figure 1. The first knock-in AD mouse model, App$^{NL\text{-}F/NL\text{-}F}$ shows an age-dependent accumulation of Aβ pathology, neuroinflammation and neurodegeneration of principal cells. (*A*) and (*B*) Immunoperoxidase labeling of Aβ in aged wild-type and App$^{NL\text{-}F/NL\text{-}F}$ brains. Photographs taken with light microscope at 20× magnification; inserts illustrate photographs taken at 40× magnification. Circles show Aβ deposits. (*C–F*) Similarly, CD68 and GFAP labeling indicating microglia and reactive astrocytes respectively, in aged wild-type and App$^{NL\text{-}F/NL\text{-}F}$ brains. The presence of strong Aβ aggregation in the AD mouse model, which correlates with increased inflammatory markers, is apparent (scale bar, 50 μm, enlarged images, scale bar, 20 μm). Circles indicate microglia and reactive astrocytes, respectively. (*G–I*) Graphs illustrating an age-dependent increase in Aβ, CD68, and GFAP levels in the 3 different age windows investigated in wild-type and *App*$^{NL\text{-}F/NL\text{-}F}$. *App* $^{NL\text{-}F/NL\text{-}F}$ mice (10–18 months) demonstrated a significant increase in Aβ and CD68 level compared with wild-type aged animals, or the other 2 age cohorts (1–2 months, 4–6 months). Results are expressed as mean ± SD (**$P < 0.01$, ***$P < 0.001$; 2-tailed student *t*-test). (*Ji-ii*) Confocal imaging experiments using antibody to selectively label the expression of calcium/calmodulin-dependent protein kinase II (CamKII) expressed in principal excitatory cells in 3 cortical regions: LEC, CA1, and layer 2/3 of the neocortex. There is gradual decline in DAPI colocalised with CamKII (secondary antibody Alexa 488, green), suggesting neurodegeneration of principal cells in the *App*$^{NL\text{-}F/NL\text{-}F}$ mouse model. Panels show representative confocal images taken at X63 magnification of tissue stained with CamKII and DAPI in wild-type animals at 13 months and in age-matched *App*$^{NL\text{-}F/NL\text{-}F}$ mouse brains (scale bar = 20 mm). (*Ki-iii*) Pyramidal cell density was counted from collapsed confocal *Z*-stacks taken at ×20 magnification. There is significant reduction in pyramidal cell density in the lateral entorhinal cortex in the *App*$^{NL\text{-}F/NL\text{-}F}$ animals compared with age-matched wild-type mice at all 3 ages investigated, which reduced significantly, (*$P < 0.05$, ***$P < 0.001$, 2-tailed Student *t*-test comparing *App*$^{NL\text{-}F/NL\text{-}F}$ animals to wild-type counterparts separately at each of the 3 age groups investigated, $n = 5$ animals per cohort).

observed during pathogenesis. The entorhinal cortex is one of the earliest and most affected by the neurodegenerative disease process, whereas the cerebellum is rarely affected. Therefore, we investigated canonical Wnt signaling activity in the cortex, entorhinal cortex and cerebellum of $App^{NL\text{-}F/NL\text{-}F}$ knock-in mice in comparison to wild-type littermate controls using an antibody against free dephosphorylated ß-catenin. We found an overall statistically significant decrease of canonical Wnt signaling activity in the cortex and entorhinal cortex to 60 ± 12% ($P < 0.01$) and 66 ± 3% ($P < 0.01$) respectively but no significant change in the cerebellum of $App^{NL\text{-}F/NL\text{-}F}$ knock-in animals (Fig. 2, Supplementary Figs S1–S7). The decrease of canonical Wnt signaling activity was already evident from 1–2 months of age in the entorhinal cortex (62 ± 3%, $P < 0.01$) and from 4–6 months in the remaining cortex (66 ± 15%, $P < 0.05$). In the cortex we observed a decrease of canonical Wnt signaling activity over time from 1–2 months (72 ± 15%, not statistically significant), 4–6 months (66 ± 15%, $P < 0.05$) to 12–14 months (42 ± 19%, $P < 0.05$) old animals suggesting a progression of the signaling defect in a special and/or temporal manner. As the Wnt signaling dysfunction is first observed in the entorhinal cortex but seems to remain at a similar level in this area over time, a spread of the canonical Wnt signaling dysfunction throughout the cortex starting from the entorhinal cortex is suggested. Our data also show that the first observed decrease in Wnt signaling activity in the entorhinal cortex and cortex precedes the above observed gliosis and Aβ pathology in the $App^{NL\text{-}F/NL\text{-}F}$ model (Fig. 1). Observed Wnt signaling activity is at its lowest point when AD pathology becomes visible in brain slices.

Distorted Excitatory–Inhibitory Synaptic Activity in the LEC Preceding Hallmarks of AD

To determine whether the decrease of Wnt signaling activity was correlated with early stage synaptic impairment, we investigated whether the excitatory and inhibitory synaptic inputs received by principal pyramidal cells were impaired in the $App^{NL\text{-}F/NL\text{-}F}$ model of AD. To examine the network effect at these cells, we first examined the presynaptic action potential-dependent synaptic release and recorded sEPSPs and sIPSPs from the 3 different age cohorts in age-matched wild-type and $App^{NL\text{-}F/NL\text{-}F}$ mice in the LEC, CA1, and neocortex. This was then followed by recording miniature postsynaptic events (mEPSPs and mIPSPs) in the presence of the sodium channel blocker tetrodotoxin (TTX), which reveals action potential-independent mechanisms of the neurotransmitter release machinery.

The vast majority of pyramidal cells studied in layer 2 of the LEC (~90%) showed impaired excitatory and inhibitory properties recorded in the youngest cohort of 1–2 months of $App^{NL\text{-}F/NL\text{-}F}$ mice (Fig. 3A). Pyramidal cells recorded in the CA1 region and neocortex did not show hyperexcitability in the $App^{NL\text{-}F/NL\text{-}F}$ mice at 1–2 months and there was no significant different between the synaptic responses recorded in age-matched wild-type mice (20–30 cells recorded in CA1 and neocortex, $n = 15$ animals). However, in the $App^{NL\text{-}F/NL\text{-}F}$ mouse model, an age-dependent spread of the hyperexcitability was observed; CA1 pyramidal cells exhibited hyperexcitability between 4 and 6 months, while neocortical pyramidal cells exhibited it at a later stage of 10 months onwards (Fig. 3B,C).

Due to the apparent aberrant hyperexcitability evident at 1–2 months in the LEC, we focused on investigating the synaptic changes in more detail here. We found that in the LEC, $GABA_A$ receptor mediated sIPSPs recorded at −55 mV membrane potential from all 3 age cohorts of $App^{NL\text{-}F/NL\text{-}F}$ mice showed a significant decrease in amplitude and frequency. The mean amplitude of sIPSPs decreased by 32 ± 9%, 32 ± 9%, 48 ± 38% of control mice for 1–2, 4–6, and 10–18 months, respectively ($P < 0.01$, $n = 12$ cells, $n = 7$ animals). The frequency of sIPSPs was also consistently lower in AD mice by 79 ± 25%, 85 ± 16%, 87 ± 18% of control mice for 1–2, 4–6, and 10–18 months, respectively (all significantly different $P < 0.0001$, $n = 10$ cells, $n = 7$ animals) (Fig. 3A,D,E). However, in contrast, both sEPSP amplitude and frequency were significantly *higher* in 1–2 months and 4–6 months aged $App^{NL\text{-}F/NL\text{-}F}$ mice, but then reduced at 10–18 months. The sEPSP amplitudes were significantly higher in the $App^{NL\text{-}F/NL\text{-}F}$ mice, by 70 ± 3%, 100 ± 22%, and 68 ± 29% of control mice at 1–2, 4–6, and 10–18 months, respectively (all significantly different $P < 0.05$, $n = 12$ cells, $n = 7$ animals per group). However, this shows a decrease of the sEPSP amplitudes at 10–18 months in the $App^{NL\text{-}F/NL\text{-}F}$ mice compared with the younger cohorts. The frequency increased by, 51 ± 13% and 167 ± 8% in 1–2 months and 4–6 months aged $App^{NL\text{-}F/NL\text{-}F}$ mice compared with control mice ($P < 0.0001$, $n = 10$ cells, $n = 7$ animals), and also reduced at 10–18 months by, 13 ± 12% of control wild-type mice (Fig. 3A,F,G).

In the presence of TTX (1 μM), the hyperexcitability in terms of increased action potential discharge, increased frequency and amplitudes of sEPSPs observed in AD mice was blocked, suggesting that the effect was mediated through changes in presynaptic action potential activity (Fig. 3H). The peak mean amplitude and frequency of mEPSPs recorded from 10 to 18 months old wild-type mice was, 0.5 ± 0.05 mV and 1.5 ± 0.34 Hz, respectively, which was not significantly different from the amplitude and frequency of mEPSPs recorded from 10 to 18 months $App^{NL\text{-}F/NL\text{-}F}$ mice (amplitudes and frequency, 98 ± 0.3% and 95 ± 1.5% of control, respectively, $P > 0.5$, $n = 10$ cells, $n = 5$ per group). Similarly, mIPSP mean amplitude and frequency recorded in the same control animals was, 0.2 ± 0.03 mV and 1.8 ± 0.4 Hz, respectively, and also did not significantly differ from the events recorded in $App^{NL\text{-}F/NL\text{-}F}$ mice (amplitudes and frequency, 90 ± 2.5% and 94 ± 4.5% of control, respectively, $P > 0.5$, $n = 10$ cells, $n = 5$ per group).

The overall reduction in excitation in the 10–18 months cohort was consistent with the pattern of neurodegeneration observed in the LEC of $App^{NL\text{-}F/NL\text{-}F}$ mice compared with other cortical regions including CA1 and the neocortex as described above (Fig. 1J,K).

Intrinsic Hyperexcitation of Principal Pyramidal Cells Correlates With Morphological Degeneration

We then investigated whether the aberrant hyperexcitation related to intrinsic firing was sustained during the 3 age cohorts over time. All pyramidal cells recorded were anatomically recovered postrecording. These cells in the $App^{NL\text{-}F/NL\text{-}F}$ mouse model at 1–2 and 4–6 months displayed greater sensitivity to intracellular current injection (Fig. 4A,B), which was very similar to previous observations made in epileptic tissue (Khan et al. 2018). This was shown by an increase in membrane resistance, reflective of a larger change in membrane voltage per current step. Further supporting this greater sensitivity, was an observed increase in the time constant, rendering neurons more excitable for the same injected positive current step. This was demonstrated from the decreased firing threshold and increased frequency of action potential discharge in the $App^{NL\text{-}F/NL\text{-}F}$ mouse model cells compared with wild-type litter mates (Fig. 4C). The increase in membrane hyperactivity was apparent from the earliest time window studied, but gradually showed significant deterioration

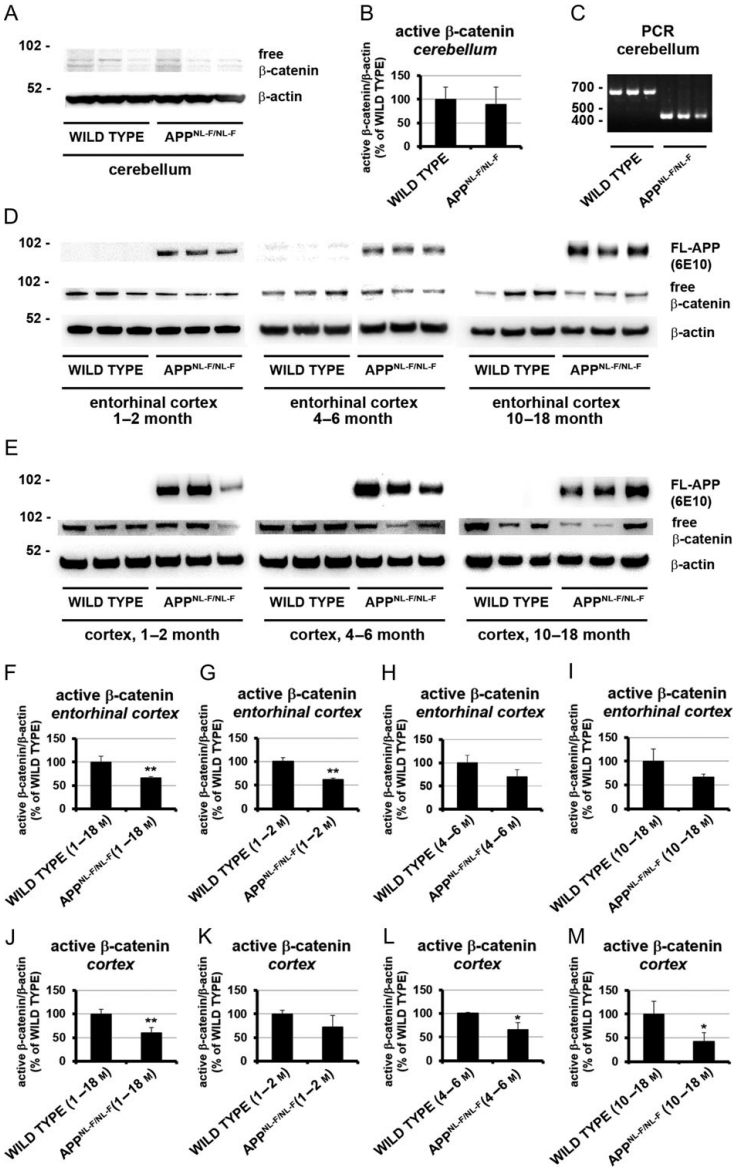

Figure 2. Tissue and age-dependent Wnt signaling analysis of wild type and $App^{NL\text{-}F/NL\text{-}F}$ *knock-in mice.* Equal amounts of protein lysates from different brain regions were analyzed from 1 to 18 months old wild-type and $App^{NL\text{-}F/NL\text{-}F}$ knock-in mice via immunoblotting. (*A*, *D*, and *E*) Representative Western blot analysis showing detection of active β-catenin in lysates from the cerebellum (*A*), entorhinal cortex (*D*), and cortex (*E*). Protein detection of human full-length APP (*D* and *E*) and mouse β-actin (*A*, *D*, and *E*) served as control. (*C*) Representative amplicon of 700 bp for wild type and 400 bp for $App^{NL\text{-}F/NL\text{-}F}$ knock-in mice, confirming the genotype of animals used in (*A*) via polymerase chain reaction using genomic DNA. (*B*, *F*–*M*) Mean signal changes of active β-catenin in cerebellum (*B*), entorhinal cortex (*F*–*I*) and cortex (*J*–*M*). Western blot labeling showing age-dependent significant reduction of active β-catenin in the cortex of $App^{NL\text{-}F/NL\text{-}F}$ knock-in mice compared with wild-type mice. Signals were divided through β-actin and normalized to wild-type (100%) represented as mean percentage ± SEM (*$P < 0.05$; **$P < 0.01$, $n = 3$–9).

with a significant reduction in membrane resistance and time constant and the inability of the neurons to fire action potentials in the 10–18 months aged mice (Fig. 4B,C). These biophysical changes correlated with the morphological alteration of pyramidal cells in the LEC that represent progressive neurodegeneration in the $App^{NL\text{-}F/NL\text{-}F}$ mouse model in

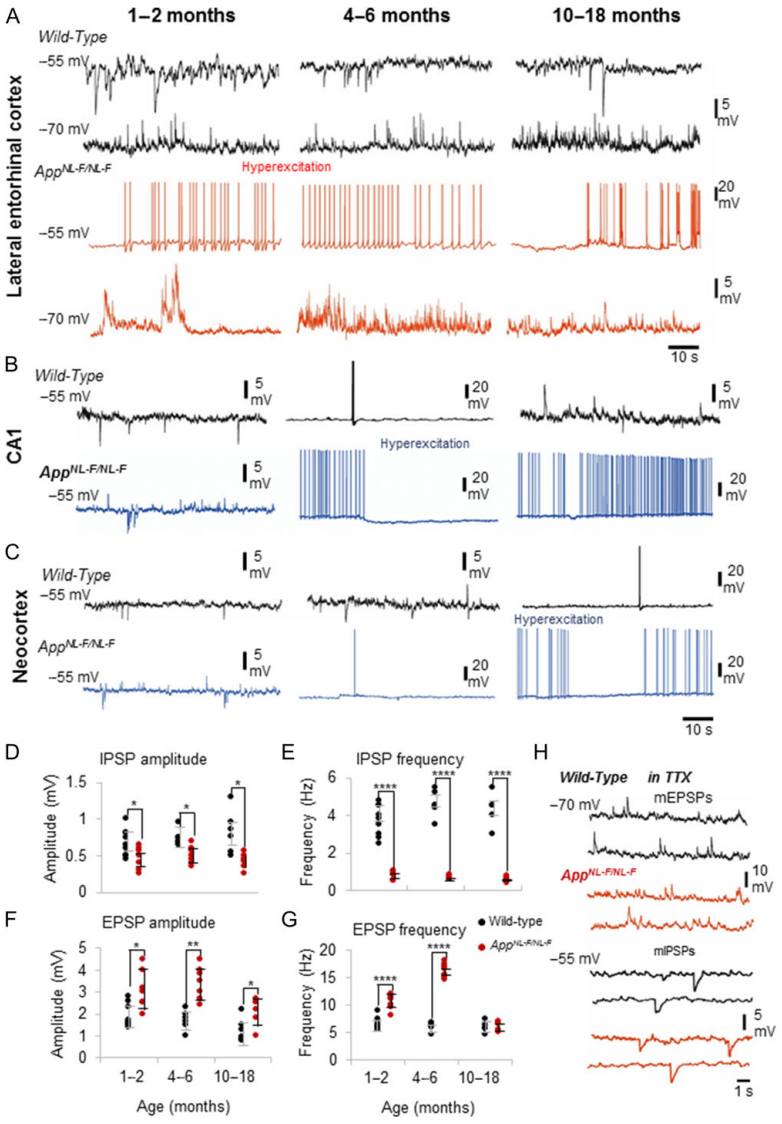

Figure 3. Persistent synaptic hyperexcitation and diminished inhibition at principal pyramidal cells in $App^{NL\text{-}F/NL\text{-}F}$ mouse model of AD. Intracellular recordings of spontaneous response of layer 2 LEC neurons recorded using whole-cell patch clamp electrodes at membrane potentials held at −55 and −70 mV (in current clamp). (*A*) Recordings from wild-type mice at 1–2 months, 4–6 months, and 10–18 months at −70 and −55 mV. Similar recordings from age-matched $App^{NL\text{-}F/NL\text{-}F}$ mice are shown in red. The principal, pyramidal cells recorded in wild-type mice showed less spontaneous firing and subthreshold oscillation compared with $App^{NL\text{-}F/NL\text{-}F}$ mice when held at firing threshold of −55 mV. Furthermore, the wild-type mice showed inward inhibitory current events as expected at all ages investigated. By contrast, similar neurons recorded in AD mice resulted in oscillation between subthreshold and spontaneous action potential discharge at firing threshold of −55 mV, which was seen to diminish from 10 months onwards. These results suggest impaired spontaneous excitation and inhibition and an increasing state of hyperexcitability upon AD progression until 10–18 months. Scale bars on the right refer to all 3 data sets. (*B* and *C*) Similar events recorded from pyramidal cells in CA1 and in the layer 2/3 of the neocortex (somatosensory region) in wild-type (black traces) and age-matched $App^{NL\text{-}F/NL\text{-}F}$ mice (blue traces). Hyperexcitation was *not* apparent in these excitatory cells in the $App^{NL\text{-}F/NL\text{-}F}$ younger mice cohorts in CA1 or neocortex, as this developed later in contrast to the LEC. (*D* and *E*), sIPSP amplitudes and frequency recorded at −55 mV in wild-type and age-matched $App^{NL\text{-}F/NL\text{-}F}$ mice. (*F* and *G*) sEPSP amplitudes and frequency recorded at −70 mV in wild-type and age-matched $App^{NL\text{-}F/NL\text{-}F}$ mice. sEPSP amplitude and frequency were significantly higher in the $App^{NL\text{-}F/NL\text{-}F}$ mouse model until 10–18 months, and correlated with a significantly reduced amplitude and frequency of sIPSPs received by pyramidal cells in the $App^{NL\text{-}F/NL\text{-}F}$ mouse model (*$P < 0.05$; **$P < 0.01$, ***$P < 0.001$, ****$P < 0.0001$, $n = 7$ animals per cohort). (*H*) Synaptic events recorded in the presence of TTX, illustrating example traces of miniature, mEPSPs and mIPSPs in wild-type and age matched $App^{NL\text{-}F/NL\text{-}F}$ mice.

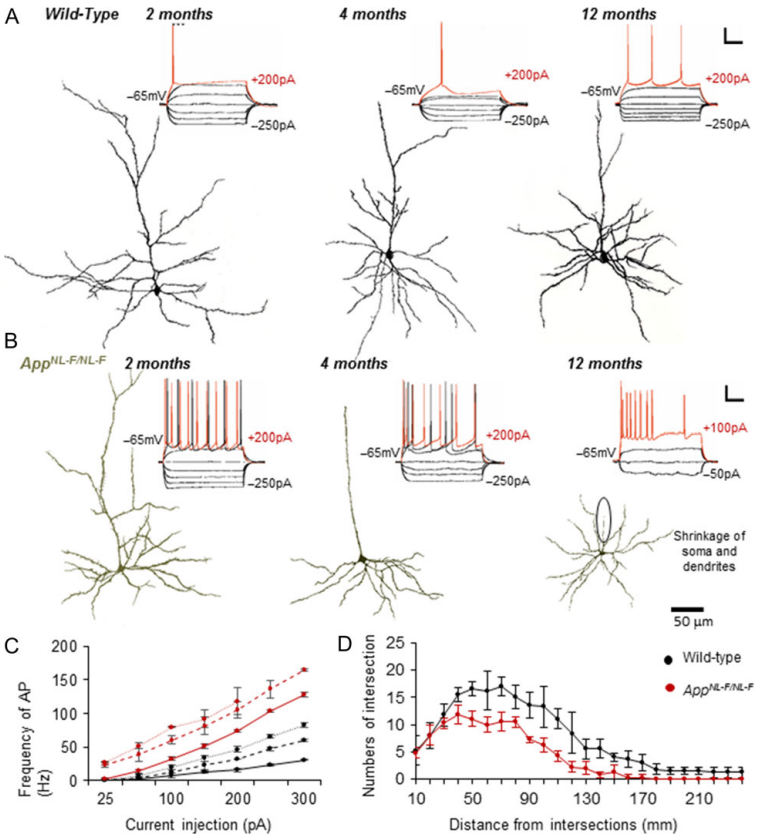

Figure 4. Pyramidal cell membrane hyperexcitability correlates with neurodegeneration. (*A*) and (*B*) Intrinsic membrane response of excitatory neurons of lateral entorhinal cortex (LEC) recorded in wild-type (WT) mice showed passive responses to intracellular current injection (range + 200–250 pA), which induced a single action potential with increased positive current injections (red traces). In $App^{NL\text{-}F/NL\text{-}F}$ mice, similar currents resulted in a significant increase in action potential discharge, increased membrane resistance and increased time constants, suggesting a more excitable membrane state ($P < 0.05$, $n = 30$ neurons; 10 animals per cohort). The hyperexcitability then declined with time, resulting in impaired membrane physiology from 10 to 18 months onwards in AD mice. This was correlated with the morphological atrophy of layer 2 LEC principal cells from 4 months onward in the AD $App^{NL\text{-}F/NL\text{-}F}$ model, (green) compared with age-matched wild-type neurons (black). Neurons were reconstructed using a light microscope and drawing tube under 100× objective. Scale refer to 20 mV and 100 ms. (*C*) Plot of action potential frequency with current injection in wild-type and age-matched $App^{NL\text{-}F/NL\text{-}F}$ mice at the 3 different age cohorts studied. (*D*) The average number and length of dendrites per groups of cells were compared and found to be significantly different and Sholl analysis, was used as a measure of dendritic complexity of pyramidal cells in LEC of aged $App^{NL\text{-}F/NL\text{-}F}$ and wild-type mice. The intersection numbers of pyramidal cells in aged $App^{NL\text{-}F/NL\text{-}F}$ mice were significantly decreased between 40 and 240 µm from soma compared with aged wild-type mice. Results are expressed as mean ± SD ($P < 0.05$; 2-tailed Student *t*-test).

comparison to the wild-type mice over time. This was also evidenced by the Sholl analysis used as a measure of dendritic complexity of LEC pyramidal cells in $App^{NL\text{-}F/NL\text{-}F}$ mice compared with age matched wild-type mice, illustrated by a downwards shift in the Sholl plot (Fig. 4D).

Impaired Functions of Major Inhibitory PV-Expressing Interneurons in LEC of $App^{NL\text{-}F/NL\text{-}F}$ Mice

Over activity of the LEC in early AD suggests a loss of the inhibitory drive that controls overexcitation, which was evident from the sIPSP studies in the $App^{NL\text{-}F/NL\text{-}F}$ mouse model. To determine the underlying mechanisms for the observed reduced inhibition, we investigated PV-expressing inhibitory interneurons. These predominantly fast-spiking neurons are the major inhibitory cells and therefore modifications of this network are likely to affect the observed imbalance between excitation and inhibition.

Immunofluorescence studies displayed a significant reduction in the neuronal density of PV-expressing cells in the dorsal LEC at 10–18 months compared with age-matched wild-type counterparts (reduction of 23 ± 4%, $P < 0.005$, $n = 8$ mice per cohort). This was in contrast to a nonsignificant change in the cell densities of PV-expressing cells in the neocortex and CA1 region of the hippocampus (Fig. 5A–E). In addition, $App^{NL\text{-}F/NL\text{-}F}$ mice at 10–18 months showed a reduction in the intensity of glutamic acid decarboxylase 67 (GAD67) within PV-expressing cells as a measure of GABA content and presynaptic function in the dorsal LEC when compared with the age-matched wild-type cohort ($P < 0.003$, Pearson's correlation coefficient, $n = 8$ animals) (Fig. 5F,G).

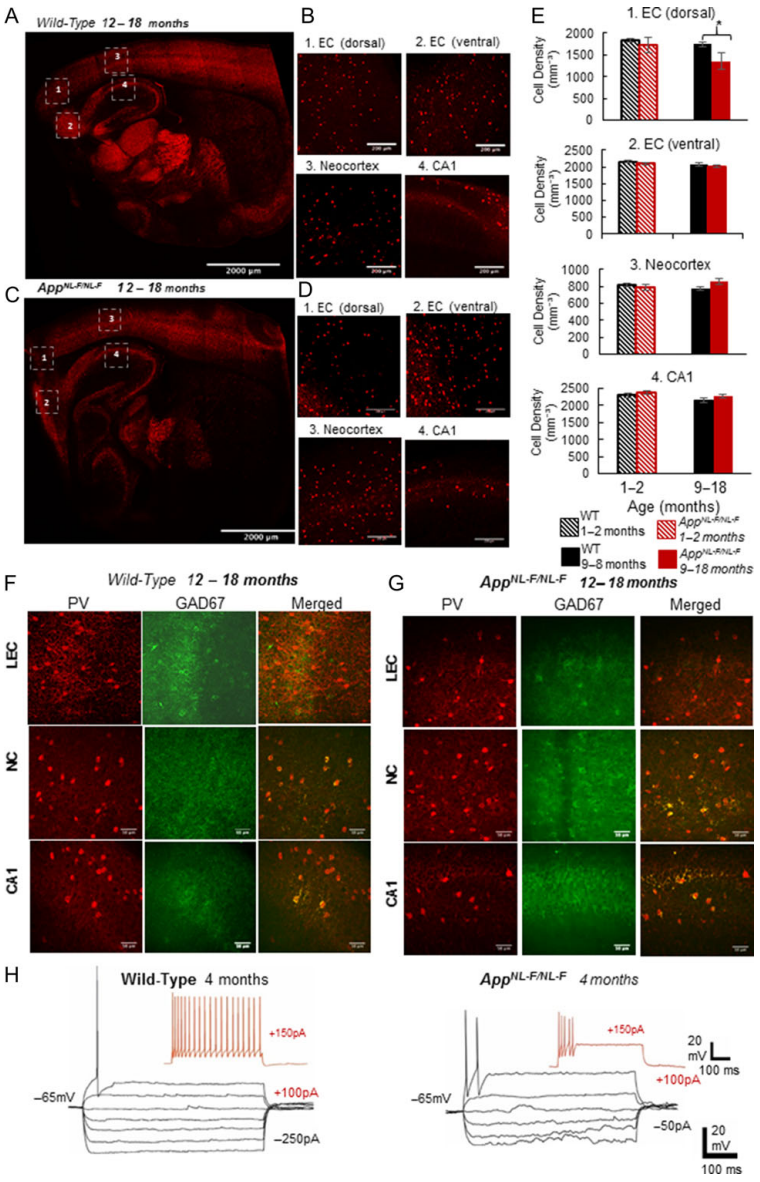

Figure 5. Fast-spiking parvalbumin-containing (PV) interneurons are reduced and functionally impaired in dorsal LEC in AD. Fast-spiking PV-expressing cells, a major class of interneurons that are known as the "pace makers" of the brain and responsible for regulating excitation. (*A–D*) Confocal microscope images from immunofluorescence labeling illustrating a significantly reduced density of PV cells in the LEC but not in neocortex or hippocampus of aged $App^{NL\text{-}F/NL\text{-}F}$ mice (red cells, primary antibody: rabbit-anti-PV, secondary antibody: Texas red). Images (*A* and *C*) are tile scans of the whole brain section, while (*B* and *D*) are 20× magnified Z-stack images (20×, scale bar = 200 μm). (*E*) The bar graph shows insignificant differences in PV cell densities in WT and $App^{NL\text{-}F/NL\text{-}F}$ mice in various cortical regions, except the dorsal LEC, suggesting that PV cells are susceptible to dysfunction in the dorsal LEC proceeding phenotypic changes of AD. PV cell counts taken from three 100 μm parasagittal brain slices of either a WT control or $App^{NL\text{-}F/NL\text{-}F}$ brains, and counts were obtained by producing a 20× magnified Z-stack image at the same positions within the different cortical regions numbered from 1 to 4 on the figure (ANOVA tests performed to show statistical significance, $n = 8$ animals per age cohort). (*F,G*) Colocalisation experiments with PV and GAD67 (an enzyme for inhibitory neurotransmitter GABA production, primary antibody: mouse anti-GAD67, secondary antibody: FITC (green)) illustrates that less GAD67 is colocalised within PV expressed cells in aged AD mice (shown in yellow/orange fluorescence, Pearson's correlation coefficient, r shown, $n = 6$ animals per cohort). This suggests that there is a decrease in the available neurotransmitter GABA in aged $App^{NL\text{-}F/NL\text{-}F}$ brains. (*H*) Impaired intrinsic membrane properties of fast-spiking PV cells in the LEC in aged $App^{NL\text{-}F/NL\text{-}F}$ brains.

These observations were accompanied by general poor health of fast-spiking interneurons recorded in the LEC, which showed a reduced action potential threshold, increased spike frequency adaption and accommodation, and inability to sustain a high frequency of firing, suggesting impaired membrane properties (Fig. 5*H*).

$GABA_A$ Receptor Allosteric Modulators Rectify Synaptic Imbalance in $App^{NL\text{-}F/NL\text{-}F}$ Mice

It has been established that pyramidal cell somata and axon initial segments receive only inhibitory synapses from axon terminals of PV-expressing interneurons. To determine whether perisomatic inhibitory terminals were still active in the $App^{NL\text{-}F/NL\text{-}F}$ mouse model, we performed immunofluorescence studies using anti-GABA transporter 1 (GAT1) (Fig. 6*A*) localized with the antibody against vesicular glutamate transporter 1 (VGluT1), that marks terminals of the major excitatory neurotransmitter glutamate pathways. Thus, the pattern and the extent of colocalisation of GAT1 with VGluT1 will reveal whether perisomatic PV axon terminals innervate pyramidal cells to the same extent in late AD as in control animals. The pattern of the punctate structures of VGluT1 were sparse but appeared as more intense clustered immunoreactivity in the aged $App^{NL\text{-}F/NL\text{-}F}$ mice. This GABAergic marker was found in puncta present in the periphery of cell bodies, which seemed to be reduced in distribution around DAPI stained somata in the $App^{NL\text{-}F/NL\text{-}F}$ mice at 10–18 months. However, there was some preservation of GAT1-positive puncta around the neuronal somata despite the apparent reduction in the functionality of PV cells (as indicated by GAD67 and PV firing properties), therefore, we investigated whether pharmacological manipulations of the existing GABAergic terminals could rectify the observed synaptic imbalance and hyperexcitation. Following bath-application of the broad spectrum $GABA_A$ receptor allosteric modulator, diazepam (1 μM) (Fig. 6*B*), the hyperexcitability of pyramidal cells in the LEC was reduced by 60 ± 6.5% ($P < 0.05$, $n =$ 6 cell, 4 animals at 6 months, and 10–18 months), and furthermore, the aberrant inhibition was restored, which resulted in an increase in amplitude and frequency of sIPSPs (increase of 330 ± 10% and 126 ± 9.5%, in amplitude and frequency, respectively, $P < 0.05$, $n = 6$ cell, 4 animals) which was consistent with previous studies (Busche et al. 2008). However, diazepam as a potential therapeutic target for AD is controversial (Nicholson et al. 2018) thus, we further investigated specific $GABA_A$ receptor allosteric modulators including zolpidem (1 μM), a modulator of α1-containing $GABA_A$ receptors, and L-838,417 (0.5 μM), a selective modulator of α2- and α3- containing $GABA_A$Rs, classed as a nonbenzodiazepine anxiolytic (Atack 2011). Like diazepam, both, zolpidem (Fig. 6*B*) and L-838,417 restored sIPSP amplitudes, which increased by 273 ± 32% and 246 ± 13% of control values, respectively ($P <$ 0.05, $n = 4$ animals) (Fig. 6*C*). The sIPSP frequency also increased with zolpidem and L-838,417 by 97 ± 36% and 85 ± 13%, respectively ($P < 0.05$, $n = 4$ animals), suggesting restoration of synaptic excitatory–inhibitory imbalance (Fig. 6*D*,*E*). However, bath-application of the $GABA_A$ receptor antagonist gabazine (50 μM) increased the sEPSP amplitude and frequency and decreased sIPSP parameters comparable to control untreated levels. The overall findings after bath application of diazepam, zolpidem and L-838,417, is that the aberrant, depleted inhibitory synaptic events observed in 10–18 months old $App^{NL\text{-}F/NL\text{-}F}$ mice was "normalized" and these events were similar in amplitude and frequency to the inhibitory events recorded in the age-matched wild-type mice. These changes with diazepam and zolpidem were also consistent with previous studies using healthy control rodents (Ali and Thomson 2008).

Discussion

Using the first AD knock-in mouse model ($App^{NL\text{-}F/NL\text{-}F}$), which faithfully recapitulates disease progression in AD patients as shown by molecular studies (Saito et al. 2014; Sasaguri et al. 2017), we explored progressive changes in synaptic mechanisms underlying AD pathology in the LEC with the following 3 key findings: firstly, we showed initial mechanistic synaptic dysfunction including a persistent hyperexcitation of pyramidal cell membrane properties and a diminished synaptic excitatory–inhibitory balance correlated with a reduction in canonical Wnt signaling activity in the LEC. Secondly, we identified that the impaired excitatory–inhibitory balance primarily originated from a decreased cellular distribution and hypoactivity of GABAergic function of PV interneurons in the LEC. Finally, we showed that the impaired synaptic imbalance was restored by applying specific $GABA_A$ receptors allosteric modulators, delineating future early stage therapeutic targets to prevent or halt mechanisms of synaptic dysfunction leading to neurodegeneration associated with AD.

The entorhinal cortex is the most vulnerable cortical region affected during early stages of AD, and our results show that the majority of principal cells are hyperactive before the presence of the hallmarks of disease, neuroinflammation or accumulation of Aβ plaques. However, others have suggested that early hyperexcited neurons in cortical regions are associated with amyloid plaques in a double transgenic (App23, PS45) AD mouse model (Busche et al. 2008).

Initial triggers of the observed hyperactivity and pathogenesis seem to be a combination of synaptic and molecular dysregulation. The results from our TTX experiments suggest a strong network-driven component that contributes to the sustained hyperexcitability, as blocking action potential discharge eliminated synaptic hyperactivity. The dysregulated network probably combines excitatory and inhibitory components. We suggest the network-driven hyperexcitability is related to changes in the fundamental inhibitory PV microcircuitry, which was significantly reduced in density, firing properties and the capacity to produce the neurotransmitter GABA in the LEC. These factors alone (due to a loss of the inhibitory drive) or in combination with other dysfunctional dis-inhibitory interneurons in the $App^{NL\text{-}F/NL\text{-}F}$ mouse model (Shi et al., manuscript under review), could potentially trigger synaptic imbalance and hyperactivity of the pyramidal cells in the LEC in early AD. The LEC was unique in this change, since we report unchanged PV cell densities in other cortical regions, including the dorsal entorhinal cortex, neocortex and hippocampus in late phenotypical expression of AD in $App^{NL\text{-}F/NL\text{-}F}$ mice, although a general loss of colocalized PV with GAD67 was consistent in all cortical regions studied, suggesting a reduction of the synthesis of GABA neurotransmitter present within cell bodies and therefore inhibitory function. Similarly, we observed a reduction in GAT-1 expression at GABAergic somatic terminals, which we propose is due to PV cells since it is well established that PV cells make only proximal postsynaptic contacts (Kawaguchi et al. 1987). Others have suggested that a direct excitatory innervation of CA1 PV cells is lost due to principal cell death in the entorhinal cortex (Yang et al. 2018a,b). Whether similar mechanisms trigger the loss of LEC PV cells in the LEC needs further investigation.

The factors that cause the initial reduction in inhibition could be related to observations showing that most diminished

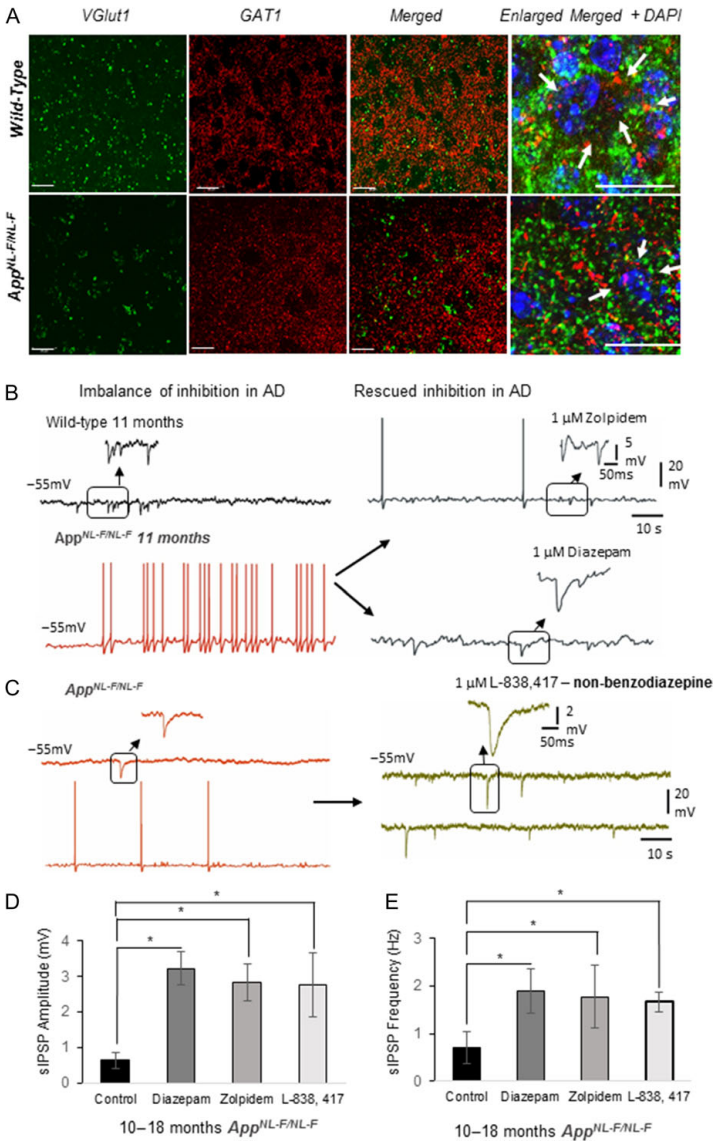

Figure 6. Restoration of the excitatory–inhibitory balance by $GABA_A$ receptor allosteric modulators. (*A*) Immunofluorescence Z-stacks of VGlut1 (green) and GABA-transporter 1 (GAT-1, red) in entorhinal cortex in both wild-type and $App^{NL\text{-}F/NL\text{-}F}$ *mice.* Although, the levels of GAT-1 remained constant ($P > 0.05$) in both wild-type and $App^{NL\text{-}F/NL\text{-}F}$ mouse model, the pattern of distribution of VGlut1 and GAT-1 merged, appear different in the $App^{NL\text{-}F/NL\text{-}F}$ mice, indicated by the arrows in the enlarged merged images. (*B*, *C*) Aberrant spontaneous synaptic events recorded in principal LEC neurons in wild-type and $App^{NL\text{-}F/NL\text{-}F}$ mice restored by bath-application of $GABA_A$ receptor allosteric modulators diazepam, α1 subunit containing $GABA_AR$, zolpidem or α2 and α3 subunit containing $GABA_A$ receptor (nonbenzo-diazepine), L-838, 417. (*D*) Bar graphs to illustrate the change in the amplitude and frequency of sIPSPs with bath-application of diazepam, zolpidem or L-383,417, (*$P < 0.05$; $n = 4$, 10–18 months old animals per cohort and $n = 6$ cells per cohort).

GABA terminals are found adjacent to Aβ plaques suggesting that Aβ plaque accumulation directly initiates cellular dysfunction in patients affected by AD (Garcia-Marin et al. 2009). However, PV is a calcium binding protein that is thought to have a buffering capacity and prevents oxidative stress, which makes these cells resilient to neurodegeneration. Thus factors such as the impaired, hypoactive intrinsic properties of PV cells as we observed, could be directly related to the initial insults. Similarly, others have also reported hypoactivity of PV cell membrane properties (Zhang et al. 2016).

In line with the electrophysiological and microscopic observations, the reduction in Wnt signaling activity was first observed in the entorhinal cortex, the region first affected in AD. The magnitude of the decrease in signaling activity remained similar in the entorhinal cortex from 1 to 18 months but increased over time throughout the remaining cortex, illustrating a direct correlation between canonical Wnt signaling activity and progress of AD pathogenesis. At this stage it is clear that Wnt signaling dysregulation occurs prior to Aβ pathology and gliosis but unclear if it is the result or the cause of the early observed synaptic dysfunction. The observed early onset of pyramidal cell hyperactivity might be a manifestation of disrupted synaptic mechanisms mediated by PV network function originating in the LEC and likely amplified by canonical Wnt signaling dysfunction. However, it is also important to note that Wnt signaling is known to be crucial during brain development including axonal outgrowth and synapse formation. In addition, evidence for the relevance of Wnt signaling for synaptic maintenance and function throughout life is accumulating (Inestrosa and Arenas 2010; Jensen et al. 2012; Park and Shen 2012; Dickins and Salinas 2013; Oliva et al. 2013a,b). Therefore, dysregulation of canonical Wnt signaling possibly caused by mutant APP gene expression during development might cause subtle neuronal changes, resulting in an increased vulnerability to neurodegenerative insults that becomes evident during aging (Zhou et al. 2012; Purro et al. 2012, 2014; Tapia-Rojas et al. 2016; Elliott et al. 2018; Tapia-Rojas and Inestrosa 2018a,b). For example, knockout of the specific canonical Wnt signaling co-receptor Lrp6 leads to age related structural and functional synaptic changes in wild type mice and accelerates pathogenic changes in AD mouse models (Liu et al. 2014). Therefore, changes observed in the $APP^{NL\text{-}F/NL\text{-}F}$ animals might be partially mimicked by knockout or knockdown of canonical Wnt signaling components such as Lrp6 in wild type animals. *Vice versa* treatment with stimulators of canonical Wnt signaling such as Wnt3a ligand or DKK1 inhibitors might alleviate some of the observed neuronal changes in the $APP^{NL\text{-}F/NL\text{-}F}$ animals (Alvarez et al. 2004; Toledo and Inestrosa 2010; Fiorentini et al. 2010; Harvey and Marchetti 2014; Yi et al. 2014; Parr et al. 2015; Marzo et al. 2016; Jin et al. 2017, Huang et al. 2018).

Consistent with the observed synaptic imbalance, there was a notable change in the intrinsic membrane properties rendering pyramidal cells in the $App^{NL\text{-}F/NL\text{-}F}$ mouse model more excitable compared with age matched wild-type mice. This membrane hyperactivity could be related to pro-inflammatory mediators, such as cytokines, reactive oxygen species and free radicals to name a few, released from the activated astrocytes and glial cells, which themselves have been shown to be altered morphologically (Olabarria et al. 2010; Rodriguez et al. 2010). Astrocytes regulate the microenvironment by providing K^+ ion homeostasis for excitable membranes, and their reduced function could lead to an accumulation of extracellular K^+ released from neurons (Verkhratsky 2010), resulting in a more depolarized membrane potential, rendering cells more excitable. These hyperactive membrane properties become weak and diminished with age, which is probably due alterations and down regulation of leak conductance responsible for generating the intrinsic firing of these cells. Moreover, hyperexcitation of neuronal populations can lead to excitotoxicity contributing to neurodegeneration, as shown in our aged $App^{NL\text{-}F/NL\text{-}F}$ mice that were associated with morphological atrophy of LEC pyramidal cells and the gradual decline in the density of principal cells as shown by the CAMKII-α labeling experiments. These cellular properties observed in vitro correlate with the behavioral abnormalities of this AD mouse model detected from 10 months onwards (Masuda et al. 2016).

Dysfunctional synaptic activity has been shown to promote the spread of Aβ (Yamamoto et al. 2015); this is further supported by the largest accumulation of Aβ plaques in postphenotypic $App^{NL\text{-}F/NL\text{-}F}$ mice found at the boundary between the neocortex and the dorsal entorhinal cortex, suggesting that the initial hyperexcitation observed in the entorhinal cortex promotes the propagation of Aβ. The observed aberrant function of the LEC is consistent with preclinical human fMRI studies that have also shown pathology to be initiated in the LEC (Khan et al. 2014). Therefore, it would be beneficial to understand whether such mechanisms could be normalized, as it may prevent the propagation of the disease. To normalize the impaired aberrant excitatory–inhibitory imbalance, we pharmacologically targeted the preserved GABAergic terminals in the aged $App^{NL\text{-}F/NL\text{-}F}$ model and our results are promising. Three different types of $GABA_A$ receptor allosteric modulators, diazepam, zolpidem and L-838,417, rectified the aberrant synaptic excitatory–inhibitory imbalance in our AD model by enhancing the amplitudes and frequency of inhibitory effects. We suggest that both, the increase in sIPSP amplitudes and frequency with these allosteric modulators are due to postsynaptic effects related to the enhanced affinity for GABA at the receptors, as well as an increase in the frequency of the opening times of the receptor ion channels. Hence, our observations support the idea of a reduced GABAergic network primarily contributing to the observed hyperexcitability of principal cells. Zolpidem is specifically known to target α1 containing $GABA_A$ receptors, while L-838,417 has been shown primarily to activate α2 and α3 subunit-containing $GABA_A$ receptors, (McKernan et al. 2000; Mathiasen et al. 2007; Ujfalussy et al. 2007), which are subtypes of $GABA_A$ receptors shown to be associated with postsynaptic domains targeted by PV interneurons (Ali and Thomson 2008), and with little sedative or amnestic effects that are associated with α1 subtypes (McKernan et al. 2000). Others have also shown that AD associated insults to cortical regions can be restored or intercepted with either pharmacological agents (Busche et al. 2008; Busche and Konnerth 2016), or by optogenetic experiments inducing specific oscillatory states such as gamma (Iaccarino et al. 2016; Nakazono et al. 2017) or theta oscillations (Yang et al. 2018a,b).

In summary, AD is a multifactorial disease, and the interplay between the molecular and cellular mechanisms probably cause an iterative remodeling of cellular pathways and redistribution of the synaptic activity during the pathogenesis of the disease. In this study, we report a combination of early stage molecular and synaptic mechanistic dysfunction that contributes to the disease pathogenesis. Canonical Wnt signaling changes in the *App* knock-in mice are observed early on in the AD disease process in areas typically also affected in AD patients and exacerbate further over time. These changes are not observed in the cerebellum, a brain area mostly spared during AD pathogenesis. Our data suggest impaired synaptic excitatory–inhibitory inputs in pyramidal cells of $App^{NL\text{-}F/NL\text{-}F}$ mice from early stages of the disease, preceding the typical hallmarks of AD, i.e., before the signs of neuroinflammation and Aβ plaque formation in the LEC, which is also corroborated by recent study using rTg4510 transgenic mouse line studying tauopthay (Jackson et al. 2017). In the present study, we suggest that the synaptic imbalance is associated with a decrement in PV interneuron density and function specific to the dorsal entorhinal cortex, which plays a vital function in the storage of

episodic and long-term memory alongside the maintenance of crucial cognitive functions in the murine brain.

In conclusion, this novel study provides a deeper understanding of the neuronal networks affected in AD which can form the basis for further mechanistic studies. Further investigation of whether early treatment preceding AD hallmarks with specific targeted $GABA_A$ receptors modulators halts the neurodegeneration could lead to novel therapeutic intervention and assist in future developments of novel targeted therapies to delay, halt or prevent memory deficits associated with AD dementia.

Supplementary Material

Supplementary material is available at *Cerebral Cortex* online.

Author Contributions

A.P.: Performed the neuroanatomical studies, confocal microscope imaging and data analysis and contributed in preparing the article. A.R.: Performed neuroanatomical studies, confocal microscope imaging of PV cells and data analysis. A.S.: Performed the neuroanatomical studies and neuronal reconstruction, data analysis and contributed in preparing the article. A.W.: Performed and analyzed western blot experiments associated with Wnt signaling and contributed in preparing the article. T.S. and T.C.S.: Provided the App^{NL_F/NL_F} mouse model of Alzheimer's disease and provided comments to the article. K.H.: Designed and analyzed Wnt signaling experiments, advised on wnt signaling and contributed in preparing the article. A.B.A.: Designed and coordinated the project, performed all electrophysiological whole-cell recordings, performed and supervised neuroanatomical studies, performed data analysis and prepared the article.

Funding

Experiments were performed using equipment funded by the Wellcome Trust (UK) and by the Medical Research Council (UK) New Investigators award (AB Ali: GO501263). This research was supported in part by the Medical Research Council [MR/M00676X/1 to K.H.].

Notes

Conflict of Interest: There are no competing interests.

References

Ali AB, Thomson AM. 2008. Synaptic alpha 5 subunit-containing GABAA receptors mediate IPSPs elicited by dendrite-preferring cells in rat neocortex. Cereb Cortex. 18: 1260–1271.

Alvarez AR, Godoy JA, Mullendorff K, Olivares GH, Bronfman M, Inestrosa NC. 2004. Wnt-3a overcomes beta-amyloid toxicity in rat hippocampal neurons. Exp Cell Res. 297:186–196.

Ascoli GA, Alonso-Nanclares L, Anderson SA, Barrionuevo G, Benavides-Piccione R, Burkhalter A, Buzsaki G, Cauli B, Defelipe J, Fairen A, et al. 2008. Petilla terminology: nomenclature of features of GABAergic interneurons of the cerebral cortex. Nat Rev Neurosci. 9:557–568.

Atack JR. 2011. GABAA receptor subtype-selective modulators. I. Alpha2/alpha3-selective agonists as non-sedating anxiolytics. Curr Top Med Chem. 11:1176–1202.

Bakker A, Krauss GL, Albert MS, Speck CL, Jones LR, Stark CE, Yassa MA, Bassett SS, Shelton AL, Gallagher M. 2012. Reduction of hippocampal hyperactivity improves cognition in amnestic mild cognitive impairment. Neuron. 74:467–474.

Bero AW, Bauer AQ, Stewart FR, White BR, Cirrito JR, Raichle ME, Culver JP, Holtzman DM. 2012. Bidirectional relationship between functional connectivity and amyloid-beta deposition in mouse brain. J Neurosci. 32:4334–4340.

Berwick DC, Harvey K. 2014. The regulation and deregulation of Wnt signaling by PARK genes in health and disease. J Mol Cell Biol. 6:3–12.

Braak H, Braak E. 1991. Demonstration of amyloid deposits and neurofibrillary changes in whole brain sections. Brain Pathol. 1:213–216.

Buckner RL, Snyder AZ, Shannon BJ, LaRossa G, Sachs R, Fotenos AF, Sheline YI, Klunk WE, Mathis CA, Morris JC, et al. 2005. Molecular, structural, and functional characterization of Alzheimer's disease: evidence for a relationship between default activity, amyloid, and memory. J Neurosci. 25:7709–7717.

Busche MA, Eichhoff G, Adelsberger H, Abramowski D, Wiederhold KH, Haass C, Staufenbiel M, Konnerth A, Garaschuk O. 2008. Clusters of hyperactive neurons near amyloid plaques in a mouse model of Alzheimer's disease. Science. 321:1686–1689.

Busche MA, Konnerth A. 2016. Impairments of neural circuit function in Alzheimer's disease. Philos Trans R Soc Lond B Biol Sci. 371.

Cerpa W, Farias GG, Godoy JA, Fuenzalida M, Bonansco C, Inestrosa NC. 2010. Wnt-5a occludes Abeta oligomer-induced depression of glutamatergic transmission in hippocampal neurons. Mol Neurodegener. 5:3.

Cerpa W, Gambrill A, Inestrosa NC, Barria A. 2011. Regulation of NMDA-receptor synaptic transmission by Wnt signaling. J Neurosci. 31:9466–9471.

Cirrito JR, Kang JE, Lee J, Stewart FR, Verges DK, Silverio LM, Bu G, Mennerick S, Holtzman DM. 2008. Endocytosis is required for synaptic activity-dependent release of amyloid-beta in vivo. Neuron. 58:42–51.

Dengler-Crish CM, Ball HC, Lin L, Novak KM, Cooper LN. 2018. Evidence of Wnt/beta-catenin alterations in brain and bone of a tauopathy mouse model of Alzheimer's disease. Neurobiol Aging. 67:148–158.

Dickins EM, Salinas PC. 2013. Wnts in action: from synapse formation to synaptic maintenance. Front Cell Neurosci. 7:162.

Elliott C, Rojo AI, Ribe E, Broadstock M, Xia W, Morin P, Semenov M, Baillie G, Cuadrado A, Al-Shawi R, et al. 2018. A role for APP in Wnt signalling links synapse loss with beta-amyloid production. Transl Psychiatry. 8:179.

Fiorentini A, Rosi MC, Grossi C, Luccarini I, Casamenti F. 2010. Lithium improves hippocampal neurogenesis, neuropathology and cognitive functions in APP mutant mice. PLoS One. 5:e14382.

Garcia-Marin V, Blazquez-Llorca L, Rodriguez JR, Boluda S, Muntane G, Ferrer I, Defelipe J. 2009. Diminished perisomatic GABAergic terminals on cortical neurons adjacent to amyloid plaques. Front Neuroanat. 3:28.

Harvey K, Marchetti B. 2014. Regulating Wnt signaling: a strategy to prevent neurodegeneration and induce regeneration. J Mol Cell Biol. 6:1–2.

Holtzman DM, Morris JC, Goate AM. 2011. Alzheimer's disease: the challenge of the second century. Sci Transl Med. 3:77sr71.

Howell O, Atack JR, Dewar D, McKernan RM, Sur C. 2000. Density and pharmacology of alpha5 subunit-containing

GABA(A) receptors are preserved in hippocampus of Alzheimer's disease patients. Neuroscience. 98:669–675.
Huang M, Liang Y, Chen H, Xu B, Chai C, Xing P. 2018. The role of fluoxetine in activating Wnt/beta-Catenin signaling and repressing beta-amyloid production in an Alzheimer mouse model. Front Aging Neurosci. 10:164.
Iaccarino HF, Singer AC, Martorell AJ, Rudenko A, Gao F, Gillingham TZ, Mathys H, Seo J, Kritskiy O, Abdurrob F, et al. 2016. Gamma frequency entrainment attenuates amyloid load and modifies microglia. Nature. 540:230–235.
Inestrosa NC, Arenas E. 2010. Emerging roles of Wnts in the adult nervous system. Nat Rev Neurosci. 11:77–86.
Inestrosa NC, Toledo EM. 2008. The role of Wnt signaling in neuronal dysfunction in Alzheimer's disease. Mol Neurodegener. 3:9.
Inestrosa NC, Varela-Nallar L. 2014. Wnt signaling in the nervous system and in Alzheimer's disease. J Mol Cell Biol. 6: 64–74.
Jackson JS, Witton J, Johnson JD, Ahmed Z, Ward M, Randall AD, Hutton ML, Isaac JT, O'Neill MJ, Ashby MC. 2017. Altered synapse stability in the early stages of tauopathy. Cell Rep. 18: 3063–3068.
Jensen M, Brockie PJ, Maricq AV. 2012. Wnt signaling regulates experience-dependent synaptic plasticity in the adult nervous system. Cell Cycle. 11:2585–2586.
Jin N, Zhu H, Liang X, Huang W, Xie Q, Xiao P, Ni J, Liu Q. 2017. Sodium selenate activated Wnt/beta-catenin signaling and repressed amyloid-beta formation in a triple transgenic mouse model of Alzheimer's disease. Exp Neurol. 297:36–49.
Kamenetz F, Tomita T, Hsieh H, Seabrook G, Borchelt D, Iwatsubo T, Sisodia S, Malinow R. 2003. APP processing and synaptic function. Neuron. 37:925–937.
Kawaguchi Y, Katsumaru H, Kosaka T, Heizmann CW, Hama K. 1987. Fast spiking cells in rat hippocampus (CA1 region) contain the calcium-binding protein parvalbumin. Brain Res. 416:369–374.
Kawaguchi Y, Kubota Y. 1993. Correlation of physiological subgroupings of nonpyramidal cells with parvalbumin- and calbindinD28k-immunoreactive neurons in layer V of rat frontal cortex. J Neurophysiol. 70:387–396.
Khan UA, Liu L, Provenzano FA, Berman DE, Profaci CP, Sloan R, Mayeux R, Duff KE, Small SA. 2014. Molecular drivers and cortical spread of lateral entorhinal cortex dysfunction in preclinical Alzheimer's disease. Nat Neurosci. 17:304–311.
Khan AA, Shekh-Ahmad T, Khalil A, Walker MC, Ali AB. 2018. Cannabidiol exerts antiepileptic effects by restoring hippocampal interneuron functions in a temporal lobe epilepsy model. Br J Pharmacol. 175:2097–2115.
Klausberger T, Marton LF, O'Neill J, Huck JH, Dalezios Y, Fuentealba P, Suen WY, Papp E, Kaneko T, Watanabe M, et al. 2005. Complementary roles of cholecystokinin- and parvalbumin-expressing GABAergic neurons in hippocampal network oscillations. J Neurosci. 25:9782–9793.
Klausberger T, Somogyi P. 2008. Neuronal diversity and temporal dynamics: the unity of hippocampal circuit operations. Science. 321:53–57.
Liu CC, Tsai CW, Deak F, Rogers J, Penuliar M, Sung YM, Maher JN, Fu Y, Li X, Xu H, et al. 2014. Deficiency in LRP6-mediated Wnt signaling contributes to synaptic abnormalities and amyloid pathology in Alzheimer's disease. Neuron. 84:63–77.
Maccaferri G, Lacaille JC. 2003. Interneuron diversity series: hippocampal interneuron classifications—making things as simple as possible, not simpler. Trends Neurosci. 26:564–571.
Marin O. 2012. Interneuron dysfunction in psychiatric disorders. Nat Rev Neurosci. 13:107–120.
Markram H, Toledo-Rodriguez M, Wang Y, Gupta A, Silberberg G, Wu C. 2004. Interneurons of the neocortical inhibitory system. Nat Rev Neurosci. 5:793–807.
Marzo A, Galli S, Lopes D, McLeod F, Podpolny M, Segovia-Roldan M, Ciani L, Purro S, Cacucci F, Gibb A, Salinas PC. 2016. Reversal of Synapse Degeneration by Restoring Wnt Signaling in the Adult Hippocampus. Curr Biol. 26: 2551–2561.
Masuda A, Kobayashi Y, Kogo N, Saito T, Saido TC, Itohara S. 2016. Cognitive deficits in single App knock-in mouse models. Neurobiol Learn Mem. 135:73–82.
Mathiasen LS, Rodgers RJ, Mirza NR. 2007. Comparative effects of nonselective and subtype-selective gamma-aminobutyric acidA receptor positive modulators in the rat-conditioned emotional response test. Behav Pharmacol. 18:191–203.
McGrath JC, Drummond GB, McLachlan EM, Kilkenny C, Wainwright CL. 2010. Guidelines for reporting experiments involving animals: the ARRIVE guidelines. Br J Pharmacol. 160:1573–1576.
McKernan RM, Rosahl TW, Reynolds DS, Sur C, Wafford KA, Atack JR, Farrar S, Myers J, Cook G, Ferris P, et al. 2000. Sedative but not anxiolytic properties of benzodiazepines are mediated by the GABA(A) receptor alpha1 subtype. Nat Neurosci. 3:587–592.
Nakazono T, Lam TN, Patel AY, Kitazawa M, Saito T, Saido TC, Igarashi KM. 2017. Impaired in vivo gamma oscillations in the medial entorhinal cortex of knock-in Alzheimer model. Front Syst Neurosci. 11:48.
Nicholson MW, Sweeney A, Pekle E, Alam S, Ali AB, Duchen M, Jovanovic JN. 2018. Diazepam-induced loss of inhibitory synapses mediated by PLCdelta/Ca (2+)/calcineurin signalling downstream of GABAA receptors. Mol Psychiatry. 23: 1851–1867.
Olabarria M, Noristani HN, Verkhratsky A, Rodriguez JJ. 2010. Concomitant astroglial atrophy and astrogliosis in a triple transgenic animal model of Alzheimer's disease. Glia. 58: 831–838.
Oliva CA, Inestrosa NC. 2015. A novel function for Wnt signaling modulating neuronal firing activity and the temporal structure of spontaneous oscillation in the entorhinal-hippocampal circuit. Exp Neurol. 269:43–55.
Oliva CA, Vargas JY, Inestrosa NC. 2013a. Wnt signaling: role in LTP, neural networks and memory. Ageing Res Rev. 12: 786–800.
Oliva CA, Vargas JY, Inestrosa NC. 2013b. Wnts in adult brain: from synaptic plasticity to cognitive deficiencies. Front Cell Neurosci. 7:224.
O'Brien JL, O'Keefe KM, LaViolette PS, DeLuca AN, Blacker D, Dickerson BC, Sperling RA. 2010. Longitudinal fMRI in elderly reveals loss of hippocampal activation with clinical decline. Neurology. 74:1969–1976.
Palop JJ, Chin J, Mucke L. 2006. A network dysfunction perspective on neurodegenerative diseases. Nature. 443:768–773.
Palop JJ, Mucke L. 2016. Network abnormalities and interneuron dysfunction in Alzheimer disease. Nat Rev Neurosci. 17: 777–792.
Park M, Shen K. 2012. WNTs in synapse formation and neuronal circuitry. EMBO J. 31:2697–2704.
Parr C, Mirzaei N, Christian M, Sastre M. 2015. Activation of the Wnt/β-catenin pathway represses the transcription of the β-amyloid precursor protein cleaving enzyme (BACE1) via

binding of T-cell factor-4 to BACE1 promoter. FASEB J. 29: 623–635.

Pelkey KA, Chittajallu R, Craig MT, Tricoire L, Wester JC, McBain CJ. 2017. Hippocampal GABAergic Inhibitory Interneurons. Physiol Rev. 97:1619–1747.

Purro SA, Dickins EM, Salinas PC. 2012. The secreted Wnt antagonist Dickkopf-1 is required for amyloid beta-mediated synaptic loss. J Neurosci. 32:3492–3498.

Purro SA, Galli S, Salinas PC. 2014. Dysfunction of Wnt signaling and synaptic disassembly in neurodegenerative diseases. J Mol Cell Biol. 6:75–80.

Rissman RA, De Blas AL, Armstrong DM. 2007. GABA(A) receptors in aging and Alzheimer's disease. J Neurochem. 103: 1285–1292.

Ristanovic D, Milosevic NT, Stulic V. 2006. Application of modified Sholl analysis to neuronal dendritic arborization of the cat spinal cord. J Neurosci Methods. 158:212–218.

Rodriguez JJ, Witton J, Olabarria M, Noristani HN, Verkhratsky A. 2010. Increase in the density of resting microglia precedes neuritic plaque formation and microglial activation in a transgenic model of Alzheimer's disease. Cell Death Dis. 1:e1.

Rudy B, Fishell G, Lee S, Hjerling-Leffler J. 2011. Three groups of interneurons account for nearly 100% of neocortical GABAergic neurons. Dev Neurobiol. 71:45–61.

Saito T, Matsuba Y, Mihira N, Takano J, Nilsson P, Itohara S, Iwata N, Saido TC. 2014. Single App knock-in mouse models of Alzheimer's disease. Nat Neurosci. 17:661–663.

Sasaguri H, Nilsson P, Hashimoto S, Nagata K, Saito T, De Strooper B, Hardy J, Vassar R, Winblad B, Saido TC. 2017. APP mouse models for Alzheimer's disease preclinical studies. EMBO J. 36:2473–2487.

Tapia-Rojas C, Burgos PV, Inestrosa NC. 2016. Inhibition of Wnt signaling induces amyloidogenic processing of amyloid precursor protein and the production and aggregation of Amyloid-beta (Abeta)42 peptides. J Neurochem. 139:1175–1191.

Tapia-Rojas C, Inestrosa NC. 2018a. Loss of canonical Wnt signaling is involved in the pathogenesis of Alzheimer's disease. Neural Regen Res. 13:1705–1710.

Tapia-Rojas C, Inestrosa NC. 2018b. Wnt signaling loss accelerates the appearance of neuropathological hallmarks of Alzheimer's disease in J20-APP transgenic and wild-type mice. J Neurochem. 144:443–465.

Toledo EM, Inestrosa NC. 2010. Activation of Wnt signaling by lithium and rosiglitazone reduced spatial memory impairment and neurodegeneration in brains of an APPswe/PSEN1DeltaE9 mouse model of Alzheimer's disease. Mol Psychiatry. 15:272–285. 228.

Ujfalussy B, Kiss T, Orban G, Hoffmann WE, Erdi P, Hajos M. 2007. Pharmacological and computational analysis of alpha-subunit preferential GABA(A) positive allosteric modulators on the rat septo-hippocampal activity. Neuropharmacology. 52:733–743.

Verkhratsky A. 2010. Physiology of neuronal-glial networking. Neurochem Int. 57:332–343.

Verret L, Mann EO, Hang GB, Barth AM, Cobos I, Ho K, Devidze N, Masliah E, Kreitzer AC, Mody I, et al. 2012. Inhibitory interneuron deficit links altered network activity and cognitive dysfunction in Alzheimer model. Cell. 149:708–721.

Wang X, Zhang C, Szabo G, Sun QQ. 2013. Distribution of CaMKIIalpha expression in the brain in vivo, studied by CaMKIIalpha-GFP mice. Brain Res. 1518:9–25.

Yamamoto K, Tanei ZI, Hashimoto T, Wakabayashi T, Okuno H, Naka Y, Yizhar O, Fenno LE, Fukayama M, Bito H, et al. 2015. Chronic optogenetic activation augments abeta pathology in a mouse model of Alzheimer disease. Cell Rep. 11:859–865.

Yang X, Yao C, Tian T, Li X, Yan H, Wu J, Li H, Pei L, Liu D, Tian Q, et al. 2018a. A novel mechanism of memory loss in Alzheimer's disease mice via the degeneration of entorhinal-CA1 synapses. Mol Psychiatry. 23:199–210.

Yang X, Yao C, Tian T, Li X, Yan H, Wu J, Li H, Pei L, Liu D, Tian Q, et al. 2018b. Synaptic mechanism in Alzheimer's disease: a selective degeneration of an excitatory synaptic pathway in the CA1 hippocampus that controls spatial learning and memory in Alzheimer's disease. Mol Psychiatry. 23:167.

Yi R, Chen B, Zhao J, Zhan X, Zhang L, Liu X, Dong Q. 2014. Krüppel-like factor 8 ameliorates Alzheimer's disease by activating β-catenin. J Mol Neurosci. 52:231–241.

Zhang W, Zhang L, Liang B, Schroeder D, Zhang ZW, Cox GA, Li Y, Lin DT. 2016. Hyperactive somatostatin interneurons contribute to excitotoxicity in neurodegenerative disorders. Nat Neurosci. 19:557–559.

Zhou F, Gong K, Song B, Ma T, van Laar T, Gong Y, Zhang L. 2012. The APP intracellular domain (AICD) inhibits Wnt signalling and promotes neurite outgrowth. Biochim Biophys Acta. 1823:1233–1241.

OXFORD

Cerebral Cortex, March 2020;30: 1272–1290

doi: 10.1093/cercor/bhz165
Advance Access Publication Date: 13 August 2019
Original Article

ORIGINAL ARTICLE

Preserved Calretinin Interneurons in an *App* Model of Alzheimer's Disease Disrupt Hippocampal Inhibition via Upregulated P2Y1 Purinoreceptors

Anqi Shi, Alexandra L. Petrache, Jiachen Shi and Afia B. Ali*

UCL School of Pharmacy, London, WC1N 1AX, UK

Address correspondence to Afia B. Ali, UCL School of Pharmacy, 29-39 Brunswick Square, London, WC1N 1AX, UK. Email: afia.b.ali@ucl.ac.uk.
http://orcid.org/0000-0001-5203-5609
†Anqi Shi and Alexandra L. Petrache have contributed equally to this work

Abstract

To understand the pathogenesis of specific neuronal circuit dysfunction in Alzheimer's disease (AD), we investigated the fate of three subclasses of "modulatory interneurons" in hippocampal CA1 using the $App^{NL\text{-}F/NL\text{-}F}$ knock-in mouse model of AD. Cholecystokinin- and somatostatin-expressing interneurons were aberrantly hyperactive preceding the presence of the typical AD hallmarks: neuroinflammation and amyloid-β (Aβ) accumulation. These interneurons showed an age-dependent vulnerability to Aβ penetration and a reduction in density and coexpression of the inhibitory neurotransmitter GABA synthesis enzyme, glutamic acid decarboxylase 67 (GAD67), suggesting a loss in their inhibitory function. However, calretinin (CR) interneurons—specialized to govern *only* inhibition, showed resilience to Aβ accumulation, preservation of structure, and displayed synaptic hyperinhibition, despite the lack of inhibitory control of CA1 excitatory pyramidal cells from midstages of the disease. This aberrant inhibitory homeostasis observed in CA1 CR cells and pyramidal cells was "normalized" by blocking P2Y1 purinoreceptors, which were "upregulated" and strongly expressed in CR cells and astrocytes in $App^{NL\text{-}F/NL\text{-}F}$ mice in the later stages of AD. In summary, AD-associated cell-type selective destruction of inhibitory interneurons and disrupted inhibitory homeostasis rectified by modulation of the upregulated purinoreceptor system may serve as a novel therapeutic strategy to normalize selective dysfunctional synaptic homeostasis during pathogenesis of AD.

Key words: Alzheimer's disease, astrocytes, interneurons, P2Y1 receptors, synapse

Introduction

Idiopathic and familial Alzheimer's disease (AD) are debilitating chronic neurodegenerative conditions characterized by accumulation of amyloid-β (Aβ) plaques, neurofibrillary tangles, dystrophic neurites, and gliosis (Holtzman et al. 2011), as well as progressive cognitive deficits leading to neurodegeneration and abnormal aging.

The Cornu Ammonis (CA) 1 region of the hippocampus together with the neighboring cortical region, the entorhinal cortex, is one of the significant brain regions that play a critical role in memory formation and retrieval and one of the initial regions to be disrupted in early AD. This region is enriched with pathways that are heavily innervated by the diverse inhibitory gamma-aminobutyric acid (GABA)–containing interneuron populations. The $GABA_A$ receptor family is known to play a vital role in cognitive functions, including learning and memory. Although there are currently 22 known subgroups of interneurons that perform distinct functions through activation of postsynaptic $GABA_A$ receptors (Klausberger and Somogyi 2008), the identity of the vulnerable and resistant subclasses of interneurons in AD needs detailed investigation.

This knowledge gap will help us understand a consistent observation that spans from human studies to various rodent models of AD, that is, the abnormal synaptic hyperexcitation preceding phenotypic alteration of the disease, which has been noted as a relevant therapeutic target (Palop et al. 2007; Busche et al. 2008; Khan et al. 2014). It has been suggested that AD-related cortical neurodegeneration is associated with overexcitation of hippocampal activity (Putcha et al. 2011), which is consistent with various in vitro and in vivo models of AD, demonstrating that increased neuronal activity stimulates tau release which further enhances tau pathology (Wu et al. 2016; Yamada et al. 2014), as well as augmentation of Aβ depositions from presynaptic terminals (Yamamoto et al. 2015). Using the first *App* knock-in mouse model of AD, $App^{NL\text{-}F/NL\text{-}F}$, we recently reported a time-dependent spread of synaptic hyperexcitability initiated in the entorhinal cortex that spreads to other cortical regions, altering the balance of excitation–inhibition in the AD model (Petrache et al. 2019). This synaptic hyperexcitation presents a paradox in AD, as others have reported that inhibitory post-synaptic $GABA_A$ receptors that govern excitation in memory-related pathways remain preserved in human brains of AD patients (Howell et al. 2000; Rissman et al. 2007).

Furthermore, recently, it has become apparent that the microcircuit pathogenesis of AD is more complex than just synaptic loss, but associated with a combination of an abnormal hyperactive interplay between neurons, and their synaptic support system—astrocytes and glial cells (Heneka et al. 2015; Palop and Mucke 2016b)—which mediate their activity through P2Y1 purinoreceptor (P2Y1R) pathways (Reichenbach et al. 2018). However, the pathophysiological effects of Aβ on the interactions of specific microcircuits with the neuronal support system remains to be fully elucidated in the field, and filling this missing gap will fulfill an unmet demand in the dementia field leading to an advance in our understanding of the underlying pathogenesis of the disease to bring us a step closer to designing early-stage therapeutic intervention to prevent or halt the disease progression.

In the present study, we asked the question of whether there is a cell-type selective destruction of inhibitory interneurons responsible for fine-tuning local circuitry in AD and whether specific neuronal populations were vulnerable to Aβ association or another key detrimental factor associated with the pathogenies of AD. Using the $App^{NL\text{-}F/NL\text{-}F}$ mouse model of AD and neuroanatomy combined with electrophysiology, we focused on investigating three subtypes of dendrite-targeting modulatory interneurons in CA1, namely, cholecystokinin (CCK)-expressing, somatostatin (SST)-expressing, and the previously "unexplored", disinhibitory calretinin (CR) circuitry. The CR—containing interneurons are a major part of the disinhibitory network governing other inhibitory cells (Gulyas et al. 1996). We hypothesize that an abnormal CR microcircuitry is the key candidate mechanism for the paradoxical hyperexcitability associated with AD and that correction of this abnormal circuit behavior by blocking overactive P2Y1Rs could offer a novel therapeutic strategy for preventing, ultimately, neurodegeneration in AD.

Methods

Animals

Experimental Animals

All of the procedures in this study were carried out in accordance with the British Home Office regulations under the Animal Scientific Procedure Act 1986, under the project license PPL: P1ADA633A held by the principal investigator, Dr Afia Ali. All procedures were approved by both internal and external UCL ethics committees and in accordance with the ARRIVE guidelines for reporting experiments involving animals (McGrath et al. 2010). A total of ~85 animals (disease model and wild-type) were used in this study. The animals had ad libitum access to food and water and were reared in cages of maximum five inhabitants, with a day:night cycle of 12 h:12 h.

The knock-in $APP^{NL\text{-}F/NL\text{-}F}$ AD mouse model was used for experiments (Saito et al. 2014). This particular mouse model was chosen because it follows the progression of human AD more faithfully. Since amyloid β-peptide (Aβ) plaque deposition is a key AD pathological hallmark, the model exhibits pathogenic Aβ accumulation while also maintaining biological amyloid precursor protein (APP) levels without overexpression artifacts. The $APP^{NL\text{-}F}$ model consists of the introduction of two familial AD (FAD) mutations: KM670/671NL and I716F. The former, identified as the Swedish mutation, increases β-site cleavage of APP to produce elevated amounts of both Aβ_{40} and Aβ_{42}, whereas the latter, known as the Beyreuther/Iberian mutation, promotes γ-site cleavage at C-terminal position 42, thereby increasing the Aβ_{42}/Aβ_{40} ratio in favor of the more hydrophobic Aβ_{42} (Saito et al. 2014). Both features are key to the integrity of the disease phenotype. The knock-in line was crossed with C57BL/6 mice, and the resulting heterozygous pairs were used for breeding, but excluded from experiments. Only male $APP^{NL\text{-}F/NL\text{-}F}$ and age-matched wild-type (C57BL/6) mice from the same breeding were used as control. $APP^{NL\text{-}F/NL\text{-}F}$ and control mice were investigated at three different ages, grouped into three age groups where no differences was observed within the time window; these were 1–3 months, 4–6 months, and 9–18 months.

Animals were genotyped via standard polymerase chain reaction using the following four primers: 5′-ATCTCGGAAG TGAAGATG-3′, 5′-TGTAGATGAGAACTTAAC-3′, 5′-ATCTCGGAA GTGAATCTA-3′, and 5′-CGTATAATGTATGCTATACGAAG-3′ as previously described (Saito et al. 2014).

Tissue Collection and Preparation

Mice were anesthetized by an intraperitoneal injection of 60 mg/kg phenobarbitone and perfused transcardially with artificial cerebrospinal fluid (ACSF) containing sucrose. The level of anesthesia was monitored using pedal and tail pinch reflexes, rate, depth, and pattern of respiration through observation and color of mucous membranes and skin. The ACSF comprised (in mM) 248 sucrose, 3.3 KCl, 1.4 NaH_2PO_4, 2.5 $CaCl_2$, 1.2 $MgCl_2$, 25.5 $NaHCO_3$, and 15 glucose, which was bubbled with 95% O_2 and 5% CO_2. The animals were then decapitated and the brain removed, and coronal slices of the cortex and hippocampus—300 µm thick—were cut in ice-cold standard ACSF using an automated vibratome (Leica, Germany). This standard ACSF contained (in mM) 121 NaCl, 2.5 KCl, 1.3 NaH_2PO_4, 2 $CaCl_2$, 1 $MgCl_2$, 20 glucose, and 26 $NaHCO_3$, equilibrated with 95% O_2 and 5% CO_2. Slices were incubated in ACSF for 1 h at room temperature (20–23 °C) prior to recording. Brain slices were placed in a submerged chamber and superperfused with ACSF at a rate of 1–2 mL min^{-1} for electrophysiological recordings. For neuroanatomical studies, brains were immediately fixed after perfusion in 4% paraformaldehyde plus 0.2% picric acid in 0.1 M phosphate buffer (PB) for 24 h prior to sectioning.

Electrophysiology

Whole-cell somatic recordings were performed using patch electrodes with resistances of 8–11 MΩ made from filamented borosilicate glass capillaries (Harvard Apparatus, United Kingdom) and filled with a solution containing (in mM) 134 K gluconate, 10 HEPES, 10 phosphocreatine, 2 Na_2ATP, 0.2 Na_2GTP, and 0.2% w/v biocytin.

CA1 pyramidal cells and interneurons in the stratum oriens, stratum radiatum, and stratum lacunosum moleculare were selected for recording based on the shape of their soma using video microscopy under near infrared differential interference contrast illumination. Cells were further characterized by their electrophysiological properties obtained from injecting a series of 500-ms depolarizing and hyperpolarizing current pulses. Action potential parameters were measured from responses to depolarizing current steps (+25–150 pA, 500 ms), which induced a single or a train of action potentials. The input resistance and membrane time constant were determined from voltage changes in response to hyperpolarizing current steps (−100 pA, 500 ms). Recorded cells were filled with biocytin dye, and neurons were further identified based on their gross morphology (see below).

Spontaneous postsynaptic potentials were recorded from passive membrane responses, and mixed spontaneous excitatory postsynaptic potentials (sEPSPs) and spontaneous inhibitory postsynaptic potentials (sIPSPs) were collected in 60-s frame samples, repeated at 0.33 Hz. Recordings were carried out under the current clamp mode of operation (NPI SEC-05LX amplifier; NPI Electronic, Germany), low pass filtered at 2 kHz, and digitized at 5 kHz using a CED 1401 interface (Cambridge Electronic Design, United Kingdom). Input resistance was monitored throughout experiments by means of a hyperpolarizing current step (−0.001 nA, 10 ms). Signal (Cambridge Electronic Design, United Kingdom) was used to acquire recordings and generate current steps. The average amplitudes of spontaneous events and their frequency were measured manually from single sweep data sets of 60-s recordings, including a total sweep range of 30–50 frames (i.e., 30–50 min of recording); synaptic noise was taken as ±0.15 mV from baseline; for example, values above +0.15 mV were considered as synaptic events.

For in vitro pharmacological studies, P2Y1 receptor modulators—MRS2365 (agonist, 0.5–1 µM, Tocris Bioscience, United Kingdom) and BPTU (inhibitor, 0.5–1 µM, Tocris Bioscience, United Kingdom)—were bath-applied. Average data points after drug application were obtained after steady-state responses were attained with the drugs, which was ~ 15–20 min after onset of the bath application.

Neuroanatomical Procedures and Analysis

Recovery of Biocytin-Labeled Cells Post Electrophysiological Recordings

After electrophysiological recordings with pharmacological protocols, the slices were only suitable for biocytin recovery due to the long recording in the range of 45–90 min. Slices were fixed in 4% paraformaldehyde plus 0.2% picric acid in 0.1 M phosphate buffer (PB) for 24 h and then resectioned at 70 µm. Slices were then incubated in avidin–biotin complex (ABC) overnight at 4 °C, followed by the DAB protocol. Anatomically recovered cells were reconstructed manually from consecutive slices at ×100 objective under a Leica DMR microscope with an attached drawing tube.

Immunofluorescence Procedures, Confocal Image Acquisition, and Analysis

Coronal sections containing the neocortex and hippocampal formation were sectioned at 100-µm thickness using a vibratome (Vibroslice, Campden Instruments, Loughborough, United Kingdom) and placed in a 24-well plate containing 10% phosphate buffer (PB). Each experiment consisted of slices from wild-type and $APP^{NL\text{-}F/NL\text{-}F}$ age-matched mice and kept in separate 24-well plates. The sections per brain were allocated to the antibody and procedure, but all sections underwent identical protocols for either immunofluorescence or immunoperoxidase procedures. Prior to these specific procedures, all sections were washed in 0.3% Triton X-100 in Tris-buffered saline (TBS-T), followed by incubation in 1% hydrogen peroxide aqueous solution for 30 min. After further rinses in TBS-T, sections were incubated in phosphate-buffered saline (PBS) containing 10% normal goat serum (Sigma-Aldrich, United States of America) for 1 h at room temperature. This followed incubation in the specific primary antibodies to target the desired proteins shown in Table 1.

When colocalization assessments were performed, both primary antibodies were added to the same well simultaneously.

Slices were incubated in primary antibody for 48 h on a platform shaker at 4 °C. Afterwards, the sections were washed (0.3% TBS-T, 3 × 10 min) and incubated in the appropriate secondary antibodies (see Table 1) for 3 h. The secondary antibody solution also contained the appropriate serum in rough proportion of 0.05% of the total solution volume. When two fluorophores were added to the same well, the serum used was normal horse serum (NHS), with the exception of solutions applied to wells stained for CR, for which normal donkey serum (NDS) was used. The sections were then washed (0.3% TBS-T, 3 × 10 min), and slices stained with CD68 and glial fibrillary acidic protein (GFAP) were incubated with DAPI (1:1000) for 15 min. After further washes, the slices were mounted on glass slides using the antifade mounting medium Vectashield (Vector Lab, United Kingdom).

Images were acquired with an LSM 710 confocal microscope and processed using Zeiss ZEN Black 2009 software. Z-stacks of the CA1 region were taken at ×20 magnification. The first and last 10 µm were discarded from each section to prevent repeated capture of the same cell. When needed, more than one image was taken per slice so as to obtain an accurate average measurement for the region.

To distinguish cells from any background fluorescence, a threshold was calculated by summing the mean intensity of the collapsed Z-stack and twice the standard deviation, using ZEN 2009. Colocalization was confirmed when fluorophores marking both the cell of interest and GAD67 or P2Y1 receptor were at an intensity that exceeded the threshold and when GAD67 was present within the cell outline. Somata that exceeded the threshold were counted, and the total number obtained was then divided by the volume of the Z-stack (4.99×10^{-2} mm^3) to determine the density of cell fluorescence + GAD67-coexpressing interneurons. GAD67 or P2Y1 receptor colocalization with CR cells was calculated similarly, by analyzing the colocalization coefficient obtained using ZEN 2009.

P2Y1R expression colocalized with either CR, GFAP, or CaMKII-α was estimated using the correlation coefficient R, which was calculated with ZEN 2009. The closer R is to 1, the stronger the positive correlation between the two variables. Z-stacks were collapsed into one image and a region-of-interest (ROI)–based analysis was used to quantify receptor

Table 1 Antibody and serum information

Antibody target	Company	Species	Dilution	Serum
		Primary antibodies		
Cholecystokinin	Frontier Institute	Rabbit	1:750	NHS
Calretinin	Swant	Goat	1:1000	NDS
Somatostatin	Santa Cruz Biotechnology	Rabbit	1:200	NHS
GAD67	Millipore	Mouse	1:2000	NHS
APP695	Thermo Fisher	Mouse	1:1000 for both IF and IP	NHS
CD68	Bio-Rad	Goat	1:500; 1:3000 for IP	NGS
GFAP	Agilent (Dako)	Rabbit	1:500; 1:2000 for IP	NGS
		Secondary antibodies		
Immunofluorescence				
Texas Red	Thermo Scientific	Rabbit	1:500	
FITC	Sigma-Aldrich	Mouse	1:875	
Alexa 488	Abcam	Rabbit	1:1000	
Alexa 568	Molecular Probes	Goat	1:500	
DAPI	Sigma-Aldrich	Multiple	1:1000	
Immunoperoxidase				
Biotinylated	Vector Laboratories	Mouse, goat, rabbit	1:500	

IF, immunofluorescence; IP, immunoperoxidase; NGS, normal goat serum. The "Serum" column refers to the serum used for the 1-h incubation step before placement in primary antibodies and the serum used in conjunction with the secondary antibody solution.

colocalization with the cell type of interest. In the "Coloc" tab, the colocalization crosshairs were set using a threshold calculated with values obtained from "Histo" using the formula Threshold = mean + (standard deviation / 2). Then, the channel for the structure of interest was turned on and the cell of interest was outlined. Afterwards, the P2Y1R channel was turned on and R was calculated by the software.

Immunoperoxidase Procedure and Analysis

After washes in TBS-T, the sections were incubated in secondary biotinylated antibodies (see Table 1). After incubation with the secondary biotinylated antibody and after washes in TBS-T, there was a further incubation in avidin–biotin complex (ABC)–horseradish peroxidase (Vector Laboratories, United Kingdom) solution, for 2 h at room temperature. The sections were then washed further in TBS-T and processed with 3,3′-diaminobenzidine (DAB) and subsequently dehydrated and mounted (Khan et al. 2018).

The darkness density of slices was measured using the Fiji imaging package. DAB-stained pictures were taken under ×10 light microscope, and the background was kept consistent. Pictures were processed by color deconvolution and "H DAB," and the "mean gray value" was used to measure the darkness density. Mean gray values were normalized into optical density numbers by the formula OD = log (max intensity / mean intensity), where max intensity = 255 for 8-bit images.

Statistics

All figures displaying error bars represent the standard deviation from the mean. The "n" is given as the number of observations and the number of animals used, unless otherwise stated.

Various statistical tests were performed depending on the parameter analyzed; each figure legends detail the specific statistical test used. For example, two-sampled unpaired Student's *t*-test was used to compare biophysical parameters between wild-type and $App^{NL\text{-}F/NL\text{-}F}$ mice. A two-way ANOVA with pairwise comparisons corrected for multiple comparisons was used with either a post hoc Tukey's test or Sidak's test.

For the comparison of P2Y1 receptor expression in CR cells, astrocytes, and pyramidal cells, correlation *R* among the three cell types was performed. Fisher's transformation was applied to *R* so as to convert it to the *Z* distribution. After the conversion, a one-way ANOVA was performed ($\alpha = 0.05$), with a post hoc Tukey test for multiple comparisons in order to compare between wild-type and $App^{NL\text{-}F/NL\text{-}F}$ mice in the three cell types: calretinin, astrocytes, and pyramidal cells.

For all statistical tests performed, a 95% confidence interval was used ($P < 0.05$).

The statistical analysis was performed using GraphPad Prism version 8.1.1 for Windows and Mac, GraphPad Software, La Jolla, CA, United States of America.

Results

CA1 Age-Dependent Phenotypical Changes in AD

Classical hallmarks of AD, such as neuroinflammatory markers, astrocytes and microglia, and Aβ deposits, were stained with antibodies to glial fibrillary acidic protein (GFAP), CD68, and APP, respectively. Using immunofluorescence and immunoperoxidase staining, our data show that the $App^{NL\text{-}F/NL\text{-}F}$ model expresses an age-dependent accumulation of these classical hallmarks of AD (Fig. 1A–F). There was a significant change in glial cells and astrocytes and accumulation of Aβ levels only at 9–18 months between the age-matched wild-type and the $App^{NL\text{-}F/NL\text{-}F}$ mice. For example, GFAP levels significantly increased by 71% (±0.64%, $P < 0.001$, $n = 10$ animals per cohort, two-way ANOVA) (Fig. 1A,B) and CD68 levels increased by 108% (±27.71%, $P < 0.05$, $n = 8$ animals, two-way ANOVA) (Fig. 1C,D) in $App^{NL\text{-}F/NL\text{-}F}$ compared with the age-matched wild-type control mice at 9–18 months. There was also a 60% increase in overall Aβ accumulation in the entire CA1 region in the disease model compared with the age-matched wild-type mice at 9–18 months (±19.21%, $P < 0.01$, $n = 8$ animals, two-way ANOVA) (Fig. 1E,F). These differences were also significantly different when compared with the 1–3-month and 4–6-month age cohorts investigated (Fig. 1B,D, F).

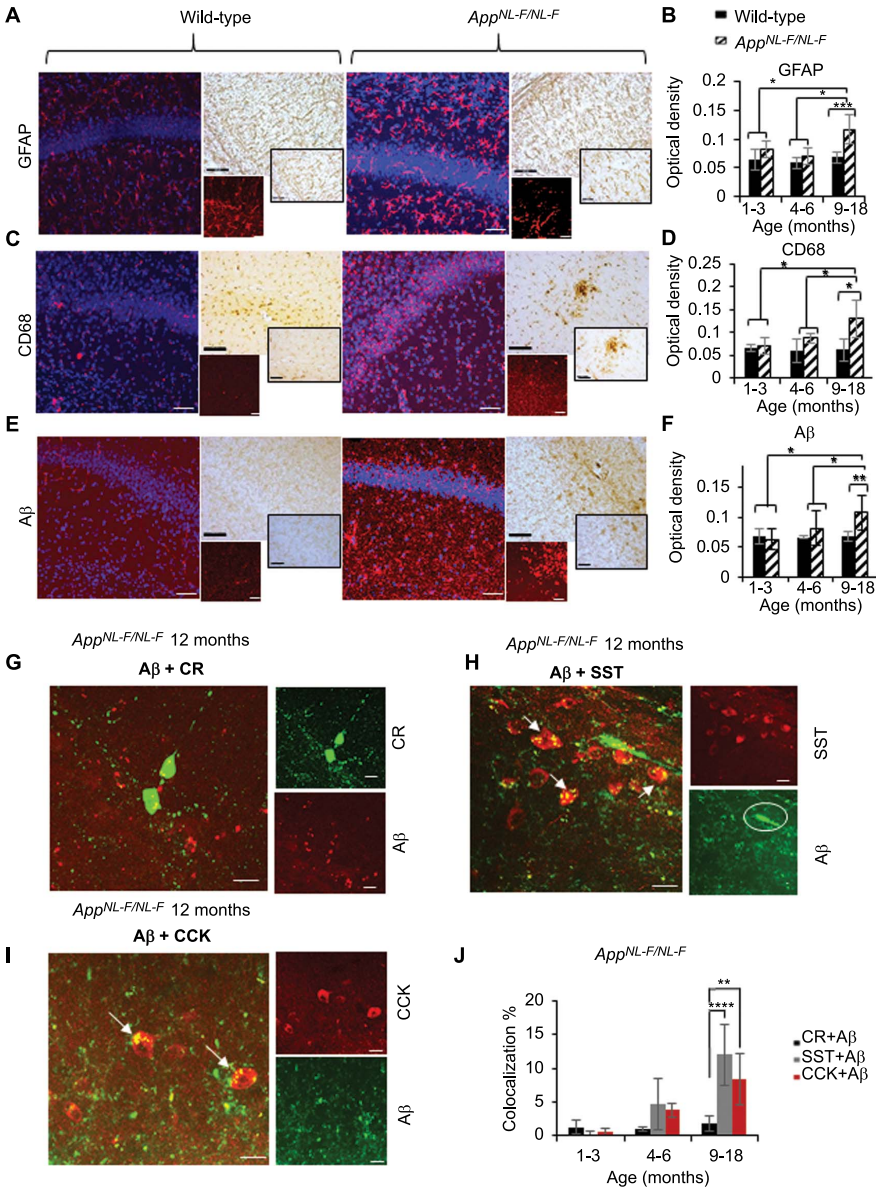

Figure 1. Age-dependent phenotypical changes in the $App^{NL\text{-}F/NL\text{-}F}$ model of AD. (*A*,*C*,*E*) Z-stack images from confocal microscopy illustrating the expression of GFAP (for reactive astrocytes), CD68 (for microglia), and Aβ (all in red, secondary antibody Texas Red) together with DAPI staining for nuclei (in blue) in 12-month age-matched wild-type and $App^{NL\text{-}F/NL\text{-}F}$ mice, respectively. Similarly, bright-field images of tissue immunostained with biotinylated antibodies show conglomerates of GFAP, CD68, and Aβ in the same animals. Both immunofluorescence and immunoperoxidase-stained images taken at ×20 magnification (larger images, scale bar = 50 µm) and ×63 magnification (inserts, scale bar = 20 µm). (*B*,*D*,*F*) Analysis of GFAP, CD68, and Aβ from immunoperoxidase-stained tissue. Significant differences in the three markers of AD were seen between wild-type and $App^{NL\text{-}F/NL\text{-}F}$ mice only at 9–18 months and when comparing quantification at 9–18 months with the other two age cohorts. (*G*,*I*) Age-dependent accumulation of Aβ in selective subtypes of interneurons in hippocampal CA1. Aβ colocalization was found at significantly higher levels in SST and CCK cells (indicated by arrows), but not in calretinin (CR) cells in the same animals at 12 months (scale = 20 µm). (*J*) Quantification of colocalization of Aβ with either CCK, SST, or calretinin cells. A two-way ANOVA was performed with pairwise comparisons corrected for multiple comparisons ($\alpha = 0.05$), with either post hoc Sidak's test or Tukey's test for multiple comparisons. $^{*}P < 0.05$, $^{**}P < 0.01$, $^{***}P < 0.001$.

Aβ Accumulated in Specific Cell Types

To investigate whether Aβ selectively accumulated in specific cell populations, we used confocal microscopy to analyze the colocalization of Aβ with the somatic expression of either: CR-, SST-, or CCK-labeled cells in the $App^{NL\text{-}F/NL\text{-}F}$ mice. Interestingly, CR cells showed no significant colocalization with Aβ (in older animals, 1.4 ± 0.9% compared with wild-type mice, $P > 0.5$, $n = 6$ animals per group, two-way ANOVA) (Fig. 1G,J). In contrast, in the same AD mice, there was an age-dependent increase in the colocalization of Aβ levels with SST- and CCK-expressing cells in the $App^{NL\text{-}F/NL\text{-}F}$ mouse model (colocalization of SST with Aβ was 13 ± 4.0%, and CCK with Aβ was 9 ± 3.7%) (Fig. 1H–J), which were significantly different when compared with CR cell colocalization with SST/Aβ and CCK/Aβ at 9–18 months ($P < 0.0001$ for SST and $P < 0.01$ for CCK, $n = 8$ animals for both SST and CCK, two-way ANOVA), suggesting that CCK and SST cells are readily penetrated by Aβ.

CCK- and SST-Expressing Interneurons Show an Age-Dependent Decline in AD, While CR Cells Remain Resilient

To determine whether general GABAergic inhibition was aberrant in the $App^{NL\text{-}F/NL\text{-}F}$ mouse model, we performed immunofluorescence studies to colocalize CCK-, SST-, and CR-expressing cells with glutamic acid decarboxylase 67 (GAD67), an enzyme for inhibitory neurotransmitter GABA production, which exists in every terminal where GABA locates and can be a reliable marker for functional GABAergic interneurons. Confocal Z-stack images showed a general age-dependent decline of GAD67 (Fig. 2E), which was significantly decreased in the oldest cohort of $App^{NL\text{-}F/NL\text{-}F}$ mice studied (1–3 months, 7.73% ± 1.20%, $P > 0.05$, $n = 5$, and at 9–18 months, 36.09% ± 2.07, $P < 0.01$, $n = 5$, two-way ANOVA). This suggests that GABAergic cells maintained their function in the early stages of the disease, but this altered as the pathology of the disease progressed, which is consistent with previous studies using alternative AD mouse models (Krantic et al. 2012; Choi et al. 2018; Leung et al. 2012). We then measured the expression of CCK, SST, and CR colocalization with GAD67 (Figs 2 and 3) from Z-stack images obtained using confocal microscopy. All somata labeled with respective neuropeptide (CCK, SST) or calcium-binding protein (CR) always colocalized GAD67, although there was a cell-type specific alteration in the expression with age in the AD model compared with the age-matched wild-type mice. For example, a significant decline in the expression of the CCK/GAD67-labeled cells was observed, as well as a decrease in CCK cells from 4 months onwards in the $App^{NL\text{-}F/NL\text{-}F}$ mice and a decrease of 24.31 ± 1.39 ($P < 0.05$, $n = 4$, two-way ANOVA) at 4–6 months and 35.91 ± 3.10% ($P < 0.01$, $n = 7$, t-test) at 9–18 months (Fig. 2F). Similarly, SST/GAD67 cells also significantly decreased in an age-dependent manner in the $App^{NL\text{-}F/NL\text{-}F}$ mouse model, and there was a reduction of 15.44 ± 2.94 ($P > 0.05$, $n = 4$, two-way ANOVA) and a significant reduction of 32.02 ± 2.65% ($P < 0.01$, $n = 8$ for wild-type, $n = 5$ $App^{NL\text{-}F/NL\text{-}F}$, two-way ANOVA) at 4–6 months and 9–18 months, respectively, in the $App^{NL\text{-}F/NL\text{-}F}$ mice age-matched to control wild-type mice (Fig. 2G). In contrast to the SST-expressing and CCK-expressing interneurons, in the $App^{NL\text{-}F/NL\text{-}F}$ mouse model, we discovered a preservation of the CR-expressing interneurons colocalized with GAD67 in all the age-matched wild-type and $App^{NL\text{-}F/NL\text{-}F}$ animals studied (Fig. 3A,B).

The changes in the cell densities were also corroborated by immune peroxidase staining, which showed a similar alteration in the densities of CCK- and SST-expressing cells in CA1 of $App^{NL\text{-}F/NL\text{-}F}$ mice age-matched to wild-type mice (Fig 4A–D), while no significant differences in the CR cell density between $App^{NL\text{-}F/NL\text{-}F}$ mice and age-matched to wild-type control were seen at any of the age cohorts (Fig. 4E,F). A nonsignificant increase of 2–3% was observed in the AD model age-matched to the wild-type mice ($P > 0.5$, $n = 9$, two-way ANOVA).

Membrane Properties of CCK and SST Interneurons Are Hyperactive While CR Cells Are Preserved in Early Stages of AD

To identify contributing factors to the loss of cell densities, we investigated the cell membrane properties of CCK, SST, and CR cells at between 1.5 and 2 months of age in both genotypes to detect possible differences preceding the classical hallmarks of AD such as Aβ accumulation and neuroinflammation. Due to the lack of identifiable CCK and SST somata under infrared-differential interference contrast (IR-DIC) in the late stages of AD (9–18 months), it was not possible in our hands to record CCK and SST cells in the older cohorts.

Recorded cells were initially identified by their somata location in CA1 and electrophysiological properties, followed by their gross morphology (post recording). Morphologically, CCK cells had triangular somata located in the stratum radiatum (SR) with dendrites predominantly radiating in SR. The axons of these cells ramified in SR with a few branches extending into the stratum pyramidale (SP) (see Ali 2007). However, the SST cell somata located in the stratum oriens (SO) had horizontally oriented dendrites restricted to SO, and the axons of these cells projected and ramified extensively in the stratum lacunosum moleculare (SLM). Furthermore, SST cells displayed a characteristic "sag" in the electronic response to hyperpolarizing current (Fig. 5C) characterization of I_h current activation in the cells (see also Ali et al. 1998).

Interestingly, the membrane properties of CCK interneurons were consistently found to be intrinsically hyperactive (Fig. 5A,B; see Table 2 for details). Similarly, SST cell membrane properties were also hyperexcited (Fig. 5C,D), which was consistent with previous studies (Zhang et al. 2016). The membrane hyperexcitability was indicated by their decreased firing threshold which was accompanied by an increased membrane input resistance, time constant, and action potential firing frequency in $App^{NL\text{-}F/NL\text{-}F}$ mice compared with the age-matched control wild-type mice with the same magnitude of current injection at the same membrane potential (Fig. 5B,D and Table 2).

In contrast to intrinsic hyperactivity observed in CCK and SST cells, the intrinsic membrane properties of CR cells were found to be unchanged at a younger age range (1.5–2 months) (Fig. 5E,F) between wild-type age-matched to $App^{NL\text{-}F/NL\text{-}F}$ mice. Furthermore, the CR cells recorded at the later stage of 9–18 months also remained unchanged between the two genotypes (Table 2). The membrane properties of CR cells—input resistance, time constants, and action potential firing properties—remained unchanged during the disease progression (Fig. 5F). Morphologically, the recorded CR cells were similar in appearance (Fig. 6A,B), and in our data sets all had oval somata located in mid SR with two to three primary dendrites that radiated into SR and never entered SP. The axons of CR cells were sparse and ramified close to the somata in SR; these cells resembled previously published CR cells (see Gulyas et al. 1996).

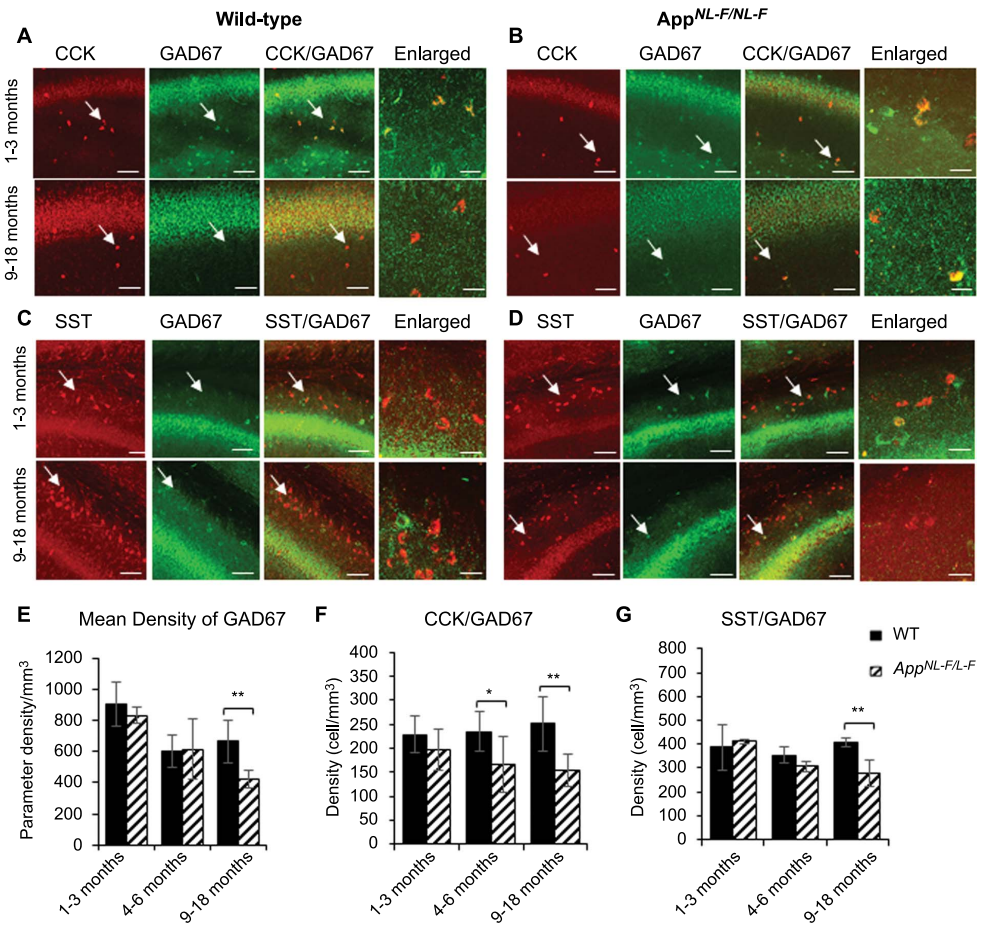

Figure 2. CCK- and SST-expressing interneurons show an age-dependent loss in the $App^{NL\text{-}F/NL\text{-}F}$ AD model. (*A–D*) Confocal microscope Z-stack images showing the expression of CCK- and SST-expressing cells (both in red channel), colocalized with GAD67, the marker for GABA production (green channel) in 1–3- and 9–18-month-old wild-type age-matched $App^{NL\text{-}F/NL\text{-}F}$ mice in CA1. Images taken at ×20 magnification (scale bar = 50 µm) and ×63 magnification (enlarged images, scale bar = 20 µm). In aged $App^{NL\text{-}F/NL\text{-}F}$ mice, CCK- and SST-positive cells were found to be weakly colocalized with GAD67 compared with the 1–3-month-old $App^{NL\text{-}F/NL\text{-}F}$ mice. (*E–G*) The graphs represent mean density of GAD67-, CCK-, and SST-positive cells in wild-type age-matched $App^{NL\text{-}F/NL\text{-}F}$ measured at three ages: 1–3 months, 4–6 months, and 9–18 months. Overall, GAD67, CCK, and SST expression showed an age-dependent decline in the AD model, which was significantly different from their control wild-type counterparts at 9–18 months. However, CCK cells also showed a significant decline in $App^{NL\text{-}F/NL\text{-}F}$ mice 4–6. A two-way ANOVA was performed with pairwise comparisons corrected for multiple comparisons ($\alpha = 0.05$), with a post hoc Tukey's test for multiple comparisons. $^{*}P < 0.05$, $^{**}P < 0.001$.

CR Interneurons Displayed Strengthened Synaptic Inhibition in AD

Spontaneous inhibitory postsynaptic potentials (sIPSPs) and spontaneous excitatory postsynaptic potentials (sEPSPs) were recorded from CR interneurons in 1–3- and 9–18-month old $App^{NL\text{-}F/NL\text{-}F}$ mice at holding membrane potentials of −55 and −75 mV (Fig. 6C–F); however, no differences were observed in the synaptic properties received by CR cells at the two age cohorts studied in either genotypes. Since our aim was to investigate whether CR cells were functionally "preserved" during the presence of significant Aβ accumulation and proliferation of glial cells and astrocytes, we have presented the data sets obtained "post phenotypic changes" of AD (9–18 months), which revealed interesting properties compared with the age-matched wild-type CR cells recorded.

The average peak frequency and amplitude of sIPSPs increased in the AD model compared with wild-type age-matched mice at both membrane potentials, but were only significantly different at a more positive membrane potential of −55 mV (due to the higher imposed driving force for Cl^{-} ions to enter $GABA_A$ receptors in our experimental condition). In the $App^{NL\text{-}F/NL\text{-}F}$ mice, sIPSP frequency and amplitude increased by 153 ± 53% ($P < 0.01$, $n = 6$, two-way ANOVA) and 157 ± 65%

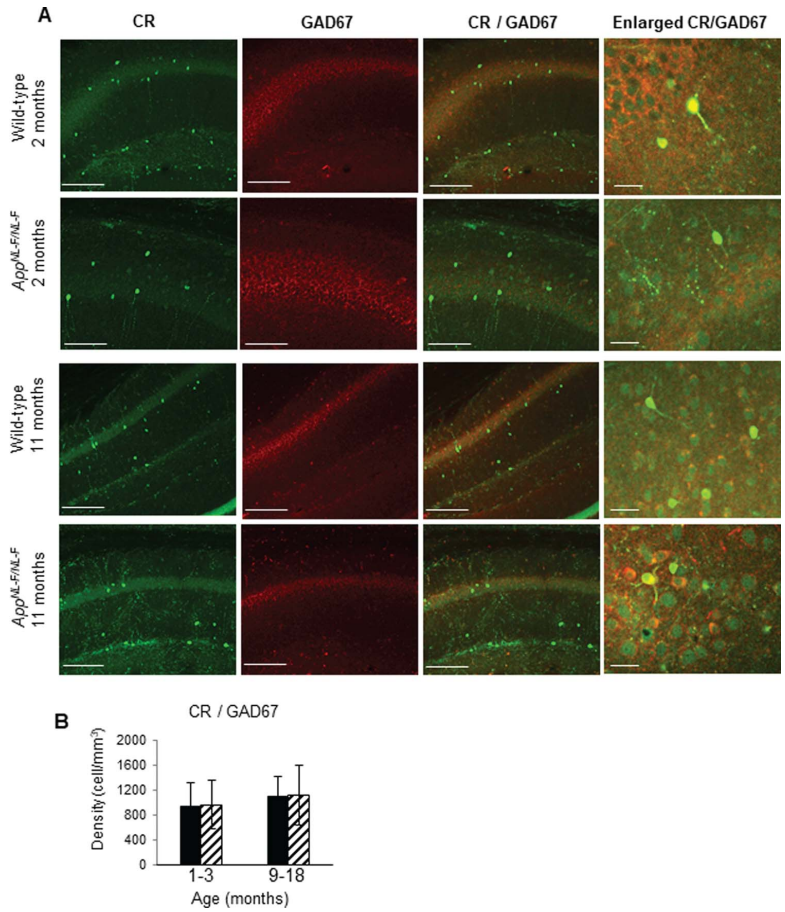

Figure 3. Calretinin (CR)-expressing interneurons are functionally and anatomically preserved in the CA1 in $App^{NL\text{-}F/NL\text{-}F}$ mice. (*A*) Z-stack confocal microscope images taken at ×20 magnification show calretinin (green, secondary antibody Alexa 488) and GAD67 (red, secondary antibody Texas Red), colocalized (yellow) in 2- and 12-month-old wild-type and $App^{NL\text{-}F/NL\text{-}F}$ mice. The nonsignificant change in the colocalization of GAD67- with CR-labeled cells between the two genotypes during the disease progression suggests that the integrity and function of the CR interneurons are preserved after postphenotypical alterations of the disease (scale bar = 50 µm). The enlarged images present wild-type and $App^{NL\text{-}F/NL\text{-}F}$ tissue imaged at ×63 magnification (scale bar = 20 µm). (*B*) Analysis of confocal images shows that the number of CR cells remains unchanged between wild-type and $App^{NL\text{-}F/NL\text{-}F}$ mice, in both young and old animals in CA1, CA2, and CA3 in the hippocampus. However, the amount of GAD67 appears to be increased significantly when colocalized with CR cells in 1–3-month-old $App^{NL\text{-}F/NL\text{-}F}$ mice when compared with age-matched wild-type mice. A two-way ANOVA ($\alpha = 0.05$) was performed with pairwise comparisons corrected for multiple comparisons with Sidak's test.

($P < 0.01$, $n = 6$, two-way ANOVA) of control sIPSPs recorded in age-matched wild-type mice, respectively (Fig. 6E). The average sEPSP frequency also changed significantly, showing a decrease at both membrane potentials, −55 and −75 mV, but without a significant change in the amplitudes (Fig. 6F). The increase in sEPSP frequency was 144 ± 35% ($P < 0.01$, $n = 6$, two-way ANOVA) and 87 ± 19% ($P > 0.05$, $n = 6$, two-way ANOVA), of control wild-type sEPSPs recorded at −55 and −75 mV, respectively.

CR interneurons during the late stages (9–18 months) of AD were readily identifiable under IR-DIC during experiments, which was in striking contrast to CCK or SST cells that were not easily visualized. These differences could be due to the decline of CCK and SST cells in the late stages of the disease; this together with the technical difficulties of performing whole-cell recordings in aged mice hampered recording of CCK and SST cells in these animals to directly compare the synaptic inputs of CCK and SST cells after postphenotypical alterations of AD.

P2Y1Rs Are Expressed Predominantly in Calretinin Cells

Previously, it has been shown that P2Y1Rs are expressed on CR cells (Bowser and Khakh 2004), and others have also evidenced that these receptors are "upregulated" in proinflammatory reactive astrocytes in AD, which facilitates the synchrony of aberrant astrocyte behavior (Delekate et al. 2014). Whether

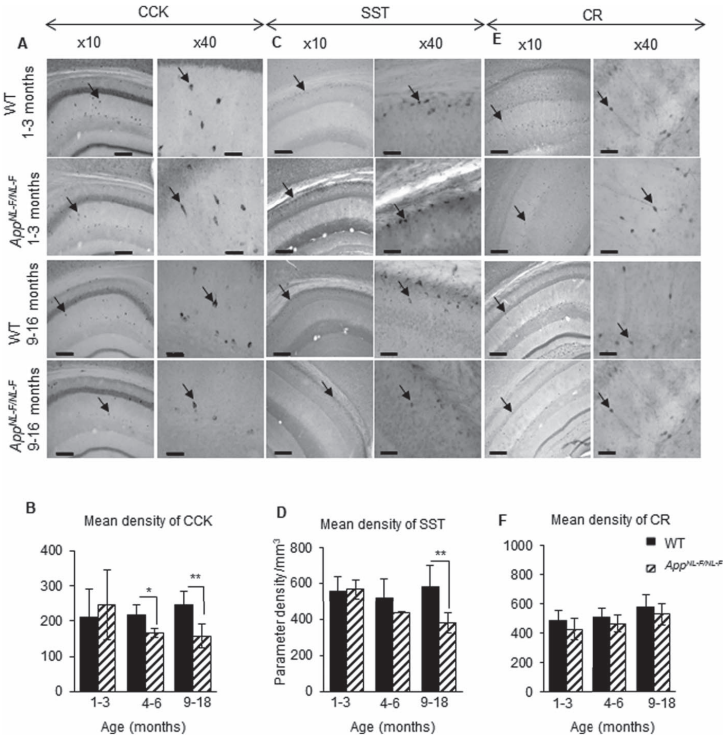

Figure 4. Cell-type–specific survival of CA1 interneurons in the $App^{NL\text{-}F/NL\text{-}F}$ AD model. (*A–C*) Immunoperoxidase staining showing CCK, SST, and CR interneurons, respectively, at ×10 and ×40 magnification in age-matched wild-type and $App^{NL\text{-}F/NL\text{-}F}$ animals (arrows indicate example interneurons). Scale bar, 100 µm for ×10 images and 50 µm for ×40. (*D–F*) Graphs illustrate a significant decrease in SST cells in the 9–18-month-old $App^{NL\text{-}F/NL\text{-}F}$ animals compared with the age-matched wild-type cohort. There was also a significant decrease in CCK cells at 4–6-month-old and 9–18-month-old $App^{NL\text{-}F/NL\text{-}F}$ animals compared with age-matched wild-type animals. In contrast, CR cell densities were not significantly different between the ages and genotypes studied. A two-way ANOVA ($\alpha = 0.05$) was performed with pairwise comparisons corrected for multiple comparisons with Sidak's test. $^{*}P < 0.05$, $^{**}P < 0.01$.

Table 2 Electrophysiological properties of CCK, SST, and CR interneurons recorded from wild-type age-matched to $App^{NL\text{-}F/NL\text{-}F}$ mice in the CA1 region of the hippocampus

Subclass of cells	**CCK** ($n = 20$ cells, 6 animals per genotype)		SST ($n = 10$ cells, 5 animals per genotype)		CR cells ($n = 14$ cells, 8 animals per genotype)		CR cells ($n = 12$ cells, 8 animals per genotype)	
	Wild-type	$App^{NL\text{-}F/NL\text{-}F}$	Wild-type	$App^{NL\text{-}F/NL\text{-}F}$	Wild-type	$App^{NL\text{-}F/NL\text{-}F}$	Wild-type	$App^{NL\text{-}F/NL\text{-}F}$
AP Amp (mV)	78 ± 2.50	68 ± 2.00	82 ± 3.00	70 ± 5.40	78 ± 1.50	78 ± 2.00	76 ± 1.50	78 ± 2.00
AP HW (ms)	1.3 ± 0.43	1.5 ± 0.320	1.2 ± 0.25	1.5 ± 0.50	1.25 ± 0.32	1.3 ± 0.22	1.25 ± 0.32	1.3 ± 0.22
AP threshold (mV)	22 ± 1.56	17.5 ± 1.30*	20 ± 1.50	14.5 ± 1.32*	22 ± 1.43	22 ± 1.47	22 ± 1.43	22 ± 1.47
AP AHP Amp (mV)	6.5 ± 0.75	4.37 ± 0.90	8.7 ± 0.63	5.50 ± 0.74	9.4 ± 0.65	9.56 ± 0.67	9.4 ± 0.65	9.56 ± 0.67
Input resistance (MΩ)	295 ± 14.52	350.45 ± 18.10**	300.54 ± 25.0	365.53 ± 30.56**	290 ± 23.00	291 ± 36.64	290 ± 23.00	291 ± 36.64
TC (ms)	12.0 ± 2.00	15.70 ± 0.62*	10.52 ± 1.42	16.47 ± 0.95**	10.50 ± 0.50	10.32 ± 0.50	10.50 ± 0.50	10.32 ± 0.50
No. of spikes at +150 pA	11 ± 1.30	21 ± 0.37****	10.75 ± 2.98	21.75 ± 2.21****	10.75 ± 0.95	11 ± 0.81	11.20 ± 0.85	10.95 ± 0.94
	1.5–2 months		1.5–2 months		1.5–2 months		9–18 months	

Results are expressed as mean ± SD. A two-sampled unpaired Student's *t*-test was used to compare between control wild-type and $App^{NL\text{-}F/NL\text{-}F}$ mice for each biophysical property per cell type. AP, action potential; Amp, amplitude; HW, half-width; AHP, after hyperpolarization; TC, time constant. Significantly different from control, unpaired *t*-test, $^{*}P < 0.05$, $^{**}P < 0.01$, $^{****}P < 0.0001$.

similar mechanisms exist among the CR cell networks that promote hyperinhibition in AD is unknown, and therefore, we investigated the level of expression colocalization of P2Y1Rs on CR cells and compared the level of P2Y1R colocalization to either GFAP (for reactive astrocytes) or CaMKII-α (for pyramidal cells) from the oldest cohort (after phenotypic changes of the disease), 9–18-month-old $App^{NL\text{-}F/NL\text{-}F}$ and wild-type mice (Fig. 7A–C). We investigated the colocalization of P2Y1Rs which was estimated

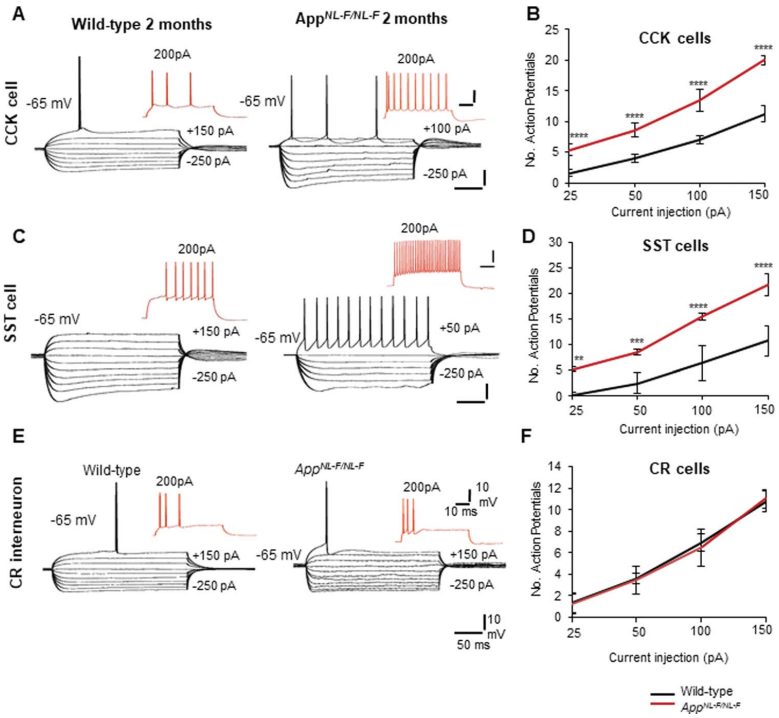

Figure 5. CCK and SST cells displayed hyperactive membrane properties, but CR cells remained unchanged in early AD. (*A*,*C*) Intrinsic membrane response of CA1 CCK interneurons and SST interneurons recorded using whole-cell patch clamp electrodes in wild-type and $App^{NL\text{-}F/NL\text{-}F}$ mice at 2 months of age. Both CCK and SST cells displayed hyperexcitable membranes at −65 mV in response to intracellular current injections (ranging from +200 to −200 pA). Red traces are the voltage response of the cells to +200 pA current injection. (*B*,*D*) Graphs illustrate the number of action potentials discharged with increasing current applied to CCK and SST cells recorded in wild-type and $App^{NL\text{-}F/NL\text{-}F}$ mice. The firing of both interneurons was dramatically increased with increasing current injections in the AD model, which was also accompanied by an increase in input resistance and time-constant illustrating hyperexcitability in the AD model. (*E*) Intrinsic membrane response of CA1 CR interneurons recorded in 2-month wild-type and $App^{NL\text{-}F/NL\text{-}F}$ mice, respectively. These showed passive responses to intracellular current injections (+200 to −200 pA) which culminated in single- or double-action potentials with current injection of +150 pA (black traces). Red traces are the voltage response of the cells to +200-pA current injection. There were no significant differences in the action potential discharge, input resistance, and time constants between the two age-matched mouse cohorts. (*F*) The input–output curves displayed a pseudolinear relationship between number of action potentials generated by adapting CR cells of healthy wild-type and $App^{NL\text{-}F/NL\text{-}F}$ mice with increasing current injections. The membrane input resistance, action potential threshold, and time constants did not appear to be different between the two genotypes studied. A two-way ANOVA was performed with genotype and treatment as factors ($\alpha = 0.05$), with a post hoc Sidak's test for multiple comparisons. $^{*}P < 0.05$, $^{**}P < 0.01$, $^{***}P < 0.001$, $^{****}P < 0.0001$.

using the correlation coefficient *R* to assess the level of correlation between the fluorophore channels that correspond to either CR, GFAP, or CaMKII-α (see Methods).

We found a high level of colocalization of P2Y1Rs in CR cells compared with astrocytes and pyramidal cells in 9–18-months age-matched wild-type and $App^{NL\text{-}F/NL\text{-}F}$ mice (Fig. 7D–F). In wild-type mice, a 13- and 23-fold increase in P2Y1 receptor colocalization in CR cells was observed compared with P2Y1 colocalization in GFAP and CaMKII-α-labeled cells, respectively ($P < 0.05$, $n = 4$ animals for CR cells, and $n = 6$ animals for GFAP and CaMKII-α labeled cells). In $App^{NL\text{-}F/NL\text{-}F}$ mice, there was an 8- and 16-fold increase in the colocalization of the P2Y1 receptor on CR cells compared with P2Y1 receptor colocalization in GFAP and CaMKII-α-labeled cells, respectively ($P < 0.05$, $n = 6$ animals). Furthermore, there was an upregulation of P2Y1R expression in the AD model, which was correlated with a higher colocalization in CR cells, astrocytes, and pyramidal cells of $App^{NL\text{-}F/NL\text{-}F}$ mice compared with the age-matched wild type. For example, there was a significant increase in the receptor coexpressed with CR cells in the $App^{NL\text{-}F/NL\text{-}F}$ mice compared with the age-matched wild-type CR cells ($28.37 \pm 0.41\%$ of control wild-type, $P < 0.001$, $n = 40$ cells, $n = 4$ animals per group). In the $App^{NL\text{-}F/NL\text{-}F}$ mice, there was also an increase in the expression of P2Y1Rs with GFAP by $102.61 \pm 113.35\%$ of control ($P < 0.05$, $n = 240$ cells, $n = 6$ animals per group) and CaMKII-α by $77.6 \pm 55.90\%$ of control wild type ($P > 0.05$, $n = 60$ cells, $n = 6$ animals per group).

P2Y1 Receptor Allosteric Inhibitor Restores Dysfunctional Inhibitory Homeostasis in CA1

Our data suggests an overall increase in the level of P2Y1R expression in the AD model; therefore, we investigated whether blocking P2Y1Rs *in vitro* could "normalize" the hyperinhibition observed in CR cells. Using $App^{NL\text{-}F/NL\text{-}F}$ knock-in mice and

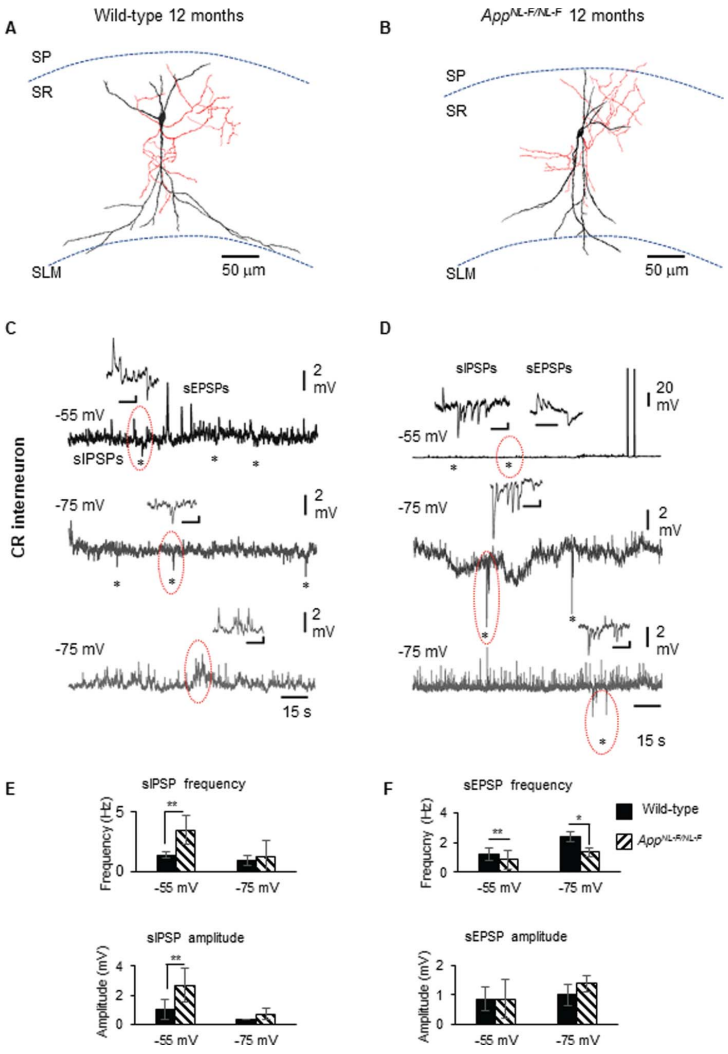

Figure 6. Calretinin cells in early AD form an enhanced inhibitory network. (*A*,*B*) Reconstruction of recorded, biocytin-labeled CR cells from wild-type mouse and $App^{NL\text{-}F/NL\text{-}F}$ mouse model, drawn at ×1000 magnification using a light microscope and drawing tube. The dendrites (black) and axon (red) were located in SR. The morphology of CR cells in both genotypes was similar in appearance. (*C*,*D*) Whole-cell current-clamp recordings of spontaneous inhibitory/excitatory postsynaptic potentials (sIPSPs and sEPSPs) recorded in CR cells in CA1 of 12-month-old $App^{NL\text{-}F/NL\text{-}F}$ mice, at membrane potentials of −55 and −75 mV in control conditions (morphology shown above). The circles indicate where synaptic events have been enlarged and shown in the inserts. (*E*,*F*) Bar graphs show the average sIPSP and sEPSP amplitude and frequency at −55 and − 75 mV in CR cells recorded in wild-type and $App^{NL\text{-}F/NL\text{-}F}$ mouse models. These data suggest a significantly enhanced frequency and amplitude of inhibition at −55 mV, while sEPSP frequency (and not amplitude) was found significantly different at both −55 and − 75 mV recorded in CR cells at 9–18 months of age in $App^{NL\text{-}F/NL\text{-}F}$ mice. A two-way ANOVA was performed with pairwise comparisons corrected for multiple comparisons ($\alpha = 0.05$), with a post hoc Tukey's test for multiple comparisons. $^{*}P < 0.05$, $^{**}P < 0.01$, $^{***}P < 0.001$, $^{****}P < 0.0001$.

age- and sex-matched wild-type controls, we bath-applied the P2Y1 receptor agonist, MRS2365 (500 nM), followed by subsequent addition of the P2Y1R allosteric inhibitor, BPTU (500 nM). Since we previously reported that principal pyramidal cells were aberrantly hyperexcited following hypoinhibition input (Petrache et al. 2019), it was of interest to also investigate the changes in synaptic activity recorded in pyramidal cells after bath application of the P2Y1R modulators.

In both wild-type and $App^{NL\text{-}F/NL\text{-}F}$ mice, bath application of MRS2365 resulted in an enhanced aberrant hyperactivity in both CR and pyramidal cells recorded at −55 mV by causing an increase in action potential discharge, an increase in sEPSP

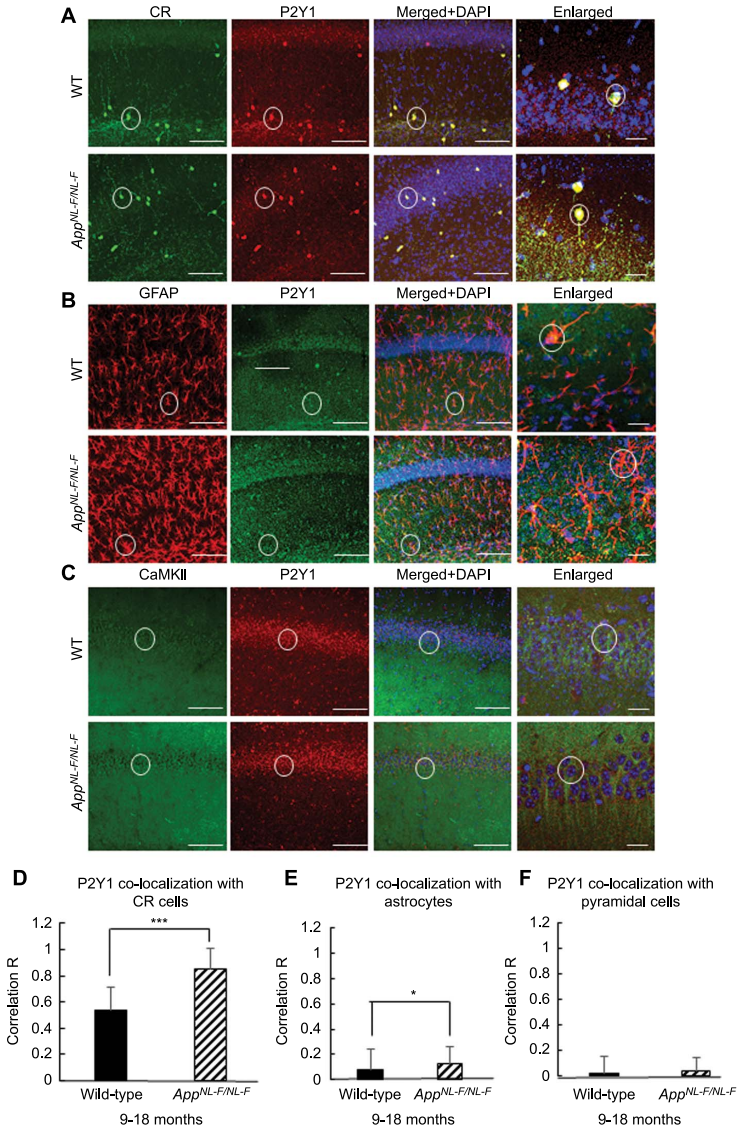

Figure 7. P2Y1Rs are predominantly expressed on CR cells and are upregulated in the $App^{NL\text{-}F/NL\text{-}F}$ AD mouse model. (*A–C*) Confocal microscope, Z-stack images of P2Y1R colocalization on CR cells (green, Alexa 488), astrocytes stained for GFAP (red, Texas Red), and pyramidal cells stained for CaMKII-α (green, FITC), respectively in 9–18-month-old wild-type and $App^{NL\text{-}F/NL\text{-}F}$ mice (taken at ×63 magnification, scale bar, 20 µm). Representative cells are outlined with white circles, and colocalization between the two channels appears yellow/orange. The merged images include the nuclear staining, DAPI (blue). (*D–F*) Graphs illustrate quantification of P2Y1Rs colocalized on CR cells, GFAP, and CaMKII-α in wild-type and $App^{NL\text{-}F/NL\text{-}F}$ mice obtained from Z-stack images at ×20 magnification. The CR cells and astrocytes show a high level of coexpression with P2Y1Rs; however, the CR cells showed the highest level of P2Y1R coexpression, which seems to be upregulated in the AD model. Error bars represent the standard deviation from the mean. Two-tailed unpaired Student's *t*-test was performed individually for panels (*D–F*) to compare wild-type and $App^{NL\text{-}F/NL\text{-}F}$ mice within their respective groups. To measure across the three cell groups studied, a one-way ANOVA was performed with pairwise comparisons corrected for multiple comparisons ($\alpha = 0.05$), with a post hoc Tukey's test for multiple comparisons. $^{*}P < 0.05$, $^{**}P < 0.01$, $^{***}P < 0.001$ (40–240 cells, $n = 4$ animals for CR cells and $n = 6$ animals for GFAP and CaMKII-α).

Table 3 P2Y1 receptor pharmacology in CR and pyramidal cells in 9–18-month wild-type and $App^{NL\text{-}F/NL\text{-}F}$ mice

	Calretinin cells		Pyramidal cells	
Genotype	MRS2365 (% change from control)	BPTU (% change from MRS2365)	MRS2365 (% change from control)	BPTU (% change from MRS2365)
sEPSP frequency				
Wild-type	↑131.72 ± 77.80 ($n = 5$)	↓ 69.64 ± 20.89 ($n = 5$)	↑ 110.38 ± 4.45 ($n = 6$)**	↓ 61.14 ± 47.93 ($n = 6$)***
$APP^{NL\text{-}F/NL\text{-}F}$	↑ 44.07 ± 10.24 ($n = 6$)***	↓ 64.31 ± 23.90 ($n = 6$)***	↑ 32.57 ± 0.44 ($n = 5$)*	↓ 53.45 ± 2.80 ($n = 5$)****
sEPSP amplitude				
Wild-type	↑ 53.91 ± 23.39 ($n = 5$)	↓ 56.44 ± 8.49 ($n = 5$)*	↑ 121.51 ± 39.96 ($n = 6$) **	↓ 42.72 ± 18.52 ($n = 6$)**
$APP^{NL\text{-}F/NL\text{-}F}$	↑ 62.16 ± 26.42 ($n = 5$)	↓ 65.42 ± 25.21 ($n = 5$)**	↑ 59.48 ± 19.03 ($n = 5$)****	↓ 53.51 ± 19.12 ($n = 5$)****
sIPSP frequency				
Wild-type	↑ 80.98 ± 30.46 ($n = 6$)**	↓ 52.54 ± 15.01 ($n = 6$)***	↑ 13.93 ± 2.10 ($n = 6$)	↑ 176.26 ± 91.11 ($n = 6$)***
$APP^{NL\text{-}F/NL\text{-}F}$	↑ 16.64 ± 4.95 ($n = 7$)*	↓ 59.37 ± 17.47 ($n = 7$)****	↓ 40.25 ± 20.24 ($n = 5$)	↑ 465.96 ± 143.54 ($n = 5$)**
sIPSP amplitude				
Wild-type	↑ 132.29 ± 50.57 ($n = 6$)*	↓ 60.0 ± 29.07 ($n = 6$)**	↑ 121.51 ± 39.96 ($n = 6$) #8	↑ 42.72 ± 18.52 ($n = 6$)***
$APP^{NL\text{-}F/NL\text{-}F}$	↑ 45.98 ± 10.21 ($n = 7$)*	↓ 64.76 ± 17.90 ($n = 7$)***	↑ 59.48 ± 19.03 ($n = 5$)	↑ 53.51 ± 19.12 ($n = 5$)**

Changes of spontaneous synaptic events recorded in CR and pyramidal cells after bath application of the P2Y1R agonist, MRS2365, followed by antagonist, BPTU, in 9–18 months of age-matched, wild-type, and $APP^{NL\text{-}F/NL\text{-}F}$ mice. Values represent % changes between conditions (MRS2365 application after control or BPTU after subsequent addition of MRS2365 to control) ± standard deviation. A one-way ANOVA followed by post hoc Tukey's test for multiple comparisons was used to determine the statistical value. Sample size n denotes the number of animals (one cell per animal was recorded in these experiments). Arrows indicate either a decrease or increase in the parameter. MRS2365, P2Y1 agonist; BPTU, P2Y1 allosteric antagonist. * $P < 0.05$, ** $P < 0.01$, *** $P < 0.001$, **** $P < 0.0001$.

amplitude and frequency (see Table 3 for details) (Fig. 8), and an average ~8-mV depolarization of the cell membrane. Subsequent addition of the inhibitor BPTU "decreased" the hyperinhibition observed in CR cells by decreasing the MRS2365-induced firing but also significantly reducing the sIPSP amplitudes and frequency in CR cells (Table 3 and Fig. 8A,B,E). However, the aberrant hyperexcitability of principal pyramidal cells was differentially affected in comparison with CR interneurons following application of P2Y1R inhibitor BPTU. Upon subsequent bath application of BPTU, there was an increase in the sIPSP amplitude and frequency (Table 3) (Fig. 8C–E), with an ~10-mV tonic hyperpolarization of pyramidal cell membranes. Thus, BPTU produced a normalization of the aberrant hyperinhibition at CR cells and consequently the aberrant hypoinhibition at pyramidal cells in the AD model.

Discussion

Using the first knock-in mouse model of AD ($App^{NL\text{-}F/NL\text{-}F}$) (Saito et al. 2014), we showed an age-dependent increase in the pathological hallmarks of AD, including Aβ and microglial and reactive astrocytes, and several novel observations in the CA1 region of the hippocampus, which are illustrated in the schematic circuit diagram in Figure 9. Firstly, we report a cell-type–specific alteration of modulatory interneuron function and association with Aβ oligomers. There was a gradual decline in the expression of CCK- and SST-expressing inhibitory interneurons together with the coexpression of GAD67, suggesting a reduction in their inhibitory function. The decrease in SST expression is consistent with the results that SST expression decreases in the cortex and hippocampus in AD patients (Liguzlecznar et al. 2016), as was the age-dependent decline in GAD67 (Krantic et al. 2012; Choi et al. 2018; Leung et al. 2012). The CCK and SST cells also colocalized a significant amount of Aβ fragments, and their biophysical properties showed aberrant hyperexcitability in the early stages of AD. In striking contrast, the density of CR cells and coexpression of GAD67 were unchanged in our AD model, consistent with anatomical studies reporting a resilience of CR cells in postmortem brains of AD patients (Fonseca and Soriano 1995). Furthermore, we demonstrate that the CR cells did not colocalize Aβ fragments and maintained their intrinsic biophysical properties, showing a surprising resilience to alteration during the pathobiology of AD in the $App^{NL\text{-}F/NL\text{-}F}$ model.

Our second key finding is related to alteration in inhibitory synaptic activity. We observed an enhanced frequency and amplitude of spontaneous synaptic inhibition among the CR cells proceeding the pathological hallmarks of AD, which suggests changes in pre- and postsynaptic factors during the pathogenesis of the disease. This enhanced inhibitory activity in CR cells in the AD model was despite a hyperexcited state of excitatory pyramidal cells. Others have also shown in a transgenic *App* mouse model of AD that pathological seizure-like activity in the cortex and hippocampus is accompanied by enhanced "compensatory" inhibitory activity (Palop et al. 2007). We demonstrate that CR cells together with astrocytes express a high level of P2Y1Rs in comparison to principal pyramidal cells in CA1, although we do not exclude the possibility that P2Y1R expression is changed in other cell types. Finally, we show that blockade of P2Y1Rs via allosteric inhibition restored inhibition to "normal" at CR interneurons and, as a consequence, corrected also the hyperexcitability of pyramidal cells to normal synaptic levels.

Selective Association of Aβ in CA1 Interneurons

The selective colocalization of Aβ peptides is correlated with the intrinsic hyperactivity of CCK and SST cells reported in our study in the early-stage, preplaque formation of AD, but in the presence of a low level of soluble Aβ peptides, probably with high Aβ 42/40 ratio. This is consistent with other studies (Shah et al. 2018; Palop and Mucke 2016a). Whether the hyperexcitability of CCK and SST cells results in Aβ production or whether Aβ infiltration in the cells results in the hyperexcited state is yet to be fully explored. Interestingly, both SST peptide and APP undergo similar cleavage processes to form SST and Aβ, which could facilitate interactions between the two even before their release from cells (LaFerla et al. 2007), which has led to the SST

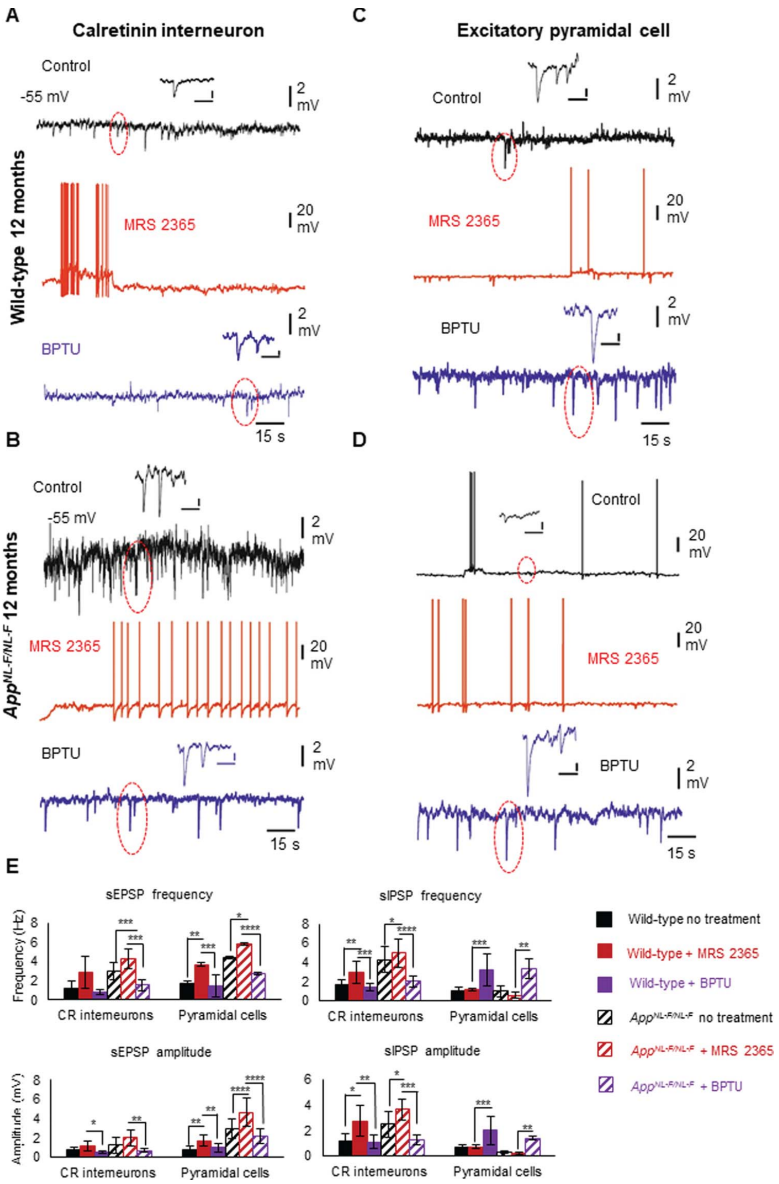

Figure 8. Enhanced inhibition among CR interneuron networks in AD is modulated by upregulated P2Y1Rs. (*A–D*) Whole-cell current-clamp recordings illustrating sIPSPs and sEPSPs in CR cells (*A*, *B*) and pyramidal cells (*C*, *D*) in CA1 of 12-month-old wild-type and $App^{NL\text{-}F/NL\text{-}F}$ mice, recorded at a membrane potential of −55 mV in control conditions and after bath application of the P2Y1R modulators. Bath application of the P2Y1R-selective agonist, MRS2365 (500 nM), resulted in membrane excitation in both cell types, increasing the aberrant hyperexcitability. However, subsequent addition of the P2Y1R inhibitor BPTU (500 nM) differentially affected the cell types; the sIPSPs (examples are highlighted in circles) were dampened in CR cells, but increased in pyramidal cells, thus normalizing the homeostatic levels of inhibition in CA1. Similar results were obtained from wild-type mice shown in bar graphs. (*E*) Bar graphs show the overall pharmacological data obtained from wild-type and $App^{NL\text{-}F/NL\text{-}F}$ mice at 9–18 months. A two-way ANOVA was performed with pairwise comparisons corrected for multiple comparisons ($\alpha = 0.05$), with a post hoc Tukey's test for multiple comparisons. *$P < 0.05$, **$P < 0.01$, ***$P < 0.001$, ****$P < 0.0001$. (see Table 3 for details).

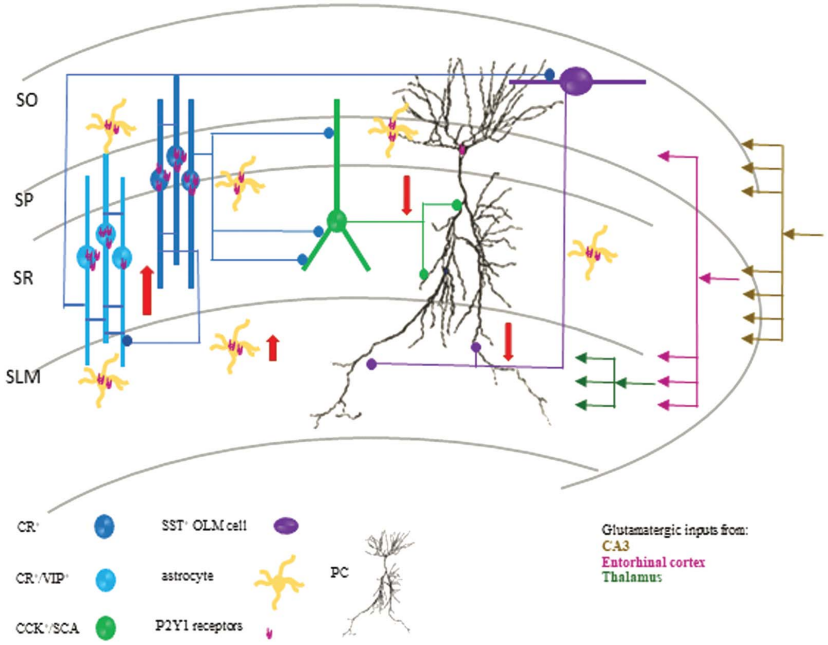

Figure 9. Schematic diagram of a CA1 circuit involving the major modulatory interneuron circuits and excitatory pyramidal cells in late AD. Red arrows depict the increase in CR cell inhibitory function and a decrease in CCK- and SST-expressing interneuron function in CA1. It has been evidenced that CCK cells fine-tune proximal pyramidal cells, while SST-expressing cells fine-tune distal dendrites of pyramidal cells; therefore, loss of their function from ~6 months will impact on CA1 pyramidal cell excitability and promote pyramidal cell hyperexcitability (due to hypoinhibition). We suggest that the early hyperactivity of CCK and SST cells facilitates increased Aβ cleavage and accumulation that subsequently leads to their destruction. These factors, in addition to the overactivity among CR cells in the later stages of the disease, leads to deficits in pyramidal cell inhibition. Furthermore, we suggest that the enhanced hyperinhibition observed in CR cells is partly due to hypertrophy of astrocytes and upregulated P2Y1Rs predominantly coexpressed on CR cells and astrocytes, which is restored by blocking upregulated P2Y1Rs.

neuropeptide being termed "amyloidogenic." Consistent with the aforementioned findings, SST has also been shown to be one of the neuropeptides that bind to Aβ fragments in vitro, enabling their oligomerization to amyloidogenic peptide (Solarski et al. 2018), and SST cells in the piriform cortex and olfactory cortex are found highly colocalized with Aβ (Saiz-Sanchez et al. 2015). Furthermore, SST is thought to regulate Aβ degradation by modulating neprilysin which is an essential protein for degrading Aβ (Saito et al. 2005). Perhaps it is these common cleavage mechanisms in combination with toxic soluble Aβ infiltration that makes SST interneurons vulnerable to Aβ infiltration that triggers the aggregation and degradation of Aβ resulting in the high-level intracellular Aβ in SST. This probably destroys the normal function of SST cells and results in cell death. Whether similar mechanisms exist for CCK cells that also colocalized high Aβ needs investigation; however, it is possible that APP and Aβ are part of a feedback loop that controls the intrinsic neuronal excitability (Kamenetz et al. 2003) which we observe in both SST and CCK cells.

The selective protection from Aβ penetration could also be related to the neurochemical and pharmacological profile of the cell type since, in our study, CR cells were preserved anatomically and physiologically. Calretinin is a calcium-binding protein parvalbumin (PV), and cells expressing this protein are also reported to be either preserved, increased, or decreased, depending on the cortical region reported in various models of AD from early to late stages of the disease (Yang et al. 2018; Zallo et al. 2018; Petrache et al. 2019) which could be associated with calcium homeostasis. In normal conditions, Ca^{2+} is able to regulate the cellular membrane properties via voltage-gated Ca^{2+} channels and maintains homeostasis with other ions (Berridge et al. 1998). However, cellular membranes in AD can be altered by Aβ, which causes increasing Ca^{2+} influx and Ca^{2+}-mediated excitotoxicity (Bezprozvanny and Mattson 2008). Studies have reported that interneurons with calcium-binding proteins such as calretinin might overcome the excitotoxicity induced by increasing intracellular Ca^{2+} concentration (Mikkonen et al. 1999), whereas interneurons without calcium-binding proteins but expressing neurotransmitters like CCK and SST are more likely to degenerate in AD (Saiz-Sanchez et al. 2015).

The Triggers for Alteration in Intrinsic and Synaptic Homeostasis During the Pathogenesis of AD

A question that remains to be addressed is why there is a persistent intrinsic hyperexcitability of specific populations of neurons such as CCK and SST cells in early AD. This could be due to specific mutations in intrinsic voltage-gated ion channels resulting in the observed hyperexcitability, for example, background "leak" potassium channels; however, we suggest

that there are multiple factors involved, including alterations in the pre- and postsynaptic synaptic release machinery and the upregulated activity of P2Y1Rs on CR cells and astrocytes leading to disrupted network behavior.

Evidence from various in vitro and in vivo studies has shown that the production and secretion of Aβ into the extracellular space are regulated by presynaptic neuronal factors such as activity-dependent presynaptic firing rates, which has been hypothesized to enhance the neurotransmitter release as a result of prolonged synaptic vesicle docking to the presynaptic membrane caused by Aβ interaction with various synaptic proteins (Russell et al. 2012; Marsh and Alifragis 2018). Furthermore, endosomal proteolytic cleavage of APP and Aβ release at synaptic terminals is thought to affect neurotransmitter recycling via interference with clathrin-dependent endocytosis (Kamenetz et al. 2003; Cirrito et al. 2005; Marsh and Alifragis 2018). Blocking such neuronal activity has been shown to oppose the Aβ toxicity effect (Kamenetz et al. 2003; Palop and Mucke 2010). According to this hypothesis, these mechanisms enhance neurotransmitter release. In particular, evidence for this comes from studies focusing on glutamatergic synapses, where the enhanced extracellular Aβ was shown to increase spontaneous excitatory postsynaptic events and facilitate presynaptic glutamatergic release in neurons with low activity but not in neurons with high activity (Abramov et al. 2009). This pathologically elevated Aβ has been shown to prevent glutamate reuptake at synapses, resulting in increased levels of glutamate in the synaptic cleft (Li et al. 2009). This would have various impacts leading to postsynaptic glutamate receptor desensitization as well as affecting neighboring synapses and the neuronal support systems such as astroglia.

Physiological Consequences of Alteration in Synaptic Excitatory–Inhibitory Homeostasis

Figure 9 illustrates our findings on and the proposed outcome of CA1 interneurons in late AD. We suggest that hyperexcited presynaptic glutamatergic networks from other cortical regions such as the entorhinal cortex, shown to be in an excitatory overdrive (Petrache et al. 2019), activate CA1 interneurons rendering them hyperexcited. With this assumption, an enhanced firing of CCK and SST cells in our model will ultimately enhance the release of neurotransmitter GABA, and since CCK and SST cells are specialized to fine-tune and provide dendritic inhibition to CA1 pyramidal cells, perhaps this overdrive of inhibitory function in early stages of AD is a protective mechanism, preventing CA1 pyramidal cell hyperexcitability that is shown to develop at midstages of the disease (Petrache et al. 2019), developing at ~6 months and correlating with a decline in CCK and SST cell function probably due to exocytotic death.

The changes in these networks perhaps contributes as a "compensatory" mechanism to enhance CR interneuron function that we observe, since these cells in the rodent are located in all layers of the hippocampus. Two populations of CR cells have been suggested to exist in CA1: CR cells that contact CCK interneurons and CR cells colocalized with a neuropeptide, vasoactive intestinal peptide (VIP), which prefer to make synaptic contact with SST-expressing cells (Katona et al. 1999) but, overall, form synapses exclusively with dendrites of other interneurons, such as CCK and SST cells (Cauli et al. 2014, Tyan et al. 2014, Chamberland and Topolnik 2012), as well as electrically with each other via gap junctions (Gulyas et al. 1996). Thus, any alterations in the CCK and SST networks in later stages of AD will severely impact CA1 disinhibition, since electrical coupling mediated by gap junctions is thought to play a role in the generation of highly synchronized electrical activity (Traub et al. 2001a, Traub et al. 2001b). However, we suggest that the enhanced function of CR cells is *more* than a compensatory mechanism, but which is due to neuron–astrocyte interaction via enhanced P2Y1R activity, particularly in the later stages of AD. Interestingly, we observed an unexpected voltage-dependent increase in sIPSP frequency in the AD model, which could be explained by the altered presynaptic release machinery during the pathogenesis of AD, the presence of extracellular Aβ accumulation, and/or the involvement of a third party such as the proliferated reactive astrocytes.

It has been well documented that astrocyte hyperactivity is prominent around Aβ plaques and produces synchronous hyperactivity in $[Ca^{2+}]_i$ transients across long distances that is uncoupled from neuronal activity (Kuchibhotla et al. 2009; Delekate et al. 2014). The nucleotides ATP and ADP released during proinflammatory responses potentiate the activity of reactive astrocytes in the APPPS1 AD mouse model, which has been suggested to be predominantly mediated by P2Y1Rs, which when activated cause an enhancement in spontaneous astrocyte calcium events (Delekate et al. 2014; Reichenbach et al. 2018). Blockade of these metabotropic P2Y1Rs on astrocytes after chronic treatment with an antagonist of P2Y1Rs normalizes the aberrant hyperactivity of reactive astrocytes and reduces neuronal hyperactivity and improves performance in the spatial memory test (Reichenbach et al. 2018). Others have also evidenced that reactive astrocytes either aberrantly produce the inhibitory gliotransmitter GABA (Jo et al. 2014) or release ATP regulating the excitability of CCK interneurons through P2Y1 receptor activation (Tan et al. 2017). It is conceivable that both of these mechanisms could also increase CR cell hyperinhibition in our system, which is yet to be determined.

Therefore, it is conceivable that the enhanced network activity of reactive astrocytes that proliferate in the later stages of AD is a result of "spillover" of glutamate from neighboring excitatory cells leading to an intracellular rise in calcium levels in astroglia leading to further release of glutamate promoting CR cell excitability, which was demonstrated previously in pyramidal neurons (Fellin et al. 2004, Jourdain et al. 2007).

Perhaps this cascade of events in addition to the upregulated P2Y1Rs results in enhanced activity of CR cells, which was normalized by blocking P2Y1Rs. In addition, the aberrant hyperexcitability of principal pyramidal cells was differentially affected, restoring the aberrant hyperexcitability of pyramidal cells and restoring the inhibition observed in control wild-type mice.

Interestingly, others have shown in healthy rodent brain that the activation of P2Y1Rs did not change the membrane effects in principal cells, in contrast to what we report here. Perhaps this difference could be due to the pathogenesis of AD. Furthermore, previous studies also report that the activation of P2Y1Rs on some interneurons causes a nonselective cationic current through the activation of transient receptor potential channels and the suppression of a resulting K^+ conductance, resulting in membrane depolarization of these interneurons (by ~10 mV). As a result, the interneurons are thought to increase their firing frequency giving rise to an increased inhibition onto principal cells (Bowser and Khakh 2004; Kawamura et al. 2004). Therefore, we suggest that blocking of P2Y1Rs on CR cells "normalizes" the aberrant excitatory–inhibitory imbalance in AD through the blockade of CR network–associated excess of disinhibition. As a

result, this allows other interneurons that were "supressed" by the CR network, such as CCK cells, to perform their intended function of directly inhibiting principal cells (Ali 2007), thus relieving the overexcitation of principal cells.

In summary, our data provides further evidence that AD pathogenesis involves complex synaptic mechanisms that lead to neurodegeneration rather than simple synaptic loss. This study demonstrates that Aβ affects excitatory and inhibitory synapses differentially but also the astrocytes and their receptors, which leads to complex synaptic imbalances in circuit and network activity. The paradoxical overexcitation observed over various cortical regions in a time-dependent fashion in AD (Petrache et al. 2019) may be related to changes in neuronal structures and their junctions of communication as suggested previously (Palop et al., 2006), but to date, the precise neuronal elements and their cellular mechanisms need to be further investigated. We show for the first time a cell-type–specific neuronal destruction and Aβ penetration and that interneuron-specific networks play an important role in altering the synaptic homeostasis of inhibition in CA1 through upregulated P2Y1Rs, and we suggest that hippocampal network dysfunction is more than a compensatory response, but due to underlying mechanistic interactions between Aβ and alterations of the expression of inhibitory neuropeptides and receptors, we propose that these data have important implications for future drug development of novel targeted therapy for AD.

Funding

Wellcome Trust (United Kingdom); Medical Research Council (United Kingdom) New Investigators award (GO501263 to A.B.A); Medical Research Council PhD studentship (MR/N013867/1).

Notes

The authors would like to thank Dr Andrew Constanti (UCL School of Pharmacy, United Kingdom) for his invaluable comments in the preparation of this manuscript. We would like to thank Profs Takashi Saito and Takaomi C. Saido, RIKEN Center for Brain Science, Japan, for the *App*$^{NL\text{-}F/NL\text{-}F}$ mouse model of AD. *Conflict of Interest*: None declared.

Author Contributions

Anqi Shi: Performed the neuroanatomical studies, confocal microscope imaging, and data analysis of cholecystokinin and somatostatin cells and contributed in preparing the article. Alexandra Petrache: Performed the neuroanatomical studies, confocal microscope imaging, and data analysis of calretinin cells and contributed in preparing the article. Jiachen Shi: Performed with the confocal analysis of P2Y1 receptor colocalization and contributed in preparing the article. Afia B. Ali: Designed and coordinated the project, performed all electrophysiological whole-cell recordings, performed and supervised neuroanatomical studies, performed the data analysis, and prepared the article.

References

Abramov E, Dolev I, Fogel H, Ciccotosto GD, Ruff E, Slutsky I. 2009. Amyloid-beta as a positive endogenous regulator of release probability at hippocampal synapses. *Nat Neurosci*. 12:1567–1576.

Ali AB. 2007. Presynaptic inhibition of GABAA receptor-mediated unitary IPSPs by cannabinoid receptors at synapses between CCK-positive interneurons in rat hippocampus. *J Neurophysiol*. 98:861–869.

Ali AB, Deuchars J, Pawelzik H, Thomson AM. 1998. CA1 pyramidal to basket and bistratified cell EPSPs: dual intracellular recordings in rat hippocampal slices. *J Physiol*. 507 (Pt 1:201–217.

Berridge MJ, Bootman MD, Lipp P. 1998. Calcium-a life and death signal. *Nature*. 395:645.

Bezprozvanny I, Mattson MP. 2008. Neuronal calcium mishandling and the pathogenesis of Alzheimer's disease. *Trends in neurosciences*. 31:454–463.

Bowser DN, Khakh BS. 2004. ATP excites interneurons and astrocytes to increase synaptic inhibition in neuronal networks. *J Neurosci*. 24:8606–8620.

Busche MA, Eichhoff G, Adelsberger H, Abramowski D, Wiederhold KH, Haass C, Staufenbiel M, Konnerth A, Garaschuk O. 2008. Clusters of hyperactive neurons near amyloid plaques in a mouse model of Alzheimer's disease. *Science*. 321:1686–1689.

Cauli B, Zhou X, Tricoire L, Toussay X, Staiger JF. 2014. Revisiting enigmatic cortical calretinin-expressing interneurons. *Front Neuroanat*. 8:52.

Chamberland S, Topolnik L. 2012. Inhibitory control of hippocampal inhibitory neurons. *Front Neurosci*. 6:165.

Choi S, Won JS, Carroll SL, Annamalai B, Singh I, Singh AK. 2018. Pathology of nNOS-expressing GABAergic neurons in mouse model of Alzheimer's disease. *Neuroscience*. .

Cirrito JR, Yamada KA, Finn MB, Sloviter RS, Bales KR, May PC, Schoepp DD, Paul SM, Mennerick S, Holtzman DM. 2005. Synaptic activity regulates interstitial fluid amyloid-beta levels in vivo. *Neuron*. 48:913–922.

Delekate A, Fuchtemeier M, Schumacher T, Ulbrich C, Foddis M, Petzold GC. 2014. Metabotropic P2Y1 receptor signalling mediates astrocytic hyperactivity in vivo in an Alzheimer's disease mouse model. *Nat Commun*. 5:5422.

Fellin T, Pascual O, Gobbo S, Pozzan T, Haydon PG, Carmignoto G. 2004. Neuronal synchrony mediated by astrocytic glutamate through activation of extrasynaptic NMDA receptors. *Neuron*. 43:729–743.

Fonseca M, Soriano E. 1995. Calretinin-immunoreactive neurons in the normal human temporal cortex and in Alzheimer's disease. *Brain Res*. 691:83–91.

Gulyas AI, Hajos N, Freund TF. 1996. Interneurons containing calretinin are specialized to control other interneurons in the rat hippocampus. *J Neurosci*. 16:3397–3411.

Heneka MT, Carson MJ, El Khoury J, Landreth GE, Brosseron F, Feinstein DL, Jacobs AH, Wyss-Coray T, Vitorica J, Ransohoff RM *et al*. 2015. Neuroinflammation in Alzheimer's disease. *Lancet Neurol*. 14:388–405.

Holtzman DM, Morris JC, Goate AM. 2011. Alzheimer's disease: the challenge of the second century. *Sci Transl Med*. 3:77sr1.

Howell O, Atack JR, Dewar D, McKernan RM, Sur C. 2000. Density and pharmacology of alpha5 subunit-containing GABA(A) receptors are preserved in hippocampus of Alzheimer's disease patients. *Neuroscience*. 98:669–675.

Jo S, Yarishkin O, Hwang YJ, Chun YE, Park M, Woo DH, Bae JY, Kim T, Lee J, Chun H *et al*. 2014. GABA from reactive astrocytes impairs memory in mouse models of Alzheimer's disease. *Nat Med*. 20:886–896.

Jourdain P, Bergersen LH, Bhaukaurally K, Bezzi P, Santello M, Domercq M, Matute C, Tonello F, Gundersen V, Volterra A.

2007. Glutamate exocytosis from astrocytes controls synaptic strength. *Nat Neurosci*. 10:331–339.

Kamenetz F, Tomita T, Hsieh H, Seabrook G, Borchelt D, Iwatsubo T, Sisodia S, Malinow R. 2003. APP processing and synaptic function. *Neuron*. 37:925–937.

Katona I, Acsady L, Freund TF. 1999. Postsynaptic targets of somatostatin-immunoreactive interneurons in the rat hippocampus. *Neuroscience*. 88:37–55.

Kawamura M, Gachet C, Inoue K, Kato F. 2004. Direct excitation of inhibitory interneurons by extracellular ATP mediated by P2Y1 receptors in the hippocampal slice. *J Neurosci*. 24:10835–10845.

Khan AA, Shekh-Ahmad T, Khalil A, Walker MC, Ali AB. 2018. Cannabidiol exerts antiepileptic effects by restoring hippocampal interneuron functions in a temporal lobe epilepsy model. *Br J Pharmacol*. .

Khan UA, Liu L, Provenzano FA, Berman DE, Profaci CP, Sloan R, Mayeux R, Duff KE, Small SA. 2014. Molecular drivers and cortical spread of lateral entorhinal cortex dysfunction in preclinical Alzheimer's disease. *Nat Neurosci*. 17:304–311.

Klausberger T, Somogyi P. 2008. Neuronal diversity and temporal dynamics: the unity of hippocampal circuit operations. *Science*. 321:53–57.

Krantic S, Isorce N, Mechawar N, Davoli MA, Vignault E, Albuquerque M, Chabot JG, Moyse E, Chauvin JP, Aubert I. 2012. Hippocampal GABAergic neurons are susceptible to amyloid-β toxicity in vitro and are decreased in number in the Alzheimer's disease TgCRND8 mouse model. *Journal of Alzheimers Disease Jad*. 29:293.

Kuchibhotla KV, Lattarulo CR, Hyman BT, Bacskai BJ. 2009. Synchronous hyperactivity and intercellular calcium waves in astrocytes in Alzheimer mice. *Science*. 323:1211–1215.

LaFerla FM, Green KN, Oddo S. 2007. Intracellular amyloid-beta in Alzheimer's disease. *Nat Rev Neurosci*. 8:499–509.

Leung L, Andrews-Zwilling Y, Yoon SY, Jain S, Ring K, Dai J, Wang MM, Tong L, Walker D, Huang Y. 2012. Apolipoprotein E4 causes age- and sex-dependent impairments of Hilar GABAergic interneurons and learning and memory deficits in mice. *Plos One*. 7: e53569.

Li S, Hong S, Shepardson NE, Walsh DM, Shankar GM, Selkoe D. 2009. Soluble oligomers of amyloid beta protein facilitate hippocampal long-term depression by disrupting neuronal glutamate uptake. *Neuron*. 62:788–801.

Liguzlecznar M, Urbanciecko J, Kossut M. 2016. Somatostatin and somatostatin-containing neurons in shaping neuronal activity and plasticity. *Frontiers in Neural Circuits*. 10.

Marsh J, Alifragis P. 2018. Synaptic dysfunction in Alzheimer's disease: the effects of amyloid beta on synaptic vesicle dynamics as a novel target for therapeutic intervention. *Neural Regen Res*. 13:616–623.

McGrath JC, Drummond GB, McLachlan EM, Kilkenny C, Wainwright CL. 2010. Guidelines for reporting experiments involving animals: the ARRIVE guidelines. *Br J Pharmacol*. 160:1573–1576.

Mikkonen M, Alafuzoff I, Tapiola T, Soininen H, Miettinen R. 1999. Subfield-and layer-specific changes in parvalbumin, calretinin and calbindin-D28K immunoreactivity in the entorhinal cortex in Alzheimer's disease. *Neuroscience*. 92:515–532.

Palop JJ, Chin J, Mucke L. 2006. A network dysfunction perspective on neurodegenerative diseases. *Nature* 443(7113): 768–773.

Palop JJ, Chin J, Roberson ED, Wang J, Thwin MT, Bien-Ly N, Yoo J, Ho KO, Yu GQ, Kreitzer A *et al*. 2007. Aberrant excitatory neuronal activity and compensatory remodeling of inhibitory hippocampal circuits in mouse models of Alzheimer's disease. *Neuron*. 55:697–711.

Palop JJ, Mucke L. 2010. Amyloid-beta-induced neuronal dysfunction in Alzheimer's disease: from synapses toward neural networks. *Nat Neurosci*. 13:812–818.

Palop JJ, Mucke L. 2016a. Network abnormalities and interneuron dysfunction in Alzheimer disease. *Nature Reviews Neuroscience*. 17:777.

Palop JJ, Mucke L. 2016b. Network abnormalities and interneuron dysfunction in Alzheimer disease. *Nat Rev Neurosci*. 17:777–792.

Petrache AL, Rajulawalla A, Shi A, Wetzel A, Saito T, Saido TC, Harvey K, Ali AB. 2019. Aberrant excitatory-inhibitory synaptic mechanisms in Entorhinal cortex microcircuits during the pathogenesis of Alzheimer's disease. *Cereb Cortex*. 29:1834–1850.

Putcha D, Brickhouse M, O'Keefe K, Sullivan C, Rentz D, Marshall G, Dickerson B, Sperling R. 2011. Hippocampal Hyperactivation associated with cortical thinning in Alzheimer's disease signature regions in non-demented elderly adults. *Journal of Neuroscience*. 31:17680–17688.

Reichenbach N, Delekate A, Breithausen B, Keppler K, Poll S, Schulte T, Peter J, Plescher M, Hansen JN, Blank N *et al*. 2018. P2Y1 receptor blockade normalizes network dysfunction and cognition in an Alzheimer's disease model. *J Exp Med*. 215:1649–1663.

Rissman RA, De Blas AL, Armstrong DM. 2007. GABA(A) receptors in aging and Alzheimer's disease. *J Neurochem*. 103: 1285–1292.

Russell CL, Semerdjieva S, Empson RM, Austen BM, Beesley PW, Alifragis P. 2012. Amyloid-beta acts as a regulator of neurotransmitter release disrupting the interaction between synaptophysin and VAMP2. *PLoS One*. 7: e43201.

Saito T, Iwata N, Tsubuki S, Takaki Y, Takano J, Huang SM, Suemoto T, Higuchi M, Saido TC. 2005. Somatostatin regulates brain amyloid beta peptide Abeta42 through modulation of proteolytic degradation. *Nat Med*. 11:434–439.

Saito T, Matsuba Y, Mihira N, Takano J, Nilsson P, Itohara S, Iwata N, Saido TC. 2014. Single App knock-in mouse models of Alzheimer's disease. *Nat Neurosci*. 17:661–663.

Saiz-Sanchez D, Rosa-Prieto CDL, Ubeda-Banon I, Martinez-Marcos A. 2015. Interneurons, tau and amyloid-β in the piriform cortex in Alzheimer's disease. *Brain Structure & Function*. 220:2011.

Shah D, Latif-Hernandez A, De SB, Saito T, Saido T, Verhoye M, D'Hooge R, dLA V. 2018. Spatial reversal learning defect coincides with hypersynchronous telencephalic BOLD functional connectivity in APP NL-F/NL-F knock-in mice. *Sci Rep*. 8.

Solarski M, Wang H, Wille H, Schmitt-Ulms G. 2018. Somatostatin in Alzheimer's disease: a new role for an old player. *Prion*. 12:1–8.

Tan Z, Liu Y, Xi W, Lou HF, Zhu L, Guo Z, Mei L, Duan S. 2017. Glia-derived ATP inversely regulates excitability of pyramidal and CCK-positive neurons. *Nat Commun*. 8:13772.

Traub RD, Kopell N, Bibbig A, Buhl EH, LeBeau FE, Whittington MA. 2001a. Gap junctions between interneuron dendrites can enhance synchrony of gamma oscillations in distributed networks. *J Neurosci*. 21:9478–9486.

Traub RD, Whittington MA, Buhl EH, LeBeau FE, Bibbig A, Boyd S, Cross H, Baldeweg T. 2001b. A possible role for

gap junctions in generation of very fast EEG oscillations preceding the onset of, and perhaps initiating, seizures. *Epilepsia*. 42:153–170.

Tyan L, Chamberland S, Magnin E, Camire O, Francavilla R, David LS, Deisseroth K, Topolnik L. 2014. Dendritic inhibition provided by interneuron-specific cells controls the firing rate and timing of the hippocampal feedback inhibitory circuitry. *J Neurosci*. 34:4534–4547.

Wu JW, Hussaini SA, Bastille IM, Rodriguez GA, Mrejeru A, Rilett K, Sanders DW, Cook C, Fu H, Boonen RA *et al*. 2016. Neuronal activity enhances tau propagation and tau pathology in vivo. *Nat Neurosci*. 19:1085–1092.

Yamada K, Holth JK, Liao F, Stewart FR, Mahan TE, Jiang H, Cirrito JR, Patel TK, Hochgrafe K, Mandelkow EM *et al*. 2014. Neuronal activity regulates extracellular tau in vivo. *J Exp Med*. 211:387–393.

Yamamoto K, Tanei ZI, Hashimoto T, Wakabayashi T, Okuno H, Naka Y, Yizhar O, Fenno LE, Fukayama M, Bito H *et al*. 2015. Chronic optogenetic activation augments abeta pathology in a mouse model of Alzheimer disease. *Cell Rep*. 11:859–865.

Yang X, Yao C, Tian T, Li X, Yan H, Wu J, Li H, Pei L, Liu D, Tian Q *et al*. 2018. A novel mechanism of memory loss in Alzheimer's disease mice via the degeneration of entorhinal-CA1 synapses. *Mol Psychiatry*. 23:199–210.

Zallo F, Gardenal E, Verkhratsky A, Rodriguez JJ. 2018. Loss of calretinin and parvalbumin positive interneurones in the hippocampal CA1 of aged Alzheimer's disease mice. *Neurosci Lett*. 681:19–25.

Zhang W, Zhang L, Liang B, Schroeder D, Zhang ZW, Cox GA, Li Y, Lin DT. 2016. Hyperactive somatostatin interneurons contribute to excitotoxicity in neurodegenerative disorders. *Nat Neurosci*. 19:557–559.

frontiers in Cellular Neuroscience

ORIGINAL RESEARCH
published: 11 November 2020
doi: 10.3389/fncel.2020.568194

Selective Modulation of α5 $GABA_A$ Receptors Exacerbates Aberrant Inhibition at Key Hippocampal Neuronal Circuits in *APP* Mouse Model of Alzheimer's Disease

*Alexandra L. Petrache†, Archie A. Khan†, Martin W. Nicholson, Alessandra Monaco, Martyna Kuta-Siejkowska, Shozeb Haider, Stephen Hilton, Jasmina N. Jovanovic and Afia B. Ali**

UCL School of Pharmacy, London, United Kingdom

OPEN ACCESS

Edited by:
Sathyanarayanan Puthanveettil, The Scripps Research Institute, United States

Reviewed by:
Tija Carey Jacob, University of Pittsburgh, United States
Marianna Crispino, University of Naples Federico II, Italy
Manish Sharma, The Scripps Research Institute, United States

***Correspondence:**
Afia B. Ali
afia.b.ali@ucl.ac.uk

†These authors have contributed equally to this work

Specialty section:
This article was submitted to Cellular Neuropathology, a section of the journal Frontiers in Cellular Neuroscience

Received: *31 May 2020*
Accepted: *28 September 2020*
Published: *11 November 2020*

Citation:
Petrache AL, Khan AA, Nicholson MW, Monaco A, Kuta-Siejkowska M, Haider S, Hilton S, Jovanovic JN and Ali AB (2020) Selective Modulation of α5 $GABA_A$ Receptors Exacerbates Aberrant Inhibition at Key Hippocampal Neuronal Circuits in APP Mouse Model of Alzheimer's Disease. Front. Cell. Neurosci. 14:568194. doi: 10.3389/fncel.2020.568194

Selective negative allosteric modulators (NAMs), targeting α5 subunit-containing $GABA_A$ receptors ($GABA_A$Rs) as potential therapeutic targets for disorders associated with cognitive deficits, including Alzheimer's disease (AD), continually fail clinical trials. We investigated whether this was due to the change in the expression of α5 $GABA_A$Rs, consequently altering synaptic function during AD pathogenesis. Using medicinal chemistry and computational modeling, we developed aqueous soluble hybrids of 6,6-dimethyl-3-(2-hydroxyethyl) thio-1-(thiazol-2-yl)-6,7-dihydro-2-benzothiophene-4(5H)-one, that demonstrated selective binding and high negative allosteric modulation, specifically for the α5 $GABA_A$R subtypes in constructed HEK293 stable cell-lines. Using a knock-in mouse model of AD ($APP^{NL-F/NL-F}$), which expresses a mutant form of human amyloid-β (Aβ), we performed immunofluorescence studies combined with electrophysiological whole-cell recordings to investigate the effects of our key molecule, α5-SOP002 in the hippocampal CA1 region. In aged $APP^{NL-F/NL-F}$ mice, selective preservation of α5 $GABA_A$Rs was observed in, calretinin- (CR), cholecystokinin- (CCK), somatostatin- (SST) expressing interneurons, and pyramidal cells. Previously, we reported that CR dis-inhibitory interneurons, specialized in regulating other interneurons displayed abnormally high levels of synaptic inhibition in the $APP^{NL-F/NL-F}$ mouse model, here we show that this excessive inhibition was "normalized" to control values with bath-applied α5-SOP002 (1 μM). However, α5-SOP002, further *impaired* inhibition onto CCK and pyramidal cells that were already largely compromised by exhibiting a *deficit* of inhibition in the AD model. In summary, using a multi-disciplinary approach, we show

Abbreviations: ACSF, Artificial cerebrospinal fluid; AD, Alzheimer's disease; CCK, Cholecystokinin; CR, Calretinin; DAB, 3–3-diaminobenzidine; DMSO, Dimethyl sulfoxide; GABA, γ-Aminobutyric acid; IPSP, Inhibitory postsynaptic potential; PB, Phosphate buffer; PBS, Phosphate-buffered saline; PFA, Paraformaldehyde; NAM, Negative allosteric modulator; RT, 10–90% rise time; SCA, Schaffer collateral-associated; SR, Stratum Radiatum; sEPSP, Spontaneous excitatory postsynaptic potential; sIPSP, Spontaneous inhibitory postsynaptic potential; SEM, Standard error of the mean; TBS-T, Triton X-100 in Tris-buffered saline.

that exposure to α5 $GABA_A$R NAMs may further compromise aberrant synapses in AD. We, therefore, suggest that the α5 $GABA_A$R is not a suitable therapeutic target for the treatment of AD or other cognitive deficits due to the widespread neuronal-networks that use α5 $GABA_A$Rs.

Keywords: Alzheimer's disease, $GABA_A$ receptors, synaptic, interneurons, hippocampus

INTRODUCTION

Over the last few decades, considerable focus has been on negative allosteric modulators (NAMs; previously referred to as inverse agonists) of the benzodiazepine site of γ-aminobutyric acid receptors ($GABA_A$Rs) as a potential therapeutic target for cognitive impairment in temporal lobe epilepsy (TLE), Huntington's disease, Down's syndrome, schizophrenia and the most common form of dementia, Alzheimer's disease (AD), which constitutes one of the most significant health problems confronting societies with an aging population.

The ionotropic $GABA_A$R family are heteropentameric structures consisting of a combination of five subunits (Sieghart and Sperk, 2002) with the α–subunit being clinically relevant, as it controls the pharmacological profile of $GABA_A$ Rs (McKernan and Whiting, 1996). Since the understanding that distinct pharmacological properties of the $GABA_A$R are reliant on the fact that different brain regions and cell types contain various subunit compositions, NAMs of the $GABA_A$R at the subunit level have been widely studied. In particular, $GABA_A$Rs containing the α5-*subunit* have been of interest, given their role in learning and memory as evidenced by various studies (Collinson et al., 2002; Crestani et al., 2002; Caraiscos et al., 2004; Yee et al., 2004; Dawson et al., 2006; Ghafari et al., 2017).

The hippocampus plays a critical role in memory formation and retrieval and is significantly affected in AD, which is characterized by short-term memory deficits as one of the first symptoms of the disease (Price et al., 2001). The strong evidence to suggest hippocampal preferential distribution of the α5-containing $GABA_A$R sub-type (Quirk et al., 1996), together with its diverse pathology in memory deficit-related disease, and particularly, its preservation in human brains of AD patients (Howell et al., 2000; Rissman et al., 2007), has led many researchers to test several α5 subunit-selective compounds for their potential cognition-enhancing effects (Liu et al., 1996; Quirk et al., 1996; Sternfeld et al., 2004; Savić et al., 2008).

Originally, Merck, Sharp, and Dohme (MSD) developed the first $GABA_A$R NAM, known as α5IA, with high efficacy at the $GABA_A$ α5 receptor sub-type without being an anxiogenic agent (Atack et al., 2006). Following the development of this compound by MSD, several other nootropic drugs (α5 sub-type selective NAMs) have been developed (e.g., RO4938581; Ballard et al., 2009). Many of these studies reported an impressive pharmacological profile of this compounds and their potential as cognitive enhancers without CNS-mediated adverse effects (Chambers et al., 2003; Collinson et al., 2006; Dawson et al., 2006; Ballard et al., 2009; Braudeau et al., 2011; Martinez-Cue et al., 2014; Duchon et al., 2019; Eimerbrink et al., 2019). These studies were initially implemented in rodent models, and unfortunately, these results were not reproducible in human subjects/patients to the same extent. Several key molecules consistently failed clinical trials at different phases including Basmisanil (code, RO5186582), a5IA (Atack, 2010), and MRK-016 (Atack et al., 2009). Basmisanil entered through Phase 1 and Phase 2 of clinical trials for Down's syndrome but failed during Phase 2 due to a lack of efficacy in adults and adolescents. It appears that despite a5IA and MRK-016 demonstrating tolerance in young males, some of these molecules were poorly tolerated in elderly patients with no cognitive improvement (Atack, 2010), thus reducing the viability of α5 as a therapeutic target. Although these molecules were shown to be selective for α5 subunit-containing $GABA_A$Rs, the lack of efficacy and poor tolerance in human patients could be related to poor brain penetration of the molecules or an age-related effect.

Whether this failure was due to low drug potency/bioavailability or due to a general lack of understanding of the synaptic mechanisms involving α5 receptors during the pathogenesis of the disease is currently unclear. To address these issues, we synthesized a novel water-soluble α5 $GABA_A$R selective NAM. These receptor subtypes are located in hippocampal extrasynaptic sites, as well as synaptic sites of postsynaptic pyramidal cells (Serwanski et al., 2006; Ali and Thomson, 2008; Glykys et al., 2008). Although it has been shown that dendrite-targeting interneuron populations elicit α5 $GABA_A$R-mediated inhibition in pyramidal cells (Ali and Thomson, 2008), it is unclear whether the α5 receptor subtype was expressed on inhibitory interneurons themselves. This was of particular interest, as we have shown previously, using the $APP^{NL-F/NL-F}$ mouse, the first β-amyloid precursor protein (*APP*) knock-in mouse AD model that is thought to be able to recapitulate the human condition more accurately (see Sasaguri et al., 2017), that synaptic excitability is disrupted in various cortical regions, including the CA1 region (Petrache et al., 2019), and that this could be related to the alteration of three key modulatory interneuron populations namely; calretinin- (CR), cholecystokinin- (CCK), and somatostatin- (SST) expressing interneurons (Shi et al., 2019). We investigated whether these key modulatory interneurons located in CA1 stratum oriens (SO), stratum radiatum (SR), together with principal pyramidal cells in stratum pyramidale (SP), expressed the α5 subunit-containing $GABA_A$Rs, in the $APP^{NL-F/NL-F}$ model, age-matched to wild-type control mice, and then characterized the synaptic effects of our newly-developed α5 compound in these four subtypes of neurons.

MATERIALS AND METHODS

Development of α5-SOP002

We re-synthesized 6,6-dimethyl-3-(2-hydroxyethyl) thio-1-(thiazol-2-yl)-6,7-dihydro-2-benzothiophene-4(5H)-one that has demonstrated selectivity for the benzodiazepine binding site and high negative allosteric modulation for the α5 $GABA_A$R sub-type following its published route, from the parent compound (Sternfeld et al., 2004; Atack, 2010) to develop hybrid derivatives (parent compound, shown in **Figure 1A**), full details of the synthetic steps are detailed in **Supplementary Scheme 1** (see also Sung and Lee, 1992). There were two main sites for modification, which we explored *via* replacement of the triazole moiety or the oxazole which enabled us to explore late-stage modification to synthesize hybrid analogs to improve potency as a NAM acting on α5 $GABA_A$Rs.

Computational Modeling

The structure of the α5 subunits contained in the A-type γ-aminobutyric acid receptor ($GABA_A$R) subtype formed by two α5, two β3, and one γ2 subunits was modeled based on the Cryo-EM structure 6A96 downloaded from the protein data bank[1]. Then, the complete $GABA_A$R was modeled. Potential pockets that were large enough to bind the ligands were identified using the icmPocketfinder tool present in the ICM-Pro software[2]. The pocket selected was present at the interface of the subunits α5 and γ2 and was analogous to that which binds benzodiazepine in the $GABA_A$R, the human β3 homopentamer (PDB id: 4COF). The volume of the pocket was 435.6 $Å^3$.

The ligands were sketched using the LigEdit module and docked in the receptor using the docking module. The template-based docking protocol was used. The spatial orientation of benzodiazepine was selected as a reference template to dock the compounds. Grid maps were generated around the template, which defined a binding site encompassed in a grid of 20 × 20 × 20 $Å^3$. Docking was run with an effort of 5, storing all alternative conformations. A maximum of 25 docked conformations was generated. The final confirmation was chosen based on the strongest interaction energy. Visualization of the docked poses was done by using the ICM-Pro Molsoft molecular modeling package.

Preparation of Stable HEK293 Cell Lines Expressing $GABA_A$Rs

To test the target selectivity of α5-SOP002, a stable cell line of HEK293 cells expressing α5β2γ2 subunits of the $GABA_A$R was developed using the previously established method based on antibiotic selection (Brown et al., 2016). HEK293 cells (2 × 106) were transfected using Lipofectamine LTX (catalog no. 15338–100, Invitrogen) with the α5 pcDNA3.1(+) construct, incorporating the G418 disulfate (Neomycin) resistance gene and β2 pcDNA3.1(+) construct, incorporating the Zeocin resistance gene. Cells were subsequently plated at the ratios of 1:3, 1:5, 1:7, 1:10, 1:15, and 1:20, and selected with G418 (Neomycin; catalog no. G5013, Sigma–Aldrich) and Zeocin (catalog no. R25001 Gibco) antibiotics (both at 800 μg/ml) until colonies were formed. After 7 days, ∼5–20 single colonies were selected and gradually scaled up. The clone expressing the highest level of $GABA_A$R α5 and β2 subunits, as well as the previously established α2β2-HEK293 (Brown et al., 2016) stable cell line were further transfected with the γ2 pcDNA3.1(+) construct, incorporating the Hygromycin resistance gene, to produce triple cell lines. The expression of all three subunits was characterized by immunoblotting and immunocytochemistry. The α1β2γ2-HEK293 was characterized previously (Fuchs et al., 2013).

Experimental Animals

All of the procedures in this study were carried out following the British Home Office regulations under the Animal Scientific Procedure Act 1986, under the project license PPL: P1ADA633A held by the principal investigator, Dr. Afia Ali. All procedures were approved by both internal and external UCL ethics committees and following the ARRIVE guidelines for reporting experiments involving animals (McGrath et al., 2010). A total of ∼100 male animals (disease model and wild-type) were used in this study. The animals had *ad-libitum* access to food and water and were reared in cages of a maximum of five inhabitants, with a day: night cycle of 12: 12 h.

The knock-in $APP^{NL-F/NL-F}$ AD mouse model was used for experiments (Saito et al., 2014), which consists of the introduction of two familial AD (FAD) mutations: KM670/671NL and I716F. The former, identified as the Swedish mutation, increases β-site cleavage of APP to produce elevated amounts of both $Aβ_{40}$ and $Aβ_{42}$, whereas the latter, known as the Beyreuther/Iberian mutation, promotes γ-site cleavage at C-terminal position 42, thereby increasing the $Aβ_{42}/Aβ_{40}$ ratio in favor of the more hydrophobic $Aβ_{42}$ (Saito et al., 2014). Both features are key to the integrity of the disease phenotype. The knock-in line was crossed with C57BL/6 mice, and male $APP^{NL-F/NL-F}$ and age-matched wild-type (C57BL/6) mice from the same breeding were used as control at 10–18 months (age ranges of mice for neuroanatomy and electrophysiology experiments were; 12–18 months and 10–12 months, respectively).

Animals were genotyped *via* standard polymerase chain reaction using the following four primers: 5′-ATCTCGGAAG TGAAGATG-3′, 5′-TGTAGATGAGAACTTAAC-3′, 5′-ATCT CGGAAGTGAATCTA-3′, and 5′-CGTATAATGTATGCTATA CGAAG-3′ as previously described (Saito et al., 2014). Further details of the rationale for selecting this mouse model can be found in Petrache et al. (2019).

For the *in vivo* radial arm maze (RAM) memory test, male Wistar rats (Harlan, UK) at post-natal days 20–27 with the same housing conditions as the mice were used. The rats were weighed, handled, and monitored daily systematically during the memory test.

Tissue Collection and Preparation

Male rodents were anesthetized by an intraperitoneal injection of 60 mg/kg phenobarbital and perfused transcardially with

[1]http://www.rcsb.org./pdb
[2]www.molsoft.com

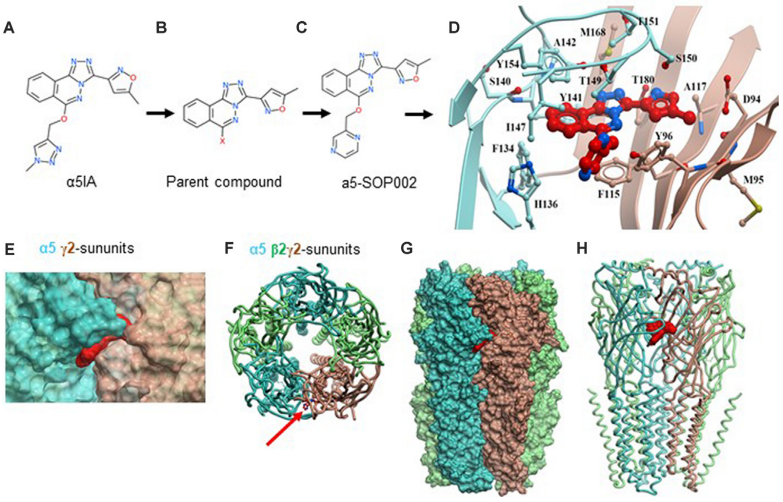

FIGURE 1 | Developing negative allosteric modulator (NAM), α5-SOP002. **(A–C)** Optimization of α5IA to α5-SOP002. **(D)** Detailed interactions of α5-SOP002 at the $GABA_AR$ binding site located at the interface between subunit α5 (blue) and γ2 (brown). **(E)** Surface representation of SH-AI-SOP002 (red) interacting with the α5 $GABA_AR$ at the α5 (blue) and γ2 (brown) subunits' interface. **(F)** The upper view of the α5 $GABA_A$ subtype is represented by ribbons. The red arrow points at α5-SOP002. Subunits α5 are shown in blue, β3 in green, and γ2 in brown. **(G)** Surface and **(H)** ribbon representation of the α5 $GABA_AR$.

artificial cerebrospinal fluid (ACSF) containing sucrose. The level of anesthesia was monitored using pedal and tail pinch reflexes, rate, depth, and pattern of respiration through observation and color of mucous membranes and skin. The ACSF comprised of (in mM): 248 sucrose, 3.3 KCl, 1.4 NaH_2PO_4, 2.5 $CaCl_2$, 1.2 $MgCl_2$, 25.5 $NaHCO_3$, and 15 glucose, which was bubbled with 95% O_2 and 5% CO_2. The animals were then decapitated and the brain removed and coronal sections hippocampus containing the neocortex ∼300 μm thick—were cut in ice-cold standard ACSF using an automated vibratome (Leica, Germany). This standard ACSF contained (in mM): 121 NaCl, 2.5 KCl, 1.3 NaH_2PO_4, 2 $CaCl_2$, 1 $MgCl_2$, 20 glucose and 26 $NaHCO_3$, equilibrated with 95% O_2 and 5% CO_2. Slices were incubated in ACSF for 1 h at room temperature (20–23°C) before recording. Brain slices were placed in a submerged chamber and superfused with ACSF at a rate of 1–2 ml min^1 for electrophysiological recordings. For neuroanatomical studies, brains were immediately fixed after perfusion in 4% paraformaldehyde (PFA) plus 0.2% picric acid in 0.1 M phosphate buffer (PB) for 24 h before sectioning.

In vitro Brain Slice Electrophysiology

All whole-cell recordings were performed using patch electrodes made from filamented borosilicate glass capillaries (Harvard Apparatus, UK) using a laser puller (Sutter Instruments, Novato, CA, USA), with resistances of 8–11 MΩ, and were visually aided by IR-DIC microscopy (Optizoom, Nikon, USA).

Whole-Cell Patch-Clamp Recordings of HEK293 Cells

Electrophysiological recordings of HEK293 cells stably expressing $GABA_ARs$ were performed in a whole-cell, voltage-clamp mode. The chamber containing coverslips with the cell line was continuously superfused at a flow rate of 1.8 ml/min with the extracellular medium composed of 130 mM NaCl, 4 mM KCl, 10 mM HEPES, 20 mM $NaHCO_3$, 10 mM glucose, 1 mM $MgCl_2$, and 2 mM $CaCl_2$, and was equilibrated with 5% CO_2/95% O_2 and maintained at room temperature (∼21–25°C). The electrodes were filled with an intracellular solution containing (in mM), 130 KCl, 3 NaCl, 4.5 phosphocreatine, 10 HEPES, 1 EGTA, 3.5 Na-ATP, 0.45 Na-GTP, and 2 $MgCl_2$ (adjusted to pH 7.2 with KOH, 290–300 mOsmol/l), and had a final resistance of 3–8 MΩ. To test the target selectivity of α5-SOP002, the responsiveness to applied GABA was investigated and measured in HEK293 cells stably expressing either, α5β2γ2, α1β2γ2 or α2β2γ2 subunits of $GABA_ARs$. The pharmacological properties of the expressed receptors were investigated by puffer-application of GABA (1 μM; Tocris Bioscience, UK) and subsequent bath-application of α5-SOP002 (0.5–1 μM), followed by diazepam (1 μM, Tocris Bioscience, UK). The change in voltage after the GABA puff application response was recorded. The statistical test used was one-way ANOVA with a 95% confidence interval.

Whole-Cell Patch-Clamp of Neurons in Acute Hippocampal Brain Slices

Whole-cell somatic recordings were performed using patch electrodes filled with a solution containing (in mM): 134 K

gluconate, 10 HEPES, 10 phosphocreatine, 2 Na_2ATP, 0.2 Na_2GTP, and 0.2% w/v biocytin.

CA1 pyramidal cells and interneurons in SR and stratum lacunosum moleculare (SLM) were selected for recording based on the shape of their soma using video microscopy under near-infrared differential interference contrast illumination. Cells were further characterized by their electrophysiological properties obtained from injecting a series of 500 ms depolarizing and hyperpolarizing current pulses and identified post-recording anatomically, as described previously in detail (Khan et al., 2018).

Spontaneous postsynaptic potentials were recorded from passive membrane responses and mixed spontaneous excitatory postsynaptic potentials (sEPSPs) and spontaneous inhibitory postsynaptic potentials (sIPSPs) were collected in 60-s frame samples, repeated at 0.33 Hz. Recordings were carried out under the current-clamp mode of operation (NPI SEC 05LX amplifier; NPI electronics, Germany), low pass filtered at 2 kHz and digitized at 5 kHz using a CED 1401 interface (Cambridge Electronic Design, UK). Input resistance was monitored throughout experiments using a hyperpolarizing current step (−10 pA, 10 ms). Signal (Cambridge Electronic Design, UK) was used to acquire recordings and generate current steps. The average amplitudes of spontaneous events and their frequency were measured manually from single sweep data sets of 60-s recordings, including a total sweep range of 30–50 frames (i.e., 30–50 min of recording); values below the baseline level of 0.1 mV were considered as noise, see Ali and Nelson (2006).

Paired whole-cell somatic recordings were obtained between CA1 CR interneurons in SR (for inhibitory connections). Unitary inhibitory postsynaptic potentials (IPSPs) were elicited by a depolarizing current step into the presynaptic neuron (+0.05 nA, 5–10 ms) repeated at 0.33 Hz. The peak IPSP amplitudes and width at half-amplitude measurements were obtained from averages including 100–200 unitary synaptic events.

Drugs for *in vitro* pharmacological studies on brain slices, zolpidem (Sigma–Aldrich, UK, 0.4 μM, dissolved first in ethanol to a final bath ethanol dilution of 1:20,000); α5-SOP002 (1–1.5 μM); diazepam (RBI, Poole UK; 1–2 μM, dissolved in ethanol to a final bath ethanol dilution of 1:5,000) were bath-applied. The α5-SOP002 concentration used was similar to the previously published parent compound, α5IA (1–1.5 μM); this was within the range of *in vitro* efficacy at which it is reported to act as an inverse agonist (NAM) with efficacy selective for α5 containing $GABA_A$Rs (Collinson et al., 2006; Dawson et al., 2006). The concentration of zolpidem used produces near-maximal effects on α1-containing receptors but submaximal effects on α2/3-containing receptors (K_d 0.2 μM for α1–containing receptors; 1.5 μM for α3 containing receptors; Munakata et al., 1998).

Neuroanatomical Procedures and Analysis

Recovery of Biocytin Labeled-Cells Post Electrophysiological Recordings

After electrophysiological recordings with pharmacological protocols, the slices were only suitable for biocytin recovery due to the long recording in the range of 45–90 min. Slices were fixed in 4% PFA plus 0.2% picric acid in 0.1 M PB for 24 h and then re-sectioned at 70 μm. Slices were then incubated in ABC overnight at 4°C, followed by the above DAB protocol. Cells were identified using a Leica DMR microscope.

Immunofluorescence Procedures, Confocal Image Acquisition, and Analysis of CA1 Neurons

Slices obtained from approximately the same medial level in CA1 were incubated as described previously (Petrache et al., 2019), using $GABA_A$R α5 primary antibody (Abcam, Cambridge, MA, USA, raised in mouse, 1:100) incubated concomitantly with the primary antibody targeting one of the following: calretinin (Swant, raised in goat, 1:1,000), somatostatin (Santa Cruz Biotechnology, Santa Cruz, CA, USA, raised in rabbit, 1:500), cholecystokinin (Frontier Institute, raised in rabbit, 1:1,000) or CaMKII-α (Invitrogen, raised in goat, 1:100). The secondary antibodies used were as follows: FITC (Sigma–Aldrich, anti-mouse, 1:200), Texas Red (Invitrogen, anti-rabbit/anti-mouse, 1:500) or Alexa Fluor 488 (Abcam, Cambridge, MA, USA, anti-goat, 1:500). The sections were counterstained with the nuclear stain, DAPI (Sigma–Aldrich, 1:1,000).

Images were acquired at 63× magnification using a ZEISS LSM 880 confocal microscope and processed using Zen Black 2009. When imaging, we maintained a consistent pinhole, exposure time, and light intensity settings between experiments. Collapsed *Z*-stacks were imported into Fiji (ImageJ) as .tif files and split into individual channels. If needed, the background was removed using the *Background subtraction* function in ImageJ, and this was applied to all channels for a given data set. In the channel corresponding to the cell staining, the outline of the cells of interest was drawn manually to obtain regions of interest (ROIs). The *Coloc2* plugin was then used to obtain Pearson's R coefficient as a measure of colocalization between the channels corresponding to the ROIs and the α5 subunit, and Fisher's transformation was applied to convert the coefficients to a normal distribution. The results so obtained were then averaged separately for wild-type and $App^{NL-F/NL-F}$ animals, respectively, for each of the cells of interest. There were no age-dependent differences observed for either wild-type and $App^{NL-F/NL-F}$ animals during confocal analysis, however, the data presented for the expression of α-5 $GABA_A$Rs were obtained from individual animals in the age bracket of 12–18 months ($n = 7$).

In vivo RAM Memory Test

A RAM was used to test the *in vivo* effects of a5-SOP002 on memory. The RAM consisted of eight identical arms and a circular platform. The maze was placed on a Table 50 cm above the floor with a digital camera recorder mounted to the ceiling directly above. All rats were first habituated in the maze for 5 days with up to two sessions of 10–30 min per day with either food scattered throughout the maze, food scattered only in the arms, and food scattered in three designated arms. The rats were further trained for another 5 days by assigning a hippocampal-dependent memory task. Three out of eight arms of the maze were baited with food. The three designated arms in which the food bait was placed were randomized between each rat. The rats

were placed at the center of the platform of the maze and allowed to retrieve food reward from the baited arms. Completion of the training was accepted if one of these criteria were met: (i) the training lasted more than 10 min; or (ii) all eight arms of the maze were visited. The fourth day of the training was assigned as the information phase where we assumed the rats have learned the task. The final day of the training was assigned as the test phase. The rats were administered a drug treatment (a5-SOP002 or L-655, 708, 1 μM in 5% DMSO) or saline (sodium chloride BP 0.9% w/v) 2 h before the beginning of the task at a dose of 1 mg/kg i.p. A 2-day interval was kept before the test day. The total time the rats took to complete the task was recorded and tracked using a video tracking software ANY-maze (Stoelting Co., Wood Dale, IL, USA).

Statistical Analyses

All data values are given as the mean ± standard error of the mean (SEM) unless otherwise stated. Before statistical analysis, normality and outlier tests were conducted. For comparisons between multiple groups of data, one-way or two-way ANOVA with a 95% confidence interval was used followed by a *post hoc* Tukey's or Bonferroni's test for multiple comparisons.

Statistical analysis for the electrophysiology in the $APP^{NL-F/NL-F}$ model and the immunofluorescence data was conducted using GraphPad Prism version 8.0.0 for Windows, GraphPad Software, San Diego, CA, USA, GraphPad.

All statistical analyses were conducted using the statistical package Origin Pro 2016 SR1. Statistical significance was accepted where $P < 0.05$ ($^{*}P < 0.05$, $^{**}P < 0.01$, $^{***}P < 0.001$, $^{****}P < 0.0001$). The "*n*" is given as the number of observations and the number of animals used unless otherwise stated.

RESULTS

In this study, we initially re-synthesized a water-soluble α5 $GABA_A$R-selective compound NAM, α5-SOP002 and determined its selectivity using HEK293 cells lines stably expressing α5β2γ2-, α2β2γ2-, or α1β2γ2-$GABA_A$Rs. To identify changes in the expression pattern of α5 $GABA_A$R during a disease that is characterized by cognitive deficits, we used an AD mouse model and wild-type mice at 10–12 months, when the typical hallmarks of AD in the hippocampus are present, including synaptic loss, accumulation of amyloid-β (Aβ) and proliferation of reactive astrocytes and microglia (Saito et al., 2014; Petrache et al., 2019). The effects of α5-SOP002 on inhibitory synaptic potentials recorded in the identified cells that co-expressed α5 $GABA_A$R were investigated.

The Development of the α5-SOP002 Compound

We initially developed four hybrid analogs of this compound with an array of biological activity ranging from inactive controls to highly potent derivatives resulting in, α5-SOP002 (**Figures 1A–C**, see also **Supplementary Scheme 1**).

The structure of the α5 subunits contained in the α5 $GABA_A$R was modeled and later used to generate the $GABA_A$R subtype containing two α5, two β3, and one γ2 subunits. Once a reliable model was obtained, our key compound, α5-SOP002 was docked into the interface of subunit α5 (**Figures 1D–H**) and subunit γ2, obtaining the best binding mode with a VlsScore of −20.35.

Overall, α5-SOP002 indicated good aqueous solubility and good blood-brain barrier penetration as evidenced by the spatial memory recall experiments in rats following intraperitoneal injection (i.p.; **Supplementary Scheme 1**). The **Supplementary Section**, which compares *in vivo* spatial memory tests (Becker et al., 1980) and *in vitro* paired whole recording data from 25 to 28 day old rats using α5-SOP002 and the published analog L-655, 708 (a similar compound to α5IA originally developed by Merck Sharp and Dome (UK) and available from Tocris (UK) were described. *In vivo*, spatial memory recall experiments were not repeated in the mouse lines due to the conclusions reached from the results (see below).

α5-SOP002 Selectively Targets α5 Subunits of $GABA_A$Rs

An α5β2γ2-HEK293 cell line was developed to investigate the selectively of α5-SOP002 towards the α5-containing $GABA_A$Rs. The cell surface expression of all three $GABA_A$R subunits in this cell line was characterized using immunocytochemistry (**Figure 2A**) with subunit-specific antibodies. The responsiveness of the α5β2γ2-HEK293 stable cell line to 10 μM puff-applied GABA in the presence α5-SOP002, confirmed its activity as a NAM (i.e., inverse agonist) of these receptors. Subsequent bath addition of diazepam, followed by puff-applied GABA resulted in an enhanced voltage change and demonstrated the presence of functional α5β2γ2-$GABA_A$Rs at the cell surface (**Figure 2D**). These experiments were repeated using the α1β2γ2-HEK293 and α2β2γ2-HEK293 stable cell lines to test the specificity of α5-SOP002. The cell surface expression of α1β2γ2-and α2β2γ2-$GABA_A$Rs was also demonstrated using immunocytochemistry with subunit-specific antibodies (**Figures 2B,C**), as shown previously (Fuchs et al., 2013; Brown et al., 2016).

HEK293 cells expressing α5β2γ2-$GABA_A$Rs responded to GABA (10 μM), puff-applied (5 s) in proximity, with a large hyperpolarization, recorded at a membrane holding potential of −60 mV. This was also recorded in the α1β2γ2-HEK293 and α2β2-HEK293 stable cell lines (**Figures 2E,F**).

The response of the three cell lines to GABA was measured and the changes of the response after bath-application of 1 μM α5-SOP002, followed by puff-application of GABA after subsequent bath application (to extracellular solution) of the broad spectrum $GABA_A$R modulator, diazepam (1 μM) was also analyzed (**Figures 2D–F**).

Bath-application of α5-SOP002 (1 μM) significantly reduced the hyperpolarizing GABA inhibitory response in cells expressing α5β2γ2- $GABA_A$Rs (mean ± SEM: control GABA: 10.0 ± 5.0 mV; α5-SOP002: 5.12 ± 2.2 mV; $P < 0.05$, $n = 8$), while bath application of diazepam had an opposite effect leading to a significant enhancement of GABA response (12.26 ± 6.94, $P < 0.05$, $n = 8$, one-way ANOVA; **Figure 2G**). In contrast, there were no significant changes in the puff-applied GABA response in the presence of α5-SOP002 in cells expressing α1β2γ2-$GABA_A$Rs (control GABA: 18.0 ± 5.0 mV; α5-SOP002: 18.0 ± 4.5, $n = 6$; **Figure 2E**) or α2β2γ2-HEK293 (control GABA:

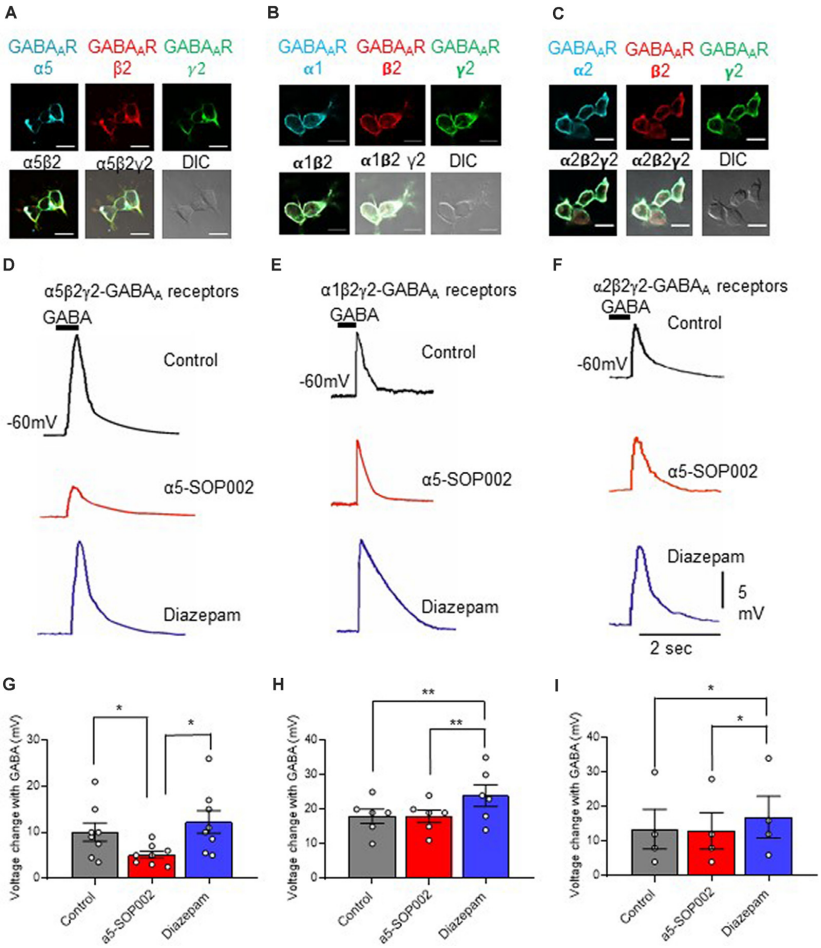

FIGURE 2 | α5-SOP002 selectively targets α5 subunits of GABA$_A$Rs. Whole-cell recordings in α5β2γ2-, α1β2γ2-, and α2β2γ2-HEK293 cells. HEK293 cells stably expressing α5β2γ2- **(A)**, α1β2γ2- **(B)**, or α2β2γ2-GABA$_A$Rs **(C)**. Immunofluorescent imaging with a 40× oil immersion objective lens shows cell surface expression of α5, α1 or α2- (cyan), β2- (red), and γ2-GABA$_A$R subunits (green). **(A–C)** also show all the three channels merged showing α-, β2-, and γ2-GABA$_A$R subunit co-localization at the cell surface (white) along with the differential interference contrast microscopy (DIC) image of the cells. The scale bar represents 10 μm. All three stable cell lines responded to 10 μM puff-applied GABA **(D–F)** in control extracellular solution (black traces), an extracellular solution containing 1 μM α5-SOP002 (red traces), and subsequent bath application of diazepam (blue traces) at a holding membrane potential of −60 mV. The corresponding plots for α5β2γ2-HEK293 cells **(G–I)** show the changes in voltage changes in response to 10 μM GABA puffed locally, in the presence of bath-applied α5-SOP002, and, subsequent addition of diazepam. Only the α5β2γ2-HEK293 cells showed an inverse agonist effect (response to GABA) of α5-SOP002. All three cell lines, however, showed an enhancement of response to GABA in the presence of diazepam. Statistically significant data are shown with $^*P < 0.05$ and $^{**}P < 0.01$.

13.5 ± 11.5 mV; α5-SOP002: 13.0 ± 10.5 mV, $n = 6$; **Figure 2F**). Puff-application GABA in the presence of diazepam enhanced the hyperpolarizing inhibitory GABA response in both, α1β2γ2-HEK293 (24.0 ± 7.6 mV, $P < 0.01$, $n = 6$) and α2β2γ2-HEK293 cells (17.0 ± 12.0, $P < 0.05$, $n = 6$; **Figures 2H,I**). This confirmed the selectivity of α5-SOP002 towards GABA$_A$Rs containing the α5 subunits.

α5-SOP002 Enhanced Memory in Healthy Rodents

As a proof of concept, experiments were performed on healthy rats, to test the effects of α5-SOP002 *in vivo*, using the RAM memory test. Rats were divided into three groups according to the treatment they received, our compound α5-SOP002 ($n = 14$), the commercially available GABA$_A$ α5 inverse agonist, L-655,

708 (n = 4; similar to α5IA), and saline-treated "sham" group (n = 9). During the first 3 days of the pre-treatment training phase, all groups took between 600 s and 800 s to complete the task and by the fourth day, the task was completed more efficiently within 450 s. The fourth day was considered as the information phase, assuming the rats have now learned the maze or gathered all the "information" to complete the task to a certain degree. All groups completed the task significantly faster on the test day in comparison to the information phase. The α5-SOP002- and L-655, 708-treated groups completed the task faster than the sham group on the test day taking almost three times less of the time and showed a bigger difference between information and test phase (**Figures 3A–C**). This validates our compound has an *in vivo* effect, potentially a memory-enhancing one.

Preservation of α5 $GABA_A$Rs in CA1 Pyramidal Cells and Three Sub-types of Interneurons in the AD Model

Using immunofluorescence and confocal microscopy analysis in the CA1 region of the hippocampus, we investigated α5 subunit-containing $GABA_A$R expression in three sub-types of modulatory inhibitory interneurons, CR-, SST- and CCK-expressing interneurons, as well as in pyramidal cells (stained for CaMKII-α) in the $APP^{NL-F/NL-F}$ mouse model and wild-type animals (**Figures 4A–D**). The imaged area in each case is shown in **Figure 4E**.

This was measures in three different ways, quantification of the total intensity of α5 signal in CA1 measured from confocal Z-stacks, followed by the quantification of α5 expression from individual cell populations measured from their somata and dendrites, using Pearson's correlation coefficient R with Fisher's transformation.

We also quantified the total intensity of α5 signal in CA1 confocal Z-stacks and observed no differences in the AD model compared to wild-type ($P > 0.05$, n = 5 wild-type animals and 6 $APP^{NL-F/NL-F}$ animals), suggesting preservation of α5 expression in the $APP^{NL-F/NL-F}$ animals (12–18 months age).

The α5 subunits expressed on all three interneuron subtypes were analyzed further from somata of the different cell types (**Figure 4F**). There was no significant change in α5 expression on CR cells in $APP^{NL-F/NL-F}$ animals compared to wild-type (only a slight increase of 11.86 ± 3.14%, $P > 0.05$, n = 6 wild-type animals and 7 $APP^{NL-F/NL-F}$ animals). Similarly, there was no change in the expression of α5 expression in SST or CCK interneurons between wild-type and $APP^{NL-F/NL-F}$ mice (changes of; 27.35 ± 12.61% and 36.09 ± 12.45% observed in SST and CCK cells, respectively, in $APP^{NL-F/NL-F}$ animals compared to wild-type animals, $P > 0.05$, n = 6). Thus, the three interneuron subtypes studies showed no significant differences in α5 subunit expression between wild-type animals and $APP^{NL-F/NL-F}$ animals, highlighting the preservation of the α5 subunit in AD.

Analysis of CaMKII-α and α5 co-staining (**Figure 4F**) showed no significant differences in the expression of α5 expression on the pyramidal cells in $APP^{NL-F/NL-F}$ animals compared to wild-type ($P > 0.05$, n = 5). This observation is consistent with previous studies, which reported α5 expression on pyramidal cells (Brünig et al., 2002).

Next, we investigated the expression of the α5 subunit on CR, SST, and pyramidal cell dendrites (**Figure 4G**), as the subunit has been reported to be located postsynaptically at dendritic sites where presynaptic CR cells target SST interneurons (Magnin et al., 2019) and on postsynaptic dendrites of pyramidal cells (Ali and Thomson, 2008). CCK cells also receive input-from dendrite-targeting interneurons (Ali, 2007), but their dendrites could not be investigated in detail here, due to the unavailability of a specific anti-CCK antibody that shows a good expression of CCK in dendrites in mouse tissue. We investigated up to 5 cells in each animal, and observed no significant difference in the α5 expression between the genotypes or neuron subtypes in their dendrites ($P > 0.05$, one-way ANOVA with *post hoc* Tukey's test for multiple comparisons).

α5-SOP002 "Normalizes" CR Interneuron Aberrant Inhibition Observed in AD

Inhibition Recorded From Spontaneous Synaptic Events

The effect of α5-SOP002 at inhibitory CR interneurons was determined on brain slices by performing whole-cell recordings under current-clamp mode. sIPSPs and sEPSPs were recorded from CR interneurons at 10–12 months old wild-type and $App^{NL-F/NL-F}$ mice at holding membrane potentials of −60 mV (to observe both excitation and inhibition; **Figures 5A–D**), the average data are shown in **Table 1**. The average peak frequency and amplitude of sIPSPs significantly increased in the AD model compared to wild-type age-matched mice at −60 mV, consistent with our previous publication that reported this interesting abnormal observation in the CR cells (Shi et al., 2019). In the $App^{NL-F/NL-F}$ mice, sIPSP frequency and amplitude were abnormally higher by 93.4 ± 7.5% ($P < 0.01$, n = 5, n = 5, two-way ANOVA with *post hoc* Turkey's test) and 55.6 ± 23.3% ($P < 0.01$, n = 5) of control sIPSPs recorded in age-matched wild-type mice, respectively (**Figure 5C**).

Bath-application of α5-SOP002 (1 μM) reduced the sIPSP frequency and amplitude in both wild-type and $App^{NL-F/NL-F}$ mice (see **Table 1** for details). The significantly reduced sIPSP frequency (48 ± 3.2%, $P < 0.01$, n = 5, two-way ANOVA with *post hoc* Turkey's test) and amplitude (56.3 ± 5.7%, $P < 0.01$, n = 5, two-way ANOVA with *post hoc* Turkey's test) recorded in CR cells from $App^{NL-F/NL-F}$ mice was comparable to the control CR cells recorded in age-matched wild-type mice. The average sEPSP frequency and amplitude also changed, but the slight increase was not significantly different from the control mean (**Figure 5D**, **Table 1**).

Interestingly, in the $App^{NL-F/NL-F}$ mice, bath-application of α5-SOP002 also caused an average ∼5 mV depolarization of the cell membrane, suggesting a reduction in tonic inhibition.

Unitary Inhibition Recorded From Two Synaptically-Connected CR Cells

CR interneurons during the late stages of AD were readily identifiable under ID-DIC during experiments (in striking

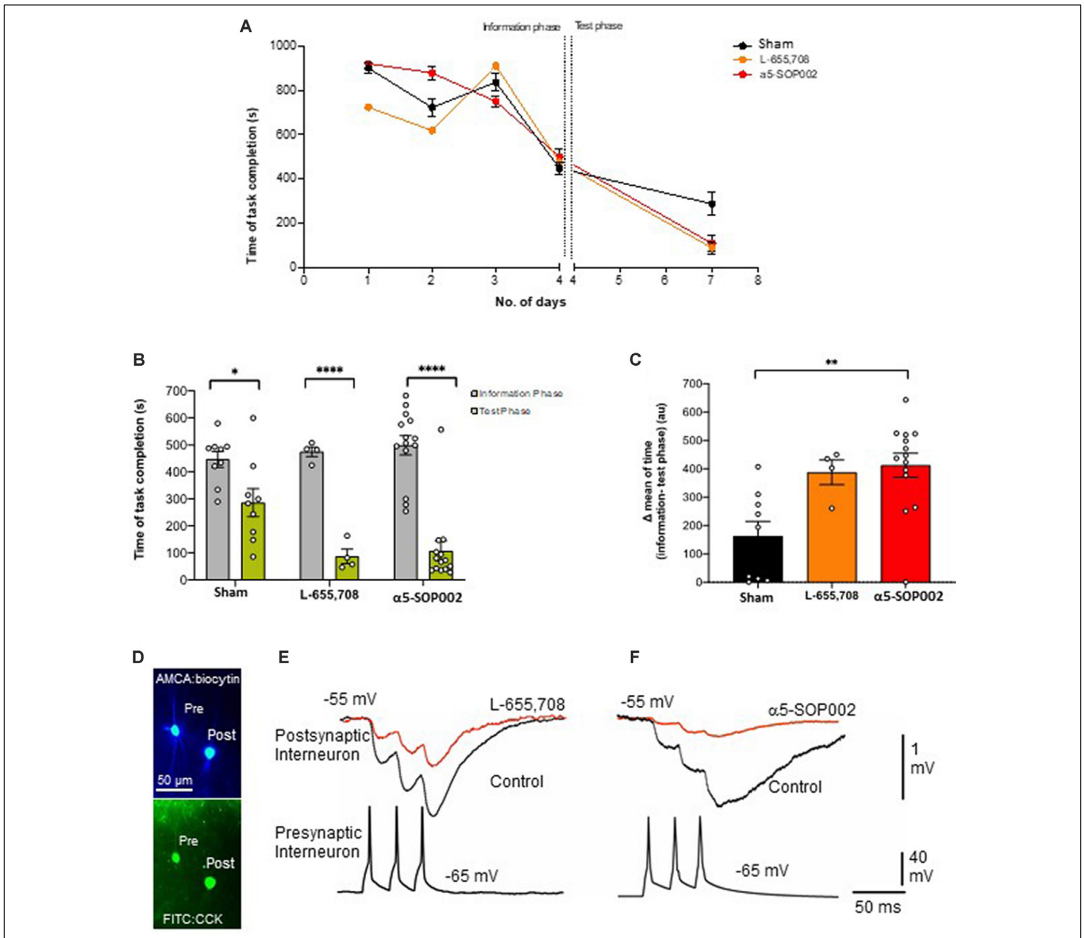

FIGURE 3 | α5-SOP002 improved memory in healthy rats performing the eight-arm radial arm maze (RAM) test, consistent with the NAM effect shown by *in vitro* electrophysiological recordings. **(A–C)** Analysis of RAM test performed in healthy rats treated with "sham," α5-SOP002- and L-655, 708. **(A)** Illustration of the variability of time taken to complete the memory task between all groups during 7 days (training + test phases). **(B)** Bar graphs compare the time taken to complete the tasks during training day 4 (defined as the information phase; gray) and day 7 (defined as test phase; green) for all groups tested. The time to complete the task during the test phase after administration of either; α5-SOP002 and L-655, 708, was reduced compared to control, suggesting potentiation of spatial memory recall. **(C)** Bar graphs representing the difference in mean time taken to complete the task between the information and test phase of each group. The a5-SOP002-treated rats had a statistically significant difference while both α5-SOP002- and L-655, 708-treated groups showed a bigger difference compared to the sham group. Results are expressed as mean ± standard error of the mean (SEM; black; sham group, $n = 9$, orange; L-6, 55 $n = 4$ and red; a5-SOP002 $n = 14$; one-way ANOVA, $^*P < 0.05$, $^{**}P < 0.01$, $^{****}P < 0.0001$). **(D)** Representative images of the anatomy of dendrite targeting, presynaptic CCK schaffer collateral-associated (SCA) cells synaptically connected to a postsynaptic CCK cell (AMCA shows the biocytin labeling during electrophysiological recordings). **(E,F)** Paired recording, trains of presynaptic action potentials elicited unitary inhibitory postsynaptic potentials (IPSPs), that were reduced by both NAMs selective for a5 GABA$_A$ receptors, L-655, 708 and α5SOP002.

contrast to CCK or SST cells that were not easily visualized), allowing us to perform paired recording between two CR cells. We performed paired recording in the $App^{NL-F/NL-F}$ animals only due to the very technically challenging nature of these experiments, hampered by the age of the mice. **Figures 3E,F** shows examples of paired recordings performed in younger healthy control rats where pre and postsynaptic cells were identified as CCK-positive (example of anatomy shown in **Figure 3D**).

Consistent with the finding that the sIPSPs recorded in "putative" CR cells (biocytin filled cells identified with a light microscope, and were not reconstructed), was sensitive

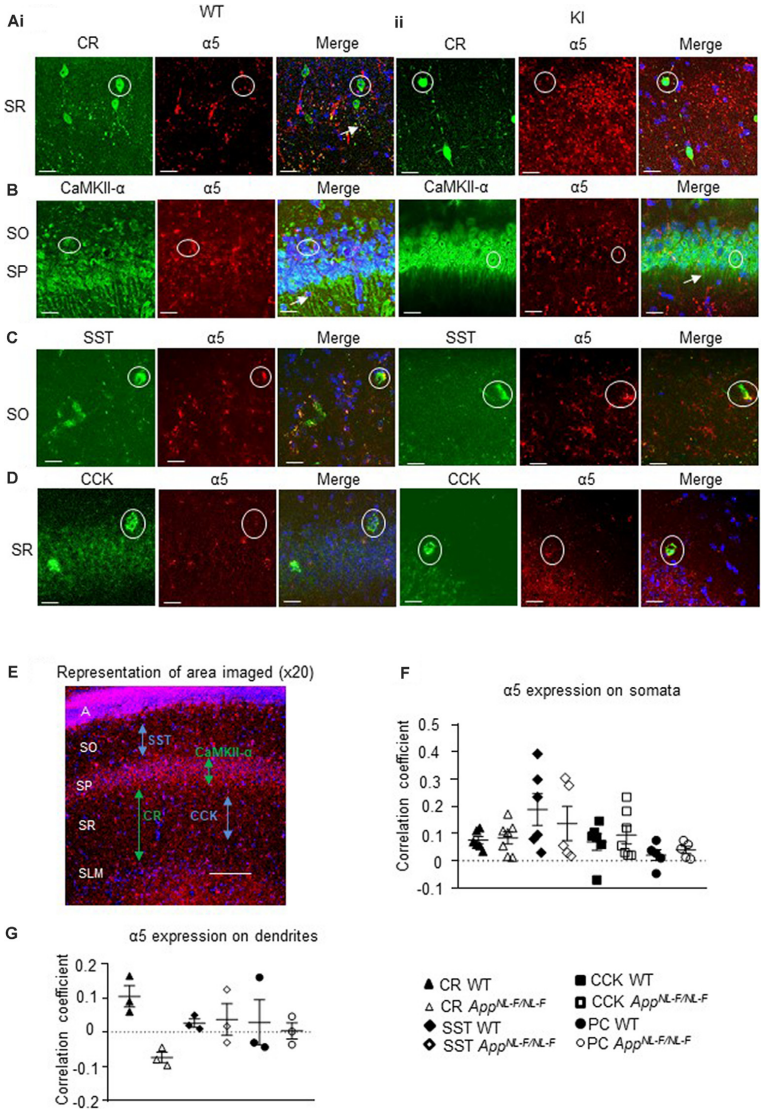

FIGURE 4 | Expression of α5 subunit-containing GABA$_A$Rs in CA1. **(A–D)** Confocal microscopy *Z*-stacks at 63× magnification showing α5 subunit-containing GABA$_A$R expression (red, Alexa 488 or Alexa 568 label) on pyramidal neurons (CaMKII- α, green, FITC), CR interneurons (green, Alexa 488), SST interneurons (green, Texas Red), and CCK interneurons (green, Texas Red) in wild-type **(i)** and *App*$^{NL-F/NL-F}$ animals **(ii)**. Panels show individual channels and merged image with the nuclear stain DAPI (blue). Representative cell somata are outlined with white circles. White arrows indicate dendritic co-localization of α5. **(E)** Representative image labeled with α5 (red) and DAPI (blue) taken at 20× magnification in the CA1 of *App*$^{NL-F/NL-F}$ to exemplify the region of data acquisition, arrows indicate the location of the sub-types of cells imaged and analyzed. Layers are labeled: alveus **(A)**, stratum oriens (SO), stratum pyramidale (SP), stratum radiatum (SR), stratum lacunosum moleculare (SLM). **(F)** Analysis of α5 subunit-containing GABA$_A$R expression on the soma of the four sub-types of neurons investigated. Each data point represents an average value (from five cells) analyzed form individual animals at 12–18 months of age (n = 5–7 mice studies per cohort). **(G)** Analysis of α5 subunit-containing GABA$_A$R expression on the dendrites of CR cells, SST cells, and pyramidal neurons (n = 3 mice per genotype with visible proximal dendrites analyzed for five cells per animal). **(F,G)** Results are expressed as a scatter plot ± (SEM; results not significant, $P > 0.05$), of Pearson correlation coefficient as a measure of co-localization, after application of Fisher's transformation. Data analyzed with a one-way ANOVA and *post hoc* Tukey test.

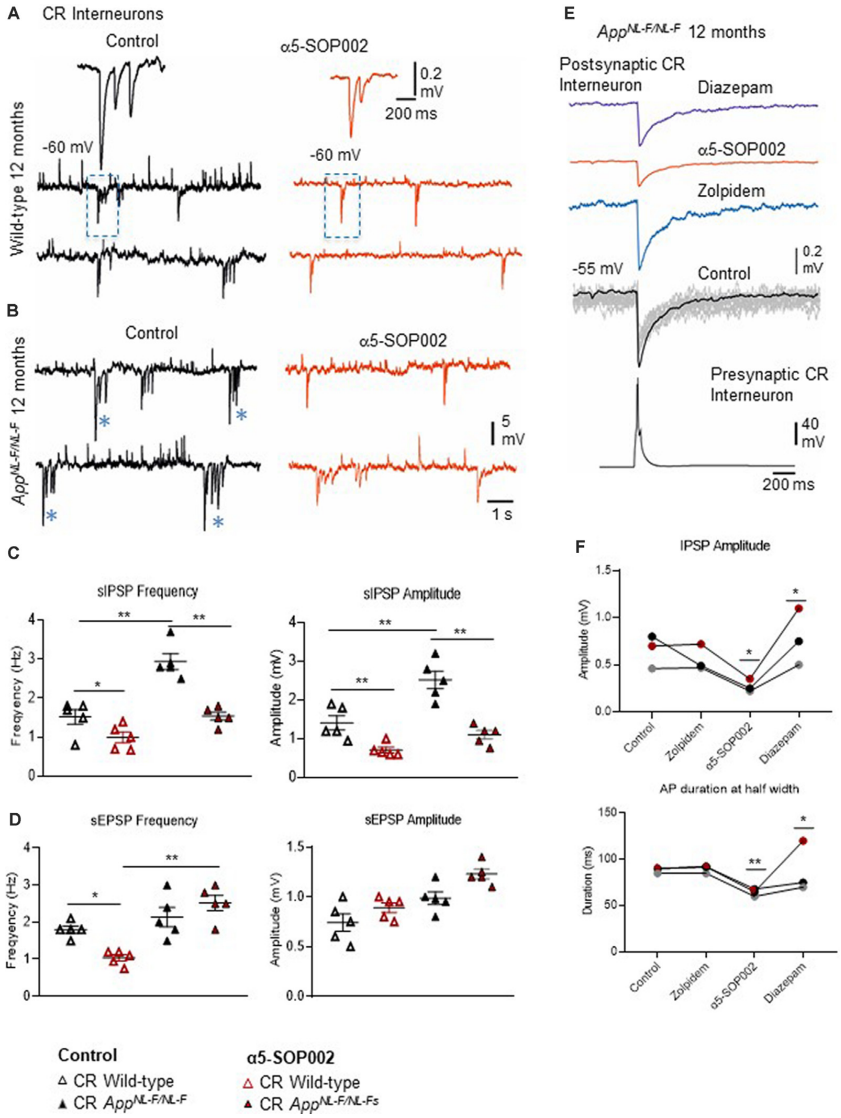

FIGURE 5 | Calretinin (CR)-expressing interneurons are functionally restored by NAM of α5 subunit-containing GABA$_A$Rs in *App*$^{NL-F/NL-F}$ mice. **(A,B)** Whole-cell current-clamp recordings of spontaneous inhibitory/excitatory postsynaptic potentials (sIPSPs and sEPSPs) recorded in CR cells in CA1 of 12-month-old wild-type and *App*$^{NL-F/NL-F}$ mice, at membrane potentials of −60 mV in control conditions, and after bath-application of α5-SOP002 (red traces). The squares indicate where synaptic events have been enlarged and shown in the inserts. *Indicate, an usually high sIPSPs recorded in the AD model. **(C,D)** Bar graphs show the average sIPSP and sEPSP amplitude and frequency at −60 mV in CR cells recorded in wild-type mice and the *App*$^{NL-F/NL-F}$ mouse model. These data suggest a significantly enhanced amplitude and frequency of inhibition in the AD model, which was "normalized" to control values after bath- application of α5-SOP002. $^{**}P < 0.01$, Data analyzed with a two-way ANOVA and *post hoc* Tukey's test. **(E)** Paired recording obtained between two putative CR cells recorded in SR of CA1 in the AD model. The unitary IPSPs were not sensitive to zolpidem, reduced by α5-SOP002, and then enhanced by subsequent addition of diazepam, indicating α5 pharmacology. **(F)** Line graphs show the average unitary IPSP amplitude and width at half amplitude change for each paired recording between two CR cells, in control, and after bath-application of zolpidem, α5-SOP002 and diazepam, recorded at −55 mV in *App*$^{NL-F/NL-F}$ mouse model. $^{*}P < 0.05$, $^{**}P < 0.01$. Data analyzed with a one-way ANOVA and *post hoc* Tukey test. Blue (*) are representative traces that have been enlarged in the inserts.

TABLE 1 | Changes of spontaneous synaptic events recorded in CR, CCK-SCA, and pyramidal cells after bath-application of a5-SOP002 in 10–12 months of age-matched, wild-type, and $APP^{NL-F/NL-F}$ mice.

Cell subtype	CR cells $n = 5$		CCK cells $n = 6$		Pyramidal cells $n = 5$	
sIPSP frequency (Hz)	**Control**	**α5-SOP002**	**Control**	**α5-SOP002**	**Control**	**α5-SOP002**
Wild-type	1.52 ± 0.19	0.99 ± 0.14**	1.18 ± 0.02	0.81 ± 0.03**	1.14 ± 0.04	0.76 ± 0.06**
$App^{NL-F/NL-F}$	2.94 ± 0.20**	1.54 ± 0.10**	0.90 ± 0.03**	0.44 ± 0.05**	0.90 ± 0.02**	0.51 ± 0.02**
sIPSP Amplitude (Hz)						
Wild-type	1.41 ± 0.19	0.71 ± 0.07**	0.57 ± 0.02	0.26 ± 0.02**	1.01 ± 0.05	0.50 ± 0.02**
$App^{NL-F/NL-F}$	2.52 ± 0.23**	1.10 ± 0.11**	0.43 ± 0.02**	0.23 ± 0.02**	0.24 ± 0.03**	0.12 ± 0.02**
sEPSP Frequency (mV)						
Wild-type	1.8 ± 0.09	1.04 ± 0.09*	1.26 ± 0.03	1.96 ± 0.04**	1.52 ± 0.02	2.52 ± 0.09
$App^{NL-F/NL-F}$	2.14 ± 0.26	2.52 ± 0.20**	2.11 ± 0.5**	3.15 ± 0.06**	3.04 ± 0.06**	4.32 ± 0.05**
sEPSP Amplitude (Hz)						
Wild-type	0.74 ± 0.09	0.89 ± 0.05	0.68 ± 0.04	1.06 ± 0.04**	0.74 ± 0.02	1.34 ± 0.06**
$App^{NL-F/NL-F}$	0.98 ± 0.06	1.23 ± 0.05	0.89 ± 0.02**	2.00 ± 0.05**	2.00 ± 0.02**	3.44 ± 0.05**

*Averaged values in control and after bath-application of a5-SOP002 ± SEM are shown, significant difference indicated as with asterisk (*P < 0.05, **P < 0.01), indicate differences between data sets obtained before and drug application with the same genotype. Significant differences between genotypes are indicated with a blue asterisk (see also* ***Figures 5***, ***6****). A two-way ANOVA followed by post hoc Tukey's test for multiple comparisons was used to determine the statistical value. The sample size n denotes the number of animals (one cell per animal was recorded in these experiments). sIPSP, spontaneous inhibitory postsynaptic potential. sEPSP, spontaneous excitatory postsynaptic potentials.*

to α5-SOP002, unitary IPSPs recorded between two CR cells in SR were also reduced in peak amplitude and width at half amplitude following bath-application of α5-SOP002 at −55 mV (**Figure 5E**). The decrease in amplitude and width was: 51.20 ± 7.36% ($P < 0.05$, $n = 3$, paired, two-tailed student's *t*-test) and 28.25 ± 1.02% ($P < 0.01$, $n = 3$, paired, two-tailed student's *t*-test) of control IPSPs recorded in $App^{NL-F/NL-F}$, respectively. Bath-application of the α1 subunit-selective agonist, zolpidem did not change the IPSP properties at these synapses, which was consistent with previous studies that reported insensitivity to zolpidem at synapses involving presynaptic dendrite-preferring cells (Ali and Thomson, 2008). Subsequent addition of the broad spectrum benzodiazepine site agonist, diazepam (after α5-SOP002) enhanced IPSP amplitude by 186.59 ± 41.45% ($P < 0.05$, $n = 3$, one-way ANOVA) and width at half amplitude by, 37.31 ± 6.71% ($P > 0.05$, $n = 3$, one-way ANOVA with *post hoc* Bonferroni's test) of control IPSPs recorded in $App^{NL-F/NL-F}$ mice (**Figures 5E,F**).

The recorded (putative) CR-expressing interneurons, recovered *post hoc* were usually oval with two to three vertically orientated primary beaded dendrites, usually from opposite poles, with fine axons containing small/medium-sized boutons originated from the soma or a primary dendrite and ramified quite sparsely in mid-SR, as described previously (Shi et al., 2019) These cells resembled previously published CR cells (Gulyas et al., 1996).

α5-SOP002 Reduced Inhibition but Exacerbated Synaptic Hyperexcitability at CCK and Principal Cells

We then attempted to record from CCK and pyramidal cells in CA1. The anatomically recovered interneurons resembled the most abundant subtype of CCK-expressing cells, the Schaffer collateral-associated (SCA) interneuron with soma/dendrites and axons predominantly located in the SR and axonal branches predominantly ramifying in SR (Ali, 2007). CCK and SST-expressing cells in aged AD mice decline in densities during the pathogenesis of AD (Shi et al., 2019), which hampered the yield of the recordings. Furthermore, we could not record from SST-expressing cells in SO due to their sparse appearance in the slices and the heavy myelination in this region at 10–12 months of age.

Bath application of the $GABA_AR$ α5 NAM, α5-SOP002, resulted in a general trend in reducing the average sIPSP amplitude and frequency recorded in both CCK-SCA and pyramidal cells in age-matched wild-type and $APP^{NL-F/NL-F}$ mice (**Figure 6**, see **Table 1** for detailed values), significant changes are indicated in **Figure 6** and **Table 1**. In $APP^{NL-F/NL-F}$ mice, the average sIPSP frequency and amplitude recorded at CCK-SCA cells reduced by 51.20 ± 1.00% and 46.18 ± 1.90%, of control values by bath- application of α5-SOP002 ($P < 0.01$, two-way ANOVA, with *post hoc* Tukey's test, $n = 5$; **Figures 6A,B,E,F**). Similarly, in $APP^{NL-F/NL-F}$ mice sIPSP frequency and amplitude recorded in pyramidal cells reduced following bath-application α5-SOP002, by 43.45 ± 1.76% ($P > 0.05$, $n = 5$, two-way ANOVA) and 62.19 ± 7.19% ($P < 0.01$, $n = 5$, two-way ANOVA with *post hoc* Tukey's test) of control sIPSPs recorded in age-matched wild-type mice, respectively (**Figures 6D,E,G,H**).

However, in contrast, with bath-application of α5-SOP002, the sEPSP properties recorded in CCK-SCA and pyramidal cells significantly *increased* in both wild-type and $App^{NL-F/NL-F}$ mice (see **Table 1**). These cells recorded in the AD model displayed an abnormal level of hyperexcitation and a deficit in inhibition compared to the healthy, wild-type mice (**Figures 6G,H**; see also Petrache et al., 2019; Shi et al., 2019), which was further exacerbated when challenged with the $GABA_AR$ α5 NAM, α5-SOP002. With bath application of α5-SOP002, in the $APP^{NL-F/NL-F}$ mice, the increase in sEPSP frequency and amplitude in CCK-SCA was 42.10 ± 0.47% and 70.29 ± 1.04% ($P < 0.01$, $n = 6$, two-way ANOVA with *post hoc* Tukey's test), and in pyramidal cells was, 48.8 ± 0.94% and 124.71 ± 3.17% ($P < 0.01$, $n = 6$, two-way ANOVA with *post hoc* Tukey's test), respectively.

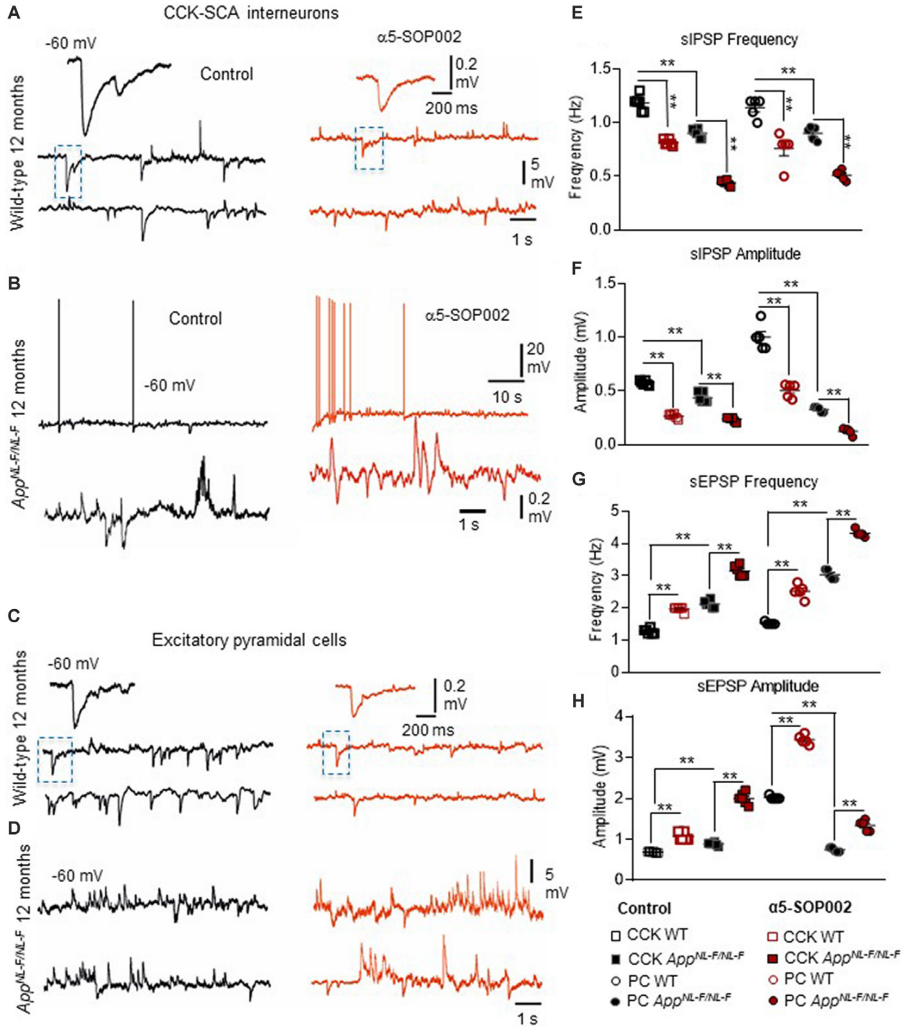

FIGURE 6 | CCK interneurons and pyramidal cells are further compromised by NAM of α5 subunit-containing $GABA_A$Rs in $App^{NL-F/NL-F}$ mice. **(A–D)** Whole-cell current-clamp recordings illustrating sIPSPs and sEPSPs recorded in CCK-SCA cells **(A,B)** and pyramidal cells **(C,D)** in CA1 of 12-month-old wild-type and $App^{NL-F/NL-F}$ mice, recorded at a membrane potential of −60 mV in control conditions and after bath-application of α5-SOP002. Bath-application of the α5-SOP002 resulted in a reduction in sIPSP amplitude and frequency, but also increased membrane excitation in both cell types, thus further increasing the aberrant hyperexcitability in the AD model. **(E–H)** Bar graphs show the overall pharmacological change after applying α5-SOP002 in CCK-SCA and pyramidal cells recorded from wild-type and $App^{NL-F/NL-F}$ mice at 10–12 months. $^{**}P < 0.01$. Data analyzed with a two-way ANOVA and *post hoc* Tukey's test, see **Table 1** for details.

DISCUSSION

In this study, we have focused on establishing whether the modulation of α5 $GABA_A$R-associated synaptic transmissions by compounds with negative allosteric effects could be a successful targeted therapeutic strategy in AD.

It has been evidenced that the $GABA_A$R α subunits form a structural basis for the different pharmacological and thus, behavioral profiles of various allosteric modulators of these receptors (Mohler et al., 2002; Whiting, 2003). In particular, allosteric modulation of α5-containing $GABA_A$Rs has been shown to gate the acquisition and modify the extinction of

associative learning in animal models (Collinson et al., 2002; Crestani et al., 2002; Yee et al., 2004; Dawson et al., 2006), while positive modulators of α5 $GABA_A$R were also found to rescue hippocampal-dependent memory deficits in memory-impaired rats tested with water and radial-arm mazes (Koh et al., 2013). Yet clinical trials aimed at alleviating cognitive deficits with selective NAMs of these receptors have failed. Our objective in the current study was to resynthesize a hybrid compound of an established NAM, 6,6-dimethyl-3-(2-hydroxyethyl)thio-1-(thiazol-2-yl)-6,7-dihydro-2-benzothiophene-4(5H)-one, to increase its' aqueous solubility, as well as its' selectivity and potency as a NAM of α5 $GABA_A$Rs. Inhibition mediated *via* these receptors is widespread in the brain but it is particularly abundant in the hippocampus (Magnin et al., 2019), where we have identified four sub-populations of neurons that express high levels of α5 $GABA_A$Rs. Using the $App^{NL-F/NL-F}$ knock-in mouse model of AD, that shows an age-dependent increase in the main pathological hallmarks of this disease, including accumulation of Aβ, activation of microglia and reactive astrocytes and neurodegeneration (Shi et al., 2019), we have revealed how the negative allosteric modulation of α5 $GABA_A$Rs can *exacerbate* the aberrant hyperexcitability and synaptic dysregulation in AD.

Mechanism of Action of Our Key Compound α5-SOP002

From computational modeling, we showed that α5-SOP002 docked into the interface of the α5 and γ2 subunits, indicating that it works *via* the benzodiazepine binding site (composed of a γ2 and either α1, α2, α3, or an α5 subunit of the $GABA_A$R). Normally, binding of benzodiazepines to these sites causes a conformational change of the receptor increasing the receptor's affinity for GABA, resulting in an enhanced inhibitory (hyperpolarizing) effect mediated *via* Cl^- flux (Sieghart, 1995). However, NAMs, such as α5-SOP002, when bound to the same $GABA_A$R sub-types *decrease* the influx of Cl^- which leads to depolarization of the membrane and a *decreased* net inhibitory effect (Haefely et al., 1993). The data obtained from various HEK cell-lines constructed to contain specific $GABA_A$R subunits and electrophysiological recordings performed, provided evidence to suggest that the developed compound, α5-SOP0002 specifically acted as a NAM at α5 $GABA_A$Rs and had no effect on α1 or α2 subunit-containing $GABA_A$Rs. However, this does not preclude an action of α5-SOP0002 as a NAM in native $GABA_A$Rs where the synaptic colocalization of the α subunits could result from a combination of the insertion of either two identical α subunits, or from insertion of a single receptor sub-type that contains two differentα subunits. Theα subunit that is adjacent to the γ2 subunit dominates the pharmacological profile of the receptor as suggested previously by binding studies on double immunopurified α1/α5 $GABA_A$Rs (Araujo et al., 1999). Thus, we suggest that α5-SOP002 acts by specifically binding at the interface of α5 and γ2 subunits, which determines a unique pharmacological profile of this compound.

Preservation of α5 $GABA_A$Rs in CA1 in the Aged Mouse Model of AD

We show for the first time, that the α5 $GABA_A$Rs in the CA1 region of the hippocampus are expressed on CR-expressing interneurons, specialized for dis-inhibition, but also SST- and CCK-expressing interneurons, specialized for fine-tuning pyramidal cell activity. The rationale for selecting CCK- and SST-expressing cells in our experiments stems from previous studies showing that dendrite-targeting interneurons form synapses with the pyramidal cells that incorporate the α5 subunit-containing $GABA_A$Rs (Ali and Thomson, 2008). However, in the current study, we show that SST- and CCK-expressing cells are also recipients of postsynaptic inhibition mediated by α5 $GABA_A$Rs.

Our findings corroborate previous studies that have demonstrated that α5 $GABA_A$Rs are preserved in post-mortem tissue obtained from AD patients (Howell et al., 2000; Palpagama et al., 2019), but also studies showing expression of α5 $GABA_A$Rs in pyramidal cells (Brünig et al., 2002). Our experiments demonstrate the expression of these receptors on the soma of CR, SST, and CCK interneurons in addition to pyramidal cells. However, the expression pattern of α5 $GABA_A$Rs in our study was in contrast to previous studies that show more diffuse staining in SR and SO compared to the pyramidal cell layer, which showed less expression of these receptors (Houser and Esclapez, 2003; Atack et al., 2005; Vidal et al., 2018). These differences could be attributed to the specificity of the antibodies, experimental protocol, or the disease model under investigation.

Since SST and CCK cells decline in the $App^{NL-F/NL-F}$ knock-in mouse model of AD (Shi et al., 2019), this distribution could be due to a subgroup of SST interneurons compensating for the reduction in numbers by upregulating α5 $GABA_A$R expression, interestingly, some studies show upregulated α5 subunits in SP and oriens of the CA1 region (Kwakowsky et al., 2018). Given that both CCK and SST cells are hyperactive in AD (Zhang et al., 2016; Shi et al., 2019), possibly the α5 expression represents a compensatory mechanism. An investigation into the levels of α5 expression on dendrites showed larger variability, notable being the level of expression on SST interneurons in the $App^{NL-F/NL-F}$ mice, which could be linked to the differential input those cells receive. Similarly, pyramidal cells showed larger variability, and we propose that this is input-dependent. Earlier studies investigating the regulation of $GABA_A$R surface expression show that, during seizures, receptors can be rapidly internalized leading to increased neuronal activity (Goodkin et al., 2007). A similar mechanism could be taking place in AD, contributing to the abnormal inhibitory-excitatory balance that characterizes this disease (Petrache et al., 2019).

Aberrant Inhibition in CR Interneurons Staining of in This Study Differs From Is "Normalized" by α5-SOP002 in the AD Model

Previously, we reported that the CR interneuron network was "preserved" in our AD model following post-phenotypic changes such as increased Aβ accumulation and proliferation

of microglial cells and astrocytes, which is consistent with anatomical studies reporting resilience of CR cells in post-mortem brains of AD patients (Fonseca and Soriano, 1995). Furthermore, the inhibitory parameters elicited in CR cells recorded in the AD models were abnormally enhanced compared to control mice, which was consistent with our previous study that suggests the involvement of the P2Y1 purinoreceptor system in regulating the abnormal inhibition expressed amongst the CR interneuron network (Shi et al., 2019). In this study, using our key NAM molecule, α5-SOP002, we have demonstrated that abnormal synaptic inhibition received by CR interneurons in the $App^{NL-F/NL-F}$ mouse model "normalized" to control levels. Moreover, paired whole-cell recordings revealed that α5-SOP002 had a pronounced effect at synapses between interneurons compared to synapses received by pyramidal cells, therefore impacting on dis-inhibition in the hippocampal CA1 region. This is important, given that we have previously demonstrated a gradual decline in the number of CCK- and SST-inhibitory interneurons in our AD model, suggesting an overall reduction in their inhibitory function, which was in stark contrast to the density of CR cells (Shi et al., 2019).

The sIPSPs recorded in this study are most likely due to the activation of synaptic α5 $GABA_A$Rs since we did not observe any significant change in either membrane potential or input resistance associated with the application of α5-SOP002 onto CR interneurons (or neither CCK nor pyramidal cells). We suggest that in the CR interneuron network, showing zolpidem insensitivity, augmentation by diazepam, and depression by α5–SOP002, the α5 subunit may coexist with another α5 subunit or either α2 or α3- subunit, where α5 pharmacology predominates.

However, interestingly, we observed a small positive (depolarization) change in membrane potential in CR interneurons with α5-SOP002 in the AD model only, suggesting that these cells may be in a state of excess tonic inhibition in the disease state. We suggest that the release from the abnormal tonic inhibition at CR cells, indicated by the depolarization of the membrane potential, could be caused by negative allosteric modulation of extrasynaptic α5-receptors (Caraiscos et al., 2004; Magnin et al., 2019), which are tonically active due to increased levels of ambient GABA (Scimemi et al., 2005). Given that α5-SOP002 requires the presence of α- and γ-subunits, it is unlikely that it can affect the activity of other types of extrasynaptic $GABA_A$Rs such as those containing the δ-subunit. However, the contribution of extrasynaptic α5 $GABA_A$Rs to the CR interneuron network remains to be fully investigated.

Negative Allosteric Modulation of α5 Subunit-Containing $GABA_A$Rs Further Exacerbates Hyperexcited Synapses in the AD Model

As previously described, there is a gradual decline in the number of CCK-SCA interneurons and CaMKII-expressing pyramidal cells in aged AD mice, with the later showing hyperexcitability when the pathological hallmarks of AD were present, clearly indicating the abnormalities in neuronal network activity (Shi et al., 2019). Since these cells express the α5 subunit, it is not surprising that α5-SOP002 can reduce inhibition at CCK and pyramidal cells, and therefore exacerbate imbalance between the excitation and inhibition at these key neuronal populations in CA1 and impact on the efficacy and precision of the fine-tuning inhibition at both temporal and spatial domains. These are reasonable assumptions, since; CCK-SCA cells, which are ideally positioned to modulate CA3 input (Iball and Ali, 2011), and are important for fine-tuning individual neurons by retrograde cannabinoid signaling (Katona et al., 1999; Ali, 2007), whereas the SST, that fine-tune distal inputs received by CA1 pyramidal cells (Leao et al., 2012; Magnin et al., 2019), and are important for coordinating neuronal assemblies and gating of memory formation (Tort et al., 2007; Cutsuridis and Wennekers, 2009). Due to the prime location of these interneurons, it is feasible to suggest that both of these interneuron subpopulations may be involved in routing information flow to CA1 from CA3 and entorhinal cortex- pathways that are important for memory acquisition and retrieval, and their destruction during the pathogenesis of AD may be a significant contributing factor to cognitive decline. This is further supported by recent studies that show SST interneuron dysfunction triggered by amyloid β oligomers underlies hippocampal oscillation important for memory functions (Chung et al., 2020).

CONCLUSION

In summary, using a multi-disciplinary approach, we have developed a novel, selective NAM for α5 $GABA_A$Rs and characterized its effects on hippocampal dis-inhibition in a well-established mouse model of AD. We have shown that this modulator can "normalize" abnormal, inhibitory synaptic activity received by CR interneurons in this model, suggesting initially its' therapeutic potential. Furthermore, our data provide evidence that α5 $GABA_A$Rs are also preserved in other types of interneurons, such as CCK, SST, and CR interneurons.

Since our data suggest that α5 $GABA_A$Rs are widely expressed by both dysfunctional and resilient neurons, and also that α5-SOP002 can compromise further the aberrant hyperexcitable network in the AD model, we propose that pharmacological modulation of α5 subunit-containing $GABA_A$R networks may not be a suitable therapeutic target for cognitive impairment in AD. Although the evidence suggests an overall improvement of memory with $GABA_A$ α5 inverse agonists in rodents, it is yet to be established what kind of short- and long-term effects these compounds might have in patients. We propose that the lack of specificity and efficacy in clinical trials could be at least in part due to a wide expression of α5 $GABA_A$Rs in the hippocampus, both by various types of interneurons and pyramidal cells. Thus, targeting the α5 subunit with NAMs would result in a global effect on the hippocampal networks and would lack the specificity required to restore the complex network alteration during the pathogenesis of AD that leads to the observed excitatory-inhibitory imbalance.

DATA AVAILABILITY STATEMENT

All datasets presented in this study are included in the article/**Supplementary Material**.

ETHICS STATEMENT

The animal study was reviewed and approved by British Home Office and UCL ethics committees.

AUTHOR CONTRIBUTIONS

AP: performed immunofluorescence studies on mouse brains to characterize the expression of α5 $GABA_A$Rs in different subtypes of interneurons and assisted in preparing the manuscript. AK: designed and produced the new α5 cell line and assisted in preparing the manuscript. AM: synthesized and refined various analogs of α5 NAMs with varying biological activity. MN: designed and produced the α5β2γ2-$GABA_A$R stable cell line. MK-S: performed molecular docking and identification of the final conformation of the developed NAM. SHa: computational modeling and assisted in preparing the manuscript. SHi: developed, refined, and synthesized the α5 compounds. JJ: supervised production and characterization of all HEK293 cell lines stably expressing $GABA_A$Rs which were used in this study. AA: designed and coordinated the project, performed and analyzed all electrophysiology and neuroanatomy experiments, and prepared the manuscript. All authors contributed to the article and approved the submitted version.

FUNDING

Experiments were performed using equipment funded by the Wellcome Trust (UK) and by the Medical Research Council (UK) New Investigators award (AA: GO501263) and MRC Ph.D. studentship (MR/N013867/1).

ACKNOWLEDGMENTS

We would like to thank Dr. Andrew Constanti (UCL School of Pharmacy) for his invaluable comments in the preparation of this manuscript. We also thank Miss Audrey Crystalia for assisting in the development and characterization of the α2β2γ2-HEK293 stable cell lines, Professor F. A. Stephenson (UCL School of Pharmacy) for the $GABA_A$R α1 subunit-specific antibody and Professor Jean-Marc Fritschy (University of Zurich) for the $GABA_A$R α5 and γ2 subunit-specific antibodies used for the HEK cell lines.

SUPPLEMENTARY MATERIAL

The Supplementary Material for this article can be found online at: https://www.frontiersin.org/articles/10.3389/fncel.2020.568194/full#supplementary-material.

REFERENCES

Ali, A. B. (2007). Presynaptic inhibition of $GABA_A$ receptor-mediated unitary IPSPs by cannabinoid receptors at synapses between CCK-positive interneurons in rat hippocampus. *J. Neurophysiol.* 98, 861–869. doi: 10.1152/jn.00156.2007

Ali, A. B., and Nelson, C. (2006). Distinct Ca^{2+} channels mediate transmitter release at excitatory synapses displaying different dynamic properties in rat neocortex. *Cereb. Cortex* 16, 386–393. doi: 10.1093/cercor/bhi117

Ali, A. B., and Thomson, A. M. (2008). Synaptic α5 subunit-containing $GABA_A$ receptors mediate IPSPs elicited by dendrite-preferring cells in rat neocortex. *Cereb. Cortex* 18, 1260–1271. doi: 10.1093/cercor/bhm160

Araujo, F., Ruano, D., and Vitorica, J. (1999). Native γ-aminobutyric acid type A receptors from rat hippocampus, containing both α1 and α5 subunits, exhibit a single benzodiazepine binding site with α5 pharmacological properties. *J. Pharmacol. Exp. Ther.* 290, 989–997.

Atack, J. R. (2010). Preclinical and clinical pharmacology of the $GABA_A$ receptor α5 subtype-selective inverse agonist α5IA. *Pharmacol. Ther.* 125, 11–26. doi: 10.1016/j.pharmthera.2009.09.001

Atack, J. R., Alder, L., Cook, S. M., Smith, A. J., and McKernan, R. M. (2005). *In vivo* labelling of α5 subunit-containing $GABA_A$ receptors using the selective radioligand [^{3}H]L-655,708. *Neuropharmacology* 49, 220–229. doi: 10.1016/j.neuropharm.2005.03.004

Atack, J. R., Bayley, P. J., Seabrook, G. R., Wafford, K. A., McKernan, R. M., and Dawson, G. R. (2006). L-655,708 enhances cognition in rats but is not proconvulsant at a dose selective for α5-containing $GABA_A$ receptors. *Neuropharmacology* 51, 1023–1029. doi: 10.1016/j.neuropharm.2006.04.018

Atack, J. R., Maubach, K. A., Wafford, K. A., O'Connor, D., Rodrigues, A. D., Evans, D. C., et al. (2009). *In vitro* and *in vivo* properties of 3-tert-butyl-7–(5-methylisoxazol-3-yl)-2–(1-methyl-1H-1,2,4-triazol-5-ylmethoxy)-pyrazolo[1,5-d]-[1,2,4]triazine (MRK-016), a $GABA_A$ receptor α5 subtype-selective inverse agonist. *J. Pharmacol. Exp. Ther.* 331, 470–484. doi: 10.1124/jpet.109.157636

Ballard, T. M., Knoflach, F., Prinssen, E., Borroni, E., Vivian, J. A., Basile, J., et al. (2009). RO4938581, a novel cognitive enhancer acting at $GABA_A$ α5 subunit-containing receptors. *Psychopharmacology* 202, 207–223. doi: 10.1007/s00213-008-1357-7

Becker, J. T., Walker, J. A., and Olton, D. S. (1980). Neuroanatomical bases of spatial memory. *Brain Res.* 200, 307–320. doi: 10.1016/0006-8993(80)90922-1

Braudeau, J., Delatour, B., Duchon, A., Pereira, P. L., Dauphinot, L., de Chaumont, F., et al. (2011). Specific targeting of the GABA-A receptor α5 subtype by a selective inverse agonist restores cognitive deficits in Down syndrome mice. *J. Psychopharmacol.* 25, 1030–1042. doi: 10.1177/0269881111405366

Brown, L. E., Nicholson, M. W., Arama, J. E., Mercer, A., Thomson, A. M., and Jovanovic, J. N. (2016). γ-aminobutyric acid type A ($GABA_A$) receptor subunits play a direct structural role in synaptic contact formation *via* their N-terminal extracellular domains. *J. Biol. Chem.* 291, 13926–13942. doi: 10.1074/jbc.M116.714790

Brünig, I., Scotti, E., Sidler, C., and Fritschy, J. M. (2002). Intact sorting, targeting and clustering of γ-aminobutyric acid A receptor subtypes in hippocampal neurons *in vitro*. *J. Comp. Neurol.* 443, 43–55. doi: 10.1002/cne.10102

Caraiscos, V. B., Elliott, E. M., You-Ten, K. E., Cheng, V. Y., Belelli, D., Newell, J. G., et al. (2004). Tonic inhibition in mouse hippocampal CA1 pyramidal neurons is mediated by α5 subunit-containing γ-aminobutyric acid type A receptors. *Proc. Natl. Acad. Sci. U S A* 101, 3662–3667. doi: 10.1073/pnas.0307231101

Chambers, M. S., Atack, J. R., Broughton, H. B., Collinson, N., Cook, S., Dawson, G. R., et al. (2003). Identification of a novel, selective $GABA_A$ α5 receptor inverse agonist which enhances cognition. *J. Med. Chem.* 46, 2227–2240. doi: 10.1021/jm020582q

Chung, H., Park, K., Jang, H. J., Kohl, M. M., and Kwag, J. (2020). Dissociation of somatostatin and parvalbumin interneurons circuit dysfunctions underlying hippocampal theta and gamma oscillations impaired by amyloid β oligomers *in vivo*. *Brain Struct. Funct.* 225, 935–954. doi: 10.1007/s00429-020-02044-3

Collinson, N., Atack, J. R., Laughton, P., Dawson, G. R., and Stephens, D. N. (2006). An inverse agonist selective for α5 subunit-containing $GABA_A$ receptors improves encoding and recall but not consolidation in the Morris water maze. *Psychopharmacology* 188, 619–628. doi: 10.1007/s00213-006-0361-z

Collinson, N., Kuenzi, F. M., Jarolimek, W., Maubach, K. A., Cothliff, R., Sur, C., et al. (2002). Enhanced learning and memory and altered GABAergic synaptic transmission in mice lacking the α5 subunit of the $GABA_A$ receptor. *J. Neurosci.* 22, 5572–5580. doi: 10.1523/JNEUROSCI.22-13-05572.2002

Crestani, F., Keist, R., Fritschy, J. M., Benke, D., Vogt, K., Prut, L., et al. (2002). Trace fear conditioning involves hippocampal α5 $GABA_A$ receptors. *Proc. Natl. Acad. Sci. U S A* 99, 8980–8985. doi: 10.1073/pnas.142288699

Cutsuridis, V., and Wennekers, T. (2009). Hippocampus, microcircuits and associative memory. *Neural Netw.* 22, 1120–1128. doi: 10.1016/j.neunet.2009.07.009

Dawson, G. R., Maubach, K. A., Collinson, N., Cobain, M., Everitt, B. J., MacLeod, A. M., et al. (2006). An inverse agonist selective for α5 subunit-containing $GABA_A$ receptors enhances cognition. *J. Pharmacol. Exp. Ther.* 316, 1335–1345. doi: 10.1124/jpet.105.092320

Duchon, J. M., Levin, M. J., and Gershon, A. A. (2019). Safety and varicella outcomes in utero-exposed newborns and preterm infants treated with varicella zoster immune globulin (VARIZIG): a subgroup analysis of an expanded-access program. *J. Pediatric. Infect. Dis. Soc.* 9, 449–453. doi: 10.1093/jpids/piz070

Eimerbrink, M. J., Pendry, R. J., Hodges, S. L., Wiles, J. D., Peterman, J. L., White, J. D., et al. (2019). The α5-$GABA_A$R inverse agonist MRK-016 upregulates hippocampal BDNF expression and prevents cognitive deficits in LPS-treated mice, despite elevations in hippocampal Aβ. *Behav. Brain Res.* 359, 871–877. doi: 10.1016/j.bbr.2018.07.013

Fonseca, M., and Soriano, E. (1995). Calretinin-immunoreactive neurons in the normal human temporal cortex and in Alzheimer's disease. *Brain Res.* 691, 83–91. doi: 10.1016/0006-8993(95)00622-w

Fuchs, C., Abitbol, K., Burden, J. J., Mercer, A., Brown, L., Iball, J., et al. (2013). $GABA_A$ receptors can initiate the formation of functional inhibitory GABAergic synapses. *Eur. J. Neurosci.* 38, 3146–3158. doi: 10.1111/ejn.12331

Ghafari, M., Falsafi, S. K., Szodorai, E., Kim, E. J., Li, L., Hoger, H., et al. (2017). Formation of $GABA_A$ receptor complexes containing α1 and α5 subunits is paralleling a multiple T-maze learning task in mice. *Brain Struct. Funct.* 222, 549–561. doi: 10.1007/s00429-016-1233-x

Glykys, J., Mann, E. O., and Mody, I. (2008). Which $GABA_A$ receptor subunits are necessary for tonic inhibition in the hippocampus? *J. Neurosci.* 28, 1421–1426. doi: 10.1523/JNEUROSCI.4751-07.2008

Goodkin, H. P., Sun, C., Yeh, J. L., Mangan, P. S., and Kapur, J. (2007). $GABA_A$ receptor internalization during seizures. *Epilepsia* 48, 109–113. doi: 10.1111/j.1528-1167.2007.01297.x

Gulyas, A. I., Hajos, N., and Freund, T. F. (1996). Interneurons containing calretinin are specialized to control other interneurons in the rat hippocampus. *J. Neurosci.* 16, 3397–3411. doi: 10.1523/JNEUROSCI.16-10-03397.1996

Haefely, W. E., Martin, J. R., Richards, J. G., and Schoch, P. (1993). The multiplicity of actions of benzodiazepine receptor ligands. *Can. J. Psychiatry* 38, S102–S108.

Houser, C. R., and Esclapez, M. (2003). Downregulation of the α5 subunit of the $GABA_A$ receptor in the pilocarpine model of temporal lobe epilepsy. *Hippocampus* 13, 633–645. doi: 10.1002/hipo.10108

Howell, O., Atack, J. R., Dewar, D., McKernan, R. M., and Sur, C. (2000). Density and pharmacology of α5 subunit-containing $GABA_A$ receptors are preserved in hippocampus of Alzheimer's disease patients. *Neuroscience* 98, 669–675. doi: 10.1016/s0306-4522(00)00163-9

Iball, J., and Ali, A. B. (2011). Endocannabinoid release modulates electrical coupling between CCK cells connected *via* chemical and electrical synapses in CA1. *Front. Neural Circuits* 5:17. doi: 10.3389/fncir.2011.00017

Katona, I., Acsady, L., and Freund, T. F. (1999). Postsynaptic targets of somatostatin-immunoreactive interneurons in the rat hippocampus. *Neuroscience* 88, 37–55. doi: 10.1016/s0306-4522(98)00302-9

Khan, A. A., Shekh-Ahmad, T., Khalil, A., Walker, M. C., and Ali, A. B. (2018). Cannabidiol exerts antiepileptic effects by restoring hippocampal interneuron functions in a temporal lobe epilepsy model. *Br. J. Pharmacol.* 175, 2097–2115. doi: 10.1111/bph.14202

Koh, M. T., Rosenzweig-Lipson, S., and Gallagher, M. (2013). Selective $GABA_A$ α5 positive allosteric modulators improve cognitive function in aged rats with memory impairment. *Neuropharmacology* 64, 145–152. doi: 10.1016/j.neuropharm.2012.06.023

Kwakowsky, A., Calvo-Flores Guzman, B., Govindpani, K., Waldvogel, H. J., and Faull, R. L. (2018). γ-aminobutyric acid A receptors in Alzheimer's disease: highly localized remodeling of a complex and diverse signaling pathway. *Neural Regen. Res.* 13, 1362–1363. doi: 10.4103/1673-5374.235240

Leao, R. N., Mikulovic, S., Leao, K. E., Munguba, H., Gezelius, H., Enjin, A., et al. (2012). OLM interneurons differentially modulate CA3 and entorhinal inputs to hippocampal CA1 neurons. *Nat. Neurosci.* 15, 1524–1530. doi: 10.1038/nn.3235

Liu, R., Hu, R. J., Zhang, P., Skolnick, P., and Cook, J. M. (1996). Synthesis and pharmacological properties of novel 8-substituted imidazobenzodiazepines: high-affinity, selective probes for α5-containing $GABA_A$ receptors. *J. Med. Chem.* 39, 1928–1934. doi: 10.1021/jm950887n

Magnin, E., Francavilla, R., Amalyan, S., Gervais, E., David, L. S., Luo, X., et al. (2019). Input-specific synaptic location and function of the α5 $GABA_A$ receptor subunit in the mouse CA1 hippocampal neurons. *J. Neurosci.* 39, 788–801. doi: 10.1523/JNEUROSCI.0567-18.2018

Martinez-Cue, C., Delatour, B., and Potier, M. C. (2014). Treating enhanced GABAergic inhibition in Down syndrome: use of GABA α5-selective inverse agonists. *Neurosci. Biobehav. Rev.* 46, 218–227. doi: 10.1016/j.neubiorev.2013.12.008

McGrath, J. C., Drummond, G. B., McLachlan, E. M., Kilkenny, C., and Wainwright, C. L. (2010). Guidelines for reporting experiments involving animals: the ARRIVE guidelines. *Br. J. Pharmacol.* 160, 1573–1576. doi: 10.1111/j.1476-5381.2010.00873.x

McKernan, R. M., and Whiting, P. J. (1996). Which $GABA_A$-receptor subtypes really occur in the brain? *Trends Neurosci.* 19, 139–143. doi: 10.1016/s0166-2236(96)80023-3

Mohler, H., Fritschy, J. M., and Rudolph, U. (2002). A new benzodiazepine pharmacology. *J. Pharmacol. Exp. Ther.* 300, 2–8. doi: 10.1124/jpet.300.1.2

Munakata, M., Jin, Y. H., Akaike, N., and Nielsen, M. (1998). Temperature-dependent effect of zolpidem on the $GABA_A$ receptor-mediated response at recombinant human $GABA_A$ receptor subtypes. *Brain Res.* 807, 199–202. doi: 10.1016/s0006-8993(98)00774-4

Palpagama, T. H., Sagniez, M., Kim, S., Waldvogel, H. J., Faull, R. L., and Kwakowsky, A. (2019). $GABA_A$ receptors are well preserved in the hippocampus of aged mice. *eNeuro* 6:ENEURO.0496-18.2019. doi: 10.1523/ENEURO.0496-18.2019

Petrache, A. L., Rajulawalla, A., Shi, A., Wetzel, A., Saito, T., Saido, T. C., et al. (2019). Aberrant excitatory-inhibitory synaptic mechanisms in entorhinal cortex microcircuits during the pathogenesis of Alzheimer's disease. *Cereb. Cortex* 29, 1834–1850. doi: 10.1093/cercor/bhz016

Price, J. L., Ko, A. I., Wade, M. J., Tsou, S. K., McKeel, D. W., and Morris, J. C. (2001). Neuron number in the entorhinal cortex and CA1 in preclinical Alzheimer disease. *Arch. Neurol.* 58, 1395–1402. doi: 10.1001/archneur.58.9.1395

Quirk, K., Blurton, P., Fletcher, S., Leeson, P., Tang, F., Mellilo, D., et al. (1996). [^{3}H]L-655,708, a novel ligand selective for the benzodiazepine site of $GABA_A$ receptors which contain the α5 subunit. *Neuropharmacology* 35, 1331–1335. doi: 10.1016/s0028-3908(96)00061-5

Rissman, R. A., De Blas, A. L., and Armstrong, D. M. (2007). $GABA_A$ receptors in aging and Alzheimer's disease. *J. Neurochem.* 103, 1285–1292. doi: 10.1111/j.1471-4159.2007.04832.x

Saito, T., Matsuba, Y., Mihira, N., Takano, J., Nilsson, P., Itohara, S., et al. (2014). Single App knock-in mouse models of Alzheimer's disease. *Nat. Neurosci.* 17, 661–663. doi: 10.1038/nn.3697

Sasaguri, H., Nilsson, P., Hashimoto, S., Nagata, K., Saito, T., De Strooper, B., et al. (2017). APP mouse models for Alzheimer's disease preclinical studies. *EMBO J.* 36, 2473–2487. doi: 10.15252/embj.201797397

Savić, M. M., Clayton, T., Furtmuller, R., Gavrilovic, I., Samardzic, J., Savic, S., et al. (2008). PWZ-029, a compound with moderate inverse agonist functional selectivity at $GABA_A$ receptors containing α5 subunits, improves passive, but not active, avoidance learning in rats. *Brain Res.* 1208, 150–159. doi: 10.1016/j.brainres.2008.02.020

Scimemi, A., Semyanov, A., Sperk, G., Kullmann, D. M., and Walker, M. C. (2005). Multiple and plastic receptors mediate tonic $GABA_A$ receptor currents in the hippocampus. *J. Neurosci.* 25, 10016–10024. doi: 10.1523/JNEUROSCI.2520-05.2005

Serwanski, D. R., Miralles, C. P., Christie, S. B., Mehta, A. K., Li, X., and De Blas, A. L. (2006). Synaptic and nonsynaptic localization of $GABA_A$ receptors

containing the α5 subunit in the rat brain. *J. Comp. Neurol.* 499, 458–470. doi: 10.1002/cne.21115

Shi, A., Petrache, A. L., Shi, J., and Ali, A. B. (2019). Preserved calretinin interneurons in an App model of Alzheimer's disease disrupt hippocampal inhibition *via* upregulated P2Y1 purinoreceptors. *Cereb. Cortex* 30, 1272–1290. doi: 10.1093/cercor/bhz165

Sieghart, W. (1995). Structure and pharmacology of γ-aminobutyric acidA receptor subtypes. *Pharmacol. Rev.* 47, 181–234.

Sieghart, W., and Sperk, G. (2002). Subunit composition, distribution and function of GABA$_A$ receptor subtypes. *Curr. Top. Med. Chem.* 2, 795–816. doi: 10.2174/1568026023393507

Sternfeld, F., Carling, R. W., Jelley, R. A., Ladduwahetty, T., Merchant, K. J., Moore, K. W., et al. (2004). Selective, orally active γ-aminobutyric acidA α5 receptor inverse agonists as cognition enhancers. *J. Med. Chem.* 47, 2176–2179. doi: 10.1021/jm031076j

Sung, K., and Lee, A.-R. (1992). Synthesis of [(4,5-disubstituted-4H-1,2,4-triazol-3-yl)thio]alkanoic acids and their analogues as possible antiinflammatory agents. *J. Het. Chem.* 29, 1101–1109. doi: 10.1002/jhet.5570290512

Tort, A. B., Rotstein, H. G., Dugladze, T., Gloveli, T., and Kopell, N. J. (2007). On the formation of γ-coherent cell assemblies by oriens lacunosum-moleculare interneurons in the hippocampus. *Proc. Natl. Acad. Sci. U S A* 104, 13490–13495. doi: 10.1073/pnas.0705708104

Vidal, V., Garcia-Cerro, S., Martinez, P., Corrales, A., Lantigua, S., Vidal, R., et al. (2018). Decreasing the expression of GABA$_A$ α5 subunit-containing receptors partially improves cognitive, electrophysiological and morphological hippocampal defects in the Ts65Dn model of down syndrome. *Mol. Neurobiol.* 55, 4745–4762. doi: 10.1007/s12035-017-0675-3

Whiting, P. J. (2003). The GABA$_A$ receptor gene family: new opportunities for drug development. *Curr. Opin. Drug Discov. Devel.* 6, 648–657.

Yee, B. K., Hauser, J., Dolgov, V. V., Keist, R., Mohler, H., Rudolph, U., et al. (2004). GABA receptors containing the α5 subunit mediate the trace effect in aversive and appetitive conditioning and extinction of conditioned fear. *Eur. J. Neurosci.* 20, 1928–1936. doi: 10.1111/j.1460-9568.2004.03642.x

Zhang, W., Zhang, L., Liang, B., Schroeder, D., Zhang, Z. W., Cox, G. A., et al. (2016). Hyperactive somatostatin interneurons contribute to excitotoxicity in neurodegenerative disorders. *Nat. Neurosci.* 19, 557–559. doi: 10.1038/nn.4257

Conflict of Interest: The authors declare that the research was conducted in the absence of any commercial or financial relationships that could be construed as a potential conflict of interest.